ABSTRACT

GAO, YUAN. A Classical Correlation Model of Resonance Raman Scattering and Surface Enhanced Infrared Absorption Spectroscopies. (Under the direction of Dr. Stefan Franzen)

Plasmonic properties of noble metals have led to a large field of investigation of the effects of plasmonic fields on molecular spectra. Molecular spectroscopic signals show enhancement near the interface of a conductor and insulator. This is most often observed when the molecule is chemically bonded to the conductor. Plasmonic enhancement has been applied to surface enhanced Raman spectroscopy (SERS), surface enhanced infrared absorption (SEIRA), and surface enhanced fluorescence (SEF) spectroscopies.

The mechanism of the enhancement has not been fully understood. Although both electromagnetic mechanism and chemical mechanism have been suggested, the enhancement factor is usually estimated by the fourth power of the enhanced incident field, where molecular properties are ignored. The development of a comprehensive model remains a challenge.

In Chapter 2, we started by demonstrating a classical correlation model (CCM) of resonance Raman spectroscopy. A spring-mass system is used to illustrate the molecule. The mass represents an electron, the wall represents the rest of the molecule. Spring represents the interaction between the electron and the molecule. By introducing an interaction term with the same frequency of the vibrational normal mode into the spring constant, the Raman excitation profile (REP) is obtained from the polarizability using methods developed previously for studies of second-harmonic generation. This theory provided the same mathematical form and matched the amplitude of the REP obtained from the quantum theory, which is derived from the Kramers-Heisenberg-Dirac equation. This work proved the feasibility of application of the CCM to elucidate electromagnetic enhancement and chemical enhancement in the surface enhanced spectroscopy.

In Chapter 3, we turned attention to CCM on SEIRA. SEIRA results can be predicted by Maxwell's equations, which is the fundamental of electromagnetic enhancement. We generalize the interactions of plasmons with molecules by considering the N_2O asymmetric stretch SEIRA signal on a Dy doped CdO (CdO:Dy) film. This semiconductor has tunable plasmon dispersion curves throughout the near-and mid-infrared that can interact directly with vibrational absorption transitions. We have demonstrated this using the Kretschmann configuration with a CaF_2 prism and a MgO substrate. The model predicts the phase behavior of SEIRA. The calculated enhancement factor relative to an Au control is 6.2, in good agreement with the value of 6.8 ± 0.5 measured under the same conditions.

In Chapter 4, we applied CCM to SERS with nanoparticle suspension. The SERS signal of various concentration of crystal violet (CV) adsorbed on a gold nanoparticle has a various radius is calculated. In the limit of a single layer, the calculated enhancement factor agrees with the experimental results for gold nanoparticles under 15 nm and CV concentration under 5 μM.

In Chapter 5, we introduced a dielectric function for a Raman-active layer. This function aimed to facilitate the computation of SERS signals within a Kretschmann configuration, serving as a previous step towards modeling the enhancement factor of a planar conductor integrated with modified nanoparticles.

We have shown the CCM is compatible with both planar and spherical geometries, with both quantum mechanics and classical electromagnetism. CCM has the potential to shed light on the mechanism of surface enhanced spectroscopies, and therefore as a guide to remove obstacles in this field.

A Classical Correlation Model of Resonance Raman Scattering and Surface Enhanced Infrared Absorption Spectroscopies

by
Yuan Gao

A dissertation submitted to the Graduate Faculty of
North Carolina State University
in partial fulfillment of the
requirements for the degree of
Doctor of Philosophy

Chemistry

Raleigh, North Carolina
2023

APPROVED BY:

_____	_____
Dr. David Aspnes	Dr. Paul Maggard
_____	_____
Dr. James Martin	Dr. Thomas Theis

_____
Dr. Stefan Franzen
Committee Chair

BIOGRAPHY

Yuan Gao obtained her B.S. in Chemistry from Zhejiang University in 2017. Her undergraduate research focused on molecular dynamics and DFT computational studies of metal-catalyzed organic reaction mechanisms, under the guidance of Dr. Xin Hong.

In 2018, Yuan started her Ph.D. journey in the Department of Chemistry at North Carolina State University. She became a member of Dr. Stefan Franzen's group, where her research project focused on theoretical and computational modeling of surface enhanced molecular infrared and Raman spectroscopies.

ACKNOWLEDGMENTS

I would like to express my heartfelt gratitude to Dr. Stefan Franzen, my advisor, for his invaluable guidance throughout this project and for teaching me the intricacies of Spectroscopy. His incredible ideas and unwavering support have been instrumental in shaping this research.

I would also like to extend my appreciation to Dr. David Aspnes, as my second advisor, who introduced me to the fascinating realm of electromagnetism and collaborated with us on this project. His continuous assistance and encouragement have been truly invaluable.

A special thanks goes to Dr. Edward Sachet for generously providing the experimental data and the CdO samples, which were crucial for the success of this study. I am also grateful to Dr. Krill Elfimenko and Dr. Jen Genzer for granting me access to their lab and allowing me to conduct the IR-VASE experiment.

I am indebted to my labmates, particularly Dr. Hniang Khamh, for introducing me to this project and for their unwavering support throughout the research process and during my internship. I would also like to acknowledge the contributions of Dr. Jessica Miranda Gonzalez-Delgado, Dr. Nikhila Kashyap Dhanvantari Madhuresh, and the future Dr. Mst Sharmin Aktar, who provided assistance and support in various aspects of the research.

I am sincerely appreciative of the Department of Chemistry in NCSU, especially Dr. Reza Ghiladi, Dr. Gavin Williams, and Amy Roosje for their continuous help with my program.

Furthermore, I am deeply grateful to my friends, my partner, and my family for their understanding, encouragement, and unconditional support throughout this endeavor. Their unwavering belief in me has been a constant source of motivation.

I would like to thank all those mentioned above, as well as anyone else who has provided support, guidance, or encouragement in any form. This research would not have been possible without their collective efforts and contributions.

TABLE OF CONTENTS

LIST OF TABLES

LIST OF FIGURES

CHAPTER 1. Background and literature review

As a collective oscillation of electrons in a conductor, on the one hand, plasmons create a localized enhanced electric field, which further enhances the local field of the molecule, providing an enhanced spectroscopic signal. On the other hand, the chemical interaction between the plasmon and molecule enabled charge transfer and selection rule relaxation, which may enhance the signal as well. In this chapter, the fundamental of plasmonic properties will be introduced. The history, achievements, and obstacles of further application of SERS and SEIRA will be deployed and discussed.

1.1. Plasmons and plasmonic properties

A plasmon is a quasiparticle which describes the plasma oscillation of the conductive electrons in the material. Plasmons can be excited with photons, by phase and frequency matching. The term "plasmon" was first used in 1956, where Pines noticed the oscillation of the conductive electrons behaves similar to the plasma oscillation in the gaseous plasma state.[1]

There are three common types of the plasmons, bulk plasmon or volume plasmon, surface plasmon, and localized surface plasmon.[2]

1.1.1. The bulk plasmon

The bulk plasmon appears when the dielectric function of the material becomes equal to zero. Given the wave equation for a planar wave,[3]

$$\vec{k}\left(\vec{k}\cdot\vec{E}\right)-k^2\vec{E}=-\frac{\mu\epsilon\omega^2}{c^2}\vec{E}, \tag{1.1}$$

the bulk plasmon is excited when the real part of the dielectric function of the material $\epsilon(\omega)=0$, the wave vector $\vec{k}$ and the electric field $\vec{E}$ share the same direction, where a longitudinal wave

is taken place. The conductive electrons encounter collective oscillation, with the direction same as the incident field. This collective oscillation is called epsilon near zero (ENZ) mode.

The Drude model has been widely used to represent free electron conductors,[4,5] where the dielectric function is described by:

$$\epsilon(\omega) = 1 - \frac{\omega_p^2}{\omega^2}, \tag{1.2a}$$

where $\omega_p = \sqrt{ne/m_e\epsilon_0}$ and n is the density of the free electron in the material. If the positive cation background is polarizable,[6]

$$\epsilon(\omega) = \epsilon_\infty - \frac{\omega_p^2}{\omega^2} = \epsilon_\infty\left(1 - \frac{\bar{\omega}_p^2}{\omega^2}\right). \tag{1.2b}$$

where ϵ_∞ is the dielectric constant to the high frequency limit, and $\bar{\omega}_p = \sqrt{ne/m_e\epsilon_0\epsilon_\infty}$.

It is obvious that when $\omega = \omega_p$ (or $\bar{\omega}_p$ when $\epsilon_\infty \neq 1$), the dielectric function $\epsilon = 0$. Thus, ω_p or $\bar{\omega}_p$ defines the plasma frequency of the material.

1.1.2. Surface plasmon polariton (SPP)

Surface plasmon is the conducting electrons oscillating along the interface between two materials with the excitation of surface wave, which is confined on the interface. The propagating excitation is the surface plasmon polariton (SPP). This feature of the surface wave is described with an imaginary wave vector on the normal direction of the interface, allows SPP attenuates exponentially from the surface.

If both materials are non-magnetic, the excitation of the surface wave requires the incident wave to be p polarized, *i.e.*, a transverse magnetic (TM) mode, where the magnetic field is parallel to the interface. The magnetic field and the electric field on both sides are given in the following equations (coordinate system based on Figure 1.1) are given:[2]

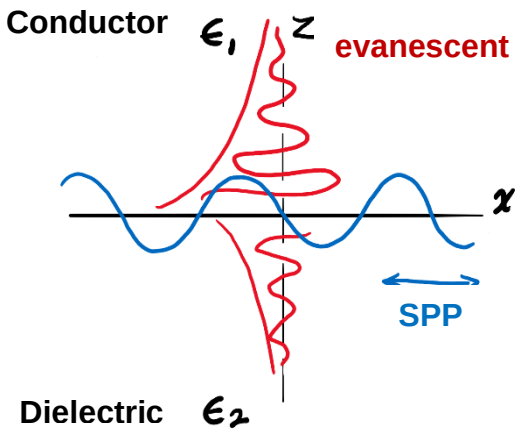

Figure 1.1 Surface wave and surface plasmon polariton

For material 1, $z > 0$:

$$H_{1y} = H_{10}e^{ik_{x1}x+ik_{z1}z-i\omega t}, \tag{1.3a}$$

$$E_{1x} = \frac{1}{i\epsilon_0\epsilon_1\omega}\frac{\partial H_{1y}}{\partial z}e^{ik_{x1}x+ik_{z1}z-i\omega t} = \frac{k_{z1}}{\epsilon_0\epsilon_1\omega}H_{10}e^{ik_{x1}x+ik_{z1}z-i\omega t}, \tag{1.3b}$$

$$E_{1z} = -\frac{1}{i\epsilon_0\epsilon_1\omega}\frac{\partial H_{1y}}{\partial x}e^{ik_{x1}x+ik_{z1}z-i\omega t} = -\frac{k_{x1}}{\epsilon_0\epsilon_1\omega}H_{10}e^{ik_{x1}x+ik_{z1}z-i\omega t}, \tag{1.3c}$$

For material 2, $z < 0$:

$$H_{2y} = H_{20}e^{ik_{x1}x+ik_{z2}z-i\omega t}, \tag{1.4a}$$

$$E_{2x} = \frac{1}{i\epsilon_0\epsilon_2\omega}\frac{\partial H_{2y}}{\partial z}e^{ik_{x1}x+ik_{z2}z-i\omega t} = \frac{k_{z2}}{\epsilon_0\epsilon_2\omega}H_{20}e^{ik_{x1}x+ik_{z2}z-i\omega t}, \tag{1.4b}$$

$$E_{2z} = -\frac{1}{i\epsilon_0\epsilon_2\omega}\frac{\partial H_{2y}}{\partial x}e^{ik_{x1}x+ik_{z2}z-i\omega t} = -\frac{k_{x2}}{\epsilon_0\epsilon_2\omega}H_{20}e^{ik_{x1}x+ik_{z2}z-i\omega t}. \tag{1.4c}$$

The boundary condition requires following restrictions at the interface when $z = 0$,

$$H_{1y} = H_{2y}, \qquad E_{1x} = E_{2x}, \qquad \epsilon_1 E_{1z} = \epsilon_2 E_{2z}, \tag{1.5}$$

which is:

$$H_{10} = H_{20}, \qquad \frac{k_{z1}}{\epsilon_1} = \frac{k_{z2}}{\epsilon_2}, \qquad k_{x1} = k_{x2}. \tag{1.6}$$

To ensure the attenuation of the surface wave, the z components of the wavevectors k_{z1} and k_{z2} must be imaginary and with different signs ($k_{z1} < 0$ and $k_{z2} > 0$). Therefore, the permittivities of the two materials must have opposite signs. A conductor and a dielectric will satisfy this requirement.

Considering the dispersion relation:[3]

$$c^2(k_{x1}^2 + k_{z1}^2) = \omega^2\epsilon_1, \tag{1.7a}$$

$$c^2(k_{x2}^2 + k_{z2}^2) = \omega^2\epsilon_2, \tag{1.7b}$$

the x component of the wave vector, also well known as the dispersion relation of SPP is obtained:[2]

$$k_{SPP} = k_{x1} = k_{x2} = \frac{\omega}{c}\sqrt{\frac{\epsilon_1\epsilon_2}{\epsilon_1 + \epsilon_2}}, \tag{1.8}$$

and the z components of the wave vectors in each material are derived:

$$k_{z1} = \frac{\omega\epsilon_1}{c}\sqrt{\frac{1}{\epsilon_1 + \epsilon_2}}, \tag{1.9a}$$

$$k_{z2} = \frac{\omega\epsilon_2}{c}\sqrt{\frac{1}{\epsilon_1 + \epsilon_2}}. \tag{1.9b}$$

From eq. (1.3) and eq. (1.4), when the wave vector becomes sufficiently large, SPP will produce an enhancement of the electric field on the molecules near the interface. There are two scenarios that can produce the enhancement.

The first scenario is when $\epsilon_1 + \epsilon_2$ is approaching 0. When applying the Drude model to the conductor,

$$1 - \frac{\omega_p^2}{\omega^2} + \epsilon_2 = 0, \tag{1.10a}$$

$$\epsilon_\infty \left(1 - \frac{\bar{\omega}_p^2}{\omega^2}\right) + \epsilon_2 = 0, \tag{1.10b}$$

the frequency required for the excitation in this case is:[2]

$$\omega = \omega_{sp} = \frac{\omega_p}{\sqrt{1+\epsilon_2}}, \tag{1.11a}$$

$$\omega = \omega_{sp} = \frac{\epsilon_\infty \bar{\omega}_p}{\sqrt{\epsilon_\infty + \epsilon_2}} = \frac{\omega_p}{\sqrt{\epsilon_\infty + \epsilon_2}}. \tag{1.11b}$$

This is the condition when the SPP becomes a stationary wave, i.e., the group velocity of SPP $d\omega/dk$ is 0.

The second situation is when the when ϵ_2 becomes large. The dielectric function of the molecule is given by the spring-mass system (derivation provided in next chapter):

$$\epsilon_2(\omega) = 1 + \frac{nq/m\epsilon_0}{\omega_0^2 - \omega^2 - 2i\omega\Gamma}. \tag{1.12}$$

where ω_0 is the resonance frequency of the molecule, q is the bounded charge of the molecule. In Raman spectroscopy, the bounded charge can represent the electron in a ground-to-excited electronic state transition; In infrared (IR) spectroscopy, it can be a part of the molecule in the vibrational normal mode. m is the effective mass of the bounded charge, and Γ describes the energy dissipation in the motion of the bounded charge. Γ is usually small compared to the resonance frequency ω_0.

When the frequency of the incident light is at the resonance of the molecule, k_{z2} will become massive. Therefore, as described in eq. (1.4b), an enhancement will be addressed on E_{2x}.

Due to the attenuated nature of SPP, the tangential component of the wave vector has a larger value compared to the wave vector itself, i.e., $k_x > k$, it is impossible to excite SPP with propagating light directly, since the Snell's law tell us that the tangential component of the wave vector is continuous, $k_1 \sin\theta_1 = k_2 \sin\theta_2 = k_x$, and the $\sin\theta$ terms are smaller than 1 unless

total internal reflection (TIR) takes place in the interface. The most famous excitation strategy of SPP was based on TIR, provided by Kretschmann-Raether,[7] and Otto[8] independently, as shown in Figure 1.2. Both methods employ the total internal reflection, which creates an evanescent field on the boundary of the substrate. SPP will be excited once the evanescent field reaches the boundary of the conductor and molecule.

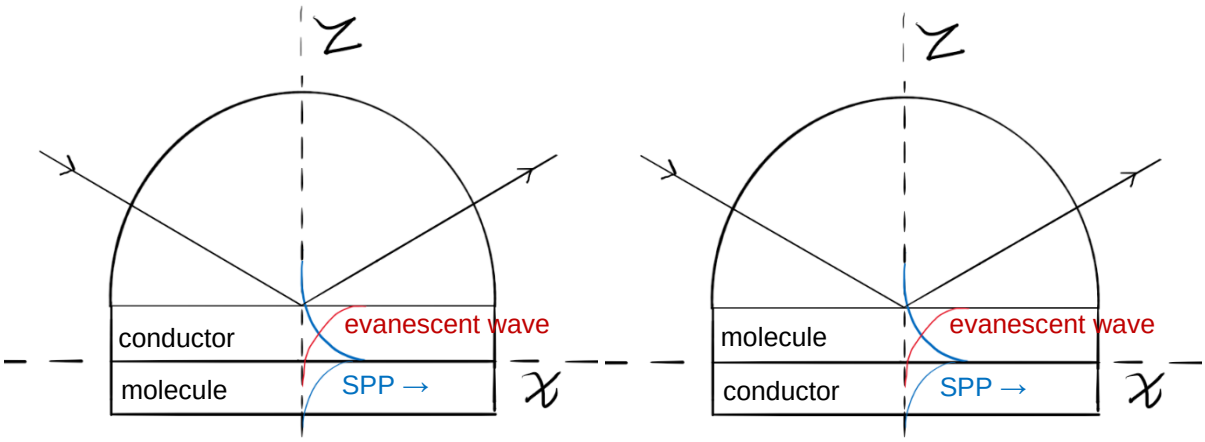

Figure 1.2 Kretschmann configuration (left) and Otto configuration (right)

1.1.3. Localized surface plasmons (LSPs)

A localized surface plasmon is when the geometry of the interface becomes curved and localized in a small region, rather than an infinite plate. When the diameter of the conductor is shorter than the wavelength of the incident light, the retardation effect is negligible, therefore, the external radiation will raise a collective oscillation of the free electrons in the conductor. The most studied geometry is spherical,[9] which refers to the shape of the nanoparticles in the colloidal solution.

The electric field of the sphere is obtained through Laplace equation of the scalar potential by series expansion.

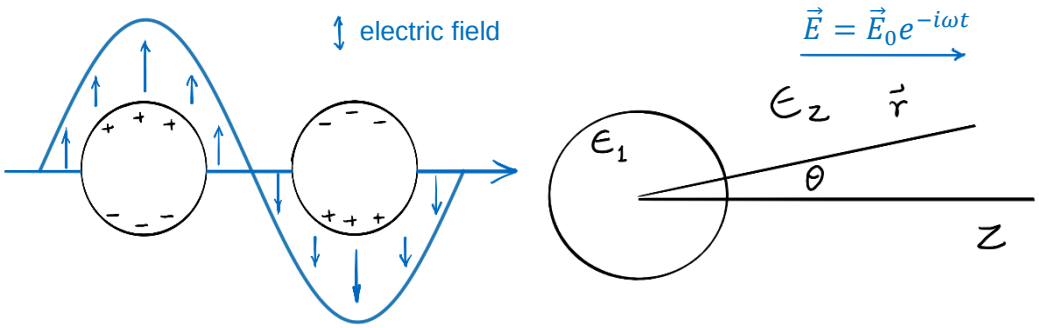

Figure 1.3 Localized surface plasmon

The scalar potential inside and outside the sphere are constructed by series expansion:[3]

$$\phi_{in} = \sum_{l=0}^{\infty} A_l r^l P_l(\cos\theta), \quad (r < a); \tag{1.13a}$$

$$\phi_{out} = -E_0 r\cos\theta + \sum_{l=0}^{\infty} B_l r^{-l-1} P_l(\cos\theta), \qquad (r \geq a). \tag{1.13b}$$

where $P_l(\cos\theta)$ is the Legendre polynomial, a is the radius of the sphere. The boundary condition gives the continuity of the scalar potential and the continuity of the normal component (r direction) of displacement field when at the interface:[3]

$$\phi_{in} = \phi_{out}, \qquad -\epsilon_1 \frac{d\phi_{in}}{dr}\bigg|_{r=a} = -\epsilon_2 \frac{d\phi_{out}}{dr}\bigg|_{r=a}. \tag{1.14}$$

By matching each terms, the potential is obtained:[3]

$$\phi_{in} = -\frac{3\epsilon_2}{\epsilon_1 + 2\epsilon_2} E_0 r\cos\theta, \tag{1.15a}$$

$$\phi_{out} = \frac{\epsilon_1 - \epsilon_2}{\epsilon_1 + 2\epsilon_2}\frac{a^3}{r^2} E_0\cos\theta - E_0 r\cos\theta. \tag{1.15b}$$

And the electric field is given by the negative gradient of the potential:[3]

$$\vec{E}_{in} = \frac{3\epsilon_2}{\epsilon_1 + 2\epsilon_2} E_0\left(\hat{r}\cos\theta - \hat{\theta}\sin\theta\right) = \frac{3\epsilon_2}{\epsilon_1 + 2\epsilon_2} E_0 \hat{z}, \tag{1.16a}$$

$$\vec{E}_{out} = \hat{r}\left(2\frac{\epsilon_1 - \epsilon_2}{\epsilon_1 + 2\epsilon_2}\frac{a^3}{r^3}E_0\cos\theta + E_0\cos\theta\right) + \hat{\theta}\left(\frac{\epsilon_1 - \epsilon_2}{\epsilon_1 + 2\epsilon_2}\frac{a^3}{r^3}E_0\sin\theta - E_0\sin\theta\right)$$

$$= \frac{\epsilon_1 - \epsilon_2}{\epsilon_1 + 2\epsilon_2}\frac{a^3}{r^3}E_0\left(2\hat{r}\cos\theta + \hat{\theta}\sin\theta\right) + E_0\hat{z}. \qquad (1.16b)$$

The electric field enhancement is given at two conditions. The first one is when $\epsilon_1 + 2\epsilon_2$ is approaching 0. In this case,

$$1 - \frac{\omega_p^2}{\omega^2} + 2\epsilon_2 = 0, \qquad (1.17a)$$

$$\epsilon_\infty\left(1 - \frac{\bar{\omega}_p^2}{\omega^2}\right) + 2\epsilon_2 = 0, \qquad (1.17b)$$

the frequency required for the excitation in this case is:[2]

$$\omega = \omega_{lsp} = \frac{\omega_p}{\sqrt{1 + 2\epsilon_2}}, \qquad (1.18a)$$

$$\omega = \omega_{lsp} = \frac{\epsilon_\infty\bar{\omega}_p}{\sqrt{\epsilon_\infty + 2\epsilon_2}} = \frac{\omega_p}{\sqrt{\epsilon_\infty + 2\epsilon_2}}. \qquad (1.18b)$$

In this situation, the conductive electrons encounter a collective oscillation with the external field. This motion is the dipole mode of LSPs because the electric field of the spherical conductor has the same form of an ideal dipole.[9]

The second case is when the incident light is on resonance with the molecule, where the dielectric function of the molecule becomes massive when the damping constant Γ is small compared to the resonance frequency of the molecule ω_0.

Comparing eq. (1.18) to eq. (1.11), the difference of the spherical geometry has an extra factor of 2 in front of the dielectric function of the molecule, ϵ_2, compared with the planar geometry. This geometric factor is linked to the aspect ratio of the nanoparticle. By modifying the geometry of the nanoparticles, the resonance frequency of the plasmon can be tuned. The

enhancement will be maximum when the frequency of the localized surface plasmon matches the molecular resonance frequency $\omega_{lsp} = \omega_0$.

1.2. Application of plasmonic properties to spectroscopic techniques

Infrared (IR) spectroscopy and Raman spectroscopy are the two most important analytical spectroscopic techniques since vibrational frequencies are fingerprints of the analyte. IR spectroscopy and Raman spectroscopy are complementary. The former characterizes dipole active vibrational modes, and the latter depicts quadruple active vibrational modes. Both IR spectroscopy and Raman spectroscopy are used extensively for detection and structural identification of all kinds of chemical and biomolecular materials.[10]

IR and Raman spectroscopy have advantages over fluorescence, which is commonly considered the most sensitive spectroscopic method known. First, IR and Raman obviate the restriction that the analyte must be fluorescent – not merely by expanding the variety of possible analytes, but also simplifying sample preparation for non-fluorescently active molecules as well. Because fluorescent labelling is no longer needed when IR or Raman is used, there is a decrease in the risk of the structural and property changes caused by chemical treatments to attach labels. Second, molecular vibrational information is provided by IR and Raman spectroscopy. This type of specific signal can be crucial for determination of the structure of the analyte. This fingerprint information is missing in fluorescence spectroscopy because of the relaxations of the excited electronic state, which lead to broad emission spectra, often with little or no structural information.

Notwithstanding these advantages, both IR and Raman spectroscopy suffer from low signal compared to fluorescence. The signal-to-noise ratio of IR is smaller than that for

fluorescence as well, because the former has a bright detection background compared to a dark background for latter. Although Raman spectroscopy has a similar dark background, the scattering mechanism restricts the cross-section to at least 10^8 times smaller than fluorescence (assuming a high fluorescence quantum yield of 0.5 or greater).[11] As a consequence, the application of IR and Raman spectroscopy for analytical detection and sensing is limited. Despite these limitations Raman spectroscopy has found many applications, including microscope,[12] optical fiber detection,[13] light detection and ranging (LIDAR) and so on.[14] IR is an excellent method for solutions that have relatively high concentration of analytes.[10] To achieve a wider application for IR and Raman spectroscopy, the enhancement of the signal for both techniques is desirable.

1.2.1. Surface enhanced infrared absorption (SEIRA)

SEIRA was discovered after surface enhanced Raman spectroscopy (SERS), as an offshoot of surface enhancement applied in IR spectroscopy. Comparing to SERS, SEIRA was believed to have small enhancement factors at an early stage, and therefore it was less attractive before 1990s when new sample preparations were proposed to enhance the signal further.[15]

SEIRA was first performed by Hartstein *et al.* in 1980.[16] They noticed the attenuated total reflectance IR (ATR-IR) signal of benzoic acid and its derivative compounds were enhanced when attached onto vacuum-evaporated thin silver layers. An enhancement of 20 was claimed with a 6 nm silver layer, compared to the IR signal without a silver layer. Because the polarization of the incident light did not create a significant change in the enhancement, the authors suggested the origin of the enhancement of benzoic acid may not be SPP.

After the first discovery, Hatta *et al.* proposed the enhancement mechanism may be different for different molecules.[17] In their work, the ATR-IR signal of p-nitrobenzoic acid and stearic acid on thin silver layer were obtained. The Kretschmann configuration was applied to establish the ATR and SPP condition. The result shows the enhancement signal of stearic acid only appears under p-polarized light; the signal generated from s-polarized light is indistinguishable from the noise background. This argued that the enhancement is indeed related to SPP. At the same time, the spectra of p-nitrobenzoic acid showed the p-polarized light led to a slightly higher absorption than s-polarized light by a factor of 1.2 – 1.4. The authors pointed out the inconsistency of the two results implied the enhancement mechanism were different.

The first type of enhancement was proved to be electromagnetic (EM) enhancement form SPP, which was supported by more evidence from the same research lab.[18] The authors showed the intensity remained unchanged if the thickness of the analyte had been increased. This suggested the enhancement appears only in a few layers near the surface, which matched the attenuative nature of SPP.

The second type of enhancement was sustained by charge transfer (CT), as a chemical enhancement mechanism. After the proposal of charge transfer as an enhancement mechanism of SERS,[19,20] the same idea was applied to SEIRA. Devlin *et al.* advocated the charge transfer leads to an enhancement of totally symmetric modes of the analytes adsorbed on metal surface.[21] Dumas *et al.*[22] showed more evidence that charge transfer would lead to an enhancement. In their experiment, temperature control was used to determine the chemisorption and physisorption of CO on a silver film. They observed an enhancement factor of 1.4 on IR spectroscopy of CO chemisorbed on a silver film, which was achieved under 40 K, and the band disappeared when temperature increased to 80 K, suggesting the adsorbates had changed to physisorption. This

phenomenon was supposed as a charge transfer effect by Otto.[23] Wadayama[24] showed the enhanced absorption band of SCN^- on Au films at 2115 cm^{-1} blue shifted when the potential of the Au film increases, which cannot be explained by EM enhancement, which suggests the intensity of the band should increase when the potential of Au raises, because SCN^- is an anion and because the position of the band would not shift if no chemical interaction existed. This evidence supported the CT is a valid mechanism of the enhancement.

After the basis of SEIRA has been established on Ag and Au, the studies on SEIRA have been expanded. On the one hand, it has been studied on various types of conductors, including metals: Pt,[25] Pd,[26] Ru,[27,28] and Fe;[29,30] semiconductors: Si,[31–33] Ge,[34,35] Sn,[36] GaN,[37,38] GaAs,[39] InAs;[40,41] metal oxide semiconductors: zinc oxide,[42,43] indium tin oxide (ITO),[44] and cadmium oxide.[45,46]; and graphene.[47,48]

On the other hand, the geometry of the conductor has evolved. Starting from the metal film, roughened metal film, immobilized metal nanoparticles,[49] and resonant nanoantennas[50] have been employed to achieve higher and higher enhancement factors. With the resonant nanoantenna, enhancement factor of up to 2.2×10^6 has been estimated.[51] The work was performed by Srajer *et al.*, where the SEIRA signal of dodecanethiol monolayer on gold film was compared to the ATR-IR signal of a dodecanethiol solution. When the absorbances of both signals were equal, the authors took the ratio of the estimated amount of the molecules in each case as the enhancement factor. However, this number is not convincing. It is well known that the structures of a long carbon chain presents linear in solid state, but twisted and folded in liquid states due to the low-frequency internal rotations.[52] Orientation and distance of the molecule from the surface are also very difficult to control. Other large enhancement factors ($> 10^3$) reported recently are based on the assumption that all the molecules are on the “hot spots”

(where the enhancement reaching the maxima).[53–56] This hot spot assumption is almost impossible to prove, but it is used frequently to justify large enhancement factors in SEIRA and SERS.

Despite the reported "high" enhancement factors of SEIRA, the mechanism of the enhancement has not been fully understood. The updated modeling theories are based on analogies. These models, including Fano resonance,[57] coupled harmonic oscillators,[58,59] and temporal coupled mode theory (TCMT)[60] as an extension of coupled harmonic oscillators, are tools to generate fits for the absorption lines, therefore only parameters for individual experiments can be described, but understanding the general interaction between the plasmon and the molecular excitation, which is the key to the enhancement mechanism is impracticable.[61] A comprehensive model which can compare chemical and electromagnetic mechanisms directly is required.

1.2.2. Surface enhanced Raman spectroscopy (SERS)

Surface enhanced Raman spectroscopy (SERS) has been developed as a highly sensitive technology to overcome the poor signal-to-noise ratio of non-resonance Raman scattering, and the fluorescence interference problem in both non-resonance Raman and resonance Raman spectroscopy due to the surface enhancing and surface fluorescence quenching.[62]

Compared to fluorescence spectroscopy, as a Raman spectroscopic technique, SERS shows the fingerprint vibrational structures of the molecule and labelling free as discussed in the previous section. In addition, the non-resonance SERS would avoid photobleaching, photodamage and thermal damage and other degradation caused by laser excitation in

fluorescence spectroscopy. These benefits from Raman spectroscopy stimulated the development of SERS with higher enhancement factors.

SERS was first discovered in 1970s. The first studied case was pyridine on silver electrode. Fleischmann *et al.*, performed cyclic potential sweeping to the silver electrode surface and found that high surface area of the electrode is required for a low limit of detection.[63] The surface-area hypothesis of SERS was disputed by van Duyne[64] and Creighton,[65] who independently discovered an enhancement factor 10^5 to 10^6 of the Raman signal of pyridine on a silver electrode. Since then, a set of molecules and metal surfaces including Ag,[11,63–66] Au,[67–70] Cu,[71,72] Pt,[73,74] Rh,[75–79] Ru,[76] Al,[80] metal oxides[81–84] and graphene[85] have been studied. Over time enhancement factors of SERS signals have increased as nanoparticles or surfaces were designed to maximize local fields. While it is clear that extremely sensitivity of detection can be achieved when resonance Raman and SERS are combined,[86] many of these claims of extreme enhancement factors have relied on assumptions regarding the number and distribution of molecules on surfaces or in solution. Single molecule SERS detection was first claimed in 1997[11,66] and has been pursued by scientists for decades. There is still no convincing theory for this effect. When combined with potential experimental artefacts and suppositions required to define the "single molecule", there is room for debate.

Single-molecule SERS (SMSERS) was aimed at the identification and dynamic studies of single molecules. The pioneer studies of SMSERS were conducted in 1997 by Nie *et al.*,[11] and Kneipp *et al.*[66] In the former work, detection of the Raman scattering signal of a designated single nanoparticle, led to the claim of an enhancement factor of 10^{15}. The assumed count of 0.1 to 1 Rhodamine 6G (R6G) molecules adsorbed on each silver nanoparticles by controlling the concentration of R6G and the nanoparticle colloid. After the nanoparticles were immobilized on

a polylysine-coated glass surface, the Raman scattering measurement was performed. The result showed that one out of 10^7 adsorbed R6G could show efficient signal enhancement imaging with evanescent-wave microscopy, while others remain silent. The authors pointed out that compared to the fluorescence signal using the same procedure with the absence of the silver nanoparticle, an active Raman signal is 10 times larger than fluorescence signal. Because the fluorescence cross-section of a fluorescent dye is typically 10^{-20} m^2, which is 10^{14} larger than a Raman cross-section of the same molecule, the enhancement factor was claimed at 10^{15}. This experiment provides us with a first example of assumptions built into the claims. The authors assumed that the distribution of the molecules was random, *i.e.*, that the molecules did not aggregate or have specific strong chemical interactions with the silver nanoparticles. No evidence was presented. They also assumed a ratio between the Raman and fluorescence cross sections for a generic molecule, not taking resonance effects or other specific attributes into account.

In the study by Kneipp *et al.*,[66] crystal violet molecule was adsorbed on the silver nanoparticle colloid. The enhancement factor 10^{14} was obtained from a comparison of the Raman signal between a 3 M methanol solution and a 3.3×10^{-14} M crystal violet molecule solution.

The bi-analyte method performed by Le Ru *et al.*,[87] reveals more evidence of single molecule signals. When two analytes with distinguishable Raman signals are presented at a high concentration in the metal colloidal solution, the Raman signal shows a mixture of the two spectra. After the concentration reduces to the single-molecule level, the Raman signal returns either one of the molecules, instead of the mixture.

The results from SMSERS seem encouraging, however its application as a probe for single molecule is still elusive based on the limitation of this technique. Fluorescence has a cross-section 10^8 larger compared to that of Raman scattering, but single-molecule fluorescence

is an extremely difficult technique and relies on statistical distributions.[88] Even if all assumptions built into the claim of SMSERS are correct, there are numerous obstacles to implementation. First, the Raman signal from SMSERS is artificial, *i.e.*, the analytes are prepared from a macroscopic ensemble to ensure a positive signal, it could be described as trace, but not as low as a single molecule in a cup of water. Second, the studies to date are measured under resonance conditions, *i.e.*, they are surface-enhanced resonance Raman (SERRS) scattering. On the one hand, the resonance effect can give rise to a larger signal with a factor of 10^6 at least compared to non-resonance Raman signals.[89] As an example, Pettinger *et al.* calculated the Raman cross-section based on their experiment for R6G in Ag colloid is 3×10^{10} times larger than that for water molecules in the same environment.[90,91] On the other hand, photobleaching and photodamage are inevitable for resonance Raman spectroscopy. The metallic surface could participate in photocatalysis of the degradation of the analyte. Lastly, the intensity of SERS signal is time and space dependent. This property relates to the migration of the adsorbed spot of the molecule,[11] and more notably, the rearrangement of surface atoms on the conductive nanoparticle.[92] The statistical data analysis method has not yet been well established.[93–96] Therefore, although SMSERS may result from the Raman signal of single molecule, understanding the mechanism of SERS via SMSERS experiment is still challenging. There are still experimental and theoretical aspects that call the interpretation of a single-molecule spectroscopy into question. Theoretical modelling is essential for understanding the mechanism of the enhancement observed in SERS.

1.3. Theories and models of SEIRA and SERS in literature

The IR signal is based on absorption. The absorbance of the molecule without the presence of the conductor is given by:

$$A = -\lg\frac{I}{I_{loc}} = \epsilon_{ext} lc, \tag{1.19}$$

where I_{loc} is the incident light on the molecule, ϵ_{ext} is the molar extinction coefficient, which is described by the cross-section (see eq. (1.23a)); l is the length of the light path; c is the concentration of the analyte. I_{loc} is related to the local electric field $E_{loc}$of the molecule in a nonmagnetic material:

$$I_{loc} = \frac{1}{2}\epsilon_0 c_0 n|E_{loc}|^2, \tag{1.20}$$

where c_0 is the speed of light in vacuum, n is the refractive index of the background material, here $n = 1$ in a microscopic view.

However, in the experiment, we measure the reflectance R or transmittance T as the signal:

$$R \; or \; T = \frac{I}{I_0}, \tag{1.21}$$

where I_0 is the incident light from the light source, which is different from I_{loc} if the conductor exists. If the local field is enhanced by the conductor, the measured absorbance will be different from eq. (1.19):

$$A' = -\lg\frac{I}{I_0}. \tag{1.22}$$

The Raman scattering signal is based on the intensity of Raman scattered light, which is described by:

$$I_{scattered} = I_{loc}\frac{d\sigma_{sca}}{d\Omega}, \tag{1.23}$$

where σ is the cross section, which relates to the polarizability. The absorption cross section is linked to the extinction coefficient, which is proportional to the imaginary part of the polarizability:[97]

$$\sigma_{abs} = \frac{\epsilon_{ext}}{N_A} = k_0 \mathrm{Im}(\alpha), \tag{1.24a}$$

The scattering cross section is proportional to the norm squared of the polarizability:[97]

$$\sigma_{sca} = \frac{k_0^4}{6\pi} |\alpha|^2. \tag{1.24b}$$

In the literature, the mechanism of the enhancement is considered from two different aspects. One is chemical enhancement, suggesting a polarizability increment by a chemical interaction, *e.g.*, charge transfer between the surface and the molecule,[98–105] and geometry distortion of the molecule which has been seldom mentioned in theoretical treatments of SEIRA and SERS. The relationship between these considerations and resonance Raman spectroscopy deserves special attention. The chemical mechanism involves a bond or chemical interaction between a molecule and a conductor. In essence, the molecule becomes part of the conductor. In this case, the excitation of plasmonic oscillations may simultaneously result in molecular displacements in the excited state, which leads to resonance enhancement. Simply put, resonance Raman enhancement is a special case of chemical enhancement mechanisms. One should not lose sight of the fact that the resonance effect in Raman can give rise to enhancements of 10^6. In the literature, the chemical enhancement is linked to the polarizability change.

The other one is EM enhancement, suggesting an enhancement to the local electric field at the position of the molecule by the surface plasmon resonance of the nanoparticle.

However, this definition may be out of date. On the one hand, a chemical interaction not only affects the polarizability, but also can generate a frequency shift to the local field, and

therefore tune the incident intensity. On the other hand, an EM interaction is able to change the polarizability, especially when the anisotropic effect is considerable.

Nevertheless, the established theories and methods will be discussed in the rest of this section.

1.3.1. Electromagnetic (EM) enhancement and the enhancement factor

Kerker and co-workers defined the basics of EM enhancement of SERS.[101] They considered the Raman scattering as two steps. The first step is absorption, and the second step is inelastic emission. Therefore, IR and Raman share the first step.

In their description of absorption, the local field of the molecule (at position r') is given by a combination of the external field E_0 and the elastically scattered fields E_s from the conductor:

$$E_{loc}(\omega_0, r') = E_0(\omega_0, r') + E_s(\omega_0, r'). \quad (1.25)$$

From eq. (1.25), we can conclude that for IR signal, the enhancement is given by the local field compared to that without the conductor. If the enhancement is large, the enhancement factor on the local field is approximate to the square of the electric field on the surface:

$$I_{loc} \propto |E_{loc}(\omega_0, r')|^2 \approx |E_s(\omega_0, r')|^2. \quad (1.26)$$

However, it is improper to say the IR absorbance enhancement factor is proportional to $|E_s(\omega_0, r')|^2$, because the absorbance signal is calculated from the light source, which is not I_{loc} due to the presence of the conductor. This complicates the EM mechanism for SEIRA. This may be the reason that the models for SEIRA are based on fitting and numerical calculations, which will be introduced after this section.

The second step of Kerker's work is the inelastic emission with the shifted frequency ω_s. Assuming the detector is at the location r'', the detected scattered field is given by:

$$E_s(\omega_s, r', r'') = E_{s,molecule}(\omega_s, r', r'') + E_{s,conductor}(\omega_s, r', r''). \quad (1.27)$$

where the first term on the right-hand side describes the Raman shifted scattering from the molecule, and the second term is the scattering from the conductor. The detected intensity:

$$I = \frac{1}{2}\epsilon_0 c_0 |E_{Raman}(\omega_s, r', r'')|^2. \quad (1.28)$$

The enhancement factor of SERS should be the ratio of the intensity in eq. (1.28) with and without the conductive nanoparticles.

Note that, the Raman scattered light from the molecule is related to the local field of the molecule by eq. (1.23):

$$\left|E_{s,molecule}(\omega_s, r', r'')\right|^2 = |E_{loc}(\omega_0, r')|^2 \frac{d\sigma}{d\Omega}. \quad (1.29)$$

This model is rigorous but challenging. Despite the interaction between the molecules, when the surface of the nanoparticle is arbitrary, the local field will be hard to solve.

Barber et al. proposed a simpler model from their experimental results.[106,107] Their model defines an intensity enhancement factor on the molecule, L^2, which is given by:

$$L^2(\omega) = \left|\frac{< E_{loc,with\ conductor}(\omega) >}{E_{loc,without\ conductor}(\omega)}\right|^2, \quad (1.30)$$

where $< E_{loc,with\ conductor} >$ is the averaged local field on the surface of the nanoparticle. They proposed the enhancement factor of SERS is:

$$EF = L^2(\omega_0) L^2(\omega_s). \quad (1.31)$$

The interpretation of eq. (1.31) is linked back to eq. (1.29), where the intensity of Raman scattered light of the molecule is proportional to the incident light feeling by the molecule (I_{loc}).

In the literature, eq. (1.31) is often "approximated" as $EF = L^4(\omega_0)$ by pretending $L^2(\omega_0)$ and $L^2(\omega_s)$ are equal, because the plasmon band is usually larger than the Stokes shift.[108] Regardless of the fact that eq. (1.31) does not have a physical derivation, $L^2(\omega_0)$ and $L^2(\omega_s)$ are not equal, at least in the case of resonance Raman scattering. When the incident light is on resonance with the molecule, $L^2(\omega_0)$ will be sufficiently large, but $L^2(\omega_s)$ is limited.[109] Unfortunately, all SMSERS experiments are based on resonance Raman scattering, the statement that enhancement is proportional to the fourth power of the local field is problematic.

1.3.2. Fano resonance

Fano resonance involves the competition of the elastic and inelastic scattering. The combination of the two processes result in an asymmetric line shape, which was elucidated in 1961 by Fano:[110]

$$\sigma \propto \frac{\left(\frac{q\Gamma}{2} + \omega - \omega_0\right)^2}{(\omega - \omega_0)^2 + \frac{\Gamma^2}{4}}, \tag{1.32}$$

where Γ describe the half band width and ω_0 is the resonance frequency of the excitation of the scattering, q is called Fano-parameter, describing the asymmetry.

Fano resonance has been applied to explain the asymmetric line shape observed in SEIRA,[111,112] by fitting the observed line shape with eq. (1.32). However, the asymmetric line shape in SEIRA has a trivial and fundamental explanation, which is nothing more than a consequence of Snell's law when the molecule absorbs the surface wave. The details will be introduced in Chapter 3.

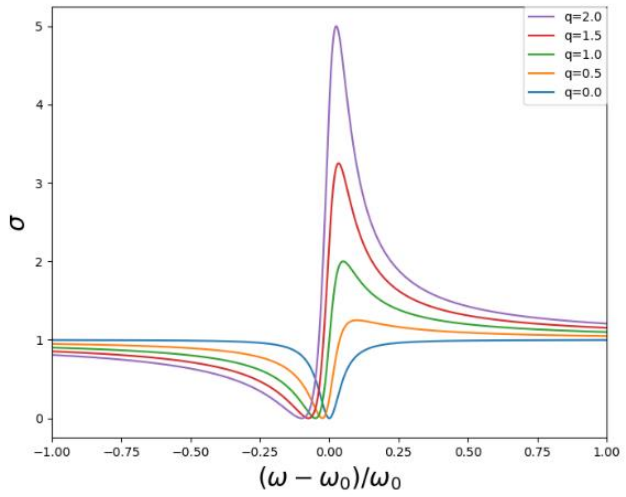

Figure 1.4 Asymmetric Fano line shapes with different q

1.3.3. Coupled harmonic oscillators

The coupled harmonic oscillator model can be adapted to represent two harmonic oscillators, the plasmon and molecule, respectively, with a connecting spring as the interaction between the molecule and the plasmon.[58]

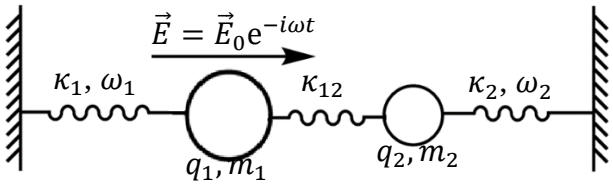

Figure 1.5 Coupled harmonic oscillators: oscillator 1 represents the plasmon, and oscillator 2 represents the molecule.

By solving the equation of motion, the absorbed power by the plasmon can be solved, in terms of the parameters shown in Figure 1.5. However, the insight from the model is limited. First and foremost, the directions of the two dipoles are restricted to the direction perpendicular to the interface. The usual direction for plasmonic interactions parallel to the surface is not accounted for. Second, the interaction term κ_{12} is an input parameter, which can be obtained only by fitting to the experimental data.

1.3.4. Numerical methods for calculating the EM enhancement

Discrete dipole approximation (DDA)[113] and finite difference time-domain (FDTD)[114] are two important numerical methods to calculate the EM enhancement factor. Both methods divide the space into cubic grids but solve the electric field on the surface of the conductor in different ways.

In the DDA method, the electric field is calculated from the dipole density. By treating each cubic grid on the conductor as a dipole with a polarizability derived from the dielectric function, the local field at each position can be simulated as the incident field plus the sum of the retarded dipole fields.

In the FDTD method, each grid is assigned a dielectric function. If the grid is in the conductor, the dielectric function is described with Drude model (a damped version of eq. (1.2b)),

$$\epsilon(\omega) = \epsilon_\infty - \frac{\omega_p^2}{\omega^2 + i\omega\gamma}. \tag{1.33}$$

Otherwise, the dielectric function is ϵ_0. The electric field will be from Maxwell's equations with an iterative algorithm.

After obtaining the electric field, the enhancement factor can be calculated in the space.

1.4. Conclusion and outlook

Since the first discovery of SERS in 1974, the mechanism of the surface enhanced IR and Raman signals has been studied for approximately five decades.[63] The electromagnetic enhancement can be estimated from first principal calculations, while the chemical enhancement are focused on charge transfer.[115–118] Although charge transfer has been proposed as the origin of the chemical enhancement,[119,120] the molecular geometry distortion, and the resulting

spectroscopic frequency shift have not yet been considered by theoreticians. The proposed electromagnetic mechanisms listed above are based on isotropic dielectric functions, *i.e.*, the dielectric function is scalar rather than tensorial.[58,101,106,107,113,114]

On the other hand, as discussed at section 1.3, both the EM and chemical enhancement can affect the polarizability, and both can manipulate the local field. In addition, resonance effects can arise due to molecular spectra as well as coupling of molecular vibrational modes to the surface due to bonding. If this is the case, then the molecule becomes part of the surface and molecular modes can be enhanced as surface plasmon scattering becomes large. The definition of EM and chemical enhancement should be reconsidered. The key to understanding the mechanism is the interaction between the molecule and the plasmon. This requires a comprehensive model which can describe both the EM enhancement and chemical enhancement.

The nonlinear bond model inspired us to treat the polarizability of the molecule as a coupling analogous to a second harmonic component explained by Aspnes.[121] This enabled us to model the excitation profile of the molecule based on its polarizability. In the following chapters, we will introduce our classical correlation model as a potential comprehensive model which can take both EM and chemical mechanism into consideration.

CHAPTER 2. Classical Correlation Model of Resonance Raman Spectroscopy

Abstract

A classical correlation model (CCM), based on forces instead of potentials, is developed and applied to resonance Raman scattering to provide a foundation for further advances in understanding the effects of fields and vibronic perturbations on the optical properties of materials by a simple, yet versatile, description. The model consists of a charge connected by a classical spring to a surface, driven by an external electric field. The spring represents the charge cloud of the electrons and the transition strength, and the surface represents the nucleus or molecule. Molecular vibrations are assumed to be many-body effects that change the configuration and hence modify the spring constant directly, as opposed to all previous classical models of Raman scattering, opposed to anisotropic bond model (ABM) of nonlinear optics, by adding anharmonic terms to the potential. The resulting expression agrees exactly with quantum mechanical models of resonance Raman scattering in the limit of weak electron-phonon coupling, agrees well when the coupling becomes strong. The result is a classical derivation of Kramers-Heisenberg-Dirac scattering theory. We show that the difference between classical and quantum approaches lies only in the interpretation of the pre-factor. In particular, the Raman excitation profile shows excellent agreement with all other methods of calculation. By comparing complementary classical and quantum solutions of the same complex system, understanding of both is enhanced.

2.1. Introduction

Models of spectroscopy based on classical electromagnetic theory provide analyses that are analytic, simple, and yet surprisingly accurate.[121] As an example, the application of an

anisotropic bond model (ABM) to second-harmonic generation provided crucial insight that identified the relevant parameters of the system in a way that tensor formulations and quantum theory had failed to do. [122,123] The basic physical idea is to reduce the system to a charge connected by a Hooke's-Law restoring force (the bond) to a fictitious immobile object (the nucleus or molecule) and driven by an oscillating electric field (light). The problem is then solved using forces, as in classical Newtonian mechanics, rather than energies, as in quantum mechanics. The savings in complexity is easily demonstrated by comparing the classical (Newton's Second Law) and quantum (Schrödinger's Equation) solutions for the new equilibrium position of the spring-mass configuration when a constant force is applied to the mass. More important, by comparing these complementary solutions, we achieve a better understanding of both perspectives.

Resonant Raman spectroscopy is an appropriate subject for this type of analysis. But is it needed? On the one hand, resonant Raman spectroscopy of Franck-Condon-allowed transitions is understood at all levels of quantum theory from sum-over-states[124,125] to the time-correlator formalism.[126–128] On the other hand, these successful theories have only been applied to Franck-Condon-active modes. There is still no closed form expression that includes vibronic processes involving intrastate Herzberg-Teller coupling for non-totally symmetric distortions of the molecule, i.e., the vibronic coupling mechanism.[129–132] Even with specific knowledge of excited state coupling, application to vibronic modes is limited to cases where we have specific knowledge of which excited states may couple to a transition by virtue of the non-totally-symmetric distortions of the molecular geometry. While the present study does not explore this question further, it is worth noting that new methods may open avenues to yet unsolved issues. The current quantum mechanical solution of the resonant Raman problem based on second order

time-dependent perturbation theory is not readily generalized when a time-dependent electric field is included in the hamiltonian.

In addition, electromagnetic theories are used routinely in an ad-hoc fashion to explain surface-enhanced Raman scattering (SERS). The SERS challenge has resulted in 50 years of theory that still has fundamental gaps. Specifically, there remains a profound disagreement about the extent to which the observed enhancement arises from chemical versus electromagnetic effects.[109,133] Nor has the role of enhancement in the first and second stages of scattering (i.e. the incident and scattered wave) been resolved by a consistent theory.

Here, we explore the possibility of treating resonant Raman spectroscopy by a classical theory that is compatible with the same electromagnetic approaches used to calculate SERS effects. We believe that a demonstration of the success of a classical approach for the Raman cross-section itself would stimulate the development of a similarly direct method for considering the role played by plasmonic fields external to the molecule.

Classical models of Raman spectroscopy presented in textbooks introduce the vibrational frequency at the level of polarizability. Such an approach implies that one already knows the polarizability, which is usually calculated based on the quantum-mechanical Kramers-Heisenberg-Dirac formalism. Thus, with respect to the issue of applying an external or plasmonic field to a molecule, this method may provide insight concerning the first and second stage of Raman enhancement, but still no prescription for how to include the applied electric field to the Hamiltonian. To develop a classical model compatible with externally applied electric fields, one must begin by developing a theory equivalent to the ABM for resonant Raman scattering and demonstrating that it can account for observed Raman excitation profiles (REPs). These are the two purposes of this paper. By introducing the term $\Delta\kappa \cos \omega_v t$ into the

electronic force constant, we reduce the complex many-body problem to a model where an effective single-electron oscillator is coupled to a collective vibrational motion. We therefore term our approach the classical correlation model (CCM). The Raman cross-section derived from the CCM agrees with that obtained from the Kramers-Heisenberg-Dirac formula.

2.2. Theory

2.2.1. Overview

Forces are the gradients of potentials. Hence, force and energy approaches are obviously related. In some cases, they only represent different ways of obtaining the same solution, as for example the constant-force problem mentioned in the Introduction. In the present context the potential is:

$$U(r) = U_0 + \frac{1}{2}\kappa(r - r_0)^2, \tag{2.1}$$

where U_0 is the reference potential, κ is the curvature (force constant), r is the location of the particle, and r_0 is its equilibrium position. If κ is independent of r, the usual assumption, this is the standard one-dimensional parabolic well, who's classical and quantum-mechanical solutions are well known.

Specifically, the restoring-force contribution to the classical equation of motion of the particle is:

$$F = m\frac{d^2r}{dt^2} = -\frac{dU}{dr} = -\kappa(r - r_0). \tag{2.2}$$

Thus U_0, even if a function of time, contributes nothing. If the particle has charge q and is located in a time-dependent electric field $\vec{E} = \hat{r}E_0\mathrm{e}^{-i\omega t}$, a new force term $qE_0\mathrm{e}^{-i\omega t}$ is added. In the absence of further perturbations $r = r(t)$ can be written

$$r(t) = r_0 + \Delta r_E e^{-i\omega t}. \qquad (2.3a)$$

When the equation of motion is solved, the result is a polarizability $p = q\Delta r_E = \alpha E_0$.

Changes of configuration will cause changes in the potential and therefore the restoring force. A phonon can be expected to affect both the shape and location of the minimum of the potential well. Considering the reference location first, if these changes occur at a vibrational frequency ω_v and to first order the reference location of the particle changes from r_0 to $r_0 + \Delta r_v \cos(\omega_v t + \theta_0)$, then from the structure of eq. (2.2) a new term is added to $r(t)$:

$$r(t) = r_0 + \Delta r_E e^{-i\omega t} + \Delta r_v \cos(\omega_v t + \theta_0). \qquad (2.3b)$$

θ_0 is a phase factor included here for generality, although it is not used in the following. Equation (2.3b) is consistent with Born-Oppenheimer approximation in quantum mechanics, where the motion of the electron and the nucleus are separated. From the structure of eq. (2.2), $\Delta r_v \cos(\omega_v t)$ in $r(t)$ combined with κ generates a term at frequency $\omega = \omega_v$. It can be ignored, because the frequency is outside the range of interest for resonant Raman scattering. In a two-body system we can stop here; there is no frequency mixing.

However, in a many-body system, any modification of the configuration can be expected to modify the shape of the well in addition to the location of its minimum. Hence κ is expected to change as well. This can be a change of curvature, or shape, or both. Taking curvature first, this is equivalent to replacing κ with

$$\kappa(t) = \kappa_0 + \Delta\kappa \cos(\omega_v t + \theta_\kappa). \qquad (2.4)$$

The second term is the electronic force constant, which is correlated with the vibrational frequency ω_v that describes the interaction between the electron and the many-body molecule.

From eq. (2.2), the interaction between $\Delta\kappa \cos(\omega_v t)$ and $\Delta r_E e^{-i\omega t}$ generates sideband harmonics $\omega \pm \omega_v$, which is what we expect in the Raman excitation profile (REP). This

contribution is equivalent to the Kramers-Heisenberg-Dirac approach in quantum mechanics and is the term of primary interest in the remainder of the paper.

However, the actual situation is more complicated. If the shape changes, then $\kappa \rightarrow \kappa(r)$, generating an additional term in eq. (2.2):

$$F = -\kappa(r - r_0) - \frac{1}{2}\frac{d\kappa(r)}{dr}(r - r_0)^2. \tag{2.5}$$

With $r(t)$ given by eq. (2.3b), the squaring operation mixes $e^{-i\omega t}$ with itself, generating $e^{-2i\omega t}$ and higher harmonics. This is the basis of the classical ABM treatment of nonlinear optics. In the present context the squaring operation also mixes Δr_E and Δr_v, which with the leading term for κ in eq. (2.4), generates Raman sideband harmonics at $\omega \pm \omega_v$. These harmonics are indistinguishable from those generated by $\kappa(t)$, and because they are generated by deviations from parabolicity, would be extremely difficult to calculate from a quantum-mechanics perspective.

In the remainder of the work, we recognize that this contribution exists, but consider it to be part of $\Delta\kappa$, since any attempt to separate curvature and shape would take us well beyond our present scope. Appendix 1 provides additional details. These two contributions arise from the charge cloud of the electrons, the strength of the transition, and the locations of the nuclei within the molecule, in short, all the many-body correlations of the system. Therefore, the model is termed the classical correlation model, or CCM.

The crucial test of the CCM is whether it has the needed accuracy to allow its predictions to be compared to the calculated REPs of quantum models. The REP is the "spectrum" of a Raman process in terms of the excitation wavelength while monitoring a given Raman shift (i.e., Raman-active vibrational mode). Experimentally, a REP is obtained by measuring the intensity of a particular Raman shift for a range of laser excitation wavelengths. We take as our theoretical

example a transition with a wave number of 20,000 cm^{-1} (500 nm) and a vibrational mode of 1000 cm^{-1}. The scattering power is related to the square of the polarizability. Thus we can calculate resonant-Raman cross sections from both classical and quantum theories to show that the REP predicted by the CCM is the same as that predicted by quantum mechanics. Finally, we show that CCM Raman polarizability can also be obtained by taking the derivative of the Lorentz polarizability with respect to model vibration-mode coordinates. This is required if this method is to be consistent with other theoretical approaches. The classical model passes all tests.

2.2.2. The Lorentz polarizability and the Raleigh scattering cross section

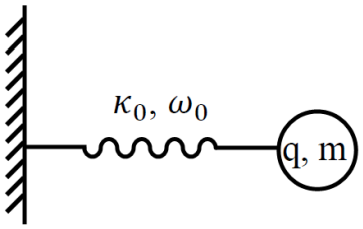

Figure 2.1 Spring-mass system.

The basic configuration is shown in Figure 2.1. The particle (usually an electron) has a mass *m* and charge *q* and is bound to an immovable object (the nucleus in a molecule or metal) by a spring (that describes the interaction between the electron and the nuclei) with a linear (Hooke's-Law) force constant κ. To represent energy loss, viscous friction described by a parameter Γ is also assumed to be present. By Newton's Second Law, the equation of motion is therefore:

$$\vec{F} = m\frac{d^2\vec{r}(t)}{dt^2} = -2m\Gamma\frac{d\vec{r}(t)}{dt} - \kappa_0(\vec{r} - \vec{r}_0). \tag{2.6}$$

If the particle is set in motion, it executes a decaying oscillation about its equilibrium position $\vec{r}_0$ at a complex frequency, ω, or

$$\vec{r}(t) = \vec{r}_0 + \Delta\vec{r}_0 e^{-i\omega t}, \tag{2.7a}$$

and the equation of motion reduces to

$$-m\omega^2 \Delta\vec{r}_0 e^{-i\omega t} = 2im\omega\Gamma\Delta\vec{r}_0 e^{-i\omega t} - \kappa_0 \Delta\vec{r}_0 e^{-i\omega t}, \tag{2.7b}$$

where $\kappa_0 = m\omega_0^2$. Solving eq. (2.7b) we obtain

$$\omega = -i\Gamma \pm \sqrt{\omega_0^2 - \Gamma^2} \approx -i\Gamma \pm \omega_0, \tag{2.8}$$

where $\omega_0 = \sqrt{\kappa_0/m}$ is the native resonant frequency of the system in the absence of friction, and κ_0 is an electronic force constant in the sense of the Lorentz polarizability. In the following, in many cases we consider $\omega_0^2 \gg \Gamma^2$ and treat Γ only to first order.

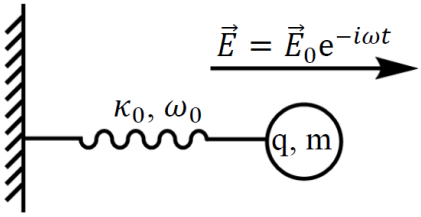

Figure 2.2 Spring-mass system with a time-harmonic driving force.

Now let the particle be driven by an incident electric field $\vec{E} = \vec{E}_0 e^{-i\omega t}$, as shown in Figure 2.2. With the electric field added, the equation of motion is now:

$$\vec{F} = m\frac{d^2\vec{r}(t)}{dt^2} = q\vec{E}_o e^{-i\omega t} - 2m\Gamma\frac{d\vec{r}(t)}{dt} - \kappa_0(\vec{r} - \vec{r}_0), \tag{2.9a}$$

which reduces to:

$$-m\omega^2 \Delta\vec{r}_0 e^{-i\omega t} = q\vec{E}_o e^{-i\omega t} + 2im\omega\Gamma\Delta\vec{r}_0 e^{-i\omega t} - \kappa_0 \Delta\vec{r}_0 e^{-i\omega t}. \tag{2.9b}$$

Solving eq. (2.9b) we obtain:

$$\Delta\vec{r}_0 = \frac{q\vec{E}_o}{m(\omega_0^2 - \omega^2) - 2im\omega\Gamma}. \tag{2.10}$$

The dipole created by the incident field is:

$$\vec{p} = q\Delta\vec{r}_0 = \frac{q^2}{m(\omega_0^2 - \omega^2) - 2im\omega\Gamma}\vec{E}_0\,. \tag{2.11}$$

From this equation the Lorentz definition of polarizability follows as:

$$\alpha_{Rayleigh} = \frac{p}{E_0} = \frac{q\Delta r_0}{E_0} = \frac{q^2}{m(\omega_0^2 - \omega^2) - 2im\omega\Gamma} \tag{2.12a}$$

$$= -\frac{q^2/m}{(\omega + \omega_0 + i\Gamma)(\omega - \omega_0 + i\Gamma) + \Gamma^2}. \tag{2.12b}$$

Since we deal with positive frequencies only, this function has a single peak at $\omega \cong \omega_0$. If $\Gamma \ll 2\omega_0$, then the first term in the denominator can be approximated by $\omega + \omega_0 + i\Gamma \approx 2\omega_0$. The result is:

$$\alpha_{Rayleigh} \approx -\frac{q^2/m}{2\omega_0(\omega - \omega_0 + i\Gamma)}\,. \tag{2.12c}$$

The Lorentz form of the resonance is immediately obvious. Note that Γ is the damping of the electron. In the following we continue to use Γ in this sense. Vibrational damping is neglected.

The radiated power is:

$$\frac{dP}{d\Omega} = \frac{\omega^4 p^2}{32\pi^2\epsilon_0 c^3} sin^2\theta. \tag{2.13}$$

The integrated value is:

$$P = \frac{\omega^4 p^2}{12\pi\epsilon_0 c^3} = \frac{\omega^4}{12\pi\epsilon_0 c^3}\left|\alpha\vec{E}_0\right|^2. \tag{2.14}$$

Therefore, the Rayleigh scattered power is:

$$P_{Rayleigh} = \frac{\omega^4}{12\pi\epsilon_0 c^3}\left|\alpha_{Rayleigh}\vec{E}_0\right|^2, \tag{2.15}$$

and the Rayleigh scattering cross section is:

$$\sigma_{Rayleigh}(\omega) = \frac{\omega^4}{6\pi\epsilon_0^2 c^4}\left|\alpha_{Rayleigh}\right|^2. \tag{2.16}$$

2.2.3. The Raman polarizability and scattering cross section; the CCM.

We now consider the Raman term specifically, writing the source term as

$$\kappa \to \kappa + \Delta\kappa\cos(\omega_v t). \tag{2.17}$$

The time dependence of the perturbation is written as the real function $\cos(\omega_v t)$ instead of $e^{\pm i\omega_v t}$ but we continue to use $e^{-i\omega t}$ for $\vec{E}$ and $\Delta\vec{r}$. By so doing we avoid crosstalk when taking the real projection at the end of the calculation.

The expression for $\Delta\vec{r}(t)$ is:

$$\Delta\vec{r}(t) = \vec{r}(t) - \vec{r}_0 = \Delta\vec{r}_0 e^{-i\omega t} + \Delta\vec{r}_+ e^{-i(\omega+\omega_v)t} + \Delta\vec{r}_- e^{-i(\omega-\omega_v)t}. \tag{2.18}$$

Second- and higher-order terms are neglected, by assumption. The equation of motion is now:

$$\left(m\frac{d^2}{dt^2} + 2m\Gamma\frac{d}{dt} + \kappa_0 + \Delta\kappa\cos(\omega_v t)\right)\left(\Delta\vec{r}_0 e^{-i\omega t} + \Delta\vec{r}_+ e^{-i(\omega+\omega_v)t} + \Delta\vec{r}_- e^{-i(\omega-\omega_v)t}\right)$$

$$= q\vec{E}_0 e^{-i\omega t}, \tag{2.19}$$

with solutions (See Appendix 1 in for more details about the algebra),

$$\Delta\vec{r}_0 = \frac{(q/m)\vec{E}_0}{(\omega_0^2 - \omega^2) - 2i\omega\Gamma} \approx -\frac{(q/m)\vec{E}_0}{2\omega_0(\omega - \omega_0 + i\Gamma)}, \tag{2.20a}$$

$$\Delta\vec{r}_\pm = \frac{(\Delta\kappa/2m)\Delta\vec{r}_0}{(\omega \pm \omega_v)^2 - \omega_0^2 + 2i(\omega \pm \omega_v)\Gamma} \approx \frac{(\Delta\kappa/2m)\Delta\vec{r}_0}{2\omega_0(\omega \pm \omega_v - \omega_0 + i\Gamma)}, \tag{2.20b}$$

where the rightmost versions use the $\Gamma \ll 2\omega_0$ approximation explicitly. The absorption lineshapes are again resonant Lorentzians.

The imaginary projection of each $\pm$ term of eq. (2.20b) is a double-peaked spectrum for the following reasons. One peak occurs at ω_0, when $\Delta\vec{r}_0$ is on-resonance but the pole in the denominator in eq. (2.20b) is off-resonance. The other occurs at $\omega_0 \pm \omega_v$, where the denominator is on-resonance but $\Delta\vec{r}_0$ is off-resonance. If $\Gamma \ll 2\omega_0$, the right-hand expressions, then the heights of the two peaks are identical. Otherwise, the lower-energy peak is higher. In the

next section we show that the $\Gamma \ll 2\omega_0$ result is obtained directly in the QM model in the limit of small displacements, although the QM derivation delivers the poles as separate terms, instead of the CCM product seen above. We return to this discussion below.

In practice only two resonances appear because the anti-Stokes shift is thermally less favorable because of its relatively low population, which is given by the Boltzmann factor:

$$P_{anti-Stokes} = P_{Stokes} \exp\left(-\frac{\hbar\omega}{kT}\right), \tag{2.21}$$

where $kT \ll \hbar\omega$. Using this reasoning, from a QM picture of vibrational energy levels we can ignore the anti-Stokes term. It is not necessary to do this, but it is practical and, as the theory is developed, we note that the semiclassical approximation can be generalized to molecules of any complexity.

The polarizability is defined as $\alpha = q\Delta r/E_0$. Hence it follows that:

$$\alpha_{Total} = \frac{q\Delta r_0}{E_0} + \frac{q\Delta r_-}{E_0} = \alpha_{Rayleigh} + \alpha_{Pert}$$

$$= \frac{q^2/m}{(\omega_0^2 - \omega^2) - 2i\omega\Gamma} + \frac{q^2\Delta\kappa/2m^2}{[(\omega-\omega_v)^2 - \omega_0^2 + 2i(\omega-\omega_v)\Gamma][(\omega_0^2-\omega^2) - 2i\omega\Gamma]}, \tag{2.22a}$$

$$\approx -\frac{q^2/m}{2\omega_0(\omega - \omega_0 + i\Gamma)} - \frac{q^2\Delta\kappa}{8m^2\omega_0^2(\omega - \omega_v - \omega_0 + i\Gamma)(\omega - \omega_0 + i\Gamma)}. \tag{2.22b}$$

where "Pert" represents "perturbation". In eq. $(2.22b)$ we use the approximation $\Gamma \ll 2\omega_0$ explicitly.

At this point we make some comments about $\Delta\kappa\cos(\omega_v t)$. Up to now, we have used only electronic coordinates and an equation of motion. The perturbation that we have introduced assumes that the time dependence arises from a separate model for nuclear motion, which we suppose is a classical harmonic oscillator with a single frequency ω_v. With a view to expanding the model to include strong coupling, we introduce Q, a variable that represents the normal

coordinates of the Raman-active vibration, and ΔQ, the difference between the normal coordinate Q and the reference Q_0 along this mode. The classical force constant is k, which is assumed to be linear in $\Delta\kappa$. The solution has the well-known sinusoidal dependence, $\cos(\omega_v t)$, in a many-body system configuration.

The CCM treats the electronic and nuclear parts of this problem separately, just as done in the quantum-mechanical wave equations. For example, in the quantum-mechanical harmonic oscillator, the force constant *k* depends on the electronic coordinates in some manner, since its magnitude depends on the bond strength and therefore on the coordinates of bonding electrons. Yet this aspect is ignored because the motions are separated, and *k* is treated as a constant in the nuclear wave equation. In the same way, the electronic perturbation term has a form that depends parametrically on a separate problem that we have defined as a classical harmonic oscillator that depends on a coordinate Q.

With this background, we compare the expression for the polarizability to that obtained in classical Raman theory:

$$\alpha_{Raman} = \frac{\partial \alpha_{Total}}{\partial Q}\Delta Q = \frac{\partial \alpha_{Pert}}{\partial Q}\Delta Q, \tag{2.23}$$

$$\alpha_{Total} = \alpha_{Rayleigh} + \alpha_{Raman} + \cdots = \alpha_{Rayleigh} + \alpha_{Pert}. \tag{2.24}$$

We introduce the vibrational potential energy, U_{vib}, of the electronic excited state of a given normal mode coupled to an electronic transition excited by the incidence light:

$$U_{vib} = \frac{1}{2}k(\Delta Q)^2 = \frac{1}{2}C\Delta\kappa(\Delta Q)^2, \tag{2.25}$$

where C is a constant, and k is the force constant of the normal mode. *k* is assumed to be linearly related to $\Delta\kappa$ because the normal mode is a combination of the interaction of the nuclei and electrons. Thus, the relationship of the normal coordinate displacement ΔQ and $\Delta\kappa$ is:

$$\Delta Q = \sqrt{\frac{2U_{vib}}{C\Delta\kappa}}, \qquad \Delta\kappa = \frac{2U_{vib}}{C(\Delta Q)^2}. \tag{2.26, 2.27}$$

We can use this term to recast the classical polarizability derivative in terms of Q into an expression in terms of $\Delta\kappa$ as follows:

$$\frac{\partial\alpha_{Pert}}{\partial Q}\Delta Q = \frac{\partial\alpha_{Pert}}{\partial\Delta\kappa}\frac{\partial\Delta\kappa}{\partial\Delta Q}\frac{\partial\Delta Q}{\partial Q}\Delta Q, \tag{2.28}$$

where

$$\frac{\partial\Delta\kappa}{\partial\Delta Q} = -\frac{4U_{vib}}{C(\Delta Q)^3} = -\frac{2\Delta\kappa}{\Delta Q}, \tag{2.29}$$

$$\frac{\partial\Delta Q}{\partial Q} = 1. \tag{2.30}$$

Thus, we have

$$\alpha_{Raman} = \frac{\partial\alpha_{Pert}}{\partial Q}\Delta Q = -2\frac{\partial\alpha_{Pert}}{\partial\Delta\kappa}\Delta\kappa$$

$$= -\frac{(q^2\,\Delta\kappa)/m^2}{[(\omega-\omega_v)^2-\omega_0^2+2i(\omega-\omega_v)\Gamma][(\omega_0^2-\omega^2)-2i\omega\Gamma]} \tag{2.31a}$$

$$\approx \frac{q^2\Delta\kappa}{4m^2\omega_0^2(\omega-\omega_v-\omega_0+i\Gamma)(\omega-\omega_0+i\Gamma)}. \tag{2.31b}$$

where in eq. (2.31b) we use the approximation $\Gamma \ll 2\omega_0$ explicitly. Following the method above to calculate the radiated power,

$$P = \frac{\omega^4}{12\pi\epsilon_0 c^3}|\alpha_{Raman}E_0|^2. \tag{2.32}$$

A resonant Raman process is a two-photon interaction that consists conceptually of an "upward" and a "downward" transition. Both transition dipole moments are included in this solution. We obtain an expression for the Raman shifted transition dipole moment:

$$\vec{p}_{-} = \alpha_{Raman}\vec{E}_0 = \frac{q^2\Delta\kappa}{4m^2\omega_0^2(\omega - \omega_v - \omega_0 + i\Gamma)(\omega - \omega_0 + i\Gamma)}\vec{E}_0. \quad (2.33)$$

Here we see the relationship between the transition dipole moment and the basic resonance at the Raman-shifted frequency. The equivalent in the classical α_{Raman} force-constant model has two resonances, as shown above. When written this way the incident electromagnetic field $\vec{E}_{incident} = \vec{E}_0\cos(\omega t)$ results in two dipolar terms, ignoring the anti-Stokes term,

$$\vec{p}_0\cos(\omega t) = \alpha_{Rayleigh}\vec{E}_0\cos(\omega t), \quad (2.34)$$

$$\vec{p}_{-}\cos\big((\omega - \omega_v)t\big) = \frac{1}{2}\alpha_{Raman}\vec{E}_0\cos\big((\omega - \omega_v)t\big). \quad (2.35)$$

2.3. Results

2.3.1. The CCM for small Δ_d, weak electron-phonon coupling

To further assess the validity of the CCM, we calculate the Raman excitation profile, *i.e.*, the wave number dependence of the resonant Raman cross section for both classical (CCM) and quantum mechanical (QM) methods. The Raman cross section is related to the Raman polarizability as given in eq. (2.36).

$$\sigma_{Raman}(\omega) = \frac{\omega^4}{6\pi\epsilon_0^2 c^4}|\alpha_{Raman}|^2, \quad (2.36)$$

where α_{Raman} is given by eq. (2.31). The quantum theory predicts that the ratio between the intensity of Stokes and anti-Stokes peaks will be approximately equal to the Boltzmann factor $e^{-\hbar\omega/kT}$ favoring the Stokes or negative shift relative to the incident frequency. The classical expression for the Raman intensity gives a route for calculation of the Raman cross section. The physically favored positive (Stokes) Raman shift that gives agreement with the QM approach in the Raman excitation profile shown in Figure 2.2. Figure 2.2 shows the Raman excitation profile

(REP) calculated explicitly using the parameters, $\omega_0 = 20{,}000\ \text{cm}^{-1}$, $\omega_v = 1{,}000\ \text{cm}^{-1}$ and $\Gamma = 100\ \text{cm}^{-1}$. We choose the Stokes shift rather than the anti-Stokes shift since the vibrational excited state is less populated than the ground state.

The QM model of the polarizability in the Kramers-Heisenberg-Dirac equation has the form:

$$\alpha_{Rayleigh,QM} = \frac{1}{\hbar}\sum_{n'} \frac{\langle 0|qr|n'\rangle\langle n'|qr|0\rangle}{(\omega_0 + n'\omega_v - \omega) - i\Gamma}, \tag{2.37}$$

$$\alpha_{Raman,QM} = \frac{1}{\hbar}\sum_{n'} \frac{\langle 0|qr|n'\rangle\langle n'|qr|1\rangle}{(\omega_0 + n'\omega_v - \omega) - i\Gamma}. \tag{2.38a}$$

Using

$$\langle 0|n'\rangle\langle n'|1\rangle = \int_{-\infty}^{+\infty} \chi_0\chi'_{n'}d\xi \int_{-\infty}^{+\infty} \chi'_{n'}\chi_1 d\xi = \left(\sqrt{S} - \frac{n'}{\sqrt{S}}\right)\frac{e^{-S}S^{n'}}{n'!}, \tag{2.39}$$

where ξ is the dimensionless normal coordinate, eq. (2.38a) can be evaluated if the transition dipoles do not interact with the nuclear wavefunctions. The result is:

$$\alpha_{Raman,QM} = \frac{1}{\hbar}\sum_{n'=0}^{+\infty} \frac{\langle 0|qr|n'\rangle\langle n'|qr|1\rangle}{(\omega_0 + n'\omega_v - \omega) - i\Gamma} = \frac{M_{if}^2}{\hbar}\sum_{n'=0}^{+\infty} \frac{\langle 0|n'\rangle\langle n'|1\rangle}{(\omega_0 + n'\omega_v - \omega) - i\Gamma}$$

$$= \frac{M_{if}^2}{\hbar\sqrt{S}}e^{-S}\sum_{n'=0}^{+\infty}(S - n')\frac{S^{n'}}{n'!}\frac{1}{(\omega_0 + n'\omega_v - \omega) - i\Gamma}$$

$$= \frac{M_{if}^2}{\hbar\sqrt{S}}e^{-S}\left[\sum_{n'=0}^{+\infty}\frac{S^{n'+1}}{n'!}\frac{1}{(\omega_0 + n'\omega_v - \omega) - i\Gamma} - \sum_{n'=1}^{+\infty}\frac{n'S^{n'}}{n'!}\frac{1}{(\omega_0 + n'\omega_v - \omega) - i\Gamma}\right]$$

$$= \frac{M_{if}^2\sqrt{S}}{\hbar}e^{-S}\sum_{n'=0}^{+\infty}\frac{S^{n'}}{n'!}\left[\frac{1}{(\omega_0 + n'\omega_v - \omega) - i\Gamma} - \frac{1}{(\omega_0 + (n'+1)\omega_v - \omega) - i\Gamma}\right], \tag{2.38b}$$

where M_{if}^2 is the square of the transition dipole moment. *S* is the constant describing the electron-phonon coupling, called the Franck-Condon factor (Huang-Rhys factor), and is described by the

dimensionless displacement of the excited electronic state from the ground excited electronic state Δ_d for a FC active mode:

$$S = \frac{1}{2}\Delta_d^2. \tag{2.40}$$

In the limit of small Δ_d, the above sum reduces to a single term. Writing

$$\langle 0|0'\rangle\langle 0'|1\rangle = \sqrt{S}e^{-S} \approx \sqrt{S}, \tag{2.41a}$$

$$\langle 0|1'\rangle\langle 1'|1\rangle = \left(S\sqrt{S} - \sqrt{S}\right)e^{-S} \approx -\sqrt{S}, \tag{2.41b}$$

we convert the $n' = 0$ term in eq. (2.38b) to

$$\begin{aligned}
\alpha_{Raman,QM} &= \frac{M_{if}^2\sqrt{S}}{\hbar}e^{-S}\sum_{n'=0}^{+\infty}\frac{S^{n'}}{n'!}\left[\frac{1}{(\omega_0 + n'\omega_v - \omega) - i\Gamma} - \frac{1}{(\omega_0 + (n'+1)\omega_v - \omega) - i\Gamma}\right] \\
&\approx \frac{M_{if}^2\sqrt{S}}{\hbar}\left[\frac{1}{(\omega_0 - \omega) - i\Gamma} - \frac{1}{(\omega_0 + \omega_v - \omega) - i\Gamma}\right] \\
&= \frac{M_{if}^2\omega_v\sqrt{S}}{\hbar(\omega_0 - \omega - i\Gamma)(\omega_0 + \omega_v - \omega - i\Gamma)}, \\
&= \frac{M_{if}^2\omega_v\Delta_d}{\sqrt{2}\hbar(\omega_0 - \omega - i\Gamma)(\omega_0 + \omega_v - \omega - i\Gamma)},
\end{aligned} \tag{2.42}$$

This is a double-peaked Raman excitation profile with exactly the lineshape given by the CCM in the limit that $\Gamma \ll 2\omega_0$ (eq. (2.31b)). By comparing coefficients, we conclude that

$$\Delta\kappa = \frac{2\sqrt{2}m^2\omega_0^2 M_{if}^2\omega_v\Delta_d}{q^2\hbar}, \tag{2.43}$$

connecting the phenomenological well parameter $\Delta\kappa$ to the dimensionless displacement of the ground to excited state Δ_d.

Thus, the two approaches converge on the same result when Γ and Δ_d are both small. In the CCM, this involves $\Gamma \ll 2\omega_0$, which leaves both peaks at the same height. In the QM, this involves discarding higher-order terms. Comparing eqs. (2.41a) and (2.41b), the two peaks in

QM should have a ratio $1:(1-S)^2 \cong 1:1$, where the second one should be slightly smaller when *S* is larger. This qualitatively agrees with the CCM when the $\Gamma \ll 2\omega_0$ approximation is not made. The comparison is shown graphically in Figure 2.3, for $\Gamma \ll 2\omega_0$ in Figure 2.3a and in the general case in Figure 2.3b.

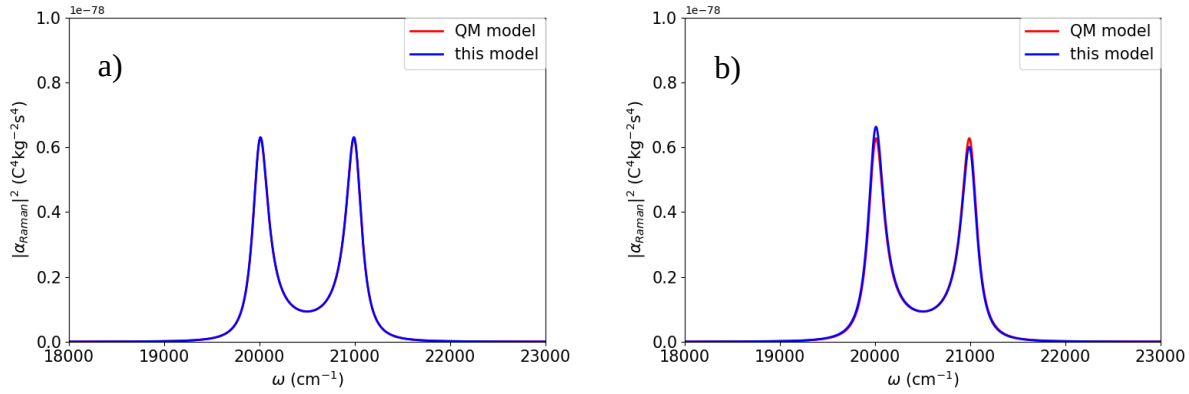

Figure 2.3 Plot of the CCM and QM results for $|\alpha_{Raman}|^2$ vs ω. a) using eq. (2.31b) with $\Gamma \ll 2\omega_0$; b) as a) but relaxing the $\Gamma \ll 2\omega_0$ condition. Parameters are provided in Appendices 2 and 3.

2.3.2. The CCM for large Δ_d, strong electron-phonon coupling; a semiclassical procedure

Combining the two terms of eq. (2.38b), we have:

$$\alpha_{Raman,QM}$$

$$= \frac{M_{if}^2\sqrt{S}}{\hbar}\sum_{n'=0}^{+\infty}\frac{e^{-S}S^{n'}}{n'!}\left[\frac{1}{(\omega_0+n'\omega_v-\omega)-i\Gamma}-\frac{1}{(\omega_0+(n'+1)\omega_v-\omega)-i\Gamma}\right], \quad (2.38b)$$

$$= \frac{M_{if}^2\omega_v\sqrt{S}}{\hbar}\sum_{n'=0}^{+\infty}\frac{e^{-S}S^{n'}}{n'!}\left[\frac{1}{\omega-(n'+1)\omega_v-\omega_0+i\Gamma}\right]\left[\frac{1}{\omega-n'\omega_v-\omega_0+i\Gamma}\right], \quad (2.38c)$$

Comparing eqs. (2.31) and eq. (2.42), we can extend eq. (2.31) to a strong coupling case by simply replacing the quantum Lorentzian terms and prefactor of eq. (2.38c) with the Lorentzian terms and prefactor of eq. (2.31), leading to

$$\alpha_{Raman,CCM}$$

$$= \frac{q^2\Delta\kappa}{m^2}\sum_{n'=0}^{+\infty}\left\{\frac{e^{-S}S^{n'}}{n'!}\left[\frac{1}{(\omega-(n'+1)\omega_v)^2-\omega_0^2+2i(\omega-(n'+1)\omega_v)\Gamma}\right]\right.$$

$$\left.\cdot\left[\frac{1}{((\omega-n'\omega_v)^2-\omega_0^2)+2i(\omega-n'\omega_v)\Gamma}\right]\right\} \qquad (2.44a)$$

$$\approx \frac{q^2\Delta\kappa}{4\omega_0^2m^2}\sum_{n'=0}^{+\infty}\frac{e^{-S}S^{n'}}{n'!}\left[\frac{1}{\omega-(n'+1)\omega_v-\omega_0+i\Gamma}\right]\left[\frac{1}{\omega-n'\omega_v-\omega_0+i\Gamma}\right]. \qquad (2.44b)$$

where in eq. (2.44b) we use the approximation $\Gamma \ll 2\omega_0$ explicitly.

The comparison of the polarizability of the CCM classical model eq. (2.44) and the fully-QM model eq. (2.38b) is shown in Figure 2.4 for various values of S. Again, Figure 2.4a shows that the QM and CCM are the same when $\Gamma \ll 2\omega_0$. Yet differences remain in Figure 2.4b: QM yields closed-form expressions for higher-order resonances with $n' \geq 1$, whereas in the fundamental case the CCM yields a closed-form expression that is valid even for $\Gamma \sim \omega_0$. By evaluating higher-order resonances, the CCM presumably yields terms that are equivalent to the $n' \geq 1$ in the QM, but since these proliferate rapidly, we have not attempted to evaluate them. The relative heights of the peaks may also exhibit some differences in the CCM and QM cases.

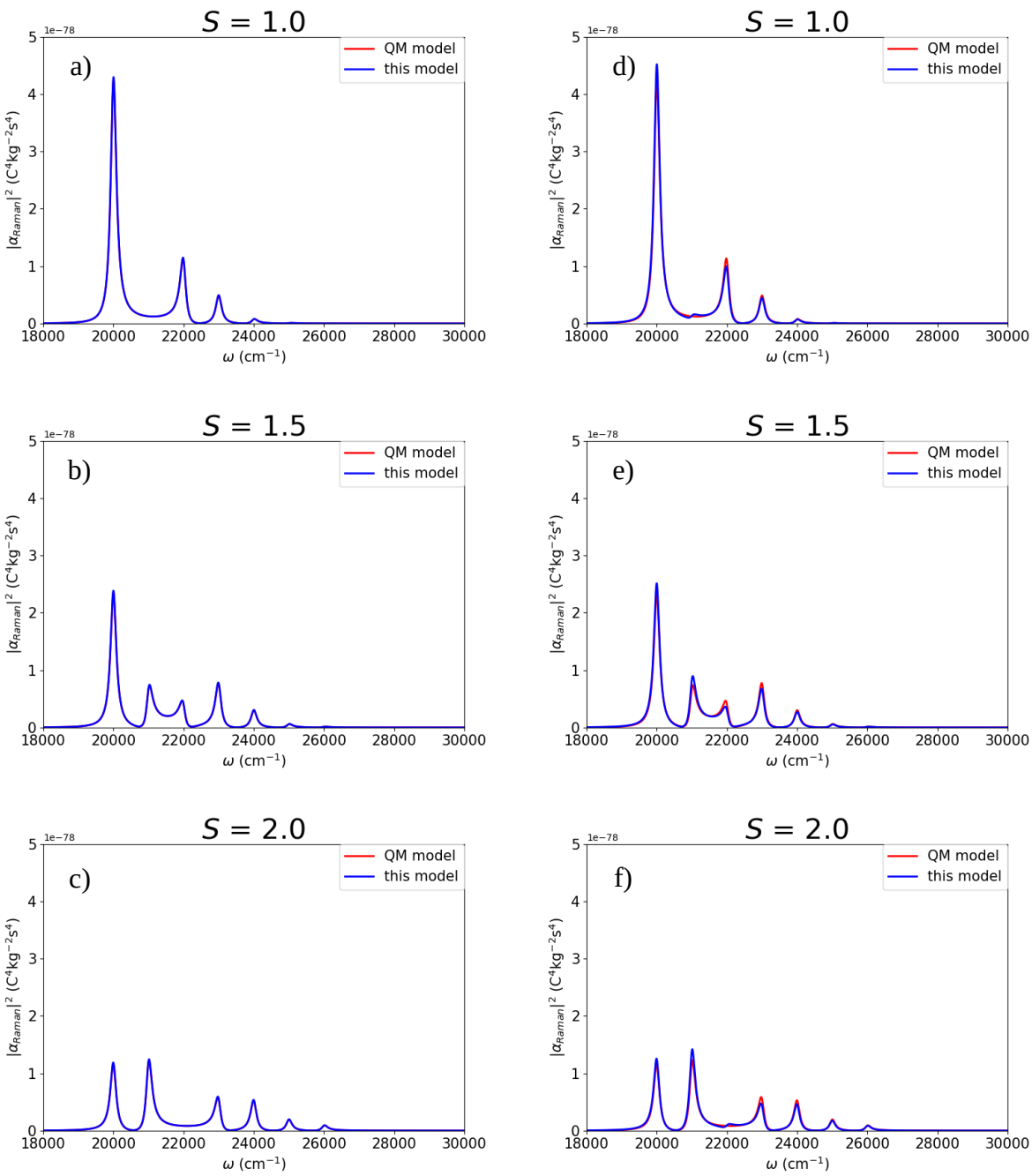

Figure 2.4 Comparison of the CCM and QM models for various values of *S*. a), b), c) eq. (2.44b) with $\Gamma \ll 2\omega_0$ assumed for the CCM; d), e), f) eq. (2.44a) with no approximation. Parameters are provided in the Appendix 2 and Appendix 3. The purpose of choosing a 1000 cm^{-1} mode in the plot is to show a better view of the progression, but it may not be valid for room temperature.

2.4. Discussion & Conclusion

The most direct comparison of the classical and quantum-mechanical formulations is in the small-displacement limit, where both predict the same REP except for prefactors. While the prefactor $\Delta\kappa$ of the CCM result is treated as phenomenological, it can be evaluated from first principles – including both shape and offset effects. Of course, the physical meaning of the correlation in the many-body system would need to be provided to obtain specific values.

In the quantum regime, studies of Raman cross sections have been based on two methods. The first is the Kramers-Heisenberg-Dirac relation, which includes the coupling of the electronic and vibronic transitions between the ground and excited states. The second is the derivative of the ground state polarizability with respect to the normal coordinate of a Raman active mode. Both approaches give rise to a Raman tensor, which has symmetric (Franck-Condon) and non-totally-symmetric (Herzberg-Teller) couplings. The depolarization ratio, $\rho = I_{\perp}/I_{\parallel}$, is widely used to determine the symmetry of the observed modes. The difference between totally symmetric, $0 < \rho < 1/3$, and non-totally symmetric modes, $\rho < 3/4$, is sufficient for these to be distinguished experimentally. The present theory provides a REP in agreement with both approaches for calculating the Raman spectrum of an isotropic model. This is easily extended to the full Raman tensor to account for polarization effects.

Thus, we find that the classical theory of the Raman cross section captures the essential physics of resonance Raman spectroscopy while maintaining a simple mathematical form. One can justify including only the Stokes-shifted modes by introducing a semiclassical population difference between frequency shifts $\omega_0 \pm \omega_v$. The pure electromagnetic theory corresponds to the limit of small ground to excited state shift Δ_d. The full quantum mechanical model parameterizes the excited-state normal mode position shift in terms of $S = \Delta_d^2/2$, where S is

called the electron-vibration coupling constant. The limit of finite nuclear displacement *e.g.*, $S > 0.05$ can be calculated as well by assuming that the Franck-Condon progression is a set of amplitude parameters, permits one to make a transition to a semi-classical model.

The application of these methods is most powerful when the absorption spectrum and REP are combined in a model that predicts the absolute resonance Raman cross sections. The fact that S is a parameter in the theory presented thus far may need further refinement to accommodate polarization effects. For simplicity we work here in one dimension, equivalent to assuming that $\Delta\kappa$ is a scalar. However, the model is easily generalized to describe anisotropic effects by replacing κ and $\Delta\kappa$ with tensorial equivalents. This would enable polarization effects to be included, permitting calculation of Raman depolarization ratios and surface selection rules, which are important for SERS spectra.[134]

The electromagnetic nature of the model is useful for tackling problems such as SERS because of the difficulty of including oscillating electric fields due to surface plasmons into the Hamiltonian for quantum-mechanical approaches to the Raman cross section. A complete treatment must account for the polarization and Raman frequency shift both in the molecular scattered radiation and in the field within the plasmonic material. The CCM is readily extended to include these fields. Thus, the demonstration above that the REP can be calculated using values of S and ω_v as parameters works well with an extension to the time-correlator method. Since S and ω_v can be calculated using a combination of density functional theory (DFT) and time-dependent density functional theory (TDDFT), we can obtain the starting point for the molecular parameters and energy levels, which serve as inputs to the time-correlator formalism.[135–138]

The time correlator formalism of Heller[139] was extended to thermalized modes by Shreve and Mathies using a two-time correlator method.[127] Comparison with experiment in such systems has provided confirmation of the time-correlator model.[140–142] Such calculations can be applied to metal-molecule adducts, which permit calculation of charge transfer contributions to SERS.[143,144] Similar approaches have employed the MP2 level of post-Hartree Fock theory for calculation of the excited-state geometry.[145,146] Polarizability derivatives have been used to provide indirect estimates for the electron-vibration coupling S in charge transfer calculations of silver-molecule adducts.[147–151]

Greater accuracy in calculation of excited state properties can be achieved by combining an electronic excited state and the ground state in a complete-active-space self-consistent field (CASSCF) approach.[152] However, these expensive methods have not been used to calculate dimensionless displacements. The contribution of Franck-Condon overlaps to the Raman polarizability have been estimated using derivatives of the potential-energy surface rather than explicitly calculating the excited potential-energy surface. Potential-energy-surface derivatives have been shown to have application in the case of large excited-state displacements, which lead to a short-time approximation in the time correlator.[142,153] Although developed initially for rapid isomerization reactions with ill-defined excited state geometries due to their intrinsic instability, the need for such approximations in computational approaches is understandable given the expense of the CASSCF calculation, which limit the number of geometries one can consider.

The method using DFT calculations of potential energy surfaces and TD-DFT for excited state energies that has been implemented previously can be used to explicitly calculate the displacement of the excited state in a multi-mode molecule, which gives the key parameters S and ω_v.[135–138] Since the vibrational modes are orthogonal in the harmonic approximation, the

calculated values can be used to create separate REPs for each mode. Alternatively, these can then be inserted into the CCM to obtain accurate multi-mode REPs, which extends the method developed here to molecules of interest for applications. Then it is relatively straightforward to extend this calculation to include secondary fields from a surface for application to SERS.

The surface selection rules present the greatest challenge. Given the electromagnetic interactions between the molecule and calculations to determine resonance Raman cross sections, the classical theory should agree with these calculations at zero applied field and thereby provide a baseline that can readily be extended to applied electric fields. This approach permits the inclusion of the phase differences in the surface field, surface selection rules and vibrational Stark effects as natural extensions of the method. These additional aspects of the problem would be exceedingly difficult to implement using DFT approaches.

The model applied in this study follows the assumptions of the Franck-Condon principle. Vibronic coupling requires inclusion of higher-lying energy states, which can couple because of distortions of the geometry of the system along a non-totally symmetric mode.[154] The inclusion of higher lying states using an CCM approach is a conceivable way of tackling the problem of vibronic coupling. In previous work, the vibronic approach to absorption and Raman spectra has been based on DFT calculations of explicit geometric distortions away from the original symmetry and estimations of matrix elements based on the strength of coupling to excited states. On the other hand, if it could be applied with the appropriate symmetry, the CCM could be extended to this approach merely by including tensorial force constants with corresponding terms in the force equation.

As noted above, classical and quantum treatments of configurations are analogous in that classical treatments involve forces and quantum treatments are based on potentials, and forces

are simply the negative gradient of the potentials. For conditions where Newton's Second Law of Motion can provide an adequate representation of phenomena under consideration, the simplicity of the classical approach can provide insights difficult to achieve in a quantum environment. Raman scattering is ideally suited for investigations of this type. This work is intended to stimulate further progress in this area.

Supporting Information

Comparison of CCM and ABM are provided in Appendix 1; Parameters of the Figures are provided in Appendices 2 and 3.

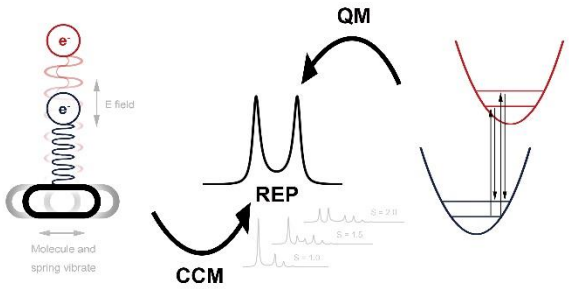

Figure 2.5 Table of content graphic

CHAPTER 3. Classical Correlation Model Applied in Surface Enhanced Infrared Absorption (SEIRA) Spectroscopy

Abstract

The molecule-plasmon interaction is the key to the mechanisms of surface enhanced infrared absorption (SEIRA) and surface enhanced Raman scattering (SERS). Since plasmons are well described by Maxwell's equations, one fundamental treatment involves the classical interpretation of infrared absorption, and resonance Raman spectroscopies. We can understand the molecule-plasmon interaction using electromagnetic theory if the classical field effect on a transition dipole moment or transition polarizability is properly described. In previous work, we derived the Raman excitation profile of a model molecule using a classical driven spring attached to a charged mass with a perturbative force constant due to vibrational oscillations. In this study we generalize the interactions of plasmons with molecules by considering N_2O asymmetric stretch SEIRA signal on a Dy doped CdO (CdO:Dy) film. This semiconductor has tunable plasmon dispersion curves throughout the near-and mid-infrared, that can interact directly with vibrational absorption transitions. We have demonstrated this using the Kretschmann configuration with a CaF_2 prism and a MgO substrate. The model predicts the phase behavior of SEIRA. The calculated enhancement factor relative to an Au control is 6.2, in good agreement with the value of 6.8 ± 0.5 measured under the same conditions.

3.1. Introduction

The fundamental nature of the interaction of surface plasmons in conducting thin films, nanoparticles or nanostructures has not been determined. While there are theories for surface-enhanced Raman, fluorescence and infrared-absorption, there is no general explanation for the

mechanism whereby electromagnetic fields on the surface of conductors can drive molecular transitions at a greater rate than electromagnetic radiation traveling through vacuum. The interaction of the field and molecule lies at the heart of the debate over chemical *vs.* electromagnetic enhancements. It is also necessary for a cohesive theory that explains all surface-enhanced spectroscopies. We have embarked on a systematic approach towards such a theory based on atomic-bond-model (ABM) methods that have antecedents in the calculation of Lorentz polarizability.[121,123,155,156] We have called this approach the Classical Correlation Method (CCM) to represent the fact that we are applying classical electrodynamics to spectroscopic problems that have heretofore been solved using quantum mechanics.

While it is possible to obtain detailed molecular descriptions using quantum-mechanical approaches, the description of a surface plasmon in a conductor has defied quantum approaches. Hence, the need for a classical correlation approach that works for both the molecular and plasmonic surface is desirable. In our first work in this series, we showed that resonance Raman spectroscopy can be derived in a form identical to the Kramers-Heisenberg-Dirac formalism using a charged mass on a spring as the model system.[157] Clearly, the calculation of resonance Raman scattering in the presence of an electric field requires understanding the effect of fields on transition dipoles, *i.e.* absorption. Effects of this type have been observed experimentally and given the name surface enhanced infrared absorption (SEIRA). Thus, in the following, we apply the CCM theory to the enhancement of infrared signals on appropriately tuned infrared plasmonic materials.

Mid-infrared (mid-IR) plasmonic materials have the potential to interact with molecular vibrational modes due to infrared absorption. The present study deepens our knowledge of how mid-IR plasmons supported by thin-film conducting metal oxides can be applied to IR

spectroscopy for chemical detection, functional group identification, and environmental analysis.[10] Using isotope editing, it is possible to extract macromolecular structural and dynamic information on peptides that rivals nuclear magnetic resonance (NMR).[158] In general, IR is a rapid and convenient technique with *in situ* and *in vivo* modes of detection of molecular vibrational modes. Although attenuated total reflection (ATR) spectroscopy has become popular, its detection region is limited to the decay length of ~ $\lambda/10$ of an evanescent wave.[159] The utility of ATR is restricted to solvents or reagents at high concentration because of this thin effective field interaction layer. Plasmon resonance spectroscopy is a special case of ATR spectroscopy, in which the interface consists of a conducting layer and a substrate or sample layer. The disadvantage of the intrinsically small path length in ATR can potentially be overcome by the inclusion of mid-IR surface plasmon resonances in the ATR geometry.

SEIRA has been employed as an IR enhancement technique that has the potential to lower the limit of detection and thereby increase the usefulness of the method. Limits of detection are in the single-molecule range for fluorescence, micromolar concentrations for resonance Raman, and millimolar concentrations for mid-IR transmission spectroscopy. All three of these techniques have been investigated for a potential role for field enhancement near a plasmonic surface to boost the signal.[160–164] The enhancement of IR spectroscopy is an attractive idea for application of IR in trace-amount detection or other applications that require high sensitivity.[165–167]

SEIRA involves application of a conductive film as an overlayer or underlayer to the sample. Metal nanoislands[168–172] and metal oxides[42,46,173–183] have been employed as conductors since their surface plasmon resonances are tunable throughout the near-and mid-infrared region. When the incident light is on resonance with the tuned surface plasmon and the molecular

vibration, the IR signal of the molecule can be enhanced. Since the first discovery of SEIRA in 1980,[16] the magnitude of the maximum reported enhancement factor has increased from twenty to a few hundreds. Some researchers have claimed that the enhancement could reach up to 10^4 at specific locations on a conductor, known as "hot spots".[53,54,184,185] Even greater enhancement of Raman signals has been reported at hot spots,[11,66] although a comprehensive theory is lacking.

The enhancement mechanism is acknowledged to involve both electromagnetic (EM) and chemical mechanisms (CM).[161] EM enhancement arises from the local electric field impinging on the analyte, where the local field experienced by the molecule is composed of both incident radiation and a reaction field in the conductor that may be on resonance with the surface plasmon. CM is associated with charge transfer and geometry distortion, since both cases arise from the molecule chemically bound to the conductor. As an example of CM enhancement, resonance Raman scattering may have a large CM enhancement of up to 10^6 for molecules that form bonds with the surface. Resonance Raman scattering theory is based on calculation of the effect of excited state displacement of Franck-Condon active modes on the transition probability. Distortions in the ground state geometry caused by binding will tend to promote coupling to vibronic (non-totally-symmetric) modes. The CM may also involve contribution of a charge transfer absorption band, Additionally, distortions in the surface caused by plasmonic waves may be communicated to the molecule through a chemical bond to the surface.

The specific enhancement considered here is a type of SEIRA measured using conducting metal oxide thin films with tunable mid-IR plasmon resonances. The models to date for SEIRA are based on either fitting or numerical, including Fano resonance,[110] coupled harmonic oscillators,[58,59,186] temporal coupled mode theory (TCMT),[60,186–188] and finite difference time-domain (FDTD).[114] However, a model that separates chemical and electromagnetic effects is

required to understand the interaction of the surface plasmon and the molecule. The first challenge of such a model is chemical interaction. This is mainly elucidated by quantum mechanics, while the surface fields are determined by the boundary conditions on classical EM using Maxwell's equations. One possible resolution to this incompatibility is to use a consistent electromagnetic theory for both molecule and surface.

Our first step in the development a comprehensive theory was to show that the CCM is an appropriate alternative theory of resonance Raman scattering.[157] The CCM is described by a charged spring-mass system shown in Figure 3.1. For electronic absorption or scattering, the mass represents an electron or a bound charge, and the wall represents the rest of the molecule. The spring represents the interaction between the electron and the molecule following the Lorentz model for the oscillator strength and polarizability. The application of an accurate first-principles model to nonlinear optics led to an analogous treatment of resonance Raman scattering. By introducing an electron-phonon coupling constant, which results from the changes in excited state geometry due to electronic excitation, the CCM Raman polarizability has the same mathematical form as the quantum model, which is usually calculated using the Kramers-Heisenberg-Dirac (KHD) formula.[189,190] The prefactors of the two expressions differ, but can be reconciled by properly accounting for quantum-to-classical correspondences. By obtaining the classical analog of the KHD polarizability, we have demonstrated the possibility of deriving a theory that involves the interaction of surface plasmonic fields with the KHD polarizability in a self-contained model. The model is accurate and the physical correspondence between quantum and classical theory are readily explained. In this study we tackle the problem of the interaction of a transition dipole moment with the plasmonic field. In future studies we plan to extend the

result for mid-IR absorption enhancement to Raman scattering in the vicinity of a conducting surface. This is the next step towards a comprehensive theory.[45]

3.2. Theory

3.2.1. Deriving the dielectric function of N_2O with rotational-vibrational coupling from classical bond model

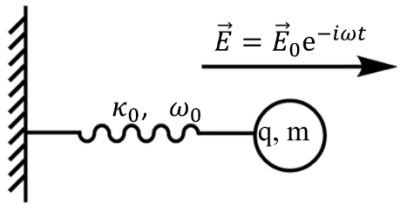

Figure 3.1 Spring mass system in classical correlation model

The classical bond model applied here differs from the previous model[157] in the interpretation of the meaning of the spring force constant and charge since this study focuses on surface field effects on vibrational absorption bands in the mid-IR. The moving charge q of the molecule in the current study arises from the change in charge distribution that accompanies molecular vibration. The mass is described by the reduced mass of the normal mode. In other words, this is our definition of the transition dipole relevant for infrared spectroscopy rather than visible spectroscopy. However, the model is versatile since it is possible to apply such a model to an electronic transition dipole as done previously.[157] The previous CCM focused on electronic transitions and the resonant Raman scattering associated with them. Therefore, in the previous model the charge represents the excited electron, and the mass is that of the electron. A second difference is in the procedure. The present CCM is applied to vibrational spectra coupled to a surface plasmon, while the previous CCM described a free molecule. It is hoped that the

synthesis of these models can be achieved in the future to study surface enhancement of Raman-active modes.

We turn to mid-IR vibrational absorption using the equation of motion for a reduced mass, *m*. Consider that the molecule is rotating with an angular velocity ω_R. If the coordinate system is set respect to the spring-mass system, the equation of motion is:

$$\vec{F} = m\frac{d^2\vec{r}(t)}{dt^2} = q\vec{E}_o e^{-i\omega t}\cos(\omega_R t) - 2m\Gamma\frac{d\vec{r}(t)}{dt} - \kappa_0(\vec{r} - \vec{r}_0), \tag{3.1a}$$

where the Γ describes energy loss. The solution to this equation is:

$$\vec{r} = \vec{r}_0 + \Delta\vec{r}_+ e^{-i(\omega+\omega_R)t} + \Delta\vec{r}_- e^{-i(\omega-\omega_R)t}. \tag{3.2}$$

Therefore, Eq. (3.1a) reduces to:

$$-m\omega^2\left(\Delta\vec{r}_+ e^{-i(\omega+\omega_R)t} + \Delta\vec{r}_- e^{-i(\omega-\omega_R)t}\right)$$

$$= \frac{1}{2}q\vec{E}_o\left(e^{-i(\omega+\omega_R)t} + e^{-i(\omega-\omega_R)t}\right) + 2im\omega\Gamma\left(\Delta\vec{r}_+ e^{-i(\omega+\omega_R)t} + \Delta\vec{r}_- e^{-i(\omega-\omega_R)t}\right)$$

$$- \kappa_0\left(\Delta\vec{r}_+ e^{-i(\omega+\omega_R)t} + \Delta\vec{r}_- e^{-i(\omega-\omega_R)t}\right). \tag{3.1b}$$

The solution gives the displacement magnitude:

$$\Delta\vec{r}_\pm = \frac{q\vec{E}_0/2m}{\omega_0^2 - (\omega \pm \omega_R)^2 - 2i\Gamma(\omega \pm \omega_R)}. \tag{3.3}$$

The dipole created by the incident field is:

$$\vec{p} = q(\Delta\vec{r}_+ + \Delta\vec{r}_-)$$

$$= \frac{q^2\vec{E}_0}{2m}\left(\frac{1}{\omega_0^2 - (\omega+\omega_R)^2 - 2i\Gamma(\omega+\omega_R)} + \frac{1}{\omega_0^2 - (\omega-\omega_R)^2 - 2i\Gamma(\omega-\omega_R)}\right). \tag{3.4}$$

The dielectric function of the material with a macroscopic number of the same system is given by the displacement field:

$$\vec{D} = \epsilon\epsilon_0\vec{E} = \epsilon_0\vec{E} + \vec{P} = \epsilon_0\vec{E} + n\vec{p}, \tag{3.5}$$

$$\epsilon = 1 + \frac{np}{E}, \tag{3.6a}$$

where n is the number density of the molecule, $\vec{P}$ is the dipole density.

In a general case where the rotation is not considered, the dielectric function has the form:

$$\epsilon = 1 + \frac{nq^2/m\epsilon_0}{(\omega_0^2 - \omega^2) - 2i\omega\Gamma}. \tag{3.6b}$$

Notice that, when $\omega_0 = 0$, the model becomes the Drude model, where the bound charge, q, becomes a free charge carrier in the material. The plasma frequency of the conductor is $\omega_p^2 = nq^2/m\epsilon_0$.

For a conductive layer described by damped Drude model, the dielectric function is:

$$\epsilon_2 = \epsilon_{\infty 2} - \frac{\omega_{p2}^2}{\omega^2 + 2i\omega\Gamma_2}, \tag{3.7}$$

where $\epsilon_{\infty 2}$ is the high frequency limit of the permittivity for the conductor. Subscript "2" corresponds to Layer 2 in Figures 3.2 and 3.3. The plasma frequency is defined as:

$$\omega_{p2} = \sqrt{\frac{n_2 e^2}{\epsilon_0 m_2}}, \tag{3.8}$$

where n_2 is the carrier density, m_2 is the effective mass of the charge in the material. Γ_2 is the energy damping parameter, which relates to the mobility μ of the charge in the conductor according to:

$$2\Gamma_2 = \frac{e}{\mu m_2}. \tag{3.9}$$

A collection of neutral molecules behaves as an insulator. If rotation is considered, the dielectric function of the molecules is described by:

$$\epsilon_3 = \epsilon_{\infty 3} + \frac{n_3 q^2}{2m_3\epsilon_0}\left(\frac{1}{\omega_0^2 - (\omega+\omega_R)^2 - 2i\Gamma_3(\omega+\omega_R)} + \frac{1}{\omega_0^2 - (\omega-\omega_R)^2 - 2i\Gamma_3(\omega-\omega_R)}\right)$$

$$\approx \epsilon_{\infty 3} + \frac{n_3 q^2}{4\omega_0 m_3\epsilon_0}\left(\frac{1}{\omega_0 - (\omega+\omega_R) - i\Gamma_3} + \frac{1}{\omega_0 - (\omega-\omega_R) - i\Gamma_3}\right). \quad (3.10)$$

where the approximation $\Gamma_3 \ll 2\omega_0$ is applied. Subscript "3" corresponds to Layer 3 in Figures 3.2 and 3.3.

The SPR effect arises at the interface between the conductor and insulator. The dispersion relation of the surface wave at that interface is well known,[191] but is derived in Appendix 4 for ease of reference:

$$k_{SPP} = \frac{\omega}{c}\sqrt{\frac{\epsilon_2\epsilon_3}{\epsilon_2+\epsilon_3}} \quad (3.11)$$

The dispersion relation is a special case of ATR. Reflectance is reduced in the region of the EM wave vector that matches the dispersion curve because of losses in the conduction electrons, which occur either due to polariton migration along the surface or enhanced electric fields interacting with molecules in layer 3.

3.2.2. The three-layer Fresnel equation and reflectance power

We can use dielectric functions obtained above to calculate the SEIRA signal excited in the Kretschmann configuration. As shown in Figures 3.2 and 3.3, three-layer Fresnel equations (Airy equations) are required. We ignore the interface between the CaF_2 prism and the MgO layer, because the MgO layer is thin and essentially index-matches the CaF_2 prism. For *s*- and *p*-polarized waves, the three-layer Fresnel equations are:

$$r_{123s} = \frac{E_{r1}}{E_{i1}} = \frac{r_{12s}e^{-ikd\cos\varphi} + r_{23s}e^{ikd\cos\varphi}}{e^{-ikd\cos\varphi} + r_{12s}r_{23s}e^{ikd\cos\varphi}} = \frac{r_{12s} + r_{23s}e^{2ikd\cos\varphi}}{1 + r_{12s}r_{23s}e^{2ikd\cos\varphi}} \quad (3.12a)$$

$$r_{123p} = \frac{H_{r1}}{H_{i1}} = \frac{r_{12p}e^{-ikd\cos\varphi} + r_{23p}e^{ikd\cos\varphi}}{e^{-ikd\cos\varphi} + r_{12p}r_{23p}e^{ikd\cos\varphi}} = \frac{r_{12p} + r_{23p}e^{2ikd\cos\varphi}}{1 + r_{12p}r_{23p}e^{2ikd\cos\varphi}} \quad (3.12b)$$

where φ is the incident angle at interface 2 or the transmitted angle at the interface 1. The derivations of Eqs.(3.12a) and (3.12b) are given in Appendix 5. These equations also accurately describe the situation for a complex wave vector k, *e.g.*, when total internal reflection takes place at interface 1, which is the case for the Kretschmann configuration used in the experiment.[45]

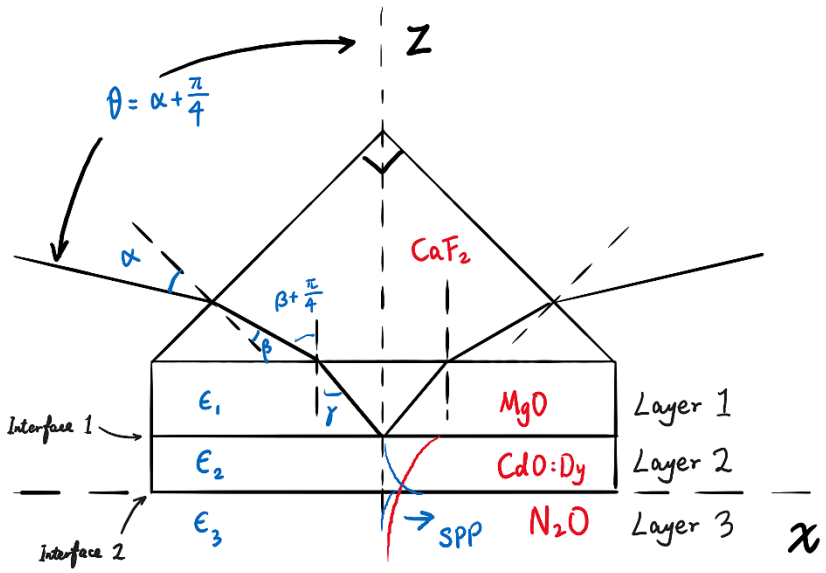

Figure 3.2 The Kretschmann configuration used in the experiment.[45] θ is the incident angle of the IR variable-angle spectroscopic ellipsometer (IR-VASE™). By varying the incident angle θ, the reflectance of the FTIR spectrum of the configuration is measured. An angle – wavenumber – reflectance map, shown below, is applied to describe the result of an IR-VASE™ measurement. The three-layer Fresnel model is based on the valid assumption that no energy is lost in the CaF_2 prism and MgO intermediate layer.

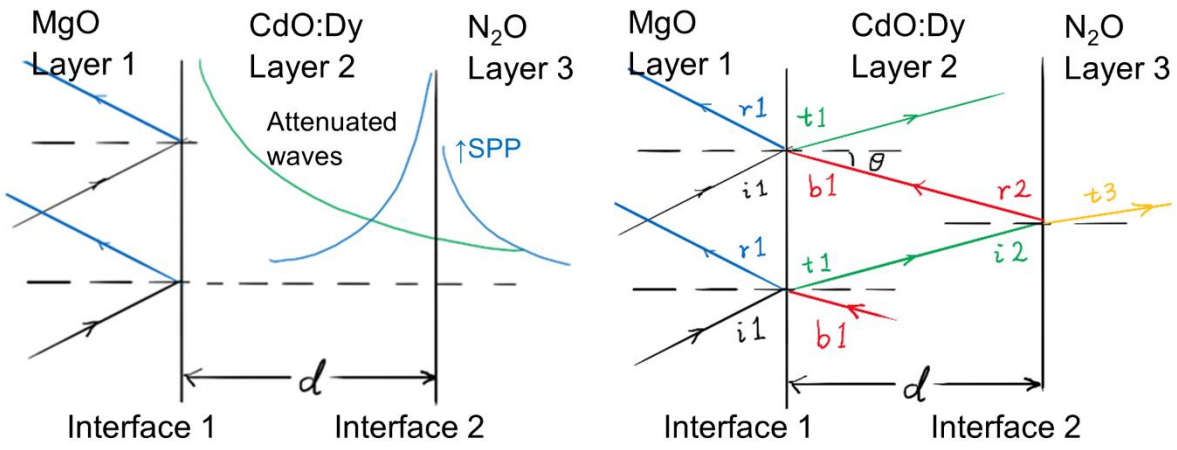

Figure 3.3 Light path in the Kretschmann configuration with (left) and without (right) total internal reflection.

3.2.3. The reflectance power derived from the Poynting vector.

Consider a general situation, where the refraction index $n = n' + in''$ and the wave vector $k = k' + ik''$ are complex. Then a phase difference exists between the electric and magnetic fields. The instantaneous Poynting vector of the incident light is:

$$\vec{S}_i = Re(\vec{E}_i) \times Re(\vec{H}_i) = \hat{k}_i$$

$$= \hat{k}_i \sqrt{\frac{\epsilon_0}{\mu_0}} n_1' E_i^2 e^{2\vec{k}_i'' \cdot \vec{r}} \cos^2(\vec{k}_i' \cdot \vec{r} - \omega t)$$

$$- \hat{k}_i \sqrt{\frac{\epsilon_0}{\mu_0}} n_1'' E_i^2 e^{2\vec{k}_i'' \cdot \vec{r}} \cos(\vec{k}_i' \cdot \vec{r} - \omega t) \sin(\vec{k}_i' \cdot \vec{r} - \omega t) \qquad (3.13)$$

where $\vec{r}$ is the position vector. When taking the time average, the cosine × sine term will average to 0, so only the first term survives. The result is:

$$\langle \vec{S}_i \rangle = \frac{1}{2} \hat{k}_i \sqrt{\frac{\epsilon_0}{\mu_0}} n_1' E_i^2 e^{2\vec{k}_i'' \cdot \vec{r}}. \qquad (3.14)$$

The Poynting vector for the reflected light is:

$$\vec{S}_r = Re(\vec{E}_r) \times Re(\vec{H}_r) = \hat{k}_r\big(r'Re(E_i) - r''Im(E_i)\big)\big(r'Re(H_i) - r''Im(H_i)\big)$$

$$= \hat{k}_r\sqrt{\frac{\epsilon_0}{\mu_0}}\big(r'Re(E_i) - r''Im(E_i)\big)\Big(r'\big(n_1'Re(E_i) - n_1''Im(E_i)\big)$$

$$- r''\big(n_1'Im(E_i) + n_1''Re(E_i)\big)\Big) \tag{3.15}$$

Note that the $Re^2(E_i)$ and $Im^2(E_i)$ terms are $E_i^2 e^{-2\vec{k}_i''\cdot\vec{r}}\cos^2\big(\vec{k}_i'\cdot\vec{r} - \omega t\big)$ and $E_i^2 e^{-2\vec{k}_i''\cdot\vec{r}}\sin^2\big(\vec{k}_i'\cdot\vec{r} - \omega t\big)$, respectively, and become $\frac{1}{2}E_i^2 e^{-2\vec{k}_i''\cdot\vec{r}}$ after time averaging,

$$\langle\vec{S}_r\rangle = \frac{1}{2}\hat{k}_r\sqrt{\frac{\epsilon_0}{\mu_0}}e^{2\vec{k}_i''\cdot\vec{r}}\big(r'^2 n_1'E_i^2 + r'r''n_1''E_i^2 - r'r''n_1''E_i^2 + r''^2 n_1'E_i^2\big)$$

$$= \frac{1}{2}\hat{k}_r\sqrt{\frac{\epsilon_0}{\mu_0}}n_1'E_i^2 e^{2\vec{k}_i''\cdot\vec{r}}\big(r'^2 + r''^2\big) \tag{3.16}$$

The reflectance power is described by the ratio of the radiation powers of the reflected and incident beams:

$$R = \frac{\langle S_r\rangle A_r}{\langle S_i\rangle A_i} = \frac{\langle S_r\rangle}{\langle S_i\rangle} = r'^2 + r''^2 = |r|^2, \tag{3.17}$$

where A_r and A_i are the cross-sections of the reflected light and the incident light beams. Since the incident and reflected angle are the same, $A_i = A_r$.

3.3. Application of the model to the SEIRA experiment on N_2O excited by CdO:Dy

3.3.1. N_2O Signal on dispersion relation and reflectance calculation

As an example of the above theory, we consider CdO:Dy as the conductor, ϵ_2; and N_2O gas as the molecule, ϵ_3. The dispersion relation is plotted in Figure 3.4, with the frequency on the

x axis, and the surface wavevector k_x on the *y* axis. The parameters are listed in Table 1, which are consistent with the data from the experiment performed by Sachet et al.[45]

Table 3.1 Parameters applied in Figure 3.4*

Parameters	CdO:Dy	N_2O
High frequency permittivity limit ϵ_∞	$\epsilon_{\infty 2} = 5.5$	$\epsilon_{\infty 3} = 1$
Carrier density of conductor	$n_2 = 3.5 \times 10^{26}\ \mathrm{m}^{-3}$	
Molecular dipole density		$n_3 = 3.238 \times 10^{25}\ \mathrm{m}^{-3}$ (4 atm)
Effective mass	$m_2 = 0.21\ m_e$	$m_3 = 2.6 \times 10^4\ m_e$
Damping parameter	$\mu = 0.03\ \mathrm{m}^2 \cdot \mathrm{V}^{-1} \cdot \mathrm{s}^{-1}$	$\Gamma_3 = 0.5\ \mathrm{cm}^{-1}$
Resonant frequency ω_0	N/A	$\omega_0 = 2225\ \mathrm{cm}^{-1}$
Rotation frequency ω_R		$\omega_R = 13\ \mathrm{cm}^{-1}$
Thickness	190 nm	

*The dielectric functions for CaF_2 and MgO used in the calculation are given by Ref.[192]

In Table 3.1, n_3 is calculated from ideal gas law $pV = nk_BT$, where $p = 4.0$ atm, $T = 298.15$ K, and k_B is the Boltzmann constant. We assume that the N_2O molecules rotate freely, and are therefore isotropic in space, so only one third of the molecules are polarized by an incident EM wave:

$$n_3 = \frac{n}{3V} = \frac{p}{3k_BT}. \tag{3.18}$$

This assumption is based on the observation that there are no N_2O molecules adsorbed on the film.[45] The effective mass m_3 for the molecule is the reduced mass of the vibrational mode, which is obtained from the eigenvectors of the Hessian matrix *l*:

$$\frac{1}{m_3} = \sum \frac{l^2}{m} = \frac{0.65}{m(N)} + \frac{0.29}{m(N)} + \frac{0.05}{m(O)}; \tag{3.19}$$

$$m_3 = 14\ a.m.u. \approx 2.6 \times 10^4\ m_e. \tag{3.20}$$

Details of the calculation are provided in Appendix 7.

The rotation frequency is estimated from the internal energy of one rotational degree of freedom $E = \frac{1}{2} I\omega^2 = \frac{1}{2} k_B T$ at room temperature.

From Snell's Law, the *x* component of the wave vector is continuous. According to Figure 3.2, the relation of the wave vector and the incident angle is given by:

$$Re(k_x) = \frac{\omega}{c} n_{MgO} \sin\gamma = \frac{\omega}{c} n_{CaF_2} \sin\left(\beta + \frac{\pi}{4}\right) = \frac{1}{\sqrt{2}} \frac{\omega}{c} n_{CaF_2} (\sin\beta + \cos\beta),$$

where

$$n_{CaF_2} \sin\beta = \sin\alpha = \sin\left(\theta - \frac{\pi}{4}\right) = \frac{1}{\sqrt{2}} (\sin\theta - \cos\theta).$$

Therefore:

$$Re(k_x) = \frac{\omega}{2c}\left(\sin\theta - \cos\theta + \sqrt{2\epsilon_{CaF_2} - 1 + \sin 2\theta}\right). \tag{3.21}$$

Figure 3.4 shows the dispersion of the real and imaginary parts of the wave vector k_x and angle θ with increasing incident light frequency. To show the perturbation of the molecule by the SPP, the damping parameter for the molecule is chosen to be $\Gamma_3 = 0.5\ \mathrm{cm}^{-1}$. The dielectric function for CaF_2 is given in Ref.[192]

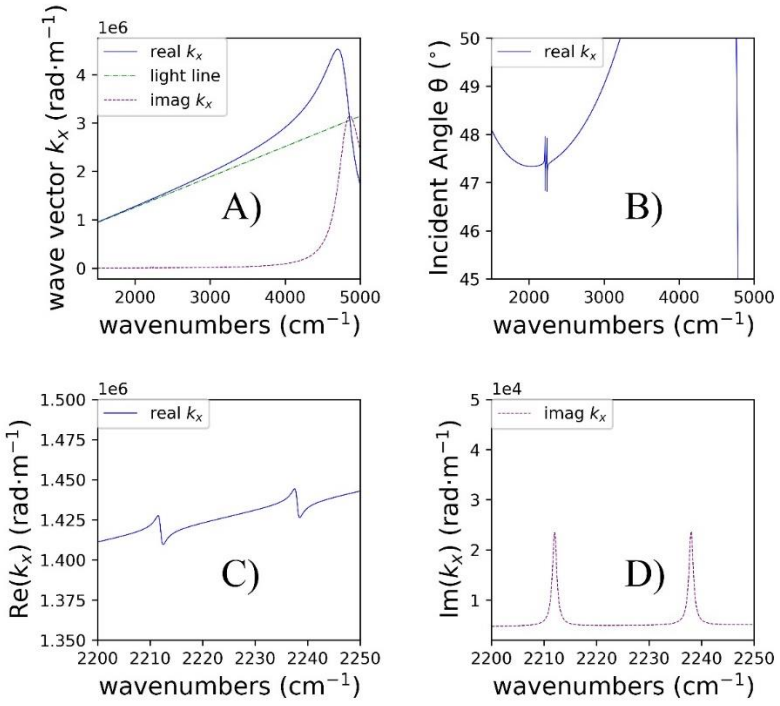

Figure 3.4 Dispersion relation of the surface wave between the CdO:Dy layer and the N_2O gas. To obtain a qualitative view of the dispersion relation, we set $\Gamma_3 = 0.5\ \mathrm{cm}^{-1}$ in the figure.

Figure. 3.4 shows that when the incident EM frequency reaches the resonant frequency of the molecule, the real part of the wave vector presents a dispersive line shape. This is consistent with the phase shift observed by Sachet *et al*.[45] in the reflected line shape as the incident angle was varied near the plasmon condition of the conductive CdO:Dy film. These data are reported in Figure 3.5. When the surface wave propagates, the reflectance decreases as required by energy conservation. In Figure 3.5 the damping parameter Γ_3 is set at $10\ \mathrm{cm}^{-1}$ for the first peak and $7.5\ \mathrm{cm}^{-1}$ for the second peak, values estimated from the full width at half maximum (FWHM) of the data in Figure 3.6B. Note that, the FWHM is equal to 2Γ.

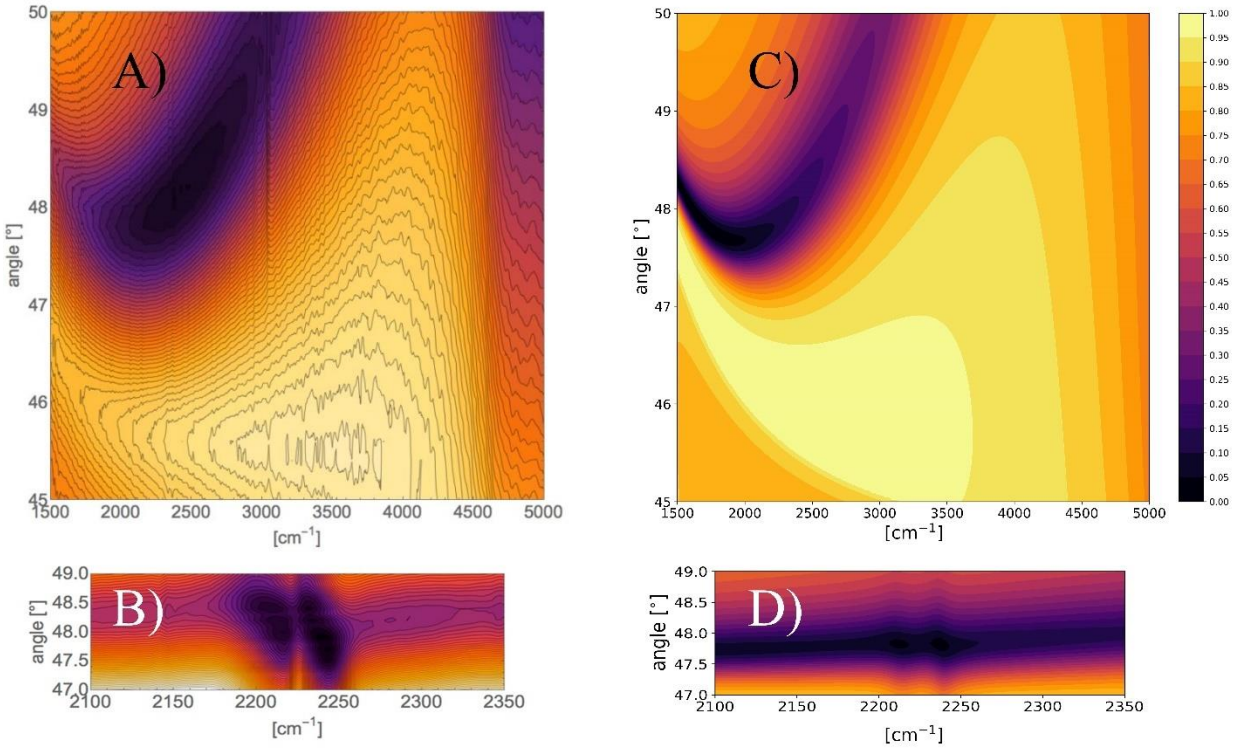

Figure 3.5 A) A control experiment without N_2O exposure. If N_2O did adsorb on the surface, coverage is below the limit of detection. B) The N_2O perturbation of the SPP signal. C) The simulation of the 3D reflectance map with the conditions of A. D) Calculated reflectance map in the region where the SPP crosses with the vibrational frequency of the molecule; θ is the incident angle of the IR variable angle spectroscopic ellipsometer (IR-VASE^{TM}) as shown in Figure 3.2. Since the resolution of the IR-VASE^{TM} is 4 cm^{-1}, rovibrational fine structure is shown as a double-envelope shape, represent for P and R branches respectively. In this figure Γ_3 is set to 10 cm^{-1} for the first peak and 7.5 cm^{-1} for the second peak. A and B are reproduced with permission: copyright 2020, American Chemical Society.[45]

Table 3.2 Parameters applied in Figure 3.5*

Parameters	CdO:Dy	N_2O
High frequency permittivity limit ϵ_∞	$\epsilon_{\infty 2} = 5.5$	$\epsilon_{\infty 3} = 1$
Carrier density of conductor	$n_2 = 3.5 \times 10^{26}\ \mathrm{m^{-3}}$	
Molecular dipole density		$3.238 \times 10^{25}\ \mathrm{m^{-3}}$ (4 atm)
Effective mass	$m_2 = 0.21\ m_e$	$m_3 = 2.6 \times 10^4\ m_e$
Damping parameter	$\mu = 0.03\ \mathrm{m^2 \cdot V^{-1} \cdot s^{-1}}$	$\Gamma_{31} = 10\ \mathrm{cm^{-1}}, \Gamma_{32} = 7.5\ \mathrm{cm^{-1}}$
Resonant frequency ω_0	N/A	$\omega_{01} = 2225\ \mathrm{cm^{-1}}$
Rotation frequency ω_R		$\omega_R = 13\ \mathrm{cm^{-1}}$
Thickness	190 nm	

*The dielectric constants for CaF_2 and MgO used in the calculation are given by Ref. [192].

3.3.2. Enhancement factor calculation.

Enhancement factors were calculated based on conversion of the reflectance data to an equivalent absorbance and comparison with simulated spectra for the plasmon-active control surface shown in Figure 3.6. The dielectric function of conducting CdO:Dy was used to simulate the SPR signal. The double-peak signals in Figure 3.6A have the baseline removed, which is done by subtracting the signal of pure SPP without N_2O presence. Figure. 3.6A shows the enhancement factors of the absorbance signal at different incident angles. The maximum enhancement factor is 50.0 when the incident angle is 47.82°. Figure 3.6B shows that a similar phase shift is observed in the reflectance spectra. The corresponding absorption spectra are presented in Ref. 45.

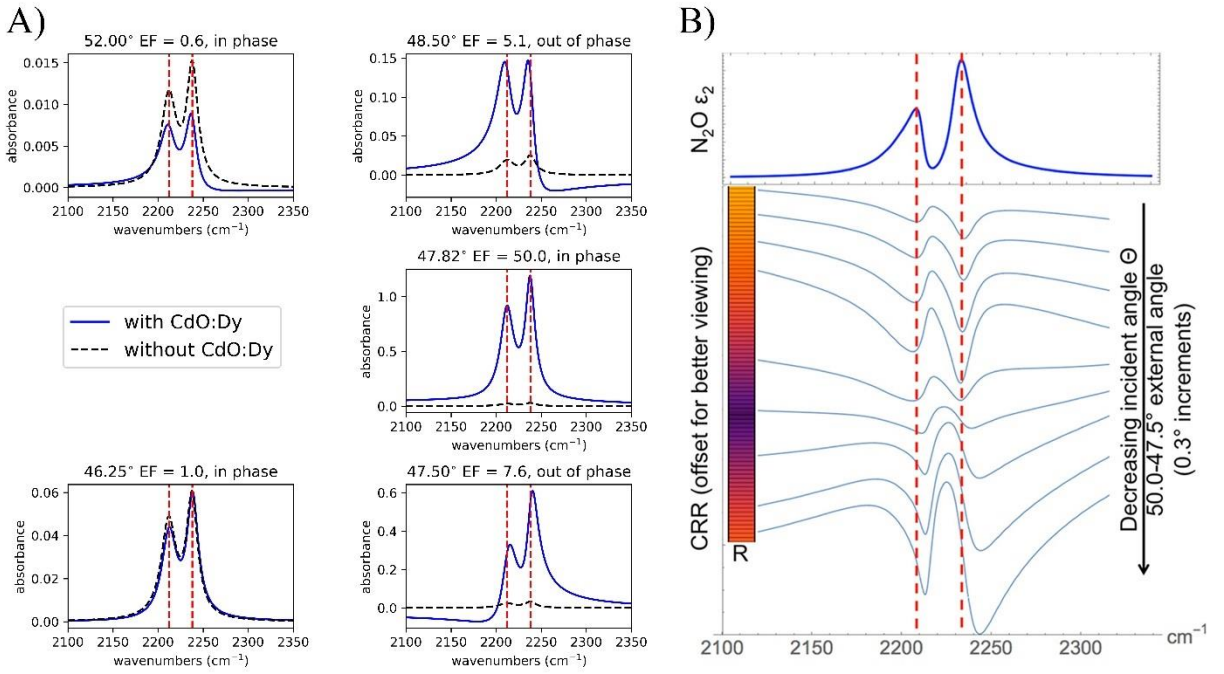

Figure 3.6 A) Absorbance signal at different incident angles. The blue lines show the SPP signal due to CdO:Dy, which is subtracted by baseline correction. The black lines are obtained using a MgO layer, *i.e.* setting the thickness of CdO:Dy layer to 0 (See Figures 3.2 and 3.3). The red dashed vertical lines represent the absorption peaks of N_2O corresponding to the maxima of the P and R branches. The enhancement factor (EF) is calculated by taking the quotient of the integral of the two signals. The largest EF = 50.0 was found at 47.82 degrees. B) Absorption spectrum of N_2O at the resolution of the IR-VASE™ (approximately 4 cm^{-1}). Below are reflectance spectra as a function of angle, showing the phase change across the resonance angle. The red dashed vertical lines represent the absorption peaks of N_2O corresponding to the maxima of the P and R branches. (Figure reproduced with permission; copyright 2020, American Chemical Society.[45])

Figure 3.6B shows that $\Gamma_{31} = 10\ cm^{-1}$ for the first peak and $\Gamma_{32} = 7.5\ cm^{-1}$ for the second peak based on a simulation of the experimental absorption spectrum. The double peak in the experiment arises from the shape of the rovibrational spectrum of the antisymmetric stretch

of N_2O. The resolution of the IR-VASE is not sufficient to observe the structure of the rovibrational spectra. Instead, the P and R branches are shown as envelopes. However, the resolution is sufficient to distinguish in phase and out-of-phase absorption line shapes. The phase shift of the reflectance signal of the N_2O gas occurs when the incident angle crosses over resonance with the SPP band. The EF for the experiment was obtained by comparing the N_2O signal on the CdO:Dy layer to that on a 5.0 ± 1.4 nm gold layer, since thin gold films are commonly used in SEIRA applications.[45]

To compare with the experimental result, the EF for a thin gold film was calculated. The relative EF is given by the ratio of the maximum EF for CdO:Dy (50.0) to that for gold layer. These results are given in Table 3.

Table 3.3 Enhancement factor (EF) of N_2O absorbance by gold film with different thickness*

Thickness of Au (nm)	EF	CdO:Dy Relative EF compared to Au	Incident angle θ (°)
3.6	8.1	6.2	47.42
4.3	10.7	4.7	47.04
5.0	11.7	4.2	46.83
5.7	12.3	4.1	46.71
6.4	13.5	3.6	46.16
Thickness of CdO:Dy (nm)	EF		Incident angle θ (°)
190	50.0	1.0	47.82

*The dielectric function of Au refers to the experimental data of Ref. [193].

The largest relative enhancement of 6.2 was found with a gold film thickness of 3.6 nm. The calculated EF agrees with the experimental relative EF 6.8, where the SEIRA signal of N_2O on CdO:Dy film was compared to that on a 5.0 ± 1.4 nm gold film.[45]

3.4. Discussion

When the incident light is on resonance with the vibrational frequency of a molecule and the conducting oscillations of a surface plasmon, the surface wave produced by the incident light can be absorbed by the molecule. In the quantum theory of absorbance, this interaction is described by the cross-section of the molecule, which is linear in the imaginary part of the wave vector.

As shown in Figure 3.4, the imaginary part of the wave vector shows two peaks corresponding to P and R branches at $\omega = \omega_0 \pm \omega_R$. As required by the Kramers-Kronig relations, the real part of the wave vector shows a dispersive line shape.

As a result of the attenuated surface wavevector, there is a phase shift in the SEIRA signal as a function of incident angle. Figure 3.6 shows the peak displacement from the vibrational frequency of N_2O. The phase shift can be described as having five stages as the incident angle increases:

i. Incident angle below the SPR angle (<47°):

As shown in the bottom left of Figure 3.6A (46.25°), the absorption line shape of SEIRA (blue line, with the presence of CdO:Dy) is in phase with that of ATR-FTIR (black line, without CdO:Dy). The maxima of P and R branches of the SEIRA signal overlap with the ones for ATR-FTIR (aligned with the red dotted lines at the maxima).

ii. Approaching the SPR angle from below (47°~47.82°):

As shown in the bottom right of Figure 3.6A (47.50°), the absorption line shape of SEIRA is out of phase with respect to ATR-FTIR. The maxima of P and R branches of the SEIRA signal are shifted to higher frequencies than the red-dotted lines, which mark the two peaks in the ATR-FTIR signal.

iii. On resonance with the SPR (~47.82°):

As shown in the center right of Figure 3.6A (47.82°), the absorption line shape of SEIRA is in phase again of that to ATR-FTIR. In this case, the enhancement factor reaches to the maximum.

iv. Surpassing the SPR angle (47.82°~51°):

As shown in the top right of Figure 3.6A (48.50°), the absorption line shape of SEIRA is out of phase again of that to ATR-FTIR. The difference compared to case ii is the peaks of SEIRA signal are associated with lower frequencies compared to the ATR-FTIR peaks rather than higher frequencies.

v. Far above the SPR angle (>51°):

As shown in the top left of Figure 3.6A (52.00°), the absorption line shape of SEIRA is in phase again of that to ATR-FTIR. The phase shift cycle is completed.

Similar phase shifts have been observed in the literature.[194,195] Their numerical calculation from Kretschmann's theory[196] shows that, the reflectance minimum shifts to a lower angle of incidence when the frequency is higher than resonance, and *vice versa*. This agreement of first principles theory and experiment shows that the phase shift is a purely electromagnetic phenomenon.

Physically, we may understand the phase shift observed in these spectra by analogy with a forced harmonic oscillator. As is well known, the phase angle of a driven oscillation with respect to the driving field changes on resonance. Below resonance the phase angle is 0^o, on resonance it is 90^o, and above resonance 180^o. It is easily shown that the difference in phase angle between the incident field and the surface plasmon oscillation is both quite small and constant across the range of resonance with the molecule (Appendix 6). When the incident light

is on resonance with the plasmon, little light is reflected, and the transmitted light is enhanced. If the plasmon is off resonance with the molecule, the dispersion is dominant; if the plasmon is on resonance with the molecule, the absorption is the major phenomenon. Thus, the observed experimental phase shift results from a forced oscillation of the molecule, which is driven by the surface plasmon.

The Lorentz polarizability itself predicts this. The imaginary part of the Lorentz polarizability corresponds to absorption of light by the molecule. The real part corresponds to dispersion and that signal changes sign by 180^{o} as electromagnetic radiation is tuned through resonance, presenting a good analogy with a forced harmonic oscillator. This is not accidental, since the CCM model is also based on a mass and spring system with an added charge to provide an interaction with the electromagnetic field. Consequently, the phase change is natural part of the CCM theory. This will also be important for further discussion of surface enhanced Raman spectroscopy.

Many researchers have applied the term Fano resonance to explain the asymmetric line shape in various contexts, including the angular dependence of the surface plasmon resonance.[111,112] Fano's result explains the line shape that results when elastic and inelastic scattering compete in helium gas.[110] The Fano model consists of a linear combination of dispersive and absorptive line shapes. The physics of the SEIRA line shapes identified as Fano line shapes is not linked to the original application of helium scattering, which has led to some confusion in the literature. The fitting of the different molecular SEIRA signals results in different parameters, and it is not trivial to summarize the intrinsic physics from the fitting parameters. In the case of SEIRA, as the angle of incidence of the exciting light is tuned near the resonance condition for driving the surface plasmon, there is a transition of the phase shift,

which causes the asymmetric line shape. The model presented here gives a physical reason for the phase shift, *i.e.*, the mixture of absorptive and dispersive components of the molecular response, which is a consequence of the damped surface wave vector. This model starts from the Kretschmann configuration, on which the experimental framework is based. Coupled harmonic oscillators and TCMT employ a simplified linear configuration where a spring represents the connection between the plasmon and the molecule. These are treated as two harmonic oscillators.[59,186,197,198] Therefore, the calculation of our model is more straightforward. The results are easier to interpret and are linked directly to the structure. Furthermore, our model has the potential to be applied to other geometries.

Comparing to FDTD, our model is analytical rather than numerical. FDTD only calculates the field in the geometry. The enhancement factor is estimated by the field on the hot spot compared to the background. However, molecules are absent in the calculation.[56,199–201] Therefore, the enhancement calculated in FDTD is purely electromagnetic. Since the CCM is based on a Lorentzian spring model for bonding, it has the potential to also account for chemical enhancement by considering models with additional springs to represent the bonding of molecules to a surface.

In conclusion, the surface plasmon dispersion relation calculated using the classical bond model provides a direct and fundamental explanation for the phase shift in reflected mid-IR light near the plasmon resonance observed in experiment. The reason for the phase shift is that Snell's law requires the wave vector along the surface to be continuous. If the molecule absorbs the surface wave, the imaginary part of the wave vector will show a peak at the resonance frequency of the molecule. Because the norm of the wave vector is conservative, the real part of the wave vector shows dispersion at the resonance of the molecule. Additional support for the model

follows in that the calculated EM enhancement factor of 6.2 agrees well with the experimental result 6.8 ± 0.5 under the same condition.[45] The difference may arise form surface imperfection in the experimental samples. In any case the model demonstrates that mid-IR SPR can be used for detection of vibrational bands and provides a rigorous measure of the SEIRA enhancement factor.

Supporting Information

The dispersion relation of the surface wave is derived in Appendix 4. The three-layer Fresnel equation (Airy equation) is derived in Appendix 5. The phase difference between the incident light and the plasmon is shown in Appendix 6. The reduced mass of the asymmetric mode is calculated in Appendix 7.

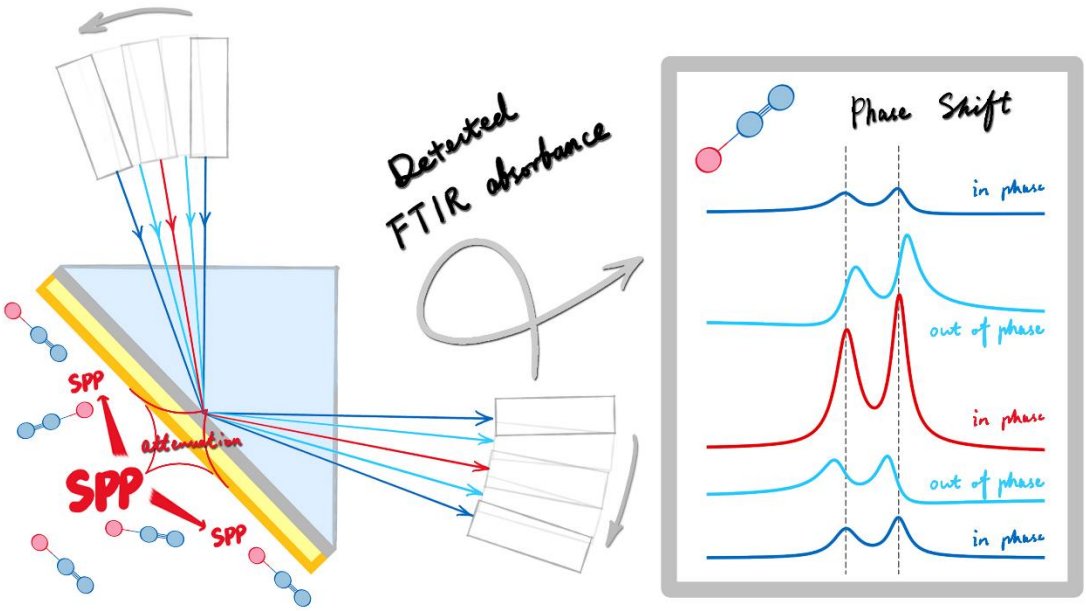

Figure 3.7 Table of content graphic

CHAPTER 4. CCM applied to SERS on spherical particles in suspension

4.1. Introduction

4.1.1. General information about SERS on spherical particles

The study of surface-enhanced Raman scattering (SERS) signal enhancement has gained significant attention as an analytical method and in the theory community. The most pronounced SERS signals have been observed when nanoparticles are immobilized or grown on conductive planar layers.[202–204] There have been many experiments in other geometries ranging from organized nanostructures to individual nanoparticles in suspension. We note that nanoparticles are colloids and the forces that keep them suspended in a solvent differ in important ways from molecular solvation. In this study we will not be concerned directly with nanoparticle stabilization as described by the Derjaguin-Landau-Verwey-Overbeek (DLVO) theory.[205–208] We will assume that nanoparticles can be stable in solution at low ionic strength due to electrostatic repulsion of like-charged colloids, but can flocculate, aggregate, and precipitate as the ionic strength is increased. In this chapter, we will focus on a model for an individual spherical nanoparticle in a suspension, which is the simplest geometry on the nanometer length scale.

The interest in SERS has been spurred by reports of extremely large enhancement factors. The disparity in reported enhancement factors has generated controversy. Yet there has not been a theory that can explain the enhancement effect in a consistent manner. Therefore, it is crucial to investigate the SERS signal enhancement by nanoparticles.

4.1.2. Traditional estimation of SERS enhancement factor

Extensive research has established that the proximity of a molecule to a conductor leads to the excitation of the localized surface plasmon (LSP), which in turn generates the electric field experienced by the molecule (referred to as the local field).[191]

$$E_{loc}(\omega) \propto \left(1 + \frac{\epsilon_p(\omega) - \epsilon_{env}(\omega)}{\epsilon_p(\omega) + 2\epsilon_{env}(\omega)}\right) E_i(\omega) \quad (4.1.1)$$

In eq. 4.1.1, $E_{loc}(\omega)$ represents the local field near the surface of the nanoparticle at the incidence laser frequency ω. It is influenced by the incident electric field, $E_i(\omega)$, as well as the dielectric functions of the nanoparticle is the incident electric field, $\epsilon_p(\omega)$ and the surrounding environment $\epsilon_{env}(\omega)$.

When $\epsilon_p(\omega)$ approaches $-2\epsilon_{env}(\omega)$, the excitation of the localized surface plasmon (LSP) occurs. This condition leads to the maximum enhancement. It is important to note that the denominator of the equation does not reach zero due to the dissipative nature of the conductor, which is reflected in the imaginary part of the dielectric function. Empirically, all conductors, including free-electron conductors, exhibit energy dissipation.

In almost all previous theoretical studies, the enhancement in surface-enhanced Raman scattering (SERS) has been estimated by considering the enhancement of the local field relative to the incident field, raised to the "fourth power". This estimation is based on the assumption that the Raman shifted frequency falls within the broad plasmon band.[209,210]

$$EF = \left|\frac{E_{loc}(\omega)}{E_i(\omega)}\right|^2 \left|\frac{E_{s,SERS}(\omega_R)}{E_{mol,RS}(\omega_R)}\right|^2 \approx \left|\frac{E_{loc}(\omega)}{E_i(\omega)}\right|^4 = \left|\frac{\epsilon_p(\omega) - \epsilon_{env}(\omega)}{\epsilon_p(\omega) + 2\epsilon_{env}(\omega)}\right|^4 \quad (4.1.2)$$

In the equation above, the ω_R represents the Raman shifted frequency. $E_{s,SERS}(\omega_R)$ corresponds to the local field near the surface at the Raman shifted frequency, while $E_{mol,RS}(\omega_R)$ refers to the Raman scattered field originating from the molecular environment in the absence of the nanoparticle. The field to the “fourth power” estimation, although a simple approach, does not accurately capture the SERS enhancement because the ratio of the electric field at the Raman scattered frequency, ω_R, is orders of magnitude smaller than the ratio at the incident frequency, ω. Moreover, the spherical geometry only applies for the incident photon, while the scattered

photon involves a molecule near a planar surface. Despite these caveats, early studies by the research terms of Kerker, Nitzan, and Moskovits, produced estimates of the fourth power dependence of the enhancement factor.[99,211–215] From a theoretical perspective the groups have made the assumption that the approximation shown in Eqn. 4.1.2 is valid.

4.1.3. Limitations of the traditional EF estimation

4.1.3.1. The EF for the incident frequency ω and the Raman shifted frequency ω_R should be considered separately

The stored energy in the conducting particle is maximum at the incident frequency, ω, and orders of magnitude smaller at ω_R. The theoretical studies have consistently avoided this issue, which is crucial for an accurate estimation of the SERS enhancement.

From a molecular perspective, it is important to note that a spectroscopic line shape is defined by the Franck-Condon (FC) factor. Transition intensity is distributed among different vibrational modes and the overall width is determined by excited state dephasing and lifetime. A large dephasing rate leads to a broad band, but also to reduction in the peak intensity. The broader the transition, the lower the peak intensity, as required for a normalized line shape function. From the nanoparticle point of view, the amplitude of the plasmonic field is larger for conductors that have less dissipation. Dissipation in a conductor is the analog of dephasing in a molecule. The local field factor described in this chapter plays a role analogous to the FC factor in a molecule. It has an amplitude and a bandwidth. Of course, the intensity is proportional to the square of the plasmonic field. Consequently, if the enhancement at a certain frequency ω is significant, the enhancement at the Raman shifted frequency ω_R is typically off-peak by 1000-1600 cm^{-1} and therefore relatively smaller. A more dissipative conductor could increase ω_R

relative to ω by increasing the bandwidth, this would occur at the expense of the overall intensity of the plasmonic field. The trade-off between large peak intensity and bandwidth intrinsically limits the two stages of enhancement which depend on ω and ω_R. Therefore, we should discuss the enhancement for the two different frequencies separately.

The enhanced field at the Raman shifted frequency ω_R consists of both the enhanced Raman scattered field emitted by the molecule and enhancement by the nanoparticle at the Raman shifted field:

$$E_{s,SERS}(\omega_R) = E_{mol}(\omega_R) + E_p(\omega_R) \tag{4.1.4}$$

The enhancement for the Raman shifted electric field is distinct from the enhancement observed in the incident field. The primary difference lies in the geometry and sources involved. In the case of incident frequency, the source is a plane wave originating from outside, while the Raman shifted wave derives from molecules within an outer layer of the nanoparticle, situated much closer to it. Consequently, this disparity gives rise to the following implications:

$$\frac{E_{s,SERS}(\omega_R)}{E_{mol,RS}(\omega_R)} \neq \frac{E_{loc}(\omega)}{E_i(\omega)} \tag{4.1.5}$$

Etchegoin et al. addresses the distinction between the two enhancements,[216] the computation of the Raman shifted signal is still indirect, as their molecular Raman polarizability is usually defined by the geometry, but not the intrinsic parameters of the molecule. As a result, the obtained results tend to primarily reflect the surface plasmon properties of the nanoparticle rather than the molecular properties of the molecule.

4.1.3.2. Molecular properties should be considered in the EF estimation

The nanoparticle and adsorbed molecules should be considered as a unit

In the experimental literature,[217–219] the enhancement factor is typically calculated by comparing the intensity ratios of two samples: one is the suspension containing the nanoparticle

and the other consists only of the Raman active molecule solution. It is not accurate to assume that the behavior of a molecule located near the nanoparticle's surface is representative of bulk solution. The molecules on the nanoparticle are often either chemically bound to the surface or, at least, they are not independent of each other. The vector sum of their dipoles must be considered in any model calculation.

For example, the intensity of a set of dependent dipoles is proportional to the square of the sum of the dipoles:

$$I_{dependant} \propto E^2 \propto \left(\sum_i \vec{p}_i\right)^2 \tag{4.1.6}$$

Whereas the intensity of individual dipoles is proportional to the sum of the dipole squares:

$$I_{independant} = \sum_i I_i \propto \sum_i E_i^2 \propto \sum_i \vec{p}_i^2 \tag{4.1.7}$$

Evaluating the enhancement factor solely based on the intensity of a randomly pointed dipole on a nanoparticle divided by the intensity of a randomly pointed dipole in the solvent is not appropriate unless each nanoparticle carries exactly one molecule.

Chemical enhancement and Resonance Raman effect

The molecular absorption spectrum may be altered when a molecule is in close proximity to a nanoparticle. This chemical effect is also difficult to estimate. All experimental studies discuss both chemical and electromagnetic enhancement. The common assumption is that the chemical enhancement is small, and the electromagnetic enhancement is large, but this is difficult to demonstrate. For example, resonance Raman effect could provide an additional EF of 10^6 to 10^8.

Van Duyne's research group has provided the most persuasive experimental demonstration of very high enhancement factors.[99,220–222] However, even an experiment showing single-molecule SERS using an isotopically labeled Rhodamine suffers from the drawback that there is simultaneous resonance enhancement of the rhodamine molecule and surface enhancement from the nanoparticle.[217] The system of rhodamine on Ag nanoparticles is very well studied and is a clear example of surface-enhanced resonance Raman spectroscopy (SERRS).[223] The enhancement of SERRS is not the same as that of SERS, which is observed for non-resonant Raman spectroscopy. Therefore, relying solely on this power-based relationship may lead to inaccurate estimations of the SERS enhancement. The enhancement factor should take the molecule into account.

Charge transfer is another situation where an electronic transition is involved. In a metal to ligand charge transfer (MLCT) band, the electronic transition from the plasmon band of the nanoparticle to the molecular empty anti-bond orbitals (usually delocalized π^* orbitals) can provide a considerable enhancement.[224,225] The molecules are bound to the nanoparticle in this case.

Aggregation

Many of the SERS-active molecules tend to aggregate in solution.[226,227] The aggregation state may be quite different in a nanoparticle suspension and comparison is therefore flawed.

In this study, we addressed the challenges involved in precisely evaluating the enhancement factor using CCM theory to relate the observations to the intrinsic electronic and vibrational parameters of the molecule. However, neither the Chemical enhancement nor aggregation were addressed by the current method.

4.2. Theory

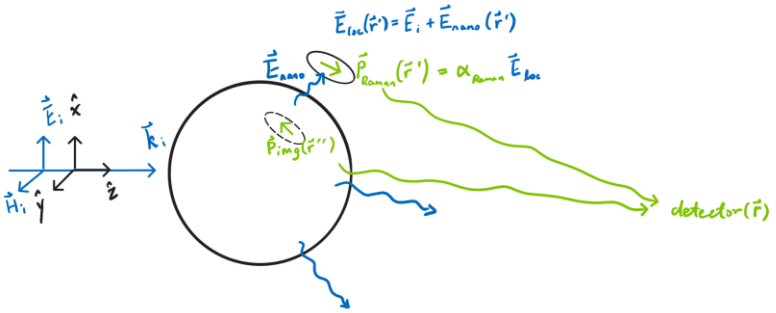

Figure 4.1 The relationship between incident light, nanoparticles, and molecules in the model setup. The local field at the location of the molecule comprises the incident field and the scattered field originating from the surface. The detected Raman signal consists of both the Raman scattered wave emitted by the molecule and the nanoparticle. The origin is set in the center of the nanoparticle.

In this study, we examine a model featuring a spherical nanoparticle coated with a Raman-active molecule. The incident light is assumed to propagate along the z-axis. Taking into account the symmetry of the spherical nanoparticle and the attached molecules, the incident electric field, denoted as E_i, is set along the x-axis. The molecules on the surface are assumed to be homogeneous, and their position is denoted as r'. The local field of the molecule at r' has two components, as described by:

$$\vec{E}_{loc}(\vec{r}',\omega) = \vec{E}_i(\vec{r}',\omega) + \vec{E}_{nano}(\vec{r}',\omega) \tag{4.2.1}$$

where the first term represents the incident field, while the second term represents the scattered field originating from the nanoparticle.

Once the local field excites the Raman-active molecule, the Raman dipole density can be expressed using CCM:

$$\vec{P}_R(\vec{r}',\omega_R) = \epsilon_0 \chi_R \vec{E}_{loc}(\vec{r}',\omega) \tag{4.2.2}$$

Next, we evaluate the Raman Scattered wave. Assume the detector at $\vec{r}$ is in a far field limit, the contribution of the molecules to the field detected at the Raman shifted frequency is given by:

$$\vec{E}_{molecule}(\vec{r},\omega_R) = \frac{\omega_R^2}{4\pi\epsilon_0 c^2 r^3}\int_{V'} d^3r'\,\vec{r}\times\left(\vec{P}_R(\vec{r}',\omega_R)\times\vec{r}\right)$$

$$= \frac{\omega_R^2 n}{4\pi\epsilon_0 c^2 r^3}\vec{r}\times\left(\int_{V'} d^3r'\vec{p}_R(\vec{r}',\omega_R)\right)\times\vec{r} \qquad (4.2.3)$$

where n is the number density for the Raman dipoles. Assuming the evenly distributed dipole layer has a thickness d. The integral becomes:

$$\vec{E}_{molecule}(\vec{r},\omega_R) = \frac{\omega_R^2 n}{4\pi\epsilon_0 c^2 r^3}\vec{r}\times\left(\int_R^{R+d} r'^2 dr'\int_{\Omega'} d\Omega'\,\vec{p}_R\,(\vec{r}',\omega_R)\right)\times\vec{r}$$

$$= \frac{\omega_R^2 n}{4\pi\epsilon_0 c^2 r^3}\left(\frac{(R+d)^3-R^3}{3}\right)\vec{r}\times\int_{\Omega'} d\Omega'\,\vec{p}_R(\theta',\varphi',\omega_R)\times\vec{r}$$

$$= \frac{\omega_R^2 n\alpha}{4\pi\epsilon_0 c^2 r^3}\left(\frac{(R+d)^3-R^3}{3}\right)\vec{r}\times\int_{\Omega'} d\Omega'\,\vec{E}_{loc}(\theta',\varphi',\omega)\times\vec{r} \qquad (4.2.4)$$

For a single layer, the molecular scattered field is a function of surface density $n_{surface}$:

$\vec{E}_{molecule}(\vec{r},\omega_R)$

$$= \frac{\omega_R^2 n_{surface}}{4\pi\epsilon_0 c^2 r^3}\vec{r}\times\left(\int_R^{R+d} r'^2 dr'\int_{\Omega'} d\Omega'\,\vec{p}_R(\delta(r'-R-d),\theta',\varphi',\omega_R)\right)\times\vec{r}$$

$$= \frac{\omega_R^2 (R+d)^2 n_{surface}}{12\pi\epsilon_0 c^2 r^3}\vec{r}\times\int_{\Omega'} d\Omega'\,\vec{p}_R(\theta',\varphi',\omega_R)\times\vec{r}$$

$$= \frac{\omega_R^2 (R+d)^2 n_{surface}\alpha_{Raman}}{12\pi\epsilon_0 c^2 r^3}\vec{r}\times\int_{\Omega'} d\Omega'\,\vec{E}_{loc}(\theta',\varphi',\omega)\times\vec{r} \qquad (4.2.5)$$

where $n_{surface}$ describes the surface number density for the Raman dipoles.

While the local field $\vec{E}_{loc}$ can be obtained by near-field Mie theory, it can also be solved using electrostatics if the particle size is smaller than the incident wavelength.

Electrostatic theory permits a near-field treatment of the interaction of molecules with conducting nanoparticles. We are interested in near-field observations, which prevents use of generalized Mie theory packages online[228,229] valid in the far field. These packages are typically used to obtain the extinction, absorption, and scattering, of nanoparticles. However, when a molecular layer is present, one must either use a near-field form of Mie theory or the electrostatic approximation as we have done here.

In the electrostatic case, the nanoparticle is equivalent as an induced dipole:

$$p_p = 4\pi\epsilon_0 \frac{\epsilon_p - \epsilon_{mol}}{\epsilon_p + 2\epsilon_{mol}} R^3 E_{xi} \tag{4.2.6}$$

The orientation of molecules on the nanoparticle is typically considered to be either parallel or perpendicular to the surface, influenced by chemical interactions with the nanoparticle. Let a represent the fraction of molecules that are perpendicular to the surface, excited by electric fields in the $\hat{r}$ direction. Similarly, let b represent the fraction of molecules parallel to the surface, excited by electric fields in tangential directions.

To simplify calculations and maintain symmetry about the x-axis (rather than the z-axis), it is preferable to use x as the polar axis in spherical coordinates. The scattered field can then be expressed as follows:

$$\begin{aligned} \vec{E}_{sca}(\vec{r}', \omega) &= \frac{1}{4\pi\epsilon_0} \frac{3(\vec{r}' \cdot \vec{p}_p)\vec{r}' - r'^2 \vec{p}_p}{r'^5} \\ &= \frac{\epsilon_p - \epsilon_{mol}}{\epsilon_p + 2\epsilon_{mol}} \frac{R^3}{r'^3} E_{xi}(2a\hat{r}\cos\eta' + b\hat{\eta}\sin\eta') \end{aligned} \tag{4.2.7}$$

where η represents the polar angle associated with the x-axis to distinguish it from the polar angle θ associated with the z-axis. It is evident that $\vec{E}_{sca}$ exhibits symmetry with respect to the x-axis, resulting in a resultant vector aligned along the x-axis. Assuming $r' = R + d$, where R

denotes the radius of the nanoparticle and d represents the distance of the molecular layer to the nanoparticle, the integration in equations 4.2.4 and 4.2.5 can be evaluated accordingly (For the detailed derivation, please refer to Appendix 8):

$$\int_{\Omega'} d\Omega' \, \vec{E}_{loc}(\theta', \varphi', \omega) = 2\pi \int_0^{\pi} \sin\eta' \, d\eta' \left(\vec{E}_i(\omega) + \vec{E}_{sca}(\eta', \omega)\right)$$

$$= 4\pi E_{xi}\hat{x}\left(\left(\frac{1}{3}a + \frac{1}{3}b\right) + \frac{\epsilon_p - \epsilon_{mol}}{\epsilon_p + 2\epsilon_{mol}} \frac{R^3}{(R+d)^3}\left(\frac{2}{3}a - \frac{2}{3}b\right)\right) \tag{4.2.8}$$

The subsequent step involves evaluating the Raman-shifted signal originating from the nanoparticle, which can be accomplished by considering the boundary conditions derived from Maxwell's equations. To address this matter, the image charge method is employed as a straightforward approach. Assuming a nanoparticle with a radius of R, the relationship between the original charge and the image charge, as described by the image charge method, is described by:[230]

$$q_{im} = -\gamma q \frac{R}{r'}, \qquad \vec{r}_{im} = \left(\frac{R}{r'}\right)^2 \vec{r}' \tag{4.2.9}$$

$$\gamma = \frac{\epsilon_p - \epsilon_{mol}}{\epsilon_p + \epsilon_{mol}} \tag{4.2.10}$$

where q and $\vec{r}'$ are the charge and the position of the source charge; q_{im} and $\vec{r}_{im}$ are the charge and the position of the image charge inside the nanoparticle; ϵ_{nano} is the dielectric function of the nanoparticle; ϵ_{mol} is the dielectric function of the molecule environment.

Consider a molecule located on the surface at position $\vec{r}'$ in the vicinity. Let $\Delta\vec{r}'_{-} = \vec{r}'_{q_+} - \vec{r}'_{q_-}$ represent the length of the molecular Raman dipole, which corresponds to the vector difference between the positive charge q and the negative charge $-q$. To maintain equilibrium and balance the potential on the surface, two image point charges are present within the nanoparticle:

$$q_{+,in} = q\gamma\frac{R}{r'_{q_-}}, \qquad q_{-,in} = -q\gamma\frac{R}{r'_{q_+}} \tag{4.2.11}$$

Note that the image charge of a positive charge is negative, and *vice versa*. The position difference between the two image charges is:

$$\Delta\vec{r}'' = \vec{r}''_{q_+} - \vec{r}''_{q_-} = \left(\frac{R}{r'_{q_-}}\right)^2 \vec{r}'_{q_-} - \left(\frac{R}{r'_{q_+}}\right)^2 \vec{r}'_{q_+} \tag{4.2.12}$$

Since the position of the positive and negative charges in the Raman active molecule may not have the same distance to the origin, therefore in the exact solution, the image point charges may not be equal in the magnitude. To obtain an exact solution, the Green function is employed. The potential of the image charge throughout the entire space can be represented as:

$$\phi(\vec{r}, \omega_R) = \frac{1}{4\pi\epsilon_0}\gamma \int d^3r'' \left[\rho_{+,in}(\omega_R)\frac{\exp\left(ik\left|\vec{r} - \vec{r}''_{q_+}\right|\right)}{\left|\vec{r} - \vec{r}''_{q_+}\right|}\right.$$
$$\left. + \rho_{-,in}(\omega_R)\frac{\exp\left(ik\left|\vec{r} - \vec{r}''_{q_-}\right|\right)}{\left|\vec{r} - \vec{r}''_{q_-}\right|}\right] \tag{4.2.13}$$

where $\frac{\exp(ik|\vec{r}-\vec{r}''|)}{|\vec{r}-\vec{r}''|}$ is the Green function, which corresponds to the potential of a point charge. $\rho_{+,in}(\omega_R)$ and $\rho_{-,in}(\omega_R)$ are the charge densities for positive image charge and negative image charges inside the nanoparticle.

The Raman shifted electric field from the nanoparticle is given by:

$$\vec{E}_{sca}(\vec{r}, \omega_R) = -\nabla\phi(\vec{r}, \omega_R) \tag{4.2.14}$$

If $r'_{q_-} \approx r'_{q_+}$, which could be the following cases: the Raman dipole is small; the molecule is parallel to the surface; or the molecule is small compared to the nanoparticle. In this case, approximation can be applied:

$$\Delta\vec{r}'_- \approx -\Delta\vec{r}'\left(\frac{R}{r'}\right)^2, q_{in} \approx -q\gamma\frac{R}{r'} \tag{4.2.15}$$

Therefore, the image dipole density is straightforward:

$$\vec{P}_{in}(\vec{r}'', \omega_R) = \vec{P}_R(\vec{r}', \omega_R)\gamma\left(\frac{R}{r'}\right)^3 \tag{4.2.16}$$

The electric field is trivial from the radiation equation:

$$\vec{E}_{sca}(\vec{r}, \omega_R) = \frac{1}{4\pi\epsilon_0}\gamma\left(\frac{R}{R+d}\right)^3 \frac{\omega_R^2}{c^2 r^3}\vec{r} \times \left(\int \vec{P}_R(\vec{r}'', \omega_R)\, d^3r''\right) \times \vec{r}$$

$$= \frac{1}{4\pi\epsilon_0}\gamma\left(\frac{R}{R+d}\right)^3 \frac{\omega_R^2}{c^2 r^3}\vec{r} \times \alpha_{Raman} \int_{\Omega'} d\Omega'\, \vec{E}_{loc}(\theta', \varphi', \omega) \times \vec{r} \tag{4.2.17}$$

The integral in eq. 4.2.17 has been evaluated in eq. 4.2.8.

The enhancement factor is compared to the SERS signal without the presence of the gold nanoparticles (Regular Raman scattering, as RS):

$$EF = \frac{I_{SERS} n_{nanoparticle} + I_{RS} n_{molecule\_in\_solution}}{I_{RS} n_{total\_molecule}} \tag{4.2.18}$$

where I_{SERS} is the intensity for one nanoparticle, $n_{nanoparticle}$ is the number of nanoparticles in the solution. $n_{total\_molecule}$ is the number of the molecules in total, $n_{molecule\_in\_solution}$ is the number of the molecules in the solution. The relationship of the numbers are given below:

$$n_{molecule_{in_{solution}}} = n_{total_{molecule}} - n_{nanoparticle} n_{molecule\_per\_nanoparticle} \tag{4.2.19}$$

In the experiment, the enhancement factor is corrected by the concentration for the signal and the control experiment without the presense of the nanoparticle:

$$EF = \frac{I_{SERS} c_{RS}}{I_{RS} c_{SERS}} \tag{4.2.20}$$

The dielectric function of the gold nanoparticle is given by Ref. 231.

4.3. Results

To assess the theory in comparison to an experiment, we have chosen to examine the study conducted by Kneipp.[219] In their research, Crystal Violet (CV) was specifically selected as the analyte for the Surface-Enhanced Raman Scattering (SERS) experiment. The structure of CV is shown in Figure 4.2. The experiment involved the use of citric-stabilized gold nanoparticles illuminated by a 633 nm He-Ne laser. In the experiment, the range of CV concentration was from 1.0×10^{-6} to 1.0×10^{-5} mol/L; the radii range of the gold nanoparticles was from 7.5 nm to 20 nm; the number density of the gold nanoparticles was from 1.4×10^{15} to 1.4×10^{14}, as shown in Table 4.2. The enhancement factors was determined by comparing the scattering intensity of the CV with AuNP suspensions with conventional Raman scattering (RS) intensity observed for 5.0×10^{-4} mol/L CV. The enhancement factor was calculated with these concentrations using equation 4.2.20. Notably, Kneipp observed that the enhancement factor increased with an increase in the nanoparticle size or the concentration of CV.

Taking into account the aforementioned study, we have opted to utilize CV as our analyte in conjunction with the experimental parameters for our calculations. Additionally, we analyzed the relationship between the enhancement factor, nanoparticle radius, and CV concentration.

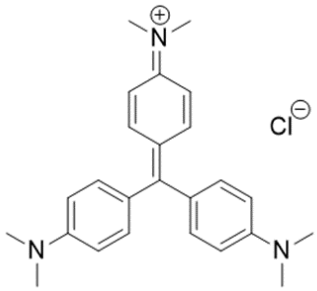

Figure 4.2 Crystal Violet structure and surface area calculations.

Table 4.1 Basic parameters for Crystal Violet (CV)

Resonance wavelength	592 nm
Raman shift	1605 cm^{-1}
Molecular surface area	4.5 nm2
Electronic damping frequency	1000 cm^{-1}
Molecular distance to the surface	2 Å

Table 4.2 The surface coverage and surface local concentration of CV on nanoparticles of different sizes

Nanoparticle radius (nm)	Nanoparticle number density (L^{-1})	Nanoparticle surface area (nm^2 L^{-1})	Molecules per nanoparticle*	Surface saturation concentration for 1 layer of perpendicular oriented CV (mol L^{-1}) *	Surface saturation concentration for 1 layer of parallel oriented CV (mol L^{-1}) *
7.5	1.4×10^{15}	1.0×10^{18}	1.6×10^{2}	3.6×10^{-7}	1.8×10^{-7}
10.0	8.6×10^{14}	1.1×10^{18}	2.8×10^{2}	6.5×10^{-7}	3.2×10^{-7}
12.5	5.1×10^{14}	1.1×10^{18}	2.8×10^{2}	1.0×10^{-6}	4.9×10^{-7}
15.0	3.2×10^{14}	1.1×10^{18}	2.8×10^{2}	1.4×10^{-6}	7.1×10^{-7}
17.5	2.1×10^{14}	1.1×10^{18}	2.8×10^{2}	1.9×10^{-6}	9.6×10^{-7}
20.0	1.4×10^{14}	7.0×10^{17}	1.1×10^{3}	2.6×10^{-6}	1.3×10^{-6}

*The molecule has a radius of 1.2 nm. The surface area is 4.5 nm^2 when parallel. Assuming one parallel oriented molecule can accommodate two perpendicular oriented molecules (with an average molecular distance of 1 nm). Therefore, the surface area for one molecule is estimated to be 2.3 nm^2 for a perpendicular oriented molecule.

4.3.1. Investigating the Relationship between Enhancement Factor and Nanoparticle Radii

Calculations using CCM were performed to determine the enhancement factor for various radii of nanoparticles, while keeping the CV concentration fixed. The experimental conditions associated with this calculation are outlined in Table 4.2.

Due to the typical high affinity constant between dye molecules and nanoparticles, our calculation assumes that all the dye molecules are located on the surface of the nanoparticle until the surface is completely saturated by one molecular layer. The equilibrium constant for Crystal Violet (CV) adsorption on a gold nanoparticle has not been reported. However, a similar molecule, rhodamine B, has been found to have an equilibrium constant $K = 2.51\times10^{8}$ L/mol on a 13 nm gold nanoparticle.[232] It can be assumed that nearly all the CV molecules are adsorbed on the nanoparticle below the saturation. If the concentration of CV exceeds the saturation concentration of the surface, the contribution of the excess molecules to the total dipole is not taken into consideration. In other words, we ignore multi-layer formation for this calculation.

The calculared enhancement compared to the experimental result is shown in Figure 4.3.

Analysis of Figure 4.3 reveals that the enhancement observed in the perpendicular orientation aligns more closely with the experimental results. However, as the particle radius increases, our model tends to underestimate the enhancement factor.

4.3.2. Relationship between Enhancement Factor and Crystal Violet concentration

Figure 4.4 shows the relationship between enhancement factors as a function of molecular concentration of the dye.The simulation shows relatively little dependence on concentration because the nanoparticles are saturated with dye.

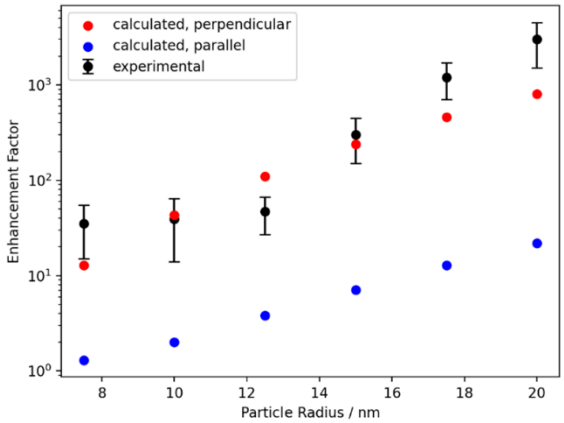

Figure 4.3 Comparison of calculated results for perpendicular orientation (red) CV and parallel orientation (blue) CV with experimental data (black with error bars). The CV concentration in the experiment is 5×10^{-6} mol L^{-1}.

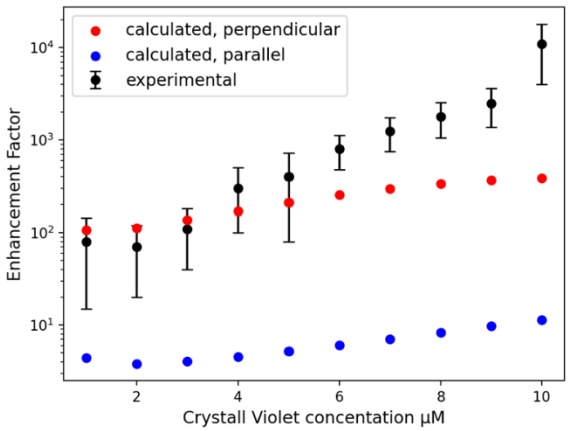

Figure 4.4 Comparison of calculated results for perpendicular orientation (red) CV with experimental data (black with error bars). The gold nanoparticle radius is 15 nm.

4.4. Discussion

Our results indicate that the radius of the nanoparticle is proportional of the SERS enhancement factor. Additionally, we observed that an increase in molecular concentration in the nanoparticle suspension leads to a higher EF.

4.4.1. The relation of the SERS EF and the CV concentrations

Our findings for lower CV concentrations exhibit good agreement with the experimental data reported by Kneipp and co-workers. However, for higher concentrations, our model yields significantly lower results compared to the experimental observations. This discrepancy can be attributed to the formation of multiple layers of CV molecules on the nanoparticle surface. Because we have assumed monolayer coverage in our model, the experimental appear to show an increase in enhancement above this level (Figure 4.4). Therefore, the observed increase in SERS EF proportional to concentration is less evident in the calculation. At relatively low concentrations, the entire surface area of the nanoparticles in the suspension will already be saturated for a monolayer model, as indicated in Table 4.2. Consequently, increasing the concentration does not contribute to the total Raman dipole of each nanoparticle but primarily affects the dielectric function. This may assist in amplifying the amplitude of the nanoparticle's surface plasmon through the relevant terms:

$$\frac{\epsilon_p(\omega) - \epsilon_{mol}(\omega)}{\epsilon_p(\omega) + 2\epsilon_{mol}(\omega)}, \qquad \frac{\epsilon_p(\omega_R) - \epsilon_{mol}(\omega_R)}{\epsilon_p(\omega_R) + \epsilon_{mol}(\omega_R)}$$

Absorption Scattering

The left term is proportional to the enhancement of the incident electric field and arises from the spherical geometry of the nanoparticle. The localized surface plasmon is excited when $\epsilon_p(\omega) = -2\epsilon_{mol}(\omega)$. The right term is proportional to the enhancement of the Raman-shifted field and is obtained from the boundary conditions using the image charge method. This term defines the surface plasmon for a planar geometry and is excited when $\epsilon_p(\omega_R) = -\epsilon_{mol}(\omega_R)$, as discussed in Chapter 3. The nanoparticle can be approximated as a planar surface because the molecular radius is at least 15 times smaller than any nanoparticle considered.

4.4.2. The relation of the molecular orientation and SERS EF

The magnitude of the SERS signal calculated using the CCM for parallel-oriented molecules is 30 to 100 times smaller than that for perpendicular-oriented molecules. This discrepancy may be attributed to the fact that on the equatorial region of the nanoparticle, that is, the scattered electric field from the nanoparticle at the incident frequency is parallel to the surface but in the opposite direction to the incident field, as shown in Figure 4.5. As a result, molecules with a parallel orientation on the equator may be less excited. On the other hand, although perpendicular-oriented molecules cannot be excited on the equator, the scattered electric field on the polar region is perpendicular to the surface and aligned with the direction of the incident field, leading to a stronger excitation of the perpendicular-oriented molecules. However, in the experiment, the orientation of the CV is not discussed. We could not assume CV is perpendicular on the surface. If the experiment has a parallel orientation, then the difference may be explained by chemical effect. For instance, metal-to-ligand charge transfer (MLCT) is a phenomenon that involves charge transfer from the plasmon band of the nanoparticle to the molecular π system.[143] Because the orbital overlap for a parallel oriented π system with the surface of the nanoparticle is much larger compared to that of a perpendicular oriented molecule, the chemical enhancement of the parallel oriented molecule should be larger in theory.

4.4.3. The relation of the SERS EF and the radius of the nanoparticle

Our findings regarding smaller nanoparticle radii exhibit good agreement with the experimental results reported by Kneipp and co-workers.[219] However, for larger nanoparticles, our model tends to underestimate the observed results. This discrepancy could potentially be attributed to the chemical enhancement effect. As the nanoparticle radius increases, the intensity

of the plasmon band also increases, thereby strengthening the MLCT. The chemical effect arises due to the mixing of wave functions between the molecule and the conductor surface, which is a quantum mechanical phenomenon. The CCM used in our calculations is purely based on electrostatics. Thus, it is reasonable to assume that the calculated enhancement is underestimated for larger nanoparticles due to the absence of the chemical effect.

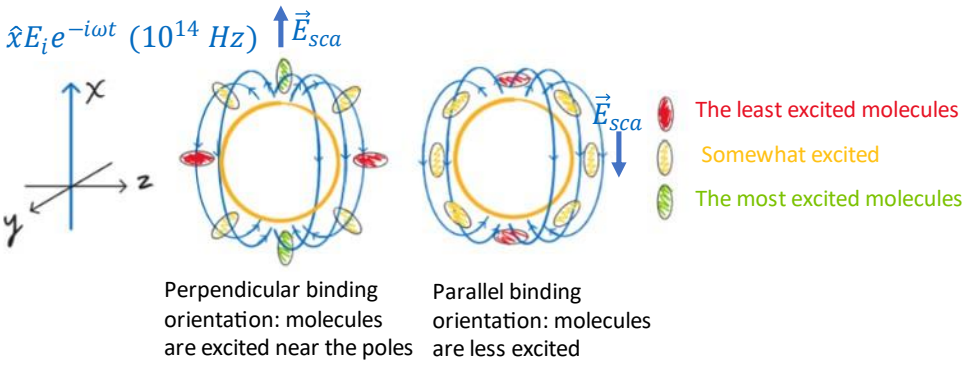

Figure 4.5 The geometry of different molecular orientation (left: perpendicular; right: parallel). The green color represents the molecules are excited the most by the local field, while the molecules with red color are not excited. The yellow colored molecules are partially excited.

Another important consideration is that when the nanoparticle size becomes larger, the assumption of purely electrostatic interactions may not hold. In such cases, it becomes necessary to incorporate Mie theory, and retardation potentials in conjunction with the CCM to accurately describe the optical properties and scattering behavior of the nanoparticle. By combining these two approaches, we can account for both the electromagnetic response of the nanoparticle and the influence of the surrounding medium, enabling a more comprehensive understanding of the system's behavior.

Nonetheless, the straightforward model provided by the CCM demonstrated agreement with experimental observations under low concentration and small nanoparticle limits. These results once again highlight the effectiveness of CCM and suggest its potential for explaining SERS enhancements even in scenarios with more intricate geometries. The success of CCM in these cases demonstrates its versatility and ability to be applied to more complex systems, offering promising prospects for further exploration and understanding of SERS phenomena.

CHAPTER 5. CCM applied on SERS associated with planar conductors

5.1. Introduction

The study of surface enhanced Raman scattering (SERS) signals has predominantly focused on surfaces that are roughened or modified with silver or gold nanoparticles.[11,64,65,67,80] These approaches led to reported significant enhancements in signal intensity up to 10^{15}.[11,233] The investigation of the SERS signal on smooth planar conductors has been limited. The difficulty of proper experimental geometry for detection of Raman scattering and predicted small enhancements have dissuaded scientists from exploring these effects. While Raman scattering from planar surfaces has been observed there are no reliable experimental measurements of the enhancement factor needed for SERS.[234] Despite the lack of data, there have been a number of theoretical studies of SERS enhancement on smooth planar surfaces.[234] Examining the smooth planar case can provide valuable insight into the underlying enhancement mechanism. In previous theoretical studies of planar SERS, the enhancement factors were obtained directly from the local field enhancement through Maxwell's equations,[235], as described in Chapter 4. The interaction between the molecule and the conductor is usually ignored. The reason is that the molecular Raman signal is obtained from electronic structural methods based on quantum mechanics. There is as yet no consistent way to describe SERS by a quantum mechanical model. Our approach has been to study the electrostatic interaction of a nanoparticle and molecule using CCM and to neglect chemical enhancement.

In this study, we employed the classical correlation model (CCM) to investigate the molecular Raman signal and SERS enhancement as it would appear on a smooth planar surface.

As discussed in Chapter 2, the CCM provides an accurate description of Raman scattering comparable to the Kramers-Heisenberg-Dirac formula. It introduces an electron-

vibration coupling term in the spring constant of a Lorentz spring-mass model of the electronic transition dipole. Moreover, the CCM successfully incorporates a planar conductor with surface plasmon polaritons, as demonstrated in Chapter 3. Using the CCM we modeled a N_2O surface enhanced infrared absorption (SEIRA) signal with rotational-vibrational coupling. The conducting surface was a doped-CdO thin film selected for its mid-IR plasmon that could couple to asymmetric stretching absorption of N_2O. The model is an extension of surface plasmon resonance (SPR) in the Kretschmann configuration. As presented previously, the Kretschmann configuration is widely used to calculate frequency shifts in surface plasmon polaritons. It also been used to calculate the theoretical enhancement in SERS experiments on a planar conductor.[234] The CCM model calculation of the SEIRA enhancement factor agreed very well with experimental results obtained in our laboratory.[45,236] In Chapter 4, we achieved successful application of the CCM to analyze the SERS signal obtained from nanoparticles. The enhancement factor we calculated demonstrated good alignment for molecules with concentrations below 5 μM and nanoparticle radii under 15 nm.

To further explore the widely studied SERS geometry of immobilized nanoparticles on a planar conductor,

in the subsequent sections of this chapter, the molecular component of the Raman scattered light will be directly obtained using the CCM. The response of the conducting surface will be evaluated under boundary conditions. By combining these two components, the Raman scattered signal can be modeled, to provide a comprehensive understanding of the electromagnetic enhancement mechanism.

5.2. Theory

The conventional approach for calculating the Raman scattered light at position $\vec{r}$ is to evaluate the scattered electric field from the integral of the dipole density $\vec{P}_R(\vec{r}', \omega_R)$ over the entire volume of interest at $\vec{r}'$, as well as the integral of the induced dipole density at $\vec{r}''$ in the conductor provided by image charge method. The Raman scattered field from the molecular layer is given by:

$$\vec{E}_{mol}(\vec{r}, \omega_R) = \frac{1}{4\pi\epsilon_0} \int \left\{ \frac{\omega_R^2}{c^2|\vec{r} - \vec{r}'|^3} (\vec{r} - \vec{r}') \times \left(\vec{P}_R(\vec{r}', \omega_R) \times (\vec{r} - \vec{r}') \right) \right.$$
$$+ \left[\frac{1}{|\vec{r} - \vec{r}'|^5} - \frac{i\omega_R}{c|\vec{r} - \vec{r}'|^4} \right] \left[3(\vec{r} - \vec{r}') \left((\vec{r} - \vec{r}') \cdot \vec{P}_R(\vec{r}', \omega_R) \right) \right.$$
$$\left. \left. - \vec{P}_R(\vec{r}', \omega_R) \right] \right\} e^{i(\vec{k}_R \cdot (\vec{r} - \vec{r}') - \omega_R t)} \, d^3\vec{r}' \qquad (5.2.1)$$

In the far field regime, i.e. when $r \gg r'$ and r'':

$$\vec{E}_{mol}(\vec{r}, \omega_R) = \frac{1}{4\pi\epsilon_0} \frac{\omega_R^2}{c^2 r^3} \int \left[(\vec{r} - \vec{r}') \times \left(\vec{P}_R(\vec{r}', \omega_R) \times (\vec{r} - \vec{r}') \right) \right] e^{i(\vec{k}_R \cdot (\vec{r} - \vec{r}') - \omega_R t)} \, d^3\vec{r}' \qquad (5.2.2)$$

The Raman shifted field from the conductor can be solved by boundary conditions, from image charge method, however, the number of image charges will expand and become more complicated.[237] Moreover, the obtained result is a numerical solution that offers limited physical insight. Notably, the equation above requires different sets of image charges for different detector locations. To overcome these limitations, an alternative approach was pursued. In this context, a key consideration is the inclusion of an additional term, the Raman susceptibility χ_R, in the dielectric function of the Raman active layer, corresponding to the Raman polarizability.

$$\epsilon_r = \epsilon_{r0} + \chi_R = 1 + \chi_0 + \chi_R \qquad (5.2.3)$$

where:

$$\chi_R = \frac{n\alpha_{Raman}}{\epsilon_0} \tag{5.2.4}$$

In Chapter 2, we showed that α_{Raman} possesses the capability to alter the frequency of the source wave from ω to the Raman shifted wave ω_R. As an illustration, the Raman dipole and dipole density can be obtained from the incident light at the laser frequency, ω, $\vec{E}_i(\omega) = \vec{E}_{i0}e^{-i\omega t}$:

$$\vec{p}_R(\omega_R) = \epsilon_0\alpha_{Raman}\vec{E}_i(\omega) \tag{5.2.5}$$

$$\vec{P}_R(\omega_R) = \epsilon_0\chi_R\vec{E}_i(\omega) \tag{5.2.6}$$

Assuming the molecular layer has a thickness much smaller than the wavelength of the propagating light source $\vec{E}_i(\vec{k},\omega)$ the resulting Raman-shifted light becomes homogeneous throughout the material, denoted as $\vec{E}_R(\vec{k}_R,\omega_R) = \vec{E}_{R0}e^{i\vec{k}_R\cdot\vec{r}\,-i\omega_R t}$. Since the Raman-shifted frequency ω_R is lower than ω, the wavelength of the Raman-shifted light is slightly longer than that of the source $\vec{E}_i(\vec{k},\omega)$. In this region, the difference between $\vec{k}_R$ and $\vec{k}$ is small. Therefore, it is reasonable to expand the function χ_R to include a wavevector shift from $\vec{k}$ to $\vec{k}_R$.

$$\vec{P}_R(\vec{k}_R,\omega_R) = \epsilon_0\chi_R\vec{E}_i(\vec{k},\omega) \tag{5.2.7}$$

On the other hand, the Raman-shifted electric field contributes to the dipole density through the conventional susceptibility as well:

$$\vec{P}_0(\vec{k}_R,\omega_R) = \epsilon_0\chi_0\vec{E}_R(\vec{k}_R,\omega_R) \tag{5.2.8}$$

The total dipole density at the Raman shifted frequency is:

$$\vec{P}(\vec{k}_R,\omega_R) = \vec{P}_R(\vec{k}_R,\omega_R) + \vec{P}_0(\vec{k}_R,\omega_R) = \epsilon_0\chi_R\vec{E}_i(\vec{k},\omega) + \epsilon_0\chi_0\vec{E}_R(\vec{k}_R,\omega_R) \tag{5.2.9}$$

Consequently, the displacement field at the Raman shifted frequency is:

$$\vec{D}_R(\vec{k}_R,\omega_R) = \vec{D}_0(\vec{k}_R,\omega_R) + \vec{P}_R(\vec{k}_R,\omega_R) = \epsilon_0\left(\epsilon_{r0}\vec{E}_R(\vec{k}_R,\omega_R) + \chi_R(\vec{k},\omega)\right) \tag{5.2.10}$$

By applying the defined displacement field to the wave equation (details see Appendix 9), the dispersion relation in the Raman active layer is obtained:

$$\left|\vec{k}_R\right|^2 = \frac{\omega_R^2}{c^2}\left(\epsilon_{r0} + \frac{\chi_R \vec{E}_0(\vec{k},\omega)}{\vec{E}_R(\vec{k}_R,\omega_R)}\right) \tag{5.2.11}$$

An equivalent dielectric function could be defined for the Raman layer:

$$\epsilon_{rR} = \epsilon_{r0} + \frac{\chi_R \vec{E}_0(\vec{k},\omega)}{\vec{E}_R(\vec{k}_R,\omega_R)} \tag{5.2.12}$$

Therefore, the dispersion relation for the Raman shifted frequency reads:

$$\left|\vec{k}_R\right|^2 = \frac{\omega_R^2}{c^2}\epsilon_{rR} \tag{5.2.13}$$

According to eq. 5.2.8, the local field at Raman shifted frequency $\vec{E}_R$ is obtained from the surrounding Raman active molecules, by considering the near-field term in the dipole scattering equation, where the difference between $\vec{r}$ and $\vec{r}'$ is small. By applying the near-field approximation, only the electrostatic term is retained:

$$\begin{aligned}\vec{E}_R(\vec{r}) = \int \frac{\omega_R^2}{c^2|\vec{r}-\vec{r}'|^3}(\vec{r}-\vec{r}') \times \left(\vec{P}_R(\vec{k}_R,\omega_R) \times (\vec{r}-\vec{r}')\right) \\ + \left[\frac{1}{|\vec{r}-\vec{r}'|^5} - \frac{i\omega_R}{c|\vec{r}-\vec{r}'|^4}\right]\left[3(\vec{r}-\vec{r}')\left((\vec{r}-\vec{r}')\cdot\vec{P}_R(\vec{k}_R,\omega_R)\right)\right. \\ \left. - \vec{P}_R(\vec{k}_R,\omega_R)\right] d^3\vec{r}'\end{aligned} \tag{5.2.14}$$

Based on this approach, the direction of $\vec{E}_R$ is found to be opposite to the incident field $\vec{E}_i$. This is in accordance with the principle of energy conservation.

Using definition of the dielectric function and local field, the Raman signal can be directly calculated from the Fresnel equations for reflectance and transmittance (see Appendix 10).

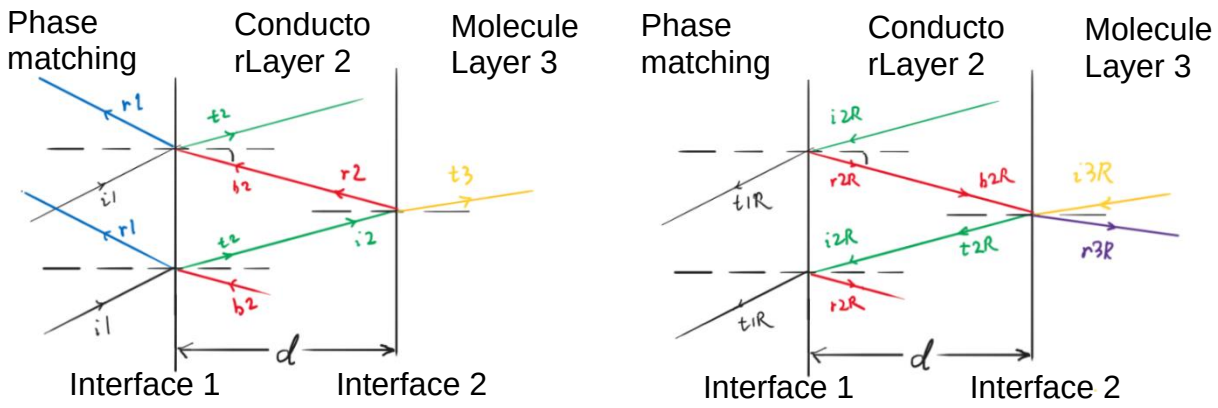

Figure 5.1 The wave propagation in Kretschmann configuration for the source wave (left) and the Raman shifted wave (right) respectively

In order to calculate the Raman signal, we employ the Kretschmann configuration, as depicted in Figure 5.1. As discussed in Chapter 3, Layer 1 is referred to as a phase matching model, designed to produce an attenuated wave within the conducting layer. This attenuated wave serves to excite the surface plasmon on the interface between the conducting layer and the Raman-active molecule layer. Once the surface plasmon excites the Raman-active molecules, another surface plasmon can be excited on the surface at the Raman-shifted frequency.

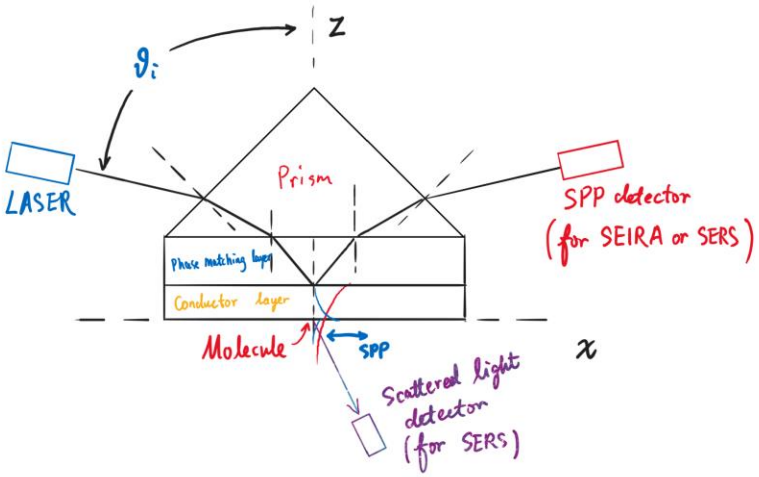

Figure 5.2 Kretschmann configuration. The detector for SERS can be on either the Laser side (red), or the molecular side (purple).

If the detector is on the laser side (see Figure 5.2), the electric field of the Raman scattered wave is given by:

$$E_{t1R} = \frac{\chi_R t_{321R} t_{123}}{(\epsilon_{rR} - \epsilon_{r0})(1 + r_{321R})} E_{i1} \tag{5.2.15}$$

If the detector is on the molecular side or sample side, the electric field of the Raman scattered wave reads:

$$E_{r3R} = \frac{\chi_R r_{321R}}{(\epsilon_{rR} - \epsilon_{r0})(1 + r_{321R})} E_{i1} \tag{5.2.16}$$

where E_{i1} is the incident source wave, t_{123} is the transmittance for the source wave, r_{321R} and t_{321R} are the reflectance and transmittance for the Raman scattered wave. The deriviation is given in Appendix 10.

Because the r3R is a propagated wave only without the surface plasmon, the signal on the molecular side is considered weak. The Raman signal is observed to be larger on the laser side than the sample side of the planar surface.[234]

5.3. Conclusion

Future work needed to understand the nanoparticle-roughened planar geometry involves two main tasks: completing the implementation of the CCM on a planar conductor and integrating the CCM with the nanoparticle to develop a comprehensive model that can explain the enhancements observed in SERS, and further enhances our understanding of SERS phenomena and provide valuable insights into the mechanisms that drive SERS enhancements.

REFERENCES

(1) Pines, D. Collective Energy Losses in Solids. *Rev. Mod. Phys.* **1956**, *28*, 184–198.

(2) Maier, S. A. *Plasmonics: Fundamentals and Applications*; 2007.

(3) Jackson, J. D. Classical Electrodynamics. American Association of Physics Teachers 1999.

(4) Drude, P. Zur Elektronentheorie Der Metalle. *Ann. Phys.* **1900**, *306*, 566–613.

(5) Drude, P. Zur Elektronentheorie Der Metalle; II. Teil. Galvanomagnetische Und Thermomagnetische Effecte. *Ann. Phys.* **1900**, *308*, 369–402.

(6) Kittel, C.; McEuen, P.; McEuen, P. *Introduction to Solid State Physics*; Wiley New York, 1996; Vol. 8.

(7) Kretschmann, E.; Raether, H. Radiative Decay of Non Radiative Surface Plasmons Excited by Light. *Zeitschrift Fur Naturforsch. Part a-Astrophysik Phys. Und Phys. Chemie* **1968**, *A 23*, 2135-.

(8) Otto, A. Excitation of Non-Radiative Surface Plasma Waves in Silver by Method of Frustrated Total Reflection. *Z Phys* **1968**, *216*, 398-.

(9) Sonnefraud, Y.; Leen Koh, A. L.; McComb, D. W.; Maier, S. A. Nanoplasmonics: Engineering and Observation of Localized Plasmon Modes. *Laser Photonics Rev.* **2012**, *6*, 277–295.

(10) Schrader, B. *Infrared and Raman Spectroscopy: Methods and Applications*; John Wiley & Sons, 2008.

(11) Nie, S. M.; Emery, S. R. Probing Single Molecules and Single Nanoparticles by Surface-Enhanced Raman Scattering. *Science (80-.).* **1997**, *275*, 1102–1106.

(12) Sijtsema, N. M.; Wouters, S. D.; Grauw, C. J. De; Otto, C.; Greve, J. Confocal Direct Imaging Raman Microscope: Design and Applications in Biology. *Appl. Spectrosc.* **1998**, *52*, 348–355.

(13) Motz, J. T.; Hunter, M.; Galindo, L. H.; Gardecki, J. A.; Kramer, J. R.; Dasari, R. R.; Feld, M. S. Optical Fiber Probe for Biomedical Raman Spectroscopy. *Appl. Opt.* **2004**, *43*, 542–554.

(14) Wandinger, U. Raman Lidar BT - Lidar: Range-Resolved Optical Remote Sensing of the Atmosphere; Weitkamp, C., Ed.; Springer New York: New York, NY, 2005; pp 241–271.

(15) Aroca, R. F.; Ross, D. J.; Domingo, C. Surface-Enhanced Infrared Spectroscopy. *Appl. Spectrosc.* **2004**, *58*, 9325.

(16) Hartstein, A.; Kirtley, J. R.; Tsang, J. C. Enhancement of the Infrared Absorption from Molecular Monolayers with Thin Metal Overlayers. *Phys. Rev. Lett.* **1980**, *45*, 201.

(17) Hatta, A.; Ohshima, T.; Suëtaka, W. Observation of the Enhanced Infrared Absorption of P-Nitrobenzoate on Ag Island Films with an ATR Technique. *Appl. Phys. A Solids Surf.* **1982**, *29*, 71.

(18) Hatta, A.; Suzuki, Y.; Suëtaka, W. Infrared Absorption Enhancement of Monolayer Species on Thin Evaporated Ag Films by Use of a Kretschmann Configuration: Evidence for Two Types of Enhanced Surface Electric Fields. *Appl. Phys. A Solids Surfaces* **1984**, *35*, 135–140.

(19) Chen, C. Y.; Burstein, E.; Lundquist, S. Giant Raman Scattering by Pyridine and CN- Adsorbed on Silver. *Solid State Commun.* **1979**, *32*, 63–66.

(20) King, F. W.; Vanduyne, R. P.; Schatz, G. C. Theory of Raman-Scattering by Molecules Adsorbed on Electrode Surfaces. *J. Chem. Phys.* **1978**, *69*, 4472–4481.

(21) Devlin, J. P.; Consani, K. Metal Surface Spectroscopy. Charge Transfer and Totally Symmetric Mode Activity. *J. Phys. Chem.* **1981**, *85*, 2597–2598.

(22) Dumas, P.; Tobin, R. G.; Richards, P. L. Study of Adsorption States and Interactions of CO on Evaporated Noble Metal Surfaces by Infrared Absorption Spectroscopy. I. Silver. *Surf. Sci.* **1986**, *171*, 555–578.

(23) Pettenkofer, C.; Mrozek, I.; Bornemann, T.; Otto, A. On the Contribution of Classical Electromagnetic Field Enhancement to Raman Scattering from Adsorbates on Coldly Deposited Silver Films. *Surf. Sci.* **1987**, *188*, 519–556.

(24) Wadayama, T.; Sakurai, T.; Ichikawa, S.; Suëtaka, W. Charge-Transfer Enhancement in Infrared Absorption of Thiocyanate Ions Adsorbed on a Gold Electrode in the Kretschmann ATR Configuration. *Surf. Sci.* **1988**, *198*, 359–364.

(25) Bjerke, A. E.; Griffiths, P. R.; Theiss, W. Surface-Enhanced Infrared Absorption of CO on Platinized Platinum. *Anal. Chem.* **1999**, *71*, 1967.

(26) Osawa, M. Dynamic Processes in Electrochemical Reactions Studied by Surface-Enhanced Infrared Absorption Spectroscopy (SEIRAS). *Bull. Chem. Soc. Jpn.* **1997**, *70*, 2861–2880.

(27) Zheng, M.-S.; Sun, S.-G.; Chen, S.-P. Abnormal Infrared Effects and Electrocatalytic Properties of Nanometer Scale Thin Film of PtRu Alloys for CO Adsorption and Oxidation. *J. Appl. Electrochem.* **2001**, *31*, 749.

(28) Hahn, F.; Melendres, C. Anodic Oxidation of Methane at Noble Metal Electrodes: An “in Situ” Surface Enhanced Infrared Spectroelectrochemical Study. *Electrochim. Acta* **2001**, *46*, 3525.

(29) Priebe, A.; Sinther, M.; Fahsold, G.; Pucci, A. The Correlation between Film Thickness and Adsorbate Line Shape in Surface Enhanced Infrared Absorption. *J. Chem. Phys.* **2003**, *119*, 4887.

(30) Priebe, A.; Fahsold, G.; Pucci, A. Strong Pyramidal Growth of Metal Films Studied with IR Transmittance and Surface Enhanced IR Absorption of CO. *J. Phys. Chem. B* **2004**, *108*, 18174.

(31) Shelton, D. J.; Brener, I.; Ginn, J. C.; Sinclair, M. B.; Peters, D. W.; Coffey, K. R.; Boreman, G. D. Strong Coupling between Nanoscale Metamaterials and Phonons. *Nano Lett.* **2011**, *11*, 2104.

(32) Shahzad, M.; Medhi, G.; Peale, R. E.; Buchwald, W. R.; Cleary, J. W.; Soref, R.; Boreman, G. D.; Edwards, O. Infrared Surface Plasmons on Heavily Doped Silicon. *J. Appl. Phys.* **2011**, *110*.

(33) Chou, L.-W.; Shin, N.; Sivaram, S. V; Filler, M. A. Tunable Mid-Infrared Localized Surface Plasmon Resonances in Silicon Nanowires. *J. Am. Chem. Soc.* **2012**, *134*, 16155–16158.

(34) Fischer, M. P.; Schmidt, C.; Sakat, E.; Stock, J.; Samarelli, A.; Frigerio, J.; Ortolani, M.; Paul, D. J.; Isella, G.; Leitenstorfer, A.; Biagioni, P.; Brida, D. Optical Activation of Germanium Plasmonic Antennas in the Mid-Infrared. *Phys. Rev. Lett.* **2016**, *117*.

(35) Samarelli, A.; Frigerio, J.; Sakat, E.; Baldassarre, L.; Gallacher, K.; Finazzi, M.; Isella, G.; Ortolani, M.; Biagioni, P.; Paul, D. J. Fabrication of Mid-Infrared Plasmonic Antennas Based on Heavily Doped Germanium Thin Films. *Thin Solid Films* **2016**, *602*, 52–55.

(36) Aroca, R.; Price, B. A New Surface for Surface-Enhanced Infrared Spectroscopy: Tin Island Films. *J. Phys. Chem. B* **1997**, *101*, 6537.

(37) Stolz, A.; Considine, L.; Faci, S.; Dogheche, E.; Tripon-Canseliet, C.; Loiseaux, B.; Pavlidis, D.; Decoster, D.; Chazelas, J. Gallium-Nitride-Based Plasmonic Multilayer Operating at 1.55 Mu M. *Opt. Lett.* **2012**, *37*, 3039–3041.

(38) KOZAWA, T.; KACHI, T.; KANO, H.; TAGA, Y.; HASHIMOTO, M.; KOIDE, N.; MANABE, K. RAMAN-SCATTERING FROM LO PHONON-PLASMON COUPLED MODES IN GALLIUM NITRIDE. *J. Appl. Phys.* **1994**, *75*, 1098–1101.

(39) Songprakob, W.; Zallen, R.; Liu, W. K.; Bacher, K. L. Infrared Studies of Hole-Plasmon Excitations in Heavily-Doped p-Type MBE-Grown GaAs : C. *Phys. Rev. B* **2000**, *62*, 4501–4510.

(40) Law, S.; Adams, D. C.; Taylor, A. M.; Wasserman, D. Mid-Infrared Designer Metals. *Opt Express* **2012**, *20*, 12155–12165.

(41) Law, S.; Yu, L.; Rosenberg, A.; Wasserman, D. All-Semiconductor Plasmonic Nanoantennas for Infrared Sensing. *NANO Lett.* **2013**, *13*, 4569–4574.

(42) Naik, G. V; Kim, J.; Boltasseva, A. Oxides and Nitrides as Alternative Plasmonic Materials in the Optical Range Invited. *Opt. Mater. Express* **2011**, *1*, 1090–1099.

(43) Noginov, M. A.; Gu, L.; Livenere, J.; Zhu, G.; Pradhan, A. K.; Mundle, R.; Bahoura, M.; Barnakov, Y. A.; Podolskiy, V. A. Transparent Conductive Oxides : Plasmonic Materials for Telecom Wavelengths. **2011**, *021101*, 2011–2013.

(44) Brewer, S. H.; Franzen, S. Indium Tin Oxide Plasma Frequency Dependence on Sheet Resistance and Surface Adlayers Determined by Reflectance FTIR Spectroscopy. *J. Phys. Chem. B* **2002**, *106*, 12986–12992.

(45) Sachet, E.; Aspnes, D. E.; Maria, J.-P.; Franzen, S. Critical Test of the Interaction of Surface Plasmon Resonances with Molecular Vibrational Transitions. *J. Phys. Chem. A* **2020**, *124*, 1744–1753.

(46) Sachet, E.; Shelton, C. T.; Harris, J. S.; Gaddy, B. E.; Irving, D. L.; Curtarolo, S.; Donovan, B. F.; Hopkins, P. E.; Sharma, P. A.; Sharma, A. L.; Ihlefeld, J.; Franzen, S.; Maria, J. P. Dysprosium-Doped Cadmium Oxide as a Gateway Material for Mid-Infrared Plasmonics. *Nat Mater* **2015**, *14*, 414–420.

(47) Jablan, M.; Buljan, H.; Soljacic, M. Plasmonics in Graphene at Infrared Frequencies. *Phys Rev B* **2009**, *80*.

(48) Chen, J.; Badioli, M.; Alonso-González, P.; Thongrattanasiri, S.; Huth, F.; Osmond, J.; Spasenović, M.; Centeno, A.; Pesquera, A.; Godignon, P. Optical Nano-Imaging of Gate-Tunable Graphene Plasmons. *Nature* **2012**, *487*, 77.

(49) Osawa, M.; Ataka, K.-I.; Yoshii, K.; Nishikawa, Y. Surface-Enhanced Infrared Spectroscopy: The Origin of the Absorption Enhancement and Band Selection Rule in the Infrared Spectra of Molecules Adsorbed on Fine Metal Particles. *Appl. Spectrosc.* **1993**, *47*, 1497–1502.

(50) Neubrech, F.; Huck, C.; Weber, K.; Pucci, A.; Giessen, H. Surface-Enhanced Infrared Spectroscopy Using Resonant Nanoantennas. *Chem. Rev.* **2017**, *117*, 5110–5145.

(51) Srajer, J.; Schwaighofer, A.; Ramer, G.; Rotter, S.; Guenay, B.; Kriegner, A.; Knoll, W.; Lendl, B.; Nowak, C. Double-Layered Nanoparticle Stacks for Surface Enhanced Infrared Absorption Spectroscopy. *Nanoscale* **2014**, *6*, 127.

(52) Sun, L.; Siepmann, J. I.; Schure, M. R. Conformation and Solvation Structure for an Isolated N-Octadecane Chain in Water, Methanol, and Their Mixtures. *J. Phys. Chem. B* **2006**, *110*, 10519–10525.

(53) Neubrech, F.; Pucci, A.; Cornelius, T. W.; Karim, S.; Garcia-Etxarri, A.; Aizpurua, J. Resonant Plasmonic and Vibrational Coupling in a Tailored Nanoantenna for Infrared Detection. *Phys. Rev. Lett.* **2008**, *101*.

(54) Yin, H.; Li, N.; Si, Y.; Zhang, H.; Yang, B.; Wang, J. Gold Nanonails for Surface-

Enhanced Infrared Absorption. *Nanoscale Horizons* **2020**, *5*, 1200–1212.

(55) Milekhin, A. G.; Cherkasova, O.; Kuznetsov, S. A.; Milekhin, I. A.; Rodyakina, E. E.; Latyshev, A. V; Banerjee, S.; Salvan, G.; Zahn, D. R. T. Nanoantenna-Assisted Plasmonic Enhancement of IR Absorption of Vibrational Modes of Organic Molecules. *BEILSTEIN J. Nanotechnol.* **2017**, *8*, 975–981.

(56) Kundu, J.; Le, F.; Nordlander, P.; Halas, N. J. Surface Enhanced Infrared Absorption (SEIRA) Spectroscopy on Nanoshell Aggregate Substrates. *Chem. Phys. Lett.* **2008**, *452*, 115–119.

(57) Fano, U. EFFECTS OF CONFIGURATION INTERACTION ON INTENSITIES AND PHASE SHIFTS. *Phys. Rev.* **1961**, *124*, 1866-.

(58) Adato, R.; Aksu, S.; Altug, H. Engineering Mid-Infrared Nanoantennas for Surface Enhanced Infrared Absorption Spectroscopy. *Mater. Today* **2015**, *18*, 436.

(59) Novotny, L. Strong Coupling, Energy Splitting, and Level Crossings: A Classical Perspective. *Am. J. Phys.* **2010**, *78*, 1199–1202.

(60) Adato, R.; Altug, H. In-Situ Ultra-Sensitive Infrared Absorption Spectroscopy of Biomolecule Interactions in Real Time with Plasmonic Nanoantennas. *Nat. Commun.* **2013**, *4*, 2154.

(61) Neubrech, F.; Huck, C.; Weber, K.; Pucci, A.; Giessen, H. Surface-Enhanced Infrared Spectroscopy Using Resonant Nanoantennas. *Chem. Rev.* **2017**, *117*, 5110–5145.

(62) Pilot, R.; Signorini, R.; Durante, C.; Orian, L.; Bhamidipati, M.; Fabris, L. A Review on Surface-Enhanced Raman Scattering. *Biosensors* **2019**, *9*, 57.

(63) Fleischmann, M.; Hendra, P. J.; McQuillan, A. J. Raman Spectra of Pyridine Adsorbed at a Silver Electrode. *Chem. Phys. Lett.* **1974**, *26*, 163–166.

(64) Jeanmaire, D. L.; Van Duyne, R. P. Surface Raman Spectroelectrochemistry: Part I. Heterocyclic, Aromatic, and Aliphatic Amines Adsorbed on the Anodized Silver Electrode. *J. Electroanal. Chem. Interfacial Electrochem.* **1977**, *84*, 1.

(65) Albrecht, M. G.; Creighton, J. A. Anomalously Intense Raman Spectra of Pyridine at a Silver Electrode. *J. Am. Chem. Soc.* **1977**, *99*, 5215–5217.

(66) Kneipp, K.; Wang, Y.; Kneipp, H.; Perelman, L. T.; Itzkan, I.; Dasari, R.; Feld, M. S. Single Molecule Detection Using Surface-Enhanced Raman Scattering (SERS). *Phys. Rev. Lett.* **1997**, *78*, 1667–1670.

(67) Dasary, S. S. R.; Singh, A. K.; Senapati, D.; Yu, H.; Ray, P. C. Gold Nanoparticle Based Label-Free SERS Probe for Ultrasensitive and Selective Detection of Trinitrotoluene. *J. Am. Chem. Soc.* **2009**, *131*, 13806–13812.

(68) Sztainbuch, I. W. The Effects of Au Aggregate Morphology on Surface-Enhanced Raman Scattering Enhancement. *J. Chem. Phys.* **2006**, *125*.

(69) Brolo, A. G.; Irish, D. E.; Szymanski, G.; Lipkowski, J. Relationship between SERS Intensity and Both Surface Coverage and Morphology for Pyrazine Adsorbed on a Polycrystalline Gold Electrode. *Langmuir* **1998**, *14*, 517–527.

(70) Kneipp, K.; Dasari, R. R.; Wang, Y. Near-Infrared Surface-Enhanced Raman-Scattering (Nir Sers) on Colloidal Silver and Gold. *Appl. Spectrosc.* **1994**, *48*, 951–957.

(71) Chen, L.; Yu, J.; Fujita, T.; Chen, M. Nanoporous Copper with Tunable Nanoporosity for SERS Applications. *Adv. Funct. Mater.* **2009**, *19*, 1221–1226.

(72) Cejkova, J.; Prokopec, V.; Brazdova, S.; Kokaislova, A.; Matejka, P.; Stepanek, F. Characterization of Copper SERS-Active Substrates Prepared by Electrochemical Deposition. *Appl. Surf. Sci.* **2009**, *255*, 7864–7870.

(73) Mahajan, S.; Baumberg, J. J.; Russell, A. E.; Bartlett, P. N.; Abdelsalam, M. E. SERS at Structured Palladium and Platinum Surfaces. *J. Am. Chem. Soc.* **2007**, *129*, 7399–7406.

(74) Lai, S. C. S.; Kleyn, S. E. F.; Rosca, V.; Koper, M. T. M. Mechanism of the Dissociation and Electrooxidation of Ethanol and Acetaldehyde on Platinum as Studied by SERS. *J. Phys. Chem. C* **2008**, *112*, 19080–19087.

(75) Tkachenko, A. G.; Xie, H.; Coleman, D.; Glomm, W.; Ryan, J.; Anderson, M. F.; Franzen, S.; Feldheim, D. L. Multifunctional Gold Nanoparticle-Peptide Complexes for Nuclear Targeting. *J. Am. Chem. Soc.* **2003**, *125*, 4700–4701.

(76) Ren, B.; Lin, X. F.; Yang, Z. L.; Liu, G. K.; Aroca, R. F.; Mao, B. W.; Tian, Z. Q. Surface-Enhanced Raman Scattering in the Ultraviolet Spectral Region: UV-SERS on Rhodium and Ruthenium Electrodes. *J. Am. Chem. Soc.* **2003**, *125*, 9598–9599.

(77) Bilmes, S. A. SERS of Pyridine Adsorbed on Rhodium Electrodes. *Chem. Phys. Lett.* **1990**, *171*, 141–146.

(78) Li, A.; Lin, J.; Huang, Z.; Wang, X.; Guo, L. Surface-Enhanced Raman Spectroscopy on Amorphous Semiconducting Rhodium Sulfide Microbowl Substrates. *Iscience* **2018**, *10*, 1–10.

(79) Li, J.-F.; Anema, J. R.; Yu, Y.-C.; Yang, Z.-L.; Huang, Y.-F.; Zhou, X.-S.; Ren, B.; Tian, Z.-Q. Core–Shell Nanoparticle Based SERS from Hydrogen Adsorbed on a Rhodium (111) Electrode. *Chem. Commun.* **2011**, *47*, 2023–2025.

(80) Tian, S.; Neumann, O.; McClain, M. J.; Yang, X.; Zhou, L.; Zhang, C.; Nordlander, P.; Halas, N. J. Aluminum Nanocrystals: A Sustainable Substrate for Quantitative SERS-Based DNA Detection. *Nano Lett.* **2017**, *17*, 5071–5077.

(81) Kudelski, A.; Grochala, W.; Janik-Czachor, M.; Bukowska, J.; Szummer, A.; Dolata, M.

Surface-enhanced Raman Scattering (SERS) at Copper (I) Oxide. *J. Raman Spectrosc.* **1998**, *29*, 431–435.

(82) Wu, H.; Wang, H.; Li, G. Metal Oxide Semiconductor SERS-Active Substrates by Defect Engineering. *Analyst* **2017**, *142*, 326–335.

(83) Zheng, Z.; Cong, S.; Gong, W.; Xuan, J.; Li, G.; Lu, W.; Geng, F.; Zhao, Z. Semiconductor SERS Enhancement Enabled by Oxygen Incorporation. *Nat. Commun.* **2017**, *8*, 1–10.

(84) Muehlethaler, C.; Considine, C. R.; Menon, V.; Lin, W. C.; Lee, Y. H.; Lombardi, J. R. Ultrahigh Raman Enhancement on Monolayer MoS2. *Acs Photonics* **2016**, *3*, 1164–1169.

(85) Xu, W.; Mao, N.; Zhang, J. Graphene: A Platform for Surface-enhanced Raman Spectroscopy. *Small* **2013**, *9*, 1206–1224.

(86) Ethegoin, P. G.; Le Ru, E. C.; Blackie, E.; Meyer, M. Surface Enhanced Raman Scattering Enhancement Factors: A Comprehensive Study. *J. Phys. Chem. C* **2007**, *111*, 13794–13803.

(87) Le Ru, E. C.; Meyer, M.; Etchegoin, P. G. Proof of Single-Mokeule Sensitivity in Surface Enhanced Raman Scattering (SERS) by Means of a Two-Analyte Technique. *J. Phys. Chem. B* **2006**, *110*, 1944–1948.

(88) Shashkova, S.; Leake, M. C. Single-Molecule Fluorescence Microscopy Review: Shedding New Light on Old Problems. *Biosci. Rep.* **2017**, *37*, BSR20170031.

(89) Morris, M. D.; Wallan, D. J. Resonance Raman Spectroscopy. Current Applications and Prospects. *Anal. Chem.* **1979**, *51*, 182A-192A.

(90) Pettinger, B.; Gerolymatou, A. DYES ADSORBED AT AG-COLLOIDS - SUBSTITUTION OF FLUORESCENCE BY SIMILARLY EFFICIENT SURFACE FLUORESCENCE AND SURFACE RAMAN-SCATTERING. *Berichte Der Bunsen-Gesellschaft-Physical Chem. Chem. Phys.* **1984**, *88*, 359–363.

(91) Pettinger, B. Light Scattering by Adsorbates at Ag Particles: Quantum-mechanical Approach for Energy Transfer Induced Interfacial Optical Processes Involving Surface Plasmons, Multipoles, and Electron-hole Pairs. *J. Chem. Phys.* **1986**, *85*, 7442–7451.

(92) Lindquist, N. C.; de Albuquerque, C. D. L.; Sobral-Filho, R. G.; Paci, I.; Brolo, A. G. High-Speed Imaging of Surface-Enhanced Raman Scattering Fluctuations from Individual Nanoparticles. *Nat. Nanotechnol.* **2019**, *14*, 981–987.

(93) Etchegoin, P. G.; Le Ru, E. C. A Perspective on Single Molecule SERS: Current Status and Future Challenges. *Phys. Chem. Chem. Phys.* **2008**, *10*, 6079–6089.

(94) Etchegoin, P. G.; Meyer, M.; Le Ru, E. C. Statistics of Single Molecule SERS Signals: Is There a Poisson Distribution of Intensities? *Phys. Chem. Chem. Phys.* **2007**, *9*, 3006–

3010.

(95) Etchegoin, P. G.; Meyer, M.; Blackie, E.; Le Ru, E. C. Statistics of Single-Molecule Surface Enhanced Raman Scattering Signals: Fluctuation Analysis with Multiple Analyte Techniques. *Anal. Chem.* **2007**, *79*, 8411–8415.

(96) Yu, Y.; Xiao, T.-H.; Wu, Y.; Li, W.; Zeng, Q.-G.; Long, L.; Li, Z.-Y. Roadmap for Single-Molecule Surface-Enhanced Raman Spectroscopy. *Adv. Photonics* **2020**, *2*, 1.

(97) Bohren, C. F. *Absorption and Scattering of Light by Small Particles*; Wiley: New York, 1983.

(98) Gersten, J.; Nitzan, A. Electromagnetic Theory of Enhanced Raman-Scattering by Molecules Adsorbed on Rough Surfaces. *J. Chem. Phys.* **1980**, *73*, 3023–3037.

(99) Schatz, G. C. Theoretical Studies of Surface Enhanced Raman Scattering. *Acc. Chem. Res.* **1984**, *17*, 370–376.

(100) METIU, H.; DAS, P. THE ELECTROMAGNETIC THEORY OF SURFACE ENHANCED SPECTROSCOPY. *Annu. Rev. Phys. Chem.* **1984**, *35*, 507–536.

(101) Kerker, M. Estimation of Surface-Enhanced Raman-Scattering from Surface-Averaged Electromagnetic Intensities. *J. Colloid Interface Sci.* **1987**, *118*, 417–421.

(102) WOKAUN, A. SURFACE-ENHANCED ELECTROMAGNETIC PROCESSES. *SOLID STATE Phys.* **1984**, *38*, 223–294.

(103) WOKAUN, A. SURFACE ENHANCEMENT OF OPTICAL-FIELDS - MECHANISM AND APPLICATIONS. *Mol. Phys.* **1985**, *56*, 1–33.

(104) Gieseking, R. L. M.; Lee, J.; Tallarida, N.; Apkarian, V. A.; Schatz, G. C. Bias-Dependent Chemical Enhancement and Nonclassical Stark Effect in Tip-Enhanced Raman Spectromicroscopy of CO-Terminated Ag Tips. *J. Phys. Chem. Lett.* **2018**, *9*, 3074–3080.

(105) Valley, N.; Greeneltch, N.; Van Duyne, R. P.; Schatz, G. C. A Look at the Origin and Magnitude of the Chemical Contribution to the Enhancement Mechanism of Surface-Enhanced Raman Spectroscopy (SERS): Theory and Experiment. *J. Phys. Chem. Lett.* **2013**, *4*, 2599–2604.

(106) Barber, P. W.; Chang, R. K.; Massoudi, H. Electrodynamic Calculations of the Surface-Enhanced Ele假装ctric Intensities on Large Ag Spheroids. *Phys. Rev. B* **1983**, *27*, 7251–7261.

(107) Cline, M. P.; Barber, P. W.; Chang, R. K. Surface-Enhanced Electric Intensities on Transition- and Noble-Metal Spheroids. *J. Opt. Soc. Am. B* **1986**, *3*, 15–21.

(108) Schatz, G. C.; Young, M. A.; Van Duyne, R. P. Electromagnetic Mechanism of SERS. *Surface-Enhanced Raman Scatt. Phys. Appl.* **2006**, *103*, 19–45.

(109) Franzen, S. Intrinsic Limitations on the |E| 4 Dependence of the Enhancement Factor for Surface-Enhanced Raman Scattering. *J. Phys. Chem. C* **2009**, *113*, 5912–5919.

(110) U. Fano. Effects of Configuration Interaction on Intensities and Phase Shifts. *Phys. Rev.* **1961**, *124*, 1866–1878.

(111) Giannini, V.; Francescato, Y.; Amrania, H.; Phillips, C. C.; Maier, S. A. Fano Resonances in Nanoscale Plasmonic Systems: A Parameter-Free Modeling Approach. *Nano Lett.* **2011**, *11*, 2835.

(112) Osley, E. J.; Biris, C. G.; Thompson, P. G.; Jahromi, R. R. F.; Warburton, P. A.; Panoiu, N. C. Fano Resonance Resulting from a Tunable Interaction between Molecular Vibrational Modes and a Double Continuum of a Plasmonic Metamolecule. *Phys. Rev. Lett.* **2013**, *110*, 1.

(113) Yang, W. H.; Schatz, G. C.; Vanduyne, R. P. Discrete Dipole Approximation for Calculating Extinction and Raman Intensities for Small Particles with Arbitrary Shapes. *J. Chem. Phys.* **1995**, *103*, 869–875.

(114) Taflove, A.; Hagness, S. C. *Computational Electrodynamics: The Finite-Difference Time-Domain Method*; Artech house, 2005.

(115) Efrima, S.; Metiu, H. Classical Theory of Light Scattering by a Molecule Located near a Solid Surface. *Chem. Phys. Lett.* **1978**, *60*, 59–64.

(116) Jensen, L.; Aikens, C. M.; Schatz, G. C. Electronic Structure Methods for Studying Surface-Enhanced Raman Scattering. *Chem. Soc. Rev.* **2008**, *37*, 1061–1073.

(117) Chen, R.; Jensen, L. Interpreting the Chemical Mechanism in SERS Using a Raman Bond Model. *J. Chem. Phys.* **2020**, *152*, 24126.

(118) Chowdhury, J. How the Charge Transfer (CT) Contributions Influence the SERS Spectra of Molecules? A Retrospective from the View of Albrecht's "A" and Herzberg-Teller Contributions. *Appl. Spectrosc. Rev.* **2015**, *50*, 240–260.

(119) Yamamoto, Y. S.; Itoh, T. Why and How Do the Shapes of Surface-enhanced Raman Scattering Spectra Change? Recent Progress from Mechanistic Studies. *J. Raman Spectrosc.* **2016**, *47*, 78–88.

(120) Lin, Q.-Y.; Li, Z.; Brown, K. A.; O'Brien, M. N.; Ross, M. B.; Zhou, Y.; Butun, S.; Chen, P.-C.; Schatz, G. C.; Dravid, V. P. Strong Coupling between Plasmonic Gap Modes and Photonic Lattice Modes in DNA-Assembled Gold Nanocube Arrays. *Nano Lett.* **2015**, *15*, 4699–4703.

(121) Aspnes, D. E. Bond Models in Linear and Nonlinear Optics. In *Ultrafast Nonlinear Imaging and Spectroscopy III*; Liu, Z., Ed.; 2015; Vol. 9584, p 95840A.

(122) Adles, E. J.; Aspnes, D. E. Application of the Anisotropic Bond Model to Second-

Harmonic Generation from Amorphous Media. *Phys. Rev. B* **2008**, *77*, 1–10.

(123) Powell, G. D.; Wang, J. F.; Aspnes, D. E. Simplified Bond-Hyperpolarizability Model of Second Harmonic Generation. *Phys. Rev. B* **2002**, *65*, 205320.

(124) Placzek, G. On the Theory of the Raman Effect. *Zeitschrift Fur Phys.* **1929**, *58*, 585–594.

(125) Guthmuller, J. Comparison of Simplified Sum-over-State Expressions to Calculate Resonance Raman Intensities Including Franck-Condon and Herzberg-Teller Effects. *J. Chem. Phys.* **2016**, *144*, 064106.

(126) Lee, S. Y.; Heller, E. J. Time-Dependent Theory of Raman Scattering. *J. Chem. Phys.* **1979**, *71*, 4777–4788.

(127) Shreve, A. P.; Mathies, R. A. Thermal Effects in Resonance Raman Scattering: Analysis of the Raman Intensities of Rhodopsin and of the Time-Resolved Raman Scattering of Bacteriorhodopsin. *J. Phys. Chem.* **1995**, *99*, 7285–7299.

(128) Myers, A. B. Resonance Raman Intensity Analysis of Excited State Dynamics. *Acc. Chem. Res.* **1997**, *30*, 519–527.

(129) Albrecht, A. C.; Hutley, M. C. Dependence of Vibrational Raman Intensity on Wavelength of Incident Light. *J. Chem. Phys.* **1971**, *55*, 4438–4443.

(130) Johnson, B. B.; Peticolas, W. L. RESONANT RAMAN EFFECT. *Annu. Rev. Phys. Chem.* **1976**, *27*, 465–491.

(131) Warshel, A.; Dauber, P. Calculations of Resonance Raman Spectra of Conjugated Molecules. *J. Chem. Phys.* **1977**, *66*, 5477–5488.

(132) Korenowski, G. M.; Ziegler, L. D.; Albrecht, A. C. Calculations of Resonance Raman Cross Sections in Forbidden Electronic Transitions: Scattering of the 992 Cm-1 Mode in the 1B2u Band of Benzene. *J. Chem. Phys.* **1978**, *68*, 1248–1252.

(133) Ding, S. Y.; You, E. M.; Tian, Z. Q.; Moskovits, M. Electromagnetic Theories of Surface-Enhanced Raman Spectroscopy. *Chem. Soc. Rev.* **2017**, *46*, 4042–4076.

(134) Moskovits, M. Surface Selection-Rules. *J. Chem. Phys.* **1982**, *77*, 4408–4416.

(135) Petrenko, T.; Neese, F. Analysis and Prediction of Absorption Band Shapes, Fluorescence Band Shapes, Resonance Raman Intensities, and Excitation Profiles Using the Time-Dependent Theory of Electronic Spectroscopy. *J. Chem. Phys.* **2007**, *127*, 164319.

(136) Petrenko, T.; Neese, F. Efficient and Automatic Calculation of Optical Band Shapes and Resonance Raman Spectra for Larger Molecules within the Independent Mode Displaced Harmonic Oscillator Model. *J. Chem. Phys.* **2012**, *137*, 234107.

(137) Gaff, J. F.; Franzen, S. Excited-State Geometry Method for Calculation of the Absolute

Resonance Raman Cross Sections of the Aromatic Amino Acids. *J. Phys. Chem. A* **2009**, *113*, 5414–5422.

(138) Gaff, J. F.; Franzen, S.; Delley, B. Ab Initio Calculation of Resonance Raman Cross Sections Based on Excited State Geometry Optimization. *J. Phys. Chem. A* **2010**, *114*, 11681–11690.

(139) Heller, E. J. Time-dependent Approach to Semiclassical Dynamics. *J. Chem. Phys.* **1975**, *62*, 1544–1555.

(140) Reid, P. J.; Mathies, R. A.; Shreve, A. P. Resonance Raman Intensity Analysis of the Photochemical Hydrogen Migration in 1, 3, 5-Cycloheptatriene. *J. Phys. Chem.* **1993**, *97*, 12691–12699.

(141) Myers, A. B.; Mathies, R. A.; Tannor, D. J.; Heller, E. J. Excited-State Geometry Changes from Pre-Resonance Raman Intensities - Isoprene and Hextriene. *J. Chem. Phys.* **1982**, *77*, 3857–3866.

(142) Myers, A. B.; Harris, R. A.; Mathies, R. A. Resonance Raman Excitation Profiles of Bacteriorhodopsin. *J. Chem. Phys.* **1983**, *79*, 603–613.

(143) Franzen, S.; Brown, D.; Gaff, J.; Delley, B. A Resonance Raman Enhancement Mechanism for Axial Vibrational Modes in the Pyridine Adduct of Myoglobin Proximal Cavity Mutant (H93G). *J. Phys. Chem. B* **2012**, *116*, 10514–10521.

(144) Jensen, L.; Autschbach, J.; Krykunov, M.; Schatz, G. C. Resonance Vibrational Raman Optical Activity: A Time-Dependent Density Functional Theory Approach. *J. Chem. Phys.* **2007**, *127*, 134101.

(145) Rush, T.; Peticolas, W. L. Ab Initio Transform Calculation of Resonance Raman Spectra of Uracil, 1-Methyluracil, and 5-Methyluracil. *J. Phys. Chem.* **1995**, *99*, 14647–14658.

(146) Torii, H.; Tasumi, M. Analysis of the Absorption-Spectrum (1-B-1(U)[-1 (1)a(G)) and Resonance Raman Excitation Profiles of Trans-1,3,5-Hexatriene Based on Ab-Initio Molecular-Orbital Calculations. *J. Chem. Phys.* **1994**, *101*, 4496–4504.

(147) Jensen, L.; Schatz, G. C. Resonance Raman Scattering of Rhodamine 6G as Calculated Using Time-Dependent Density Functional Theory. *J. Phys. Chem. A* **2006**, *110*, 5973–5977.

(148) Zhao, L. L.; Jensen, L.; Schatz, G. C. Pyridine-Ag-20 Cluster: A Model System for Studying Surface-Enhanced Raman Scattering. *J. Am. Chem. Soc.* **2006**, *128*, 2911–2919.

(149) Zhao, L. L.; Jensen, L.; Schatz, G. C. Surface-Enhanced Raman Scattering of Pyrazine at the Junction between Two Ag-20 Nanoclusters. *Nano Lett.* **2006**, *6*, 1229–1234.

(150) Aikens, C. M.; Schatz, G. C. TDDFT Studies of Absorption and SERS Spectra of Pyridine Interacting with Au-20. *J. Phys. Chem. A* **2006**, *110*, 13317–13324.

(151) Jensen, L.; Zhao, L. L.; Autschbach, J.; Schatz, G. C. Theory and Method for Calculating Resonance Raman Scattering from Resonance Polarizability Derivatives. *J. Chem. Phys.* **2005**, *123*, 20–23.

(152) Li, P.; Xue, J.; Zheng, X. Decay Dynamics of 6-azauracil from the Light Absorbing S2 (Ππ*) State. *J. Raman Spectrosc.* **2019**, *50*, 345–359.

(153) Harris, R. A.; Mathies, R.; Myers, A. A Simple Sum Rule in Raman Theory. *Chem. Phys. Lett.* **1983**, *94*, 327–330.

(154) Franzen, S.; Fritsch, K.; Brewer, S. H. Experimental Observation of Anharmonic Coupling of the Heme- Doming and Iron-Ligand out-of-Plane Vibrational Modes Confirmed by Density Functional Theory. *J. Phys. Chem. B* **2002**, *106*, 11641–11646.

(155) Aspnes, D. E. Bond Models in Linear and Nonlinear Optics. *Phys. Status Solidi Basic Res.* **2010**, *247*, 1873–1880.

(156) Adles, E. J.; Aspnes, D. E. Application of the Anisotropic Bond Model to Second-Harmonic Generation from Amorphous Media. *Phys. Rev. B* **2008**, *77*.

(157) Gao, Y.; Aspnes, D. E.; Franzen, S. Classical Correlation Model of Resonance Raman Spectroscopy. *J. Phys. Chem. A* **2020**, *124*, 9177–9186.

(158) Decatur, S. M. Elucidation of Residue-Level Structure and Dynamics of Polypeptides via Isotope-Edited Infrared Spectroscopy. *Acc. Chem. Res.* **2006**, *39*, 169–175.

(159) Kazarian, S. G.; Chan, K. L. A. ATR-FTIR Spectroscopic Imaging: Recent Advances and Applications to Biological Systems. *Analyst* **2013**, *138*, 1940–1951.

(160) Osawa, M. Surface-Enhanced Infrared Absorption. In *Near-Field Optics and Surface Plasmon Polaritons*; Kawata, S., Ed.; 2001; Vol. 81, pp 163–187.

(161) Osawa, M. Surface-Enhanced Infrared Absorption Spectroscopy. In *Compendium of Surface and Interface Analysis*; Springer, 2018; pp 697–706.

(162) Itoh, T.; Yamamoto, Y. S. Between Plasmonics and Surface-Enhanced Resonant Raman Spectroscopy: Toward Single-Molecule Strong Coupling at a Hotspot. *Nanoscale* **2021**.

(163) Yang, X.; Sun, Z.; Low, T.; Hu, H.; Guo, X.; de Abajo, F. J.; Avouris, P.; Dai, Q. Nanomaterial-Based Plasmon-Enhanced Infrared Spectroscopy. *Adv. Mater.* **2018**, *30*.

(164) Li, J.-F.; Li, C.-Y.; Aroca, R. F. Plasmon-Enhanced Fluorescence Spectroscopy. *Chem. Soc. Rev.* **2017**, *46*, 3962–3979.

(165) Kozuch, J.; Steinem, C.; Hildebrandt, P.; Millo, D. Combined Electrochemistry and Surface-Enhanced Infrared Absorption Spectroscopy of Gramicidin A Incorporated into Tethered Bilayer Lipid Membranes. *Angew. Chemie Int. Ed.* **2012**, *51*, 8114–8117.

(166) Wisitruangsakul, N.; Lenz, O.; Ludwig, M.; Friedrich, B.; Lendzian, F.; Hildebrandt, P.; Zebger, I. Monitoring Catalysis of the Membrane-Bound Hydrogenase from Ralstonia Eutropha H16 by Surface-Enhanced IR Absorption Spectroscopy. *Angew. Chemie Int. Ed.* **2009**, *48*, 611–613.

(167) Gkogkou, D.; Schreiber, B.; Shaykhutdinov, T.; Ly, H. K.; Kuhlmann, U.; Gernert, U.; Facsko, S.; Hildebrandt, P.; Esser, N.; Hinrichs, K. Polarization-and Wavelength-Dependent Surface-Enhanced Raman Spectroscopy Using Optically Anisotropic Rippled Substrates for Sensing. *Acs Sensors* **2016**, *1*, 318–323.

(168) Suzuki, Y.; Ishigo, Y.; Tsushima, M.; Nakashima, H.; Shimada, T. Simulation of Enhanced Infrared Absorption Spectra by Rigorous Coupled Wave Analysis. *Mater. Res. Express* **2019**, *6*, 1050d7.

(169) Suzuki, Y.; Nakashima, H. Verifying Electromagnetic First Layer Effect on Surface Enhanced Infrared Absorption with Evaporated Gold Nano Island Film. *Mater. Res. Express* **2019**, *6*, 85038.

(170) Shimada, T.; Nakashima, H.; Kumagai, Y.; Ishigo, Y.; Tsushima, M.; Ikari, A.; Suzuki, Y. What Is the Key Structural Parameter for Infrared Absorption Enhancement on Nanostructures? *J. Phys. Chem. C* **2016**, *120*, 534–541.

(171) Nakashima, H.; Sasaki, Y.; Osozawa, R.; Kon, Y.; Nakazawa, H.; Suzuki, Y. Surface Enhanced Infrared Absorption Spectra on Pulsed Laser Deposited Silver Island Films. *Thin Solid Films* **2013**, *536*, 166–171.

(172) Gkogkou, D.; Shaykhutdinov, T.; Kratz, C.; Oates, T. W. H.; Hildebrandt, P.; Weidinger, I. M.; Ly, K. H.; Esser, N.; Hinrichs, K. Gradient Metal Nanoislands as a Unified Surface Enhanced Raman Scattering and Surface Enhanced Infrared Absorption Platform for Analytics. *Analyst* **2019**, *144*, 5271–5276.

(173) Cerruti, M.; Rhodes, C.; Losego, M.; Efremenko, A.; Maria, J.-P.; Fischer, D.; Franzen, S.; Genzer, J. Influence of Indium–Tin Oxide Surface Structure on the Ordering and Coverage of Carboxylic Acid and Thiol Monolayers. *J. Phys. D. Appl. Phys.* **2007**, *40*, 4212.

(174) Losego, M. D.; Efremenko, A. Y.; Rhodes, C. L.; Cerruti, M. G.; Franzen, S.; Maria, J. P. Conductive Oxide Thin Films: Model Systems for Understanding and Controlling Surface Plasmon Resonance. *J. Appl. Phys.* **2009**, *106*.

(175) Losego, M. D.; Guske, J. T.; Efremenko, A.; Maria, J.-P.; Franzen, S. Characterizing the Molecular Order of Phosphonic Acid Self-Assembled Monolayers on Indium Tin Oxide Surfaces. *Langmuir* **2011**, *27*, 11883–11888.

(176) Brewer, S. H.; Franzen, S. Calculation of the Electronic and Optical Properties of Indium Tin Oxide by Density Functional Theory. *Chem. Phys.* **2004**, *300*, 285–293.

(177) Franzen, S.; Maria, J.-P.; Aspnes, D. E.; Gerber, R. W.; Cerruti, M.; Losego, M.; Rhodes,

C. Plasmonic Phenomena in Indium Tin Oxide and ITO-Au Hybrid Films. *Opt. Lett.* **2009**, *34*, 2867.

(178) Rhodes, C.; Cerruti, M.; Efremenko, A.; Losego, M.; Aspnes, D. E.; Maria, J. P.; Franzen, S. Dependence of Plasmon Polaritons on the Thickness of Indium Tin Oxide Thin Films. *J. Appl. Phys.* **2008**, *103*.

(179) Franzen, S. Surface Plasmon Polaritons and Screened Plasma Absorption in Indium Tin Oxide Compared to Silver and Gold. *J. Phys. Chem. C* **2008**, *112*, 6027–6032.

(180) Rhodes, C.; Franzen, S.; Maria, J.-P.; Losego, M.; Leonard, D. N.; Laughlin, B.; Duscher, G.; Weibel, S. Surface Plasmon Resonance in Conducting Metal Oxides. *J. Appl. Phys.* **2006**, *100*, 54905.

(181) Kang, M. S.; Losego, M.; Sachet, E.; Maria, J. P.; Franzen, S. Near-Infrared Optical Extinction of Indium Tin Oxide Structures Prepared by Nanosphere Lithography. *Acs Phot* **2016**, *3*, 1993–1999.

(182) Cerruti, M.; Franzen, S.; Efremenko, A.; Rhodes, C.; Losego, M.; Aspnes, D. E.; Maria, J.-P. Dependence of Plasmon Polaritons on the Thickness of Indium Tin Oxide Thin Films. *J. Appl. Phys.* **2008**, *103*, 093108.

(183) Sachet, E.; Losego, M. D.; Guske, J.; Franzen, S.; Maria, J. P. Mid-Infrared Surface Plasmon Resonance in Zinc Oxide Semiconductor Thin Films. *Appl Phys Lett* **2013**, *102*.

(184) Milekhin, A. G.; Cherkasova, O.; Kuznetsov, S. A.; Milekhin, I. A.; Rodyakina, E. E.; Latyshev, A. V; Banerjee, S.; Salvan, G.; Zahn, D. R. T. Nanoantenna-Assisted Plasmonic Enhancement of IR Absorption of Vibrational Modes of Organic Molecules. *Beilstein J. Nanotechnol.* **2017**, *8*, 975–981.

(185) Kundu, J.; Le, F.; Nordlander, P.; Halas, N. J. Surface Enhanced Infrared Absorption (SEIRA) Spectroscopy on Nanoshell Aggregate Substrates. *Chem. Phys. Lett.* **2008**, *452*, 115.

(186) Adato, R.; Artar, A.; Erramilli, S.; Altug, H. Engineered Absorption Enhancement and Induced Transparency in Coupled Molecular and Plasmonic Resonator Systems. *Nano Lett.* **2013**, *13*, 2584.

(187) Fan, S.; Suh, W.; Joannopoulos, J. D. Temporal Coupled-Mode Theory for the Fano Resonance in Optical Resonators. *J. Opt. Soc. Am. A* **2003**, *20*, 569.

(188) Verslegers, L.; Yu, Z.; Catrysse, P. B.; Fan, S. Temporal Coupled-Mode Theory for Resonant Apertures. *J. Opt. Soc. Am. B* **2010**, *27*, 1947.

(189) Tang, J.; Albrecht, A. C. Developments in the Theories of Vibrational Raman Intensities. In *Raman spectroscopy*; Springer, 1970; pp 33–68.

(190) Tannor, D. J.; Heller, E. J. Polyatomic Raman Scattering for General Harmonic Potentials.

J. Chem. Phys. **1982**, *77*, 202–218.

(191) Maier, S. A.; Atwater, H. A. Plasmonics: Localization and Guiding of Electromagnetic Energy in Metal/Dielectric Structures. *J. Appl. Phys.* **2005**, *98*, 1–10.

(192) Sachet, E. Transition Metal Oxides for Infrared Optoelectronics. *PhD Diss. North Carolina State Univ.* **2015**.

(193) Olmon, R. L.; Slovick, B.; Johnson, T. W.; Shelton, D.; Oh, S.-H.; Boreman, G. D.; Raschke, M. B. Optical Dielectric Function of Gold. *Phys. Rev. B* **2012**, *86*, 235147.

(194) Kurihara, K.; Suzuki, K. Theoretical Understanding of an Absorption-Based Surface Plasmon Resonance Sensor Based on Kretchmann's Theory. *Anal. Chem.* **2002**, *74*, 696–701.

(195) Kurihara, K.; Nakamura, K.; Hirayama, E.; Suzuki, K. An Absorption-Based Surface Plasmon Resonance Sensor Applied to Sodium Ion Sensing Based on an Ion-Selective Optode Membrane. *Anal. Chem.* **2002**, *74*, 6323–6333.

(196) Kretschmann, E. Die Bestimmung Optischer Konstanten von Metallen Durch Anregungen Oberflaechenplasmaschwingungen. *Z. Phys.* **1971**, *241*, 313–324.

(197) Chen, C.; Oh, S.-H.; Li, M. Coupled-Mode Theory for Plasmonic Resonators Integrated with Silicon Waveguides towards Mid-Infrared Spectroscopic Sensing. *Opt. Express* **2020**, *28*.

(198) Agrawal, A.; Singh, A.; Yazdi, S.; Singh, A.; Ong, G. K.; Bustillo, K.; Johns, R. W.; Ringe, E.; Milliron, D. J. Resonant Coupling between Molecular Vibrations and Localized Surface Plasmon Resonance of Faceted Metal Oxide Nanocrystals. *NANO Lett.* **2017**, *17*, 2611–2620.

(199) Brown, L. V; Yang, X.; Zhao, K.; Zheng, B. Y.; Nordlander, P.; Halas, N. J. Fan-Shaped Gold Nanoantennas above Reflective Substrates for Surface-Enhanced Infrared Absorption (SEIRA). *Nano Lett.* **2015**, *15*, 1272.

(200) Le, F.; Brandl, D. W.; Urzhumov, Y. A.; Wang, H.; Kundu, J.; Halas, N. J.; Aizpurua, J.; Nordlander, P. Metallic Nanoparticle Arrays: A Common Substrate for Both Surface-Enhanced Raman Scattering and Surface-Enhanced Infrared Absorption. *ACS Nano* **2008**, *2*, 707.

(201) Brown, L. V; Zhao, K.; King, N. S.; Sobhani, H.; Nordlander, P.; Halas, N. J. Surface-Enhanced Infrared Absorption Using Individual Cross Antennas Tailored to Chemical Moieties. *J. Am. Chem. Soc.* **2013**, *135*, 3688.

(202) Nie, S. Probing Single Molecules and Single Nanoparticles by Surface-Enhanced Raman Scattering. *Science (80-.).* **2002**, *275*, 1102–1106.

(203) Etchegoin, P. G.; Le Ru, E. C. Resolving Single Molecules in Surface-Enhanced Raman

Scattering within the Inhomogeneous Broadening of Raman Peaks. *Anal. Chem.* **2010**, *82*, 2888–2892.

(204) Kneipp, K.; Kneipp, H.; Itzkan, I.; Dasari, R. R.; Feld, M. S. Surface-Enhanced Non-Linear Raman Scattering at the Single-Molecule Level. *Chem. Phys.* **1999**, *247*, 155–162.

(205) Derjaguin, B. V. Theory of the Stability of Strongly Charged Lyophobic Sol and of the Adhesion of Strongly Charged Particles in Solutions of Electrolytes. *Acta phys. chim. URSS* **1941**, *14*, 633.

(206) Derjaguin, B. V; Churaev, N. V; Muller, V. M.; Derjaguin, B. V; Churaev, N. V; Muller, V. M. The Derjaguin—Landau—Verwey—Overbeek (DLVO) Theory of Stability of Lyophobic Colloids. *Surf. forces* **1987**, 293–310.

(207) Derjaguin, B. A Theory of Interaction of Particles in Presence of Electric Double Layers and the Stability of Lyophobe Colloids and Disperse Systems. *Prog. Surf. Sci.* **1993**, *43*, 1–14.

(208) Verwey, E. J. W.; Overbeek, J. T. G. Theory of the Stability of Lyophobic Colloids. Elsevier, Amsterdam. *Theory Stab. lyophobic colloids. Elsevier, Amsterdam.* **1948**.

(209) Kneipp, K.; Kneipp, H.; Itzkan, I.; Dasari, R. R.; Feld, M. S. Surface-Enhanced Raman Scattering and Biophysics. *J. Physics-Condensed Matter* **2002**, *14*, R597–R624.

(210) Schatz, G. C.; Young, M. A.; Van Duyne, R. P. Electromagnetic Mechanism of SERS. In *Surface-Enhanced Raman Scattering: Physics and Applications*; 2006; Vol. 103, pp 19–45.

(211) Kerker, M. Electromagnetic Model for Surface-Enhanced Raman Scattering (SERS) on Metal Colloids. *Acc. Chem. Res.* **1984**, *17*, 271–277.

(212) Nitzan, A. Phenomenology of Resonance Raman-Scattering and Resonance Fluorescence from Thermally Relaxing Systems. *Chem. Phys.* **1979**, *41*, 163–181.

(213) Gao, P.; Weaver, M. J. Surface-Enhanced Raman Spectroscopy as a Probe of Adsorbate-Surface Bonding: Benzene and Monosubstituted Benzenes Adsorbed at Gold Electrodes. *J. Phys. Chem.* **1985**, *89*, 5040–5046.

(214) Wang, J. A.; Zhu, T.; Zhang, X.; Liu, Z. F. The SERS Intensity vs the Size of Au Nanoparticles. *Acta Physico-Chimica Sin.* **1999**, *15*, 476–480.

(215) Maher, R. C.; Cohen, L. F.; Le Ru, E. C.; Etchegoin, P. G. On the Experimental Estimation of Surface Enhanced Raman Scattering (SERS) Cross Sections by Vibrational Pumping. *J. Phys. Chem. B* **2006**, *110*, 19469–19478.

(216) Wang, D. S.; Kerker, M. Enhanced Raman Scattering by Molecules Adsorbed at the Surface of Colloidal Spheroids. *Phys. Rev. B* **1981**, *24*, 1777–1790.

(217) Hildebrandt, P.; Stockburger, M. Surface-Enhanced Resonance Raman-Spectroscopy of Rhodamine-6g Adsorbed on Colloidal Silver. *J. Phys. Chem.* **1984**, *88*, 5935–5944.

(218) Cotton, T. M.; Schultz, S. G.; Vanduyne, R. P. Surface-Enhanced Resonance Raman-Scattering from Water-Soluble Porphyrins Adsorbed on a Silver Electrode. *J. Am. Chem. Soc.* **1982**, *104*, 6528–6532.

(219) Joseph, V.; Matschulat, A.; Polte, J.; Rolf, S.; Emmerling, F.; Kneipp, J. SERS Enhancement of Gold Nanospheres of Defined Size. *J. Raman Spectrosc.* **2011**, *42*, 1736–1742.

(220) Yamaguchi, Y.; Ishikawa, M.; Maruyama, Y.; Futamata, M. Trigonal Silver Nanostructure for Single Molecule Detection with Surface Enhanced Raman Scattering; 2005; pp S56–S62.

(221) Haes, A. J.; Zou, S. L.; Schatz, G. C.; Van Duyne, R. P. Nanoscale Optical Biosensor: Short Range Distance Dependence of the Localized Surface Plasmon Resonance of Noble Metal Nanoparticles. *J. Phys. Chem. B* **2004**, *108*, 6961–6968.

(222) Zhang, X. Y.; Zhao, J.; Whitney, A. V; Elam, J. W.; Van Duyne, R. P. Ultrastable Substrates for Surface-Enhanced Raman Spectroscopy: Al2O3 Overlayers Fabricated by Atomic Layer Deposition Yield Improved Anthrax Biomarker Detection. *J. Am. Chem. Soc.* **2006**, *128*, 10304–10309.

(223) Maher, R. C.; Cohen, L. F.; Le Ru, E. C.; Etchegoin, P. G. A Study of Local Heating of Molecules under Surface Enhanced Raman Scattering (SERS) Conditions Using the Anti-Stokes/Stokes Ratio. *Faraday Discuss.* **2006**, *132*, 77–83.

(224) Aikens, C. M.; Schatz, G. C. TDDFT Studies of Absorption and SERS Spectra of Pyridine Interacting with Au20. *J. Phys. Chem. A* **2006**, *110*, 13317–13324.

(225) Huan, M.; Thompson, M. K.; Gaff, J.; Franzen, S. Kinetic Analysis of a Naturally Occurring Bioremediation Enzyme: Dehaloperoxidase-Hemoglobin from Amphitrite Ornata. *J. Phys. Chem. B* **2010**, *114*, 13823–13829.

(226) Otto, A. On the Significance of Shalaev's "hot Spots" in Ensemble and Single-Molecule SERS by Adsorbates on Metallic Films at the Percolation Threshold. *J. Raman Spectrosc.* **2006**, *37*, 937–947.

(227) Caruso, F.; Furlong, D. N.; Kingshott, P. Characterization of Ferritin Adsorption onto Gold. *J. Colloid Interface Sci.* **1997**, *186*, 129–140.

(228) Scott, P. Miepython. *https://miepython.readthedocs.io/en/latest/index.html* **2023**.

(229) Sumlin, B. PyMieScatt. *https://pymiescatt.readthedocs.io/en/latest/index.html* **2020**.

(230) Norris, W. T. Charge Images in a Dielectric Sphere. *IEE Proceedings-Science, Meas. Technol.* **1995**, *142*, 142–150.

(231) Derkachova, A.; Kolwas, K.; Demchenko, I. Dielectric Function for Gold in Plasmonics Applications: Size Dependence of Plasmon Resonance Frequencies and Damping Rates for Nanospheres. *Plasmonics* **2016**, *11*, 941–951.

(232) Zheng, A.; Chen, J.; Wu, G.; Wei, H.; He, C.; Kai, X.; Wu, G.; Chen, Y. Optimization of a Sensitive Method for the "Switch-on" Determination of Mercury(II) in Waters Using Rhodamine B Capped Gold Nanoparticles as a Fluorescence Sensor. *Microchim. Acta* **2009**, *164*, 17–27.

(233) Kneipp, K.; Kneipp, H.; Deinum, G.; Itzkan, I.; Dasari, R. R.; Feld, M. S. Single-Molecule Detection of a Cyanine Dye in Silver Colloidal Solution Using near-Infrared Surface-Enhanced Raman Scattering. *Appl. Spec.* **1998**, *52*, 175–178.

(234) A. Meyer, S.; C. Le Ru, E.; G. Etchegoin, P. Combining Surface Plasmon Resonance (SPR) Spectroscopy with Surface-Enhanced Raman Scattering (SERS). *Anal. Chem.* **2011**, *83*, 2337–2344.

(235) Le Ru, E. C.; Etchegoin, P. G. *Principles of Surface-Enhanced Raman Spectroscopy and Related Plasmonic Effects*; Elsevier, 2009.

(236) Gao, Y.; Aspnes, D.; Franzen, S. Classical Model of Surface Enhanced Infrared Absorption (SEIRA) Spectroscopy. *J. Phys. Chem. A 126*, 341–351.

(237) Valencia, F.; Arcos, H. Method of Images for a Charge inside a Three-Layer Medium and Implementation of a Dirichlet Border Condition. *Rev. Politécnica* **2020**, *44*, 7–14.

APPENDICES

APPENDIX 1. Comparison of the anharmonic solution (ABM) and the CCM

The equation of motion for the CCM is described by eq. (2.19),

$$\left(m\frac{d^2}{dt^2}+2m\Gamma\frac{d}{dt}+\kappa_0+\Delta\kappa\cos(\omega_v t)\right)\left(\Delta\vec{r}_0 e^{-i\omega t}+\Delta\vec{r}_+ e^{-i(\omega+\omega_v)t}+\Delta\vec{r}_- e^{-i(\omega-\omega_v)t}\right)$$

$$=q\vec{E}_0 e^{-i\omega t}, \qquad (2.19)$$

Equation (2.19) can be reduced to two equations:

one involving $e^{-i\omega t}$:

$$-m\omega^2\Delta\vec{r}_0=q\vec{E}_0+2im\omega\Gamma\Delta\vec{r}_0-\kappa_0\Delta\vec{r}_0. \qquad (2.9b)$$

and the other involving $e^{-i(\omega\pm\omega_v)t}$:

$$-m(\omega\pm\omega_v)^2\Delta\vec{r}_\pm-2im(\omega\pm\omega_v)\Gamma\Delta\vec{r}_\pm+\frac{1}{2}\Delta\kappa\Delta\vec{r}_0=0$$

Terms involving $\Delta\kappa\Delta\vec{r}_\pm$ are of second order and hence small. They can be discarded.

For nonlinear optics, which is described by the ABM, the important term is anharmonicity. The equation of motion is:

$$m\frac{d^2r}{dt^2}=q\vec{E}_0\cos\omega t-\kappa_0(\vec{r}-\vec{r}_0)-\frac{1}{2}\frac{d\kappa}{dr}(\vec{r}-\vec{r}_0)^2,$$

where for simplicity the damping is not considered. Usually, $\frac{1}{2}\frac{d\kappa}{dr}$ is written as a second order restoring-force constant κ_2, equivalent to assuming that the asymmetric part is linear in *r*. The solution is:

$$\vec{r}=\vec{r}_0+\sum_l\sum_n\Delta\vec{r}_{ln}\cos(n\omega+l\omega_v)t\,,\qquad n\in\mathbb{N},\qquad l\in\mathbb{Z}$$

Thus, the Stokes Raman shift (the $\cos(\omega-\omega_v)t$ terms) could be separated from the equation of motion:

$$-m(\omega-\omega_v)^2\Delta\vec{r}_{-1,1}=-\kappa_0\Delta\vec{r}_{-1,1}-\frac{1}{2}\frac{d\kappa}{dr}\left(\sum_{\substack{l_1+l_2=-1\\ n_1+n_2=1}}\Delta\vec{r}_{l_1,n_1}\Delta\vec{r}_{l_2,n_2}+\sum_{\substack{l_1-l_2=-1\\ n_1-n_2=1}}\Delta\vec{r}_{l_1,n_1}\Delta\vec{r}_{l_2,n_2}\right)$$

If we can discard the higher order terms,

$$-m(\omega-\omega_v)^2\Delta\vec{r}_{-1,1}=-\kappa_0\Delta\vec{r}_{-1,1}-\frac{1}{2}\frac{d\kappa}{dr}\left(\Delta\vec{r}_{-1,1}\Delta\vec{r}_{0,0}+\Delta\vec{r}_{1,1}\Delta\vec{r}_{0,0}\right)$$

Comparing the CCM without the damping term,

$$-m(\omega-\omega_v)^2\Delta\vec{r}_{-}=-\frac{1}{2}\Delta\kappa\Delta\vec{r}_0$$

On this basis the two mechanisms cannot be distinguished because the two models have the same mathematical form. But CCM is much cleaner in algebra and physics, by defining the meaning of $\Delta\kappa$.

APPENDIX 2. The polarizability amplitude in the classic model

The terms in Re and Im have units of m^{-4}. The Raman cross section is related to the total scattering power P by

$$P = \sigma I$$

where I is the intensity and σ is the Raman cross section. Given the intensity:

$$I = \frac{1}{2}\epsilon_0 c|E_0|^2,$$

the Raman cross section can be related to the Raman polarizability according to:

$$\sigma = \frac{\omega^4}{6\pi\epsilon_0^2 c^4}|\alpha_{Raman}|^2.$$

From the derivation in the text, we have

$$\alpha_{Raman} = \frac{q^2\Delta\kappa}{4m^2\omega_0^2(\omega - \omega_v - \omega_0 + i\Gamma)(\omega - \omega_0 + i\Gamma)} \qquad (2.31b)$$

$$\Delta\vec{r}_- = \frac{\Delta\kappa\Delta\vec{r}_0}{4m\omega_0^2(\omega - \omega_v - \omega_0 + i\Gamma)} \qquad (2.20b)$$

As constants and parameters use

$$q = -e = 1.60217662 \times 10^{-19}\ \mathrm{C}$$

$$m = m_e = 9.10938356 \times 10^{-31}\ \mathrm{kg}$$

$$c_0 = 2.99792458 \times 10^8\ \frac{\mathrm{m}}{\mathrm{s}}$$

$$\omega_0 = 20000\ \mathrm{cm}^{-1} = 2\pi \times 5.9958 \times 10^{14}\ \mathrm{Hz} = 3.7673 \times 10^{15}\ \mathrm{rad/s}$$

$$\omega_v = 1000.0\ \mathrm{cm}^{-1} = 2\pi \times 2.9979 \times 10^{13}\ \mathrm{Hz} = 1.8836 \times 10^{14}\ \mathrm{rad/s}$$

$$\Gamma = 100.00\ \mathrm{cm}^{-1} = 2\pi \times 2.9979 \times 10^{12}\ \mathrm{Hz} = 1.8836 \times 10^{13}\ \mathrm{rad/s}$$

If $\Delta\kappa$ is constant, then the polarizability at $\omega = \omega_0 = 20000\ \mathrm{cm}^{-1}$ is (Stokes):

$$|\alpha_{Raman}|_{20000} = \frac{q^2}{4\omega_0^2 m^2}\left|\frac{1}{-\omega_v + i\Gamma}\cdot\frac{1}{i\Gamma}\right|\Delta\kappa_{20000} = 1.5278 \times 10^{-37}\ \Delta\kappa_{20000}\ (\mathrm{SI})$$

$$|\alpha_{Raman}|^2_{20000} = 2.3341 \times 10^{-74}\ \Delta\kappa^2_{20000}\ (\text{SI})$$

From Eq. (2.20b)

$$\Delta\vec{r}_{-} = \frac{\Delta\kappa\Delta\vec{r}_0}{4m\omega_0(\omega - \omega_v - \omega_0 + i\Gamma)}. \qquad (2.20b)$$

We can estimate:

$$\Delta\kappa_{20000} = \left|\frac{4m\omega_0\Delta\vec{r}_{-}}{\Delta\vec{r}_0}(\omega - \omega_v - \omega_0 + i\Gamma)\right|.$$

Assuming that $\frac{\Delta\vec{r}_{-}}{\Delta\vec{r}_0} = 0.020000$ when at Raman resonance $\omega - \omega_v - \omega_0 = 0$,

$$\Delta\kappa_{20000} = 5.1715 \times 10^{-3}\ \text{kg s}^{-2}$$

Also, using the polarizability at $\omega_0 = 20000\ \text{cm}^{-1}$:

$$|\alpha_{Raman}|_{20000} = 7.9008 \times 10^{-40}\ \text{C}^2\text{kg}^{-1}\text{s}^2$$

$$|\alpha_{Raman}|^2_{20000} = 6.2423 \times 10^{-79}\ \text{C}^4\text{kg}^{-2}\text{s}^4$$

Then the Raman cross section at $\omega_0 = 20000\ \text{cm}^{-1}$ is:

$$\sigma_{20000} = \frac{\omega_0^4}{6\pi\epsilon_0^2 c^4}|\alpha_{Raman}|^2_{20000} = 1.0534 \times 10^{-29}\ \text{m}^2$$

APPENDIX 3. The amplitude of polarizability of the quantum model

$$\alpha_{Raman} = \frac{M_{if}^2}{\hbar}\sqrt{S}\left[\frac{1}{(\omega_0 - \omega) - i\Gamma} - \frac{1}{(\omega_0 + \omega_v - \omega) - i\Gamma}\right] \tag{2.42}$$

Assume each transition dipole is $1\ \mathrm{D} = 3.33564 \times 10^{-30}$ C m, and $S = 0.0200000$.

Thus $\Delta\kappa = 3.6568 \times 10^{-2}\sqrt{S}$ (SI) and $\Delta_d = 10\frac{\Delta\vec{r}_-}{\Delta\vec{r}_0}$. Note that these parameters depends on Γ.

Next, apply the constants and parameters

$$\omega_0 = 20000\ \mathrm{cm}^{-1} = 2\pi \times 5.9958 \times 10^{14}\ \mathrm{Hz} = 3.7673 \times 10^{15}\ \mathrm{rad/s}$$

$$\omega_v = 1000.0\ \mathrm{cm}^{-1} = 2\pi \times 2.9979 \times 10^{13}\ \mathrm{Hz} = 1.8836 \times 10^{14}\ \mathrm{rad/s}$$

$$\Gamma = 100.00\ \mathrm{cm}^{-1} 2\pi \times 2.9979 \times 10^{12}\ \mathrm{Hz} = 1.8836 \times 10^{13}\ \mathrm{rad/s}$$

$$\hbar = 1.054571817 \times 10^{-34}\ \mathrm{J\ s}$$

The quantum polarizability at $\omega_0 = 20000\ \mathrm{cm}^{-1}$ is therefore

$$|\alpha_{Raman}|_{20000} = \frac{1}{\hbar}\left|\left[\frac{1}{-i\Gamma} - \frac{1}{\omega_v - i\Gamma}\right]\right| \mathrm{D}^2\sqrt{S} = 7.8818 \times 10^{-40}\ \mathrm{C^2 kg^{-1} s^2},$$

which is of the same order of magnitude as obtained with the classic model.

The cross section at $\omega_0 = 20000\ \mathrm{cm}^{-1}$ is:

$$\sigma_{20000} = \frac{\omega_0^4}{6\pi\epsilon_0^2 c^4}|\alpha|_{20000}^2 = 1.0483\ \times 10^{-29}\ \mathrm{m}^2$$

APPENDIX 4. Dispersion relation of the surface wave

The surface plasmon consists of conduction electrons oscillating at the interface between two materials. The oscillations are confined to the interface, and hence are described by imaginary wave vectors normal to the interface in both directions, resulting in exponential attenuation from the interface. The solution requires that these excitations propagate, and the resulting surface waves are called surface plasmon polaritons (SPP) (see Figure A4.1.)

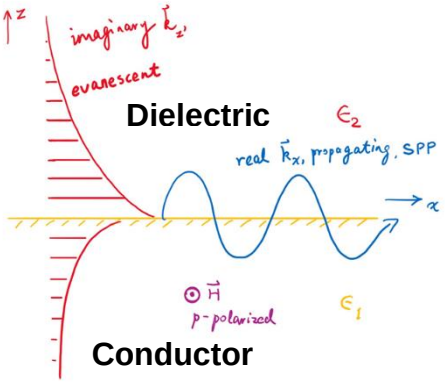

Figure A 4.1 Surface wave and surface plasmon polariton

For nonmagnetic materials these surface waves can be excited by incoming plane waves of TM (transverse magnetic) polarization, with the magnetic field parallel to the interface. The magnetic field and the electric field on both sides are given by the following equations, using the coordinate system of Figure A4.1:

For material 1, $z > 0$:

$$H_{1y} = H_{10} e^{ik_{x1}x + ik_{z1}z - i\omega t}, \tag{1.1a}$$

$$E_{1x} = \frac{1}{i\epsilon_0\epsilon_1\omega}\frac{\partial H_{1y}}{\partial z} e^{ik_{x1}x + ik_{z1}z - i\omega t} = \frac{k_{z1}}{\epsilon_0\epsilon_1\omega} H_{10} e^{ik_{x1}x + ik_{z1}z - i\omega t}, \tag{1.1b}$$

$$E_{1z} = -\frac{1}{i\epsilon_0\epsilon_1\omega}\frac{\partial H_{1y}}{\partial x} e^{ik_{x1}x + ik_{z1}z - i\omega t} = -\frac{k_{x1}}{\epsilon_0\epsilon_1\omega} H_{10} e^{ik_{x1}x + ik_{z1}z - i\omega t}, \tag{1.1c}$$

For material 2, $z < 0$:

$$H_{2y} = H_{20}e^{ik_{x1}x+ik_{z2}z-i\omega t}, \tag{1.2a}$$

$$E_{2x} = \frac{1}{i\epsilon_0\epsilon_2\omega}\frac{\partial H_{2y}}{\partial z}e^{ik_{x1}x+ik_{z2}z-i\omega t} = \frac{k_{z2}}{\epsilon_0\epsilon_2\omega}H_{20}e^{ik_{x1}x+ik_{z2}z-i\omega t}, \tag{1.2b}$$

$$E_{2z} = -\frac{1}{i\epsilon_0\epsilon_2\omega}\frac{\partial H_{2y}}{\partial x}e^{ik_{x1}x+ik_{z2}z-i\omega t} = -\frac{k_{x2}}{\epsilon_0\epsilon_2\omega}H_{20}e^{ik_{x1}x+ik_{z2}z-i\omega t}. \tag{1.2c}$$

The boundary condition requires following restrictions at the interface when $z = 0$,

$$H_{1y} = H_{2y}, \qquad E_{1x} = E_{2x}, \qquad \epsilon_1 E_{1z} = \epsilon_2 E_{2z}, \tag{1.3}$$

which is:

$$H_{10} = H_{20}, \qquad \frac{k_{z1}}{\epsilon_1} = \frac{k_{z2}}{\epsilon_2}, \qquad k_{x1} = k_{x2}. \tag{1.4}$$

To ensure the attenuation of the surface wave, the z components of the wavevectors k_{z1} and k_{z2} must be imaginary and with different signs ($k_{z1} < 0$ and $k_{z2} > 0$). Therefore, the permittivities of the two materials must have opposite signs. A conductor and a dielectric will satisfy this requirement.

Considering the dispersion relation:[3]

$$c^2(k_{x1}^2 + k_{z1}^2) = \omega^2\epsilon_1, \tag{1.5a}$$

$$c^2(k_{x2}^2 + k_{z2}^2) = \omega^2\epsilon_2, \tag{1.5b}$$

the x component of the wave vector, also well known as the dispersion relation of the SPP, is obtained:[2]

$$k_{SPP} = k_{x1} = k_{x2} = \frac{\omega}{c}\sqrt{\frac{\epsilon_1\epsilon_2}{\epsilon_1 + \epsilon_2}}. \tag{1.6}$$

The *z* components of the wave vectors in each material follow:

$$k_{z1} = \frac{\omega\epsilon_1}{c}\sqrt{\frac{1}{\epsilon_1 + \epsilon_2}}, \tag{1.7a}$$

$$k_{z2} = \frac{\omega\epsilon_2}{c}\sqrt{\frac{1}{\epsilon_1 + \epsilon_2}}. \quad (1.7b)$$

From Eqs.(1.1) and (1.2), when the wave vector becomes sufficiently large, SPP will produce an enhancement of the electric field on the molecules near the interface. There are two scenarios that can produce enhancement.

The first scenario occurs when $\epsilon_1 + \epsilon_2$ approaches 0. When applying the Drude model to the conductor,

$$1 - \frac{\omega_p^2}{\omega^2} + \epsilon_2 = 0, \quad (1.8a)$$

$$\epsilon_\infty\left(1 - \frac{\bar{\omega}_p^2}{\omega^2}\right) + \epsilon_2 = 0, \quad (1.8b)$$

the frequency required for the excitation in this case is:[2]

$$\omega = \omega_{sp} = \frac{\omega_p}{\sqrt{1 + \epsilon_2}}, \quad (1.9a)$$

$$\omega = \omega_{sp} = \frac{\epsilon_\infty\bar{\omega}_p}{\sqrt{\epsilon_\infty + \epsilon_2}}. \quad (1.9b)$$

This is the condition when the SPP becomes a stationary wave, *i.e.*, the group velocity of SPP $d\omega/dk$ is 0.

The second situation is when the when ϵ_2 becomes large. The dielectric function of the molecule is given by the spring-mass system (derivation provided in next chapter):

$$\epsilon_2(\omega) = 1 + \frac{nq/m\epsilon_0}{\omega_0^2 - \omega^2 - 2i\omega\Gamma}. \quad (1.10)$$

where ω_0 is the resonance frequency of the molecule, q is the bound charge of the molecule. In Raman spectroscopy, the bound charge can represent the electron in a ground-to-excited electronic state transition; In infrared (IR) spectroscopy, it can be a part of the molecule

in the vibrational normal mode. m is the effective mass of the bound charge, and Γ describes the energy dissipation in the motion of this charge. Γ is usually small compared to the resonance frequency ω_0.

When the frequency of the incident light is at the resonance of the molecule, k_{z2} will become massive. Therefore, as described in Eq.(1.2b), an enhancement will be addressed on E_{2x}.

APPENDIX 5. Derivation of the three-layer Fresnel equation (Airy equation)

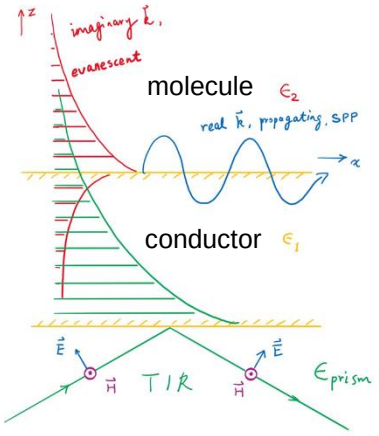

Figure A 5.1 Kretschmann configuration

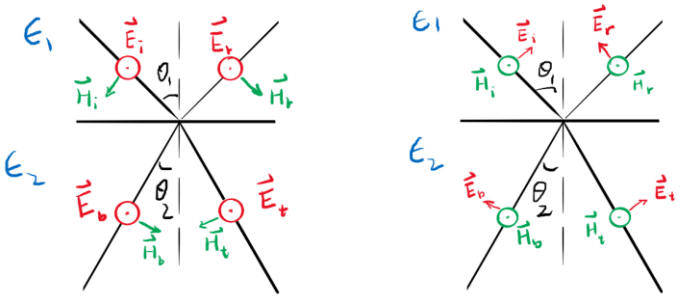

Figure A 5.2 TE (s polarized, left) and TM (p polarized, right) modes.

The derivation of the three-layer Fresnel equation is based on the two-layer Fresnel equations since the final expression is composed of two two-layer reflectances combined with a phase factor that depends on the thickness of the conductor. For an s-polarized wave (TE mode, as transverse electric field, as shown on the left side of Figure 2.2), given boundary conditions, where the tangential electric field and magnetic field should be continuous on the interface, and noting that there are no back-reflected waves for a two-layer model:

$$E_i + E_r = E_t, \tag{2.1a}$$

$$H_i \cos\theta_1 - H_r \cos\theta_1 = H_t \cos\theta_2 \tag{2.1b}$$

For a p-polarized wave (TM mode, as transverse magnetic field, see the right side of Figure 2.2), the boundary conditions are:

$$H_i + H_r = H_t, \tag{2.1c}$$

$$E_i \cos\theta_1 - E_r \cos\theta_1 = E_t \cos\theta_2 \tag{2.1d}$$

From the Maxwell-Ampère equation, we obtained the relation of magnetic field H and electric field E:

$$\nabla \times \vec{H} = i\vec{k} \times \vec{H} = \vec{J} + \frac{\partial \vec{D}}{\partial t} = \frac{\partial \vec{D}}{\partial t} = \epsilon_0 \epsilon \frac{\partial \vec{E}}{\partial t} = -i\omega\epsilon_0\epsilon\vec{E}, \tag{2.2}$$

$$H = -\frac{\omega\epsilon_0\epsilon}{k}E = -\frac{c_0\epsilon_0 n^2}{n}E = -\sqrt{\frac{\epsilon_0}{\mu_0}}nE, \tag{2.3}$$

where the refractive index $n = \frac{c_0 k}{\omega} = \sqrt{\epsilon_r \mu_r}$, and $c_0 = \frac{1}{\sqrt{\epsilon_0 \mu_0}}$ is the speed of light in vacuum.

The reflectance r and the transmittance t of the s-polarized light are:

$$r_s = \frac{E_r}{E_i} = \frac{n_1 \cos\theta_1 - n_2 \cos\theta_2}{n_1 \cos\theta_1 + n_2 \cos\theta_2}, \tag{2.4a}$$

$$t_s = \frac{E_t}{E_i} = \frac{2n_1 \cos\theta_1}{n_1 \cos\theta_1 + n_2 \cos\theta_2}. \tag{2.4b}$$

For the p-polarized wave:

$$r_p = \frac{H_r}{H_i} = \frac{n_2 \cos\theta_1 - n_1 \cos\theta_2}{n_2 \cos\theta_1 + n_1 \cos\theta_2}, \tag{2.4c}$$

$$t_p = \frac{H_t}{H_i} = \frac{2n_2 \cos\theta_1}{n_2 \cos\theta_1 + n_1 \cos\theta_2}. \tag{2.4d}$$

The boundary conditions for s-polarized light are:

$$E_i + E_r = E_t + E_b, \tag{2.5a}$$

$$H_i \cos\theta_1 - H_r \cos\theta_1 = H_t \cos\theta_2 - H_b \cos\theta_2 \tag{2.5b}$$

The boundary conditions for p-polarized light are:

$$H_i + H_r = H_t + H_b, \tag{2.5c}$$

$$E_i \cos\theta_1 - E_r \cos\theta_1 = E_t \cos\theta_2 - E_b \cos\theta_2 \tag{2.5d}$$

which leads to the relation of the waves on the two sides of the interface, for a s-polarized light:

$$\begin{bmatrix} E_i \\ E_r \end{bmatrix} = \frac{1}{t_s}\begin{bmatrix} 1 & r_s \\ r_s & 1 \end{bmatrix}\begin{bmatrix} E_t \\ E_b \end{bmatrix} \tag{2.6a}$$

This relation remains the same form for the p-polarized light,

$$\begin{bmatrix} H_i \\ H_r \end{bmatrix} = \frac{1}{t_p}\begin{bmatrix} 1 & r_p \\ r_p & 1 \end{bmatrix}\begin{bmatrix} H_t \\ H_b \end{bmatrix} \tag{2.6b}$$

Next, consider the phase shift of propagation. As shown in Figure 3 in the main text, the back reflected wave on the interface 1 is the propagated reflected wave of interface 2; the incident wave of the interface 2 is the propagated transmitted wave of interface 1. The matrix describes the phase shift:

$$\begin{bmatrix} E_{t1} \\ E_{b1} \end{bmatrix} = \begin{bmatrix} e^{-ikd\cos\gamma} & 0 \\ 0 & e^{ikd\cos\gamma} \end{bmatrix}\begin{bmatrix} E_{i2} \\ E_{r2} \end{bmatrix} \ , \tag{2.7}$$

where γ is the incident angle at the interface 2. Note that the attenuation is built into the matrix. Now, linking the beam reflected from the second interface to the first interface, the 3-layer Fresnel equation is obtained:

$$\begin{bmatrix} E_{i1} \\ E_{r1} \end{bmatrix} = \frac{1}{t_{12}} \begin{bmatrix} 1 & r_{12} \\ r_{12} & 1 \end{bmatrix} \begin{bmatrix} e^{-ikd\cos\gamma} & 0 \\ 0 & e^{ikd\cos\gamma} \end{bmatrix} \frac{1}{t_{23}} \begin{bmatrix} 1 & r_{23} \\ r_{23} & 1 \end{bmatrix} \begin{bmatrix} E_{t3} \\ 0 \end{bmatrix}$$

$$= \frac{E_{t3}}{t_{12}t_{23}} \begin{bmatrix} 1 & r_{12} \\ r_{12} & 1 \end{bmatrix} \begin{bmatrix} e^{-ikd\cos\gamma} & 0 \\ 0 & e^{ikd\cos\gamma} \end{bmatrix} \begin{bmatrix} 1 \\ r_{23} \end{bmatrix}$$

$$= \frac{E_{t3}}{t_{12}t_{23}} \begin{bmatrix} 1 & r_{12} \\ r_{12} & 1 \end{bmatrix} \begin{bmatrix} e^{-ikd\cos\gamma} \\ r_{23}e^{ikd\cos\gamma} \end{bmatrix}$$

$$= \frac{E_{t3}}{t_{12}t_{23}} \begin{bmatrix} e^{-ikd\cos\gamma} + r_{12}r_{23}e^{ikd\cos\gamma} \\ r_{12}e^{-ikd\cos\gamma} + r_{23}e^{ikd\cos\gamma} \end{bmatrix} \tag{2.8}$$

$$r_{123} = \frac{E_{r1}}{E_{i1}} = \frac{r_{12}e^{-ikd\cos\gamma} + r_{23}e^{ikd\cos\gamma}}{e^{-ikd\cos\gamma} + r_{12}r_{23}e^{ikd\cos\gamma}} = \frac{r_{12} + r_{23}e^{2ikd\cos\gamma}}{1 + r_{12}r_{23}e^{2ikd\cos\gamma}} \tag{2.9}$$

$$t_{123} = \frac{E_{t3}}{E_{i1}} = \frac{t_{12}t_{23}e^{ikd\cos\gamma}}{1 + r_{12}r_{23}e^{2ikd\cos\gamma}} \tag{2.10}$$

APPENDIX 6. Phase difference of the incident light and the plasmon

The phase difference between the plasmon and the incident light is determined by the exponential part in the three-layer Fresnel equation, which is the exponential part in the propagation matrix from Eq.(2.7) in Appendix 2:

$$e^{ikd\cos\gamma} \tag{3.1}$$

In the equation, *d* is the thickness of the conductor, *k* is the wave vector in the conductor, and γ is the incident angle at the interface between MgO and CdO. The difference between γ and the incident angle θ of the whole configuration is not large (see Figure 3.1):

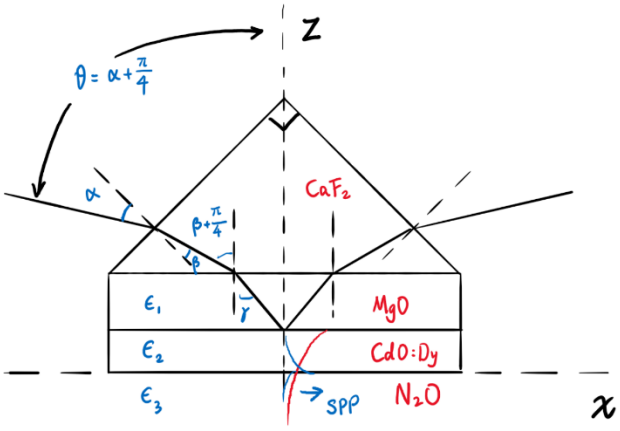

Figure A 6.1 Kretschmann configuration

We can expect that the phase should not change very much at a single wavelength because

1. k is fixed by the dispersion relation, $k = n\omega/c$.

2. d is fixed.

Therefore:

$$e^{ikd\cos\gamma} = e^{kd}e^{i\cos\gamma} = Constant * [\cos(\cos\gamma) + i\sin(\cos\gamma)] \tag{3.2}$$

Because theta basically ranges from 45 to 90 degrees, it does not even go through a range of π. Therefore, $\cos(\cos\gamma)$ and $\sin(\cos\gamma)$ are basically constants. The phase difference between the plasmon and the incident light is basically constant, as shown in Figure 3.2:

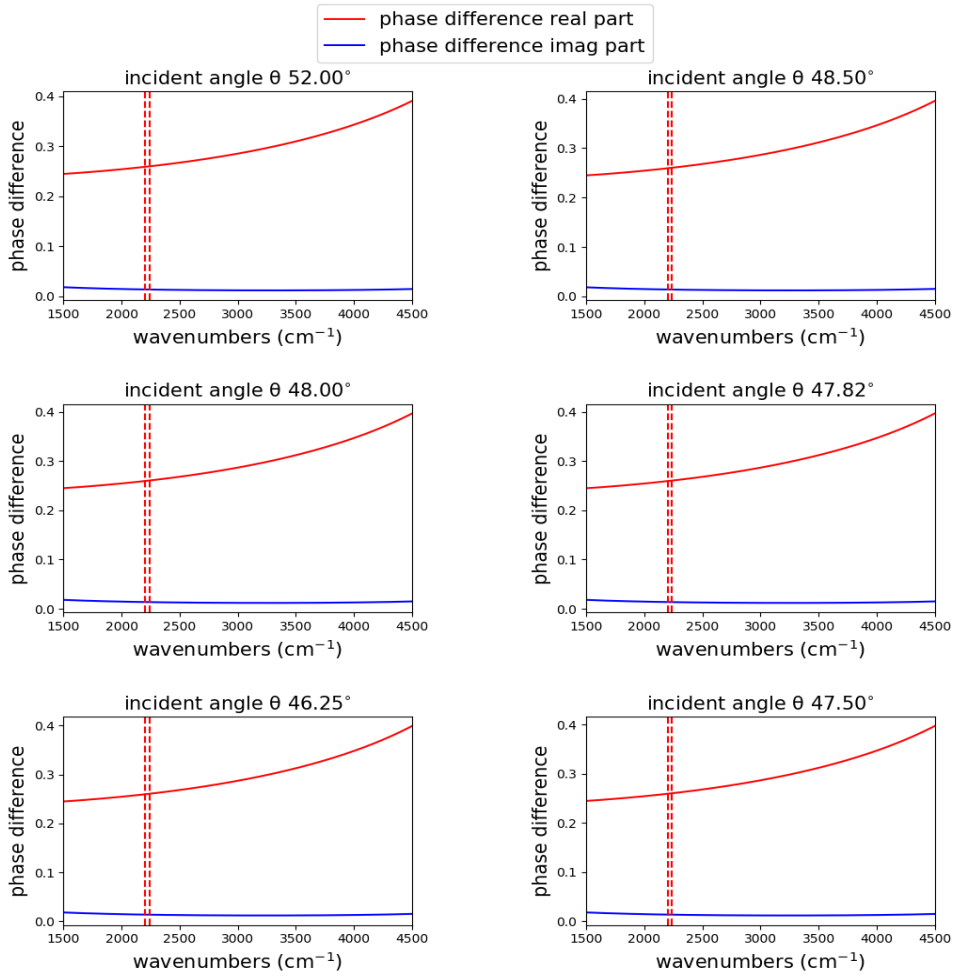

Figure A 6.2 Phase differences between the incident light and the surface wave. The red dashed lines are N_2O absorption peaks.

APPENDIX 7. Reduced-mass calculation for the asymmetric stretch mode

The literature values for the force constants of the N-N and N-O bonds in N_2O are:[237]

N-N: 1788 N/m; N-O: 1139 N/m.

If we define the molecule to be on the *x* axis, the Hessian matrix is therefore:

$$\begin{pmatrix} \frac{1788}{\sqrt{14\times14}} & -\frac{1788}{\sqrt{14\times14}} & 0 \\ -\frac{1788}{\sqrt{14\times14}} & \frac{1788+1139}{\sqrt{14\times14}} & -\frac{1139}{\sqrt{14\times16}} \\ 0 & -\frac{1139}{\sqrt{14\times16}} & \frac{1139}{\sqrt{16\times16}} \end{pmatrix} \begin{pmatrix} \sqrt{14}x_1 \\ \sqrt{14}x_2 \\ \sqrt{16}x_3 \end{pmatrix} = \frac{4\pi c^2\tilde{\nu}^2}{N_A \times 1000\ \text{g/kg}} \begin{pmatrix} \sqrt{14}x_1 \\ \sqrt{14}x_2 \\ \sqrt{16}x_3 \end{pmatrix}$$

$$= \frac{4\pi c^2\tilde{\nu}^2}{N_A \times 1000\ \text{g/kg}} \begin{pmatrix} \sqrt{14}x_1 \\ \sqrt{14}x_2 \\ \sqrt{16}x_3 \end{pmatrix}$$

$$= 1.875\times10^{-5}\tilde{\nu}^2 \begin{pmatrix} \sqrt{14}x_1 \\ \sqrt{14}x_2 \\ \sqrt{16}x_3 \end{pmatrix} \qquad (4.1)$$

where the mass of the atoms is in units of g/mol, and $\tilde{\nu}$ is the frequency in cm^{-1}. The eigenvectors are the reduced-coordinate displacements associated with each mode, where x_1 is the displacement for the proximal nitrogen, x_2 is the central nitrogen, and x_3 is the oxygen.

The eigenvalues and normalized eigenvectors are shown in the following table:

Eigenvalue ($N \cdot mol \cdot m^{-1} \cdot g^{-1}$)	Frequency (cm^{-1})	Eigenvector ($g^{1/2} \cdot mol^{-1/2}$)	Displacements	Displacement squared
$9.35\times10^{-6}\approx0$	(Translation)	0.5641 0.5641 0.6030	0.5774 0.5774 0.5774	0.3333 0.3333 0.3333
89.81	1235	0.6251 0.1855 -0.7582	0.6489 0.1926 -0.7361	0.4210 0.03708 0.5419
318.2	2324	-0.5395 0.8047 -0.2479	-0.5416 0.8078 -0.2328	0.2933 0.6525 0.0542

The reduced mass m_3 is thus obtained:

$$\frac{1}{m_3} = \sum \frac{l^2}{m} = \frac{0.65}{m(N)} + \frac{0.29}{m(N)} + \frac{0.05}{m(O)}. \quad (19)$$

$$m_3 = 14\ a.m.u. \approx 2.6 \times 10^4\ m_e. \quad (20)$$

APPENDIX 8. Derivation of the local field in Chapter 4.

$$\int_{\Omega'} d\Omega'\, \vec{E}_{loc}(\theta', \varphi', \omega) = 2\pi \int_0^{\pi} \sin\eta'\, d\eta' \left(\vec{E}_i(\omega) + \vec{E}_{nano}(\eta', \omega)\right)$$

$$= 2\pi E_{xi} \int_0^{\pi} \sin\eta'\, d\eta'\, (\hat{x}) + 2\pi \frac{\epsilon_{nano} - \epsilon_{mol}}{\epsilon_{nano} + 2\epsilon_{mol}} \frac{R^3 E_{xi}}{(R+d)^3} \int_0^{\pi} \sin\eta'\, d\eta'\, (2a\hat{r}\cos\eta' + b\hat{\eta}\sin\eta')$$

$$= 2\pi E_{xi}\hat{x} \int_0^{\pi} \sin\eta'\, d\eta'\, (a\cos^2\eta' + b\sin^2\eta')$$

$$+ 2\pi \frac{\epsilon_{nano} - \epsilon_{mol}}{\epsilon_{nano} + 2\epsilon_{mol}} \frac{R^3 E_{xi}}{(R+d)^3} \hat{x} \int_0^{\pi} \sin\eta'\, d\eta'\, (2a\cos^2\eta' - b\sin^2\eta')$$

$$= 2\pi E_{xi}\hat{x} \int_{-1}^{1} d(\cos\eta')\, (a\cos^2\eta' + b\sin^2\eta')$$

$$+ 2\pi \frac{\epsilon_{nano} - \epsilon_{mol}}{\epsilon_{nano} + 2\epsilon_{mol}} \frac{R^3 E_{xi}}{(R+d)^3} \hat{x} \int_{-1}^{1} d(\cos\eta') \left(2a\cos^2\eta' - b(1 - \cos^2\eta')\right)$$

$$= 2\pi E_{xi}\hat{x} \left(\frac{2}{3}a + \frac{2}{3}b\right) + 2\pi \frac{\epsilon_{nano} - \epsilon_{mol}}{\epsilon_{nano} + 2\epsilon_{mol}} \frac{R^3 E_{xi}}{(R+d)^3} \hat{x} \left(\frac{4}{3}a - \frac{4}{3}b\right)$$

$$= 4\pi E_{xi}\hat{x} \left(\left(\frac{1}{3}a + \frac{1}{3}b\right) + \frac{\epsilon_{nano} - \epsilon_{mol}}{\epsilon_{nano} + 2\epsilon_{mol}} \frac{R^3}{(R+d)^3} \left(\frac{2}{3}a - \frac{2}{3}b\right)\right)$$

APPENDIX 9. Derivation of the dispersion relation in Raman active layer

The magnetic field is given by the Maxwell-Ampère equation:

$$\nabla \times \vec{H} = \frac{\partial \vec{D}}{\partial t}$$

$$i\vec{k}_R \times \vec{H}_R e^{i\vec{k}_R\cdot\vec{r}-i\omega_R t} = -i\omega_R \vec{D}_R e^{i\vec{k}_R\cdot\vec{r}-i\omega_R t} = -i\epsilon_0\omega_R\left(\epsilon_{r0}\vec{E}_R e^{i\vec{k}_R\cdot\vec{r}-i\omega_R t} + \chi_R \vec{E}_0 e^{i\vec{k}\cdot\vec{r}-i\omega t}\right)$$

Note that the Raman shifted term yields a frequency ω_R rather than ω, because the χ_R has shifted the frequency of $\vec{E}_0 e^{i\vec{k}\cdot\vec{r}-i\omega t}$ before evaluating the partial derivative to time.

The wave equation in the Raman dielectric can be solved from Maxwell's equations.

$$\nabla \times \left(\nabla \times \vec{E}\right) = \nabla\left(\nabla \cdot \vec{E}\right) - \nabla^2\vec{E} = -\frac{\partial \mu_0\mu_r\left(\nabla \times \vec{H}\right)}{\partial t} = -\mu_0\mu_r\frac{\partial^2\vec{D}}{\partial t^2}$$

$$\nabla \times \left(\nabla \times \vec{H}\right) = \nabla\left(\nabla \cdot \vec{H}\right) - \nabla^2\vec{H} = \frac{\partial\left(\nabla \times \vec{D}\right)}{\partial t}$$

Setting $\mu_r = 1$, and $c^2 = 1/\mu_0\epsilon_0$. Applying the displacement field we derived above, with $\nabla \cdot \vec{E} = 0$ (setting the total net charge as 0 in the volume of the interest), and $\nabla \cdot \vec{H} = 0$:

$$\nabla^2\left(\vec{E}_R e^{i\vec{k}_R\cdot\vec{r}-i\omega_R t}\right) = \mu_0\frac{\partial^2\left(\vec{D}_R e^{i\vec{k}_R\cdot\vec{r}-i\omega_R t}\right)}{\partial t^2} = \frac{1}{c^2}\frac{\partial^2\left(\epsilon_{r0}\vec{E}_R e^{i\vec{k}_R\cdot\vec{r}-i\omega_R t} + \chi_R\vec{E}_0 e^{i\vec{k}\cdot\vec{r}-i\omega t}\right)}{\partial t^2}$$
$$= -\frac{\omega_R^2}{c^2}\left(\epsilon_{r0}\vec{E}_R e^{i\vec{k}_R\cdot\vec{r}-i\omega_R t} + \chi_R\vec{E}_0 e^{i\vec{k}\cdot\vec{r}-i\omega t}\right)$$

$$\nabla^2\left(\vec{H}_R e^{i\vec{k}_R\cdot\vec{r}-i\omega_R t}\right) = -\frac{\partial\left(\nabla \times \left(\vec{D}_R e^{i\vec{k}_R\cdot\vec{r}-i\omega_R t}\right)\right)}{\partial t}$$
$$= -\epsilon_0\frac{\partial\left(\epsilon_{r0}\nabla \times \left(\vec{E}_R e^{i\vec{k}_R\cdot\vec{r}-i\omega_R t}\right) + \nabla \times \chi_R\left(\vec{E}_0 e^{i\vec{k}\cdot\vec{r}-i\omega t}\right)\right)}{\partial t}$$
$$= \frac{1}{c^2}\frac{\partial^2\left(\epsilon_{r0}\vec{H}_R e^{i\vec{k}_R\cdot\vec{r}-i\omega_R t} + \chi_R\vec{H}_0 e^{i\vec{k}\cdot\vec{r}-i\omega t}\right)}{\partial t^2}$$
$$= -\frac{\omega_R^2}{c^2}\left(\epsilon_{r0}\vec{H}_R e^{i\vec{k}_R\cdot\vec{r}-i\omega_R t} + \chi_R\vec{H}_0 e^{i\vec{k}\cdot\vec{r}-i\omega t}\right)$$

We obtained:

$$\left|\vec{k}_R\right|^2 \vec{E}_R e^{i\vec{k}_R\cdot\vec{r}-i\omega_R t} = \frac{\omega_R^2}{c^2}\left(\epsilon_{r0}\vec{E}_R e^{i\vec{k}_R\cdot\vec{r}-i\omega_R t} + \chi_R \vec{E}_0 e^{i\vec{k}\cdot\vec{r}-i\omega t}\right)$$

$$\left|\vec{k}_R\right|^2 = \frac{\omega_R^2}{c^2}\left(\epsilon_{r0} + \frac{\chi_R \vec{E}_0 e^{i\vec{k}\cdot\vec{r}-i\omega t}}{\vec{E}_R e^{i\vec{k}_R\cdot\vec{r}-i\omega_R t}}\right) = \frac{\omega_R^2}{c^2}\epsilon_R$$

When on resonance with 0-0' at $\omega = \omega_0$, the scattered wave has a frequency $\omega_R = \omega_0 - \omega_{vib}$.

$$\chi_R = \frac{n\alpha_R}{\epsilon_0} \approx \frac{10^{25}\times 10^{-39}}{10^{-12}} \approx 10^{-2}\ (if\ \Gamma\ is\ 100\ \mathrm{cm}^{-1})$$

$$Re\left(\epsilon_{r0}(\omega_R)\right) \approx 1.1,\ \ Im\left(\epsilon_{r0}(\omega_R)\right) \approx 0.02\ (if\ \Gamma\ is\ 100\ \mathrm{cm}^{-1})$$

When on resonance with 0-1' transition, $\omega = \omega_0 + \omega_{vib}$, $\omega_R = \omega_0$, $0 < \chi_R \ll 1$,

$$Re\left(\epsilon_{r0}(\omega_R)\right) \approx 1.0,\ \ Im\left(\epsilon_{r0}(\omega_R)\right) \approx 1.0\ (if\ \Gamma\ is\ 100\ \mathrm{cm}^{-1})$$

APPENDIX 10. Derivation for Fresnel equations with Raman active layer

The magnetic field is given by the Maxwell-Ampère equation:

$$\nabla \times \vec{H} = \frac{\partial \vec{D}}{\partial t}$$

$$i\vec{k}_R \times \vec{H}_R e^{i\vec{k}_R\cdot\vec{r}-i\omega_R t} = -i\omega_R \vec{D}_R e^{i\vec{k}_R\cdot\vec{r}-i\omega_R t} = -i\epsilon_0\omega_R\left(\epsilon_{r0}\vec{E}_R e^{i\vec{k}_R\cdot\vec{r}-i\omega_R t} + \chi_R \vec{E}_0 e^{i\vec{k}\cdot\vec{r}-i\omega t}\right)$$

Note that the Raman shifted term yields a frequency ω_R rather than ω, because the χ_R has shifted the frequency of $\vec{E}_0 e^{i\vec{k}\cdot\vec{r}-i\omega t}$ before evaluating the partial derivative to time.

The wave equation in the Raman dielectric can be solved from Maxwell's equations.

$$\nabla \times \left(\nabla \times \vec{E}\right) = \nabla\left(\nabla \cdot \vec{E}\right) - \nabla^2\vec{E} = -\frac{\partial \mu_0\mu_r\left(\nabla \times \vec{H}\right)}{\partial t} = -\mu_0\mu_r\frac{\partial^2\vec{D}}{\partial t^2}$$

$$\nabla \times \left(\nabla \times \vec{H}\right) = \nabla\left(\nabla \cdot \vec{H}\right) - \nabla^2\vec{H} = \frac{\partial\left(\nabla \times \vec{D}\right)}{\partial t}$$

Setting $\mu_r = 1$, and $c^2 = 1/\mu_0\epsilon_0$. Applying the displacement field we derived above, with

$\nabla \cdot \vec{E} = 0$ (setting the total net charge as 0 in the volume of the interest), and $\nabla \cdot \vec{H} = 0$:

$$\nabla^2\left(\vec{E}_R e^{i\vec{k}_R\cdot\vec{r}-i\omega_R t}\right) = \mu_0\frac{\partial^2\left(\vec{D}_R e^{i\vec{k}_R\cdot\vec{r}-i\omega_R t}\right)}{\partial t^2} = \frac{1}{c^2}\frac{\partial^2\left(\epsilon_{r0}\vec{E}_R e^{i\vec{k}_R\cdot\vec{r}-i\omega_R t} + \chi_R\vec{E}_0 e^{i\vec{k}\cdot\vec{r}-i\omega t}\right)}{\partial t^2}$$

$$= -\frac{\omega_R^2}{c^2}\left(\epsilon_{r0}\vec{E}_R e^{i\vec{k}_R\cdot\vec{r}-i\omega_R t} + \chi_R\vec{E}_0 e^{i\vec{k}\cdot\vec{r}-i\omega t}\right)$$

$$\nabla^2\left(\vec{H}_R e^{i\vec{k}_R\cdot\vec{r}-i\omega_R t}\right) = -\frac{\partial\left(\nabla\times\left(\vec{D}_R e^{i\vec{k}_R\cdot\vec{r}-i\omega_R t}\right)\right)}{\partial t}$$

$$= -\epsilon_0\frac{\partial\left(\epsilon_{r0}\nabla\times\left(\vec{E}_R e^{i\vec{k}_R\cdot\vec{r}-i\omega_R t}\right)+\nabla\times\chi_R\left(\vec{E}_0 e^{i\vec{k}\cdot\vec{r}-i\omega t}\right)\right)}{\partial t}$$

$$= \frac{1}{c^2}\frac{\partial^2\left(\epsilon_{r0}\vec{H}_R e^{i\vec{k}_R\cdot\vec{r}-i\omega_R t}+\chi_R\vec{H}_0 e^{i\vec{k}\cdot\vec{r}-i\omega t}\right)}{\partial t^2}$$

$$= -\frac{\omega_R^2}{c^2}\left(\epsilon_{r0}\vec{H}_R e^{i\vec{k}_R\cdot\vec{r}-i\omega_R t}+\chi_R\vec{H}_0 e^{i\vec{k}\cdot\vec{r}-i\omega t}\right)$$

We obtained:

$$\left|\vec{k}_R\right|^2\vec{E}_R e^{i\vec{k}_R\cdot\vec{r}-i\omega_R t} = \frac{\omega_R^2}{c^2}\left(\epsilon_{r0}\vec{E}_R e^{i\vec{k}_R\cdot\vec{r}-i\omega_R t}+\chi_R\vec{E}_0 e^{i\vec{k}\cdot\vec{r}-i\omega t}\right)$$

$$\left|\vec{k}_R\right|^2 = \frac{\omega_R^2}{c^2}\left(\epsilon_{r0}+\frac{\chi_R\vec{E}_0 e^{i\vec{k}\cdot\vec{r}-i\omega t}}{\vec{E}_R e^{i\vec{k}_R\cdot\vec{r}-i\omega_R t}}\right) = \frac{\omega_R^2}{c^2}\epsilon_R$$

When on resonance with 0-0' at $\omega = \omega_0$, the scattered wave has a frequency $\omega_R = \omega_0 - \omega_{vib}$.

$$\chi_R = \frac{n\alpha_R}{\epsilon_0} \approx \frac{10^{25}\times 10^{-39}}{10^{-12}} \approx 10^{-2}\ (if\ \Gamma\ is\ 100\ \mathrm{cm}^{-1})$$

$$Re\left(\epsilon_{r0}(\omega_R)\right) \approx 1.1,\ \ Im\left(\epsilon_{r0}(\omega_R)\right) \approx 0.02\ (if\ \Gamma\ is\ 100\ \mathrm{cm}^{-1})$$

When on resonance with 0-1' transition, $\omega = \omega_0 + \omega_{vib}$, $\omega_R = \omega_0$, $0 < \chi_R \ll 1$,

$$Re\left(\epsilon_{r0}(\omega_R)\right) \approx 1.0,\ \ Im\left(\epsilon_{r0}(\omega_R)\right) \approx 1.0\ (if\ \Gamma\ is\ 100\ \mathrm{cm}^{-1})$$

APPENDIX 11. Python codes

A11.1. *Python code for Chapter 2.*

A11.1.1. S is small (Accurate CCM, no approximation)

```
#import pandas as pd
import matplotlib.pyplot as plt
import numpy as np
import matplotlib.ticker as ticker

#these frequencies are in cm-1 unit
w = 20000
wv = 1000
gamma = 100
gamma_quantum = gamma

#basic parameters, in SI units
c0 = 2.99792458e8
me = 9.10938356e-31
qe = 1.60217662e-19
e0 = 8.8541878128e-12
h_bar = 1.054571817e-34
debye = 3.33564e-30

x = np.arange(18000,23000,0.1)
w_raman = x - wv

r0rm = 0.020

#unit convergance
x_SI = x * c0 * 100 * 2 * np.pi
w_raman_SI = w_raman * c0 * 100 * 2 * np.pi
wv_SI = wv * c0 * 100 * 2 * np.pi
w_SI = w * c0 * 100 * 2 * np.pi
gamma_SI = gamma * c0 * 100 * 2 * np.pi
gamma_quantum_SI = gamma_quantum * c0 * 100 * 2 * np.pi

delta_k = 4 * me * w_SI * r0rm * gamma_SI
#delta_k = 0.0362
S = 0.02
prefactor = qe*qe/me/me*delta_k
a_raman = - prefactor / (w_raman_SI**2 - w_SI**2 + 2 * w_raman_SI * gamma_SI * 1j) /
(x_SI**2 - w_SI**2 - 2 * x_SI * gamma_SI * 1j)
prefactor_qtm = 1/h_bar*debye*debye
a_qtm = prefactor_qtm * np.sqrt(S) * (1 / (w_SI - x_SI - 1j * gamma_quantum_SI) - 1 / (w_SI -
w_raman_SI - 1j * gamma_quantum_SI))
a_raman_sq = abs(a_raman)**2
```

```
a_qtm_sq = abs(a_qtm)**2
#a_qtmabsq =abs(prefactor_qtm * (-1 / (1j * gamma_SI) + 1 / (wv_SI - 1j * gamma_SI)))**2
#print (a_qtmabsq*w_SI**4/6/np.pi/e0/e0/c0**4)
fig, ax1 = plt.subplots(figsize=(8,5.5))
#ax1.set_title('Real Part',fontsize=30)
ax1.set_xlabel('${\omega}$ ($\mathregular{cm^{-1}}$)',fontsize=15)
ax1.tick_params(axis='both', which='major', labelsize=15)
ax1.set_ylabel('${|\\alpha_{Raman}|^{2}}$ ($\mathregular{C^{4}kg^{-
2}s^{4}}$)',fontsize=15)
#2e-68 for raman in delta_k, 1e-74 for SI
#ax1.yaxis.set_major_formatter(ticker.FormatStrFormatter('%.1e'))
ax1.set_ylim([0,1e-78])  #need change
#ax1.set_yticks([0,4.5e-75,0.5e-75])
ax1.set_xlim([18000,23000]) #need change
ax1.plot(x,a_qtm_sq,color='red', label='QM model', linewidth=2.0)
ax1.plot(x,a_raman_sq,color='blue', label='this model', linewidth=2.0)
ax1.legend( loc='upper right', borderaxespad=0.,fontsize=15)
plt.show()
```

A11.1.2. S is small (CCM in Lorentzian approximation)

```
#import pandas as pd
import matplotlib.pyplot as plt
import numpy as np
import matplotlib.ticker as ticker

#these frequencies are in cm-1 unit
w = 20000
wv = 1000
gamma = 100
gamma_quantum = gamma

#basic parameters, in SI units
c0 = 2.99792458e8
me = 9.10938356e-31
qe = 1.60217662e-19
e0 = 8.8541878128e-12
h_bar = 1.054571817e-34
debye = 3.33564e-30

x = np.arange(18000,23000,0.1)
w_raman = x - wv

r0rm = 0.02

#unit convergance
x_SI = x * c0 * 100 * 2 * np.pi
```

```
w_raman_SI = w_raman * c0 * 100 * 2 * np.pi
wv_SI = wv * c0 * 100 * 2 * np.pi
w_SI = w * c0 * 100 * 2 * np.pi
gamma_SI = gamma * c0 * 100 * 2 * np.pi
gamma_quantum_SI = gamma_quantum * c0 * 100 * 2 * np.pi

delta_k = 4 * me * w_SI * r0rm * gamma_SI
#delta_k = 0.0362
S = 0.5 * r0rm**2 *100
prefactor = qe*qe/me/me*delta_k
a_raman = - prefactor / (w_raman_SI - w_SI + gamma_SI * 1j) / (x_SI - w_SI - gamma_SI * 1j)
/ 2 / w_SI / (2 * w_SI)
prefactor_qtm = 1/h_bar*debye*debye*np.sqrt(S)
a_qtm = prefactor_qtm * (1 / (w_SI - x_SI - 1j * gamma_quantum_SI) - 1 / (w_SI - w_raman_SI
- 1j * gamma_quantum_SI))
a_raman_sq = abs(a_raman)**2
a_qtm_sq = abs(a_qtm)**2
#a_qtmabsq =abs(prefactor_qtm * (-1 / (1j * gamma_SI) + 1 / (wv_SI - 1j * gamma_SI)))**2
#print (a_qtmabsq*w_SI**4/6/np.pi/e0/e0/c0**4)
fig, ax1 = plt.subplots(figsize=(8,5.5))
#ax1.set_title('Real Part',fontsize=30)
ax1.set_xlabel('${\omega}$ ($\mathregular{cm^{-1}}$)',fontsize=15)
ax1.tick_params(axis='both', which='major', labelsize=15)
ax1.set_ylabel('${|\\alpha_{Raman}|^{2}}$ ($\mathregular{C^{4}kg^{-
2}s^{4}}$)',fontsize=15)
#2e-68 for raman in delta_k, 1e-74 for SI
#ax1.yaxis.set_major_formatter(ticker.FormatStrFormatter('%.1e'))
#ax1.set_ylim([0,1e-78])  #need change
#ax1.set_yticks([0,4.5e-75,0.5e-75])
ax1.set_xlim([18000,23000]) #need change
ax1.plot(x,a_qtm_sq,color='red', label='QM model', linewidth=2.0)
ax1.plot(x,a_raman_sq,color='blue', label='this model', linewidth=2.0)
ax1.legend( loc='upper right', borderaxespad=0.,fontsize=15)
plt.show()
```

A11.1.3. CCM under different S (accurate)

```
#import pandas as pd
import matplotlib.pyplot as plt
import numpy as np
#basic parameters, in SI units
c0 = 2.998e8
me = 9.109e-31
qe = 1.602e-19
e0 = 8.8541878128e-12
```

```
h_bar = 1.054571817e-34
debye = 3.33564e-30

#parameters in SI units

r0rm = 0.020
n = 5
#S = 1.5

#these frequencies are in cm-1 unit
w0 = 20000
wv = 1000
gamma = 100
gamma_quantum = 100



x = np.arange(18000,30000,0.1)
#unit convergance
x_SI = x * c0 * 100 * 2 * np.pi
wv_SI = wv * c0 * 100 * 2 * np.pi
w0_SI = w0 * c0 * 100 * 2 * np.pi
gamma_SI = gamma * c0 * 100 * 2 * np.pi
gamma_quantum_SI = gamma_quantum * c0 * 100 * 2 * np.pi
delta_k = 0.0367  #delta_k in sqrt S

def classica(n,S):
  prefactor = np.sqrt(S) * qe * qe * delta_k * np.exp(-1 * S) / me / me
  a_raman = 0
  for i in range(0, n + 1):
    w_SI = x_SI - i * wv_SI
    w_raman_SI = x_SI - (i + 1) * wv_SI
    a_temp = ( S ** i ) / np.math.factorial(i) / (w_raman_SI**2 - w0_SI**2 + 2 * w_raman_SI *
gamma_SI * 1j) / (w_SI**2 - w0_SI**2 + 2 * w_SI * gamma_SI * 1j)
    a_raman = a_raman + a_temp
  a_raman_abs = abs(a_raman) * prefactor
  return a_raman_abs

def quantuma(n, S):
  prefactor_qtm = np.sqrt(S) * debye * debye * np.exp(-1 * S) / h_bar
  a_raman = 0
  for i in range(0, n + 1):
    w_SI = x_SI - i * wv_SI
    w_raman_SI = x_SI - (i + 1) * wv_SI
    a_temp = S ** (i) / np.math.factorial(i) * (1 / (w0_SI - w_raman_SI - 1j *
gamma_quantum_SI) - 1 / (w0_SI - w_SI - 1j * gamma_quantum_SI))
```

```
    a_raman = a_raman + a_temp
  a_qtm_abs = abs(a_raman) * prefactor_qtm
  return a_qtm_abs

for S in np.arange (0.01, 2.5, 0.5):
  a_raman_abs = classica(n, S)
  a_raman_sqare = a_raman_abs * a_raman_abs
  a_qtm_abs = quantuma(n, S)
  a_qtm_sqare = a_qtm_abs * a_qtm_abs
  fig, ax1 = plt.subplots(figsize=(8,5.5))
  ax1.set_title('${\it{S}}$ = %.1f'%S,fontsize=30)
  ax1.set_xlabel('${\omega}$ ($\mathregular{cm^{-1}}$)',fontsize=15)
  ax1.tick_params(axis='both', which='major', labelsize=15)
  ax1.set_ylabel('${|\\alpha_{Raman}|^{2}}$ ($\mathregular{C^{4}kg^{-
2}s^{4}}$)',fontsize=15)
  #2e-68 for raman in delta_k, 1e-74 for SI
  ax1.set_ylim([0.0,5e-78])  #need change
  ax1.set_xlim([18000,30000]) #need change
  ax1.plot(x,a_qtm_sqare,color='red', label='QM model', linewidth=2.0)
  ax1.plot(x,a_raman_sqare,color='blue', label='this model', linewidth=2.0)
  ax1.legend( loc='upper right', borderaxespad=0.,fontsize=15)
  plt.show()
```

A11.1.4. CCM under different S (Lorentzian)

```
#import pandas as pd
import matplotlib.pyplot as plt
import numpy as np
#basic parameters, in SI units
c0 = 2.998e8
me = 9.109e-31
qe = 1.602e-19
e0 = 8.8541878128e-12
h_bar = 1.054571817e-34
debye = 3.33564e-30

#parameters in SI units

r0rm = 0.020
n = 5
#S = 1.5

#these frequencies are in cm-1 unit
w0 = 20000
wv = 1000
gamma = 100
gamma_quantum = 100
```

```
x = np.arange(18000,30000,0.1)
#unit convergance
x_SI = x * c0 * 100 * 2 * np.pi
wv_SI = wv * c0 * 100 * 2 * np.pi
w0_SI = w0 * c0 * 100 * 2 * np.pi
gamma_SI = gamma * c0 * 100 * 2 * np.pi
gamma_quantum_SI = gamma_quantum * c0 * 100 * 2 * np.pi
delta_k = 0.0367  #delta_k in sqrt S

def classica(n,S):
  prefactor = np.sqrt(S) * qe * qe * delta_k * np.exp(-1 * S) / me / me / 4 / w0_SI / w0_SI
  a_raman = 0
  for i in range(0, n + 1):
    w_SI = x_SI - i * wv_SI
    w_raman_SI = x_SI - (i + 1) * wv_SI
    a_temp = ( S ** i ) / np.math.factorial(i) / (w_raman_SI - w0_SI + gamma_SI * 1j) / (w_SI -
w0_SI + gamma_SI * 1j)
    a_raman = a_raman + a_temp
  a_raman_abs = abs(a_raman) * prefactor
  return a_raman_abs

def quantuma(n, S):
  prefactor_qtm = np.sqrt(S) * debye * debye * np.exp(-1 * S) / h_bar
  a_raman = 0
  for i in range(0, n + 1):
    w_SI = x_SI - i * wv_SI
    w_raman_SI = x_SI - (i + 1) * wv_SI
    a_temp = S ** (i) / np.math.factorial(i) * (1 / (w0_SI - w_raman_SI - 1j *
gamma_quantum_SI) - 1 / (w0_SI - w_SI - 1j * gamma_quantum_SI))
    a_raman = a_raman + a_temp
  a_qtm_abs = abs(a_raman) * prefactor_qtm
  return a_qtm_abs

for S in np.arange (0.0, 2.5, 0.5):
  a_raman_abs = classica(n, S)
  a_raman_sqare = a_raman_abs * a_raman_abs
  a_qtm_abs = quantuma(n, S)
  a_qtm_sqare = a_qtm_abs * a_qtm_abs
  fig, ax1 = plt.subplots(figsize=(8,5.5))
  ax1.set_title('${\it{S}}$ = %.1f'%S,fontsize=30)
  ax1.set_xlabel('${\omega}$ ($\mathregular{cm^{-1}}$)',fontsize=15)
  ax1.tick_params(axis='both', which='major', labelsize=15)
```

```
  ax1.set_ylabel('${|\\alpha_{Raman}|^{2}}$ ($\mathregular{C^{4}kg^{-
2}s^{4}}$)',fontsize=15)
  #2e-68 for raman in delta_k, 1e-74 for SI
  ax1.set_ylim([0.0,5e-78])  #need change
  ax1.set_xlim([18000,30000]) #need change
  ax1.plot(x,a_qtm_sqare,color='red', label='QM model', linewidth=2.0)
  ax1.plot(x,a_raman_sqare,color='blue', label='this model', linewidth=2.0)
  ax1.legend( loc='upper right', borderaxespad=0.,fontsize=15)
  plt.show()
```

A11.2. Python Code and dielectric functions for Chapter 3

A11.2.1. Dispersion relation plot

```
import numpy as np
import matplotlib.pyplot as plt
from pandas import read_csv
import scipy.interpolate as inp

#constants
c = 2.99792458e8
e = 1.6021773e-19
h = 6.6260755e-34
hb = 1.05457e-34
kb = 1.380658e-23
me = 9.109389e-31
 ε 0 = 8.85419e-12 # epsilon 0
q = 1.6021773e-19
def prism(wcm):
    dprism = read_csv("CaF2.csv")
    xprism = dprism['wavn']
    yprism = dprism['e']
    tprism = inp.splrep(xprism,yprism)
    eprism = inp.splev(wcm,tprism)
    return eprism

#parameters for CdO
n1 = 3.5e26 # in m^3
 ε inf = 5.5
meff1 = 0.21
 μ  = 0.03 # m^2 / V / s
 Γ 1 = q / (μ * meff1 * me)
#Γ1 = 0

#parameters for the molecule
 ω 0 = 2212 * 2*np.pi * c * 100
 ω 02 = 2238 * 2*np.pi * c * 100
#ω0 = 0
n2 = 4e5 / kb / 298.15 /3 # via pV = NkT, V = 1 m^3
meff2 = 2.6e4
 Γ 2 = 0.5 * 2*np.pi * c * 100
 Γ 3 = 0.5 * 2*np.pi * c * 100
#Γ2 = 0 * 2*np.pi * c * 100


#the permittivities
range = [1500,5000,0.01]
```

```
ωcm = np.arange(range[0],range[1],range[2]) # in wavenumbers cm-1
ω  = ωcm * 2*np.pi * c * 100 #convert to SI
ωp = np.sqrt(n1 * q**2 / (meff1 * me * ε0))
ε CaF2 = prism(ωcm)
nCaF2 = np.sqrt(εCaF2)
print(n2)
ε 1 = εinf + n1 * q**2 / (me * meff1 * ε0) / ( - ω**2 - 2 * ω * Γ1*1j)
#ε2 = 1 + n2 * q**2 / (me * meff2 * ε0) / (2 * ω0 * (ω0 - ω - Γ2*1j))
ε 2 = 1 + n2 * 0.5 * q**2 / (me * meff2 * ε0) / (ω0**2 - ω**2 - 2 * ω * Γ2*1j) + n2 * 0.5 *
q**2 / (me * meff2 * ε0) / (ω02**2 - ω**2 - 2 * ω * Γ3*1j)
#ε2 = 1
#ε2 = 1 + 0.1 * Γ2 / (ω0 - ω - Γ2 * 1j)
sign = np.sign(ε1*ε2)
#the wave vector
kx = ω / c * np.sqrt(ε1 * ε2 / (ε1 + ε2))
kz1 = np.sqrt(ω**2 / c**2 * ε1 - kx**2)
kz2 = np.sqrt(ω**2 / c**2 * ε2 - kx**2)
kx_real = kx.real
kx_imag = kx.imag
k_vacuum = ω / c
sinbeta_p_45 = kx * c / ω / nCaF2
beta = np.arcsin(sinbeta_p_45) - np.pi/4
sinalpha = nCaF2*np.sin(beta)
alpha = np.arcsin(sinalpha)
theta = alpha + np.pi/4
#sin2theta = -1 + np.sqrt(1 - ((2 * c**2 / ω**2 * kx **2 -2)**2 -3))
#since sin2theta are always grater than 90 degrees
#theta2 = np.arcsin(sin2theta)
#theta = (np.pi - theta2)/2
#convert to degrees
theta_deg = theta * 180 / np.pi
fig = plt.figure(figsize=(8,6.5))
plt.subplot(221)
ax1 = plt.gca()
ax1.set_xlim(range[0], range[1])
#ax1.set_ylim(0, 1000)
ax1.set_xlabel('wavenumbers ($\mathregular{cm^{-1}}$)',size = 15)
ax1.set_ylabel('wave vector ${k_x}$ ($\mathregular{rad{\cdot}m^{-1}}$)',size = 15)
ax1.ticklabel_format(axis='y', style='sci', scilimits=(0,1))
ax1.plot(ωcm, kx_real, label = "real ${k_x}$", color = "blue")
ax1.plot(ωcm, kx_imag, label = "imag ${k_x}$", color = "purple")
ax1.plot(ωcm, k_vacuum, label = "light line", color = "green")
ax1.legend(borderaxespad=0., loc='upper left')
plt.subplot(222)
ax2 = plt.gca()
ax2.set_xlim(range[0], range[1])
```

```
#ax2.set_ylim(45, 50)
ax2.set_xlabel('wavenumbers ($\mathregular{cm^{-1}}$)',size = 15)
ax2.set_ylabel('Incident Angle θ (${^{\circ}}$)',size = 15)
ax2.set_ylim([45,50])
ax2.plot(ωcm, theta_deg, color = "blue", linewidth = 0.5)
#ax2.plot(ωcm, theta_deg.imag, color = "purple")
#ax2.legend(borderaxespad=0., loc='upper right')
plt.subplot(223)
ax3 = plt.gca()
#ax3.autoscale_view(tight=None, scalex=False, scaley=True)
ax3.set_xlim(2200, 2250)
ax3.set_ylim(1.35e6, 1.5e6)
ax3.set_xlabel('wavenumbers ($\mathregular{cm^{-1}}$)',size = 15)
ax3.set_ylabel('Re(${k_x}$) ($\mathregular{rad{\cdot}m^{-1}}$)',size = 15)
ax3.ticklabel_format(axis='y', style='sci', scilimits=(0,1))
ax3.plot(ωcm, kx_real, label = "real ${k_x}$", color = "blue")
#ax3.plot(ωcm, k_vacuum, label = "light line")
ax3.legend(borderaxespad=0., loc='upper left')

plt.subplot(224)
ax4 = plt.gca()
ax4.set_xlim(2200, 2250)
ax4.set_ylim(2000, 50000)
ax4.set_xlabel('wavenumbers ($\mathregular{cm^{-1}}$)',size = 15)
ax4.set_ylabel('Im(${k_x}$) ($\mathregular{rad{\cdot}m^{-1}}$)',size = 15)
ax4.ticklabel_format(axis='y', style='sci', scilimits=(0,1))
ax4.plot(ωcm, kx_imag, label = "imag ${k_x}$", color = "purple")
#ax4.plot(ωcm, k_vacuum, label = "light line")
ax4.legend(borderaxespad=0., loc='upper left')
plt.subplots_adjust(wspace =0.5, hspace =0.5, top = 0.9, left = 0.2)
plt.show()
```

A11.2.2. Reflectance Map

```
import numpy as np
import matplotlib.pyplot as plt
import scipy.interpolate as inp
from pandas import read_csv
from scipy.signal import argrelextrema
from matplotlib.colors import ListedColormap,LinearSegmentedColormap
from matplotlib.ticker import MultipleLocator, FormatStrFormatter

## The constants
c = 2.99792458e8
e = 1.6021773e-19
h = 6.6260755e-34
```

```
hb = 1.05457e-34
kB = 1.380658e-23
me = 9.109389e-31
ep0 = 8.85419e-12 # epsilon 0
mu0 = 4*np.pi*1e-7


## Parameters of CdO
D = 190 #nm
ne2 = 3.5 * 1e26 # per cubic meter
mu = 300 / 10000
EINF2 = 5.5

meff2 = 0.21*me
wp2 = np.sqrt(ne2*e**2/(meff2*ep0))
EPL2 = wp2 / (2*np.pi*c*100)
EPL22 = EPL2**2
Gamma2 = e / (2*mu*meff2)
GAM2 = Gamma2 / (2*np.pi*c*100)
#GAM2 = 74.1
#EPL2 = 12050

## Parameters of Gold
#EINFGOLD = 9.5 # unitless
#EPLGOLD = 9.06 * e / h / c / 100 # convert eV to cm-1
#GAMGOLD = 0.071 * e / h / c / 100 # convert eV to cm-1
#EPGOLD = EINFGOLD - EPLGOLD**2/(Energy*(Energy + 1j*GAMGOLD))
DG = 6.4 # nm
def gold(wcm):
    dgold = read_csv("Gold.csv")
    xgold = dgold['wavn']
    ygold_real = dgold['ep1']
    ygold_imag = dgold['ep2']
    tgold_real = inp.splrep(xgold,ygold_real)
    tgold_imag = inp.splrep(xgold,ygold_imag)
    egold_real = inp.splev(wcm,tgold_real)
    egold_imag = inp.splev(wcm,tgold_imag)
    egold = egold_real + 1j* egold_imag
    return egold

## Parameters of N2O
p = 1.333333 * 1e5 #Pascal
ne3 = p / kB / 298.15 # number per cubic meter
meff3 = 2.6e4*me # calculated from Hessian matrix and reduced mass
wp3 = np.sqrt(ne3*e**2/(meff3*ep0))
EPL3 = wp3 / (2*np.pi*c*100)
```

```
EINF3 = 1
EG3_1 = 2205 #absorbing frequency
EG3_12 = EG3_1**2
EG3_2 = 2240 #absorbing frequency
EG3_22 = EG3_2**2
GAM3_1 = 10
GAM3_2 = 7.5
#EPL3 = 10.6
EPL32 = EPL3**2

## Parameters of substrate and prism
#EP1 = 2.0
#EPP = 2.0
H_0 = 1
def prism(wcm):
    dprism = read_csv("CaF2.csv")
    xprism = dprism['wavn']
    yprism = dprism['e']
    tprism = inp.splrep(xprism,yprism)
    eprism = inp.splev(wcm,tprism)
    return eprism

def substrate(wcm):
    dsubstrate = read_csv("MgO.csv")
    xsubstrate = dsubstrate['wavn']
    ysubstrate = dsubstrate['e'] #e means epsilon
    tsubstrate = inp.splrep(xsubstrate,ysubstrate)
    esubstrate = inp.splev(wcm,tsubstrate)
    return esubstrate

def kretschmann(THET,EPP):
    ALPA = THET - np.pi/4
    BETA = np.arcsin(np.sin(ALPA)/np.sqrt(EPP))
    ANGL = BETA + np.pi/4
    return ANGL

def find_maxima(nparrayx, nparrayy):
    nparrayy = np.array(nparrayy)
    nparrayy_max_indices = argrelextrema(nparrayy, np.greater)
    ## need to find if the maximum is the absorbing peak
    interval = 20 # cm-1
    peaks_indices = []
    for i in nparrayy_max_indices[0]:
        x = nparrayx[i]
        if abs(x - EG3_1) < interval or abs(x - EG3_2) < interval:
            peaks_indices.append(i)
```

```
    return np.array(peaks_indices)

def EF_average(a,b):
    a_avr = np.average(a)
    b_avr = np.average(b)
    return a_avr/b_avr

def EF_int(a):
    sum_a = np.sum(a)
    #sum_a = np.sum(np.maximum(a,0))
    int_a = sum_a*E_STEP
    return int_a

def phase(a,b):
    c = abs(a[0] - b[0])
    if c < 1.5:
        return "in phase"
    else:
        return "out of phase"

def fresnel(THET, Energy, D, Conductor, Ambient):
    ## Layer 0: Prism
    EPP = prism(Energy)
    ANGL = kretschmann(THET,EPP)
    S2 = np.sin(ANGL)
    EPPS2 = EPP*S2*S2

    ## Layer 1: Substrate: Al2O3
    EP1 = substrate(Energy)
    N1Z = np.sqrt(EP1 - EPPS2)

    ## Layer 2: Conductor
    if Conductor == "CdO":
        EP2 = EINF2 - EPL22/(Energy*(Energy + 2j*GAM2))
        print("cdo")
    elif Conductor == "Gold":
        EP2 = gold(Energy)
        print("gold")
    elif Conductor == "None":
        EP2 = EP1
        print("no conductor")
    N2Z = np.sqrt(EP2 - EPPS2)
    Z = (2*np.pi*1e-7*Energy*N2Z*D)*1j #1e-7 convert cm-1 from Energy and nm from D to m

    ## Layer 3: Ambient
    if Ambient == "N2O":
```

```
        EP3 = EINF3 + EPL32 * (0.5 / (EG3_12 - Energy**2 - 2j*Energy*GAM3_1) + 0.5 /
(EG3_22 - Energy**2 - 2j*Energy*GAM3_2))
        print("n2o")
    elif Ambient == "None":
        EP3 = 1 + 0*1j #which is a unit array
        print("no ambient")
    N3Z = np.sqrt(EP3 - EPPS2)

    ## Fresnel Equations:
    X12P = EP2*N1Z + EP1*N2Z
    X12M = EP2*N1Z - EP1*N2Z
    X23P = EP3*N2Z + EP2*N3Z
    X23M = EP3*N2Z - EP2*N3Z
    #All of these reflectance and transmittance are the ratios of magnetic fields
    r12 = X12M/X12P
    r23 = X23M/X23P
    t12 = 2*EP2*N1Z/X12P
    t23 = 2*EP3*N2Z/X23P

    ## Transition matrix, propagation phase shift

    EX = np.exp(Z)
    rNUM = r12 + r23*EX**2
    DENOM = 1 + r12*r23*EX**2
    tNUM = t12*t23*EX
    denom = abs(DENOM)
    t123 = tNUM/DENOM
    r123 = rNUM/DENOM
    R123 = abs(r123)**2
    return R123


#fig, ax = plt.subplots(figsize=(9,2.5),dpi=600)
fig, ax = plt.subplots(figsize=(12,10))
#ax.set(xlim = [15000,25000], ylim = [15,70])
ax.set(xlim = [1500,5000], ylim = [45,50])
ax.set_xlabel('[$\mathregular{cm^{-1}}$]',size=20)
wcm = np.arange(1500,5000,10)
theta = np.arange(15,70,0.03)
#X,Y = np.meshgrid(wcm, theta)
Y,X = np.meshgrid(theta, wcm)
#data = fresnel(Y, X, D, "CdO", "None")
data = fresnel(np.deg2rad(Y), X, D, "CdO", "N2O")
#xmajorLocator = MultipleLocator(500)
#ymajorLocator = MultipleLocator(1)
ax.set_ylabel('angle [${^{\circ}}$]',size=20)
```

```
ax.tick_params(axis='x', labelsize=15)
ax.tick_params(axis='y', labelsize=15)
levels = np.linspace(0,1,21)
sc = ax.contourf(X, Y, data, levels=levels, cmap='inferno')
ax.contour(X, Y, data, levels, cmap='inferno', linewidths=0, linestyles='None')
cbar = fig.colorbar(sc, ticks=levels)
#show figure on canvas
plt.show()
```

A11.2.3. EF calculation

```
import numpy as np
import matplotlib.pyplot as plt
import scipy.interpolate as inp
from pandas import read_csv
from scipy.signal import argrelextrema

## The constants
c = 2.99792458e8
e = 1.6021773e-19
h = 6.6260755e-34
hb = 1.05457e-34
kB = 1.380658e-23
me = 9.109389e-31
ep0 = 8.85419e-12 # epsilon 0
mu0 = 4*np.pi*1e-7

## Parameters of plot and else
#THET = np.deg2rad(48)
EI = 1900
EF = 2500
d = 20000 # integral total thickness, nm, for the energy density
NPTS = 10000 # points for energy, frequence
DSTP = 2 # step for the thickness, nm

Energy = np.linspace(EI, EF, NPTS)
E_STEP = (EF - EI) / (NPTS - 1)
Energy_eV = Energy / e * h * c * 100

THETfigure8 = [46.25,47.50,47.81,48.50,52.00]
THETI = 47.81
THETF = 47.9
## Parameters of CdO
D = 190 #nm
ne2 = 3.5 * 1e26 # per cubic meter
mu = 300 / 10000
```

```
EINF2 = 5.5

meff2 = 0.21*me
wp2 = np.sqrt(ne2*e**2/(meff2*ep0))
EPL2 = wp2 / (2*np.pi*c*100)
EPL22 = EPL2**2
Gamma2 = e / (2*mu*meff2)
GAM2 = Gamma2 / (2*np.pi*c*100)
#GAM2 = 74.1
#EPL2 = 12050

## Parameters of Gold
#EINFGOLD = 9.5 # unitless
#EPLGOLD = 9.06 * e / h / c / 100 # convert eV to cm-1
#GAMGOLD = 0.071 * e / h / c / 100 # convert eV to cm-1
#EPGOLD = EINFGOLD - EPLGOLD**2/(Energy*(Energy + 1j*GAMGOLD))
DG = 3.6 # nm
def gold(wcm):
    dgold = read_csv("Gold.csv")
    xgold = dgold['wavn']
    ygold_real = dgold['ep1']
    ygold_imag = dgold['ep2']
    tgold_real = inp.splrep(xgold,ygold_real)
    tgold_imag = inp.splrep(xgold,ygold_imag)
    egold_real = inp.splev(wcm,tgold_real)
    egold_imag = inp.splev(wcm,tgold_imag)
    egold = egold_real + 1j* egold_imag
    return egold

## Parameters of N2O
p = 1.333333 * 1e5 #Pascal
ne3 = p / kB / 298.15 # number per cubic meter
meff3 = 2.6e4*me # calculated from Hessian matrix and reduced mass
wp3 = np.sqrt(ne3*e**2/(meff3*ep0))
EPL3 = wp3 / (2*np.pi*c*100)
EINF3 = 1
EG3_1 = 2205 #absorbing frequency
EG3_12 = EG3_1**2
EG3_2 = 2240 #absorbing frequency
EG3_22 = EG3_2**2
GAM3_1 = 10
GAM3_2 = 7.5
#EPL3 = 10.6
EPL32 = EPL3**2

## Parameters of substrate and prism
```

```
#EP1 = 2.0
#EPP = 2.0
H_0 = 1
def prism(wcm):
    dprism = read_csv("CaF2.csv")
    xprism = dprism['wavn']
    yprism = dprism['e']
    tprism = inp.splrep(xprism,yprism)
    eprism = inp.splev(wcm,tprism)
    return eprism

def substrate(wcm):
    dsubstrate = read_csv("MgO.csv")
    xsubstrate = dsubstrate['wavn']
    ysubstrate = dsubstrate['e'] #e means epsilon
    tsubstrate = inp.splrep(xsubstrate,ysubstrate)
    esubstrate = inp.splev(wcm,tsubstrate)
    return esubstrate

def kretschmann(THET,EPP):
    ALPA = THET - np.pi/4
    BETA = np.arcsin(np.sin(ALPA)/np.sqrt(EPP))
    ANGL = BETA + np.pi/4
    return ANGL

def find_maxima(nparrayx, nparrayy):
    nparrayy = np.array(nparrayy)
    nparrayy_max_indices = argrelextrema(nparrayy, np.greater)
    ## need to find if the maximum is the absorbing peak
    interval = 20 # cm-1
    peaks_indices = []
    for i in nparrayy_max_indices[0]:
        x = nparrayx[i]
        if abs(x - EG3_1) < interval or abs(x - EG3_2) < interval:
            peaks_indices.append(i)
    return np.array(peaks_indices)

def EF_average(a,b):
    a_avr = np.average(a)
    b_avr = np.average(b)
    return a_avr/b_avr

def EF_int(a):
    sum_a = np.sum(a)
    #sum_a = np.sum(np.maximum(a,0))
    int_a = sum_a*E_STEP
```

```
    return int_a

def phase(a,b):
    c = abs(a[0] - b[0])
    if c < 1.5:
        return "in phase"
    else:
        return "out of phase"

def fresnel(THET, Energy, D, Conductor, Ambient):
    ## Layer 0: Prism
    EPP = prism(Energy)
    ANGL = kretschmann(THET,EPP)
    S2 = np.sin(ANGL)
    EPPS2 = EPP*S2*S2

    ## Layer 1: Substrate: Al2O3
    EP1 = substrate(Energy)
    N1Z = np.sqrt(EP1 - EPPS2)

    ## Layer 2: Conductor
    if Conductor == "CdO":
        EP2 = EINF2 - EPL22/(Energy*(Energy + 2j*GAM2))
        print("cdo")
    elif Conductor == "Gold":
        EP2 = gold(Energy)
        print("gold")
    elif Conductor == "None":
        EP2 = EP1
        print("no conductor")
    N2Z = np.sqrt(EP2 - EPPS2)
    Z = (2*np.pi*1e-7*Energy*N2Z*D)*1j #1e-7 convert cm-1 from Energy and nm from D to m

    ## Layer 3: Ambient
    if Ambient == "N2O":
        EP3 = EINF3 + EPL32 * (0.5 / (EG3_12 - Energy**2 - 2j*Energy*GAM3_1) + 0.5 /
(EG3_22 - Energy**2 - 2j*Energy*GAM3_2))
        print("n2o")
    elif Ambient == "None":
        EP3 = 1 + 0*1j #which is a unit array
        print("no ambient")
    N3Z = np.sqrt(EP3 - EPPS2)

    ## Fresnel Equations:
    X12P = EP2*N1Z + EP1*N2Z
    X12M = EP2*N1Z - EP1*N2Z
```

```
    X23P = EP3*N2Z + EP2*N3Z
    X23M = EP3*N2Z - EP2*N3Z
    #All of these reflectance and transmittance are the ratios of magnetic fields
    r12 = X12M/X12P
    r23 = X23M/X23P
    t12 = 2*EP2*N1Z/X12P
    t23 = 2*EP3*N2Z/X23P

    ## Transition matrix, propagation phase shift

    EX = np.exp(Z)
    rNUM = r12 + r23*EX**2
    DENOM = 1 + r12*r23*EX**2
    tNUM = t12*t23*EX
    denom = abs(DENOM)
    t123 = tNUM/DENOM
    r123 = rNUM/DENOM
    R123 = abs(r123)**2
    return R123


## plots
n_row = 3
n_column = 2
n_count = 1
fig = plt.figure(figsize=(10,12))
for THETDEG in THETfigure8:
    THET = np.deg2rad(THETDEG)
    R123C = fresnel(THET, Energy, D, "CdO", "N2O")
    R123CB = fresnel(THET, Energy, D, "CdO", "None")
    R123G = fresnel(THET, Energy, DG, "Gold", "N2O")
    R123GB = fresnel(THET, Energy, DG, "Gold", "None")
    R123B = fresnel(THET, Energy, 0, "None", "N2O")
    R123BB = fresnel(THET, Energy, 0, "None", "None")
    A123C = -1*np.log(R123C / R123CB)
    A123G = -1*np.log(R123G / R123GB)
    A123B = -1*np.log(R123B / R123BB)
    #find maxima indices
    A123C_maxind = find_maxima(Energy, A123C)
    A123G_maxind = find_maxima(Energy, A123G)
    A123B_maxind = find_maxima(Energy, A123B)
    #calculate the averaged EF
    EF_C = EF_average(A123C[A123C_maxind],A123B[A123B_maxind])
    EF_G = EF_average(A123G[A123G_maxind],A123B[A123B_maxind])
#calculate the integrated EF
    EF_b_int = EF_int(A123B)
```

```
    EF_c_int = EF_int(A123C)
    EF_g_int = EF_int(A123G)
    EF_C_int = EF_c_int/EF_b_int
    EF_G_int = EF_g_int/EF_b_int
    plt.subplot(n_row, n_column, n_count)
    ax1 = plt.gca()
    PHASE = phase(Energy[A123C_maxind],Energy[A123B_maxind])
    ax1.plot(Energy,A123C, color = 'b', label = 'with CdO:Dy')
 #   ax1.plot(Energy,A123G, color = 'r', label = 'Gold')
    ax1.plot(Energy,A123B, color = 'k', label = 'without CdO:Dy')
    ax1.axvline(x = 2205, color='red',linestyle = '--')
    ax1.axvline(x = 2240, color='red',linestyle = '--')
    ax1.set(xlim = [2100, 2350])
## annotate the maxima
 #   ax1.plot(Energy[A123C_maxind],A123C[A123C_maxind],'o',color = 'b')
 #   ax1.plot(Energy[A123G_maxind],A123G[A123G_maxind],'o',color = 'r')
 #   ax1.plot(Energy[A123B_maxind],A123B[A123B_maxind],'o',color = 'k')
#    ax2 = plt.twiny()
#    ax2.plot(Energy_eV,A123G, color = 'b')
    ax1.set_xlabel('wavenumbers ($\mathregular{cm^{-1}}$)',size = 10)
    ax1.set_ylabel('absorbance',size = 10)
    #plt.title("incident angle %.2f${^{\circ}}$"%(THETDEG))
    #plt.title("%.2f${^{\circ}}$ EF = %.1f, %s"%(THETDEG,EF_C_int,PHASE))
    plt.title("%.2f${^{\circ}}$ EF_CdO = %.1f, EF_Au =
%.1f"%(THETDEG,EF_C_int,EF_G_int))
    n_count += 1
#plt.suptitle("Abs and EF, Au layer: %.1f nm, int. ref. baseline: x = 0"%DG, fontsize = 18)
handles, labels = plt.gca().get_legend_handles_labels()
plt.figlegend(handles, labels, ncol = 1, loc = "lower center", borderaxespad = 0, fontsize = 15)
plt.subplots_adjust(wspace =0.5, hspace =0.5)
plt.show()
```

A11.2.4. Dielectric function for Gold in Gold.csv

```
wavn,ep1,ep2,n,k
4.01E+02,-1.71E+04,1.09E+04,3.98E+01,1.37E+02
4.17E+02,-1.63E+04,1.02E+04,3.83E+01,1.33E+02
4.32E+02,-1.55E+04,9.57E+03,3.69E+01,1.30E+02
4.47E+02,-1.47E+04,8.99E+03,3.56E+01,1.26E+02
4.63E+02,-1.40E+04,8.45E+03,3.43E+01,1.23E+02
4.78E+02,-1.34E+04,7.95E+03,3.30E+01,1.20E+02
4.94E+02,-1.28E+04,7.49E+03,3.19E+01,1.18E+02
5.09E+02,-1.23E+04,7.06E+03,3.07E+01,1.15E+02
5.25E+02,-1.17E+04,6.66E+03,2.97E+01,1.12E+02
5.40E+02,-1.13E+04,6.29E+03,2.86E+01,1.10E+02
5.55E+02,-1.08E+04,5.95E+03,2.77E+01,1.08E+02
5.71E+02,-1.04E+04,5.63E+03,2.67E+01,1.05E+02
```

5.86E+02,-9.99E+03,5.33E+03,2.58E+01,1.03E+02
6.02E+02,-9.62E+03,5.05E+03,2.49E+01,1.01E+02
6.17E+02,-9.26E+03,4.78E+03,2.41E+01,9.92E+01
6.33E+02,-8.93E+03,4.54E+03,2.33E+01,9.73E+01
6.48E+02,-8.61E+03,4.31E+03,2.26E+01,9.55E+01
6.63E+02,-8.31E+03,4.09E+03,2.18E+01,9.37E+01
6.79E+02,-8.02E+03,3.89E+03,2.12E+01,9.20E+01
6.94E+02,-7.75E+03,3.70E+03,2.05E+01,9.04E+01
7.10E+02,-7.49E+03,3.52E+03,1.98E+01,8.88E+01
7.25E+02,-7.25E+03,3.36E+03,1.92E+01,8.73E+01
7.41E+02,-7.01E+03,3.20E+03,1.87E+01,8.58E+01
7.56E+02,-6.79E+03,3.05E+03,1.81E+01,8.44E+01
7.71E+02,-6.58E+03,2.91E+03,1.75E+01,8.30E+01
7.87E+02,-6.37E+03,2.78E+03,1.70E+01,8.16E+01
8.02E+02,-6.18E+03,2.66E+03,1.65E+01,8.03E+01
8.18E+02,-5.99E+03,2.54E+03,1.61E+01,7.90E+01
8.33E+02,-5.81E+03,2.43E+03,1.56E+01,7.78E+01
8.49E+02,-5.64E+03,2.32E+03,1.52E+01,7.66E+01
8.64E+02,-5.48E+03,2.22E+03,1.47E+01,7.55E+01
8.79E+02,-5.32E+03,2.13E+03,1.43E+01,7.43E+01
8.95E+02,-5.17E+03,2.04E+03,1.39E+01,7.33E+01
9.11E+02,-5.03E+03,1.96E+03,1.36E+01,7.22E+01
9.26E+02,-4.89E+03,1.88E+03,1.32E+01,7.12E+01
9.41E+02,-4.76E+03,1.80E+03,1.28E+01,7.02E+01
9.57E+02,-4.63E+03,1.73E+03,1.25E+01,6.92E+01
9.72E+02,-4.51E+03,1.66E+03,1.22E+01,6.82E+01
9.87E+02,-4.39E+03,1.60E+03,1.19E+01,6.73E+01
1.00E+03,-4.27E+03,1.54E+03,1.16E+01,6.64E+01
1.02E+03,-4.16E+03,1.48E+03,1.13E+01,6.55E+01
1.03E+03,-4.06E+03,1.42E+03,1.10E+01,6.46E+01
1.05E+03,-3.96E+03,1.37E+03,1.07E+01,6.38E+01
1.06E+03,-3.86E+03,1.32E+03,1.05E+01,6.30E+01
1.08E+03,-3.76E+03,1.27E+03,1.02E+01,6.22E+01
1.10E+03,-3.67E+03,1.22E+03,9.96E+00,6.14E+01
1.11E+03,-3.58E+03,1.18E+03,9.72E+00,6.06E+01
1.13E+03,-3.50E+03,1.14E+03,9.50E+00,5.99E+01
1.14E+03,-3.42E+03,1.10E+03,9.27E+00,5.92E+01
1.16E+03,-3.34E+03,1.06E+03,9.06E+00,5.85E+01
1.17E+03,-3.26E+03,1.02E+03,8.86E+00,5.78E+01
1.19E+03,-3.18E+03,9.88E+02,8.66E+00,5.71E+01
1.20E+03,-3.11E+03,9.55E+02,8.46E+00,5.64E+01
1.22E+03,-3.04E+03,9.23E+02,8.28E+00,5.58E+01
1.23E+03,-2.98E+03,8.93E+02,8.09E+00,5.52E+01
1.25E+03,-2.91E+03,8.64E+02,7.92E+00,5.45E+01
1.27E+03,-2.85E+03,8.36E+02,7.75E+00,5.39E+01
1.28E+03,-2.79E+03,8.09E+02,7.58E+00,5.33E+01

1.30E+03,-2.73E+03,7.83E+02,7.42E+00,5.27E+01
1.31E+03,-2.67E+03,7.59E+02,7.27E+00,5.22E+01
1.33E+03,-2.61E+03,7.35E+02,7.12E+00,5.16E+01
1.34E+03,-2.56E+03,7.12E+02,6.97E+00,5.11E+01
1.36E+03,-2.51E+03,6.90E+02,6.83E+00,5.05E+01
1.37E+03,-2.46E+03,6.70E+02,6.69E+00,5.00E+01
1.39E+03,-2.41E+03,6.49E+02,6.56E+00,4.95E+01
1.40E+03,-2.36E+03,6.30E+02,6.43E+00,4.90E+01
1.42E+03,-2.31E+03,6.12E+02,6.30E+00,4.85E+01
1.43E+03,-2.27E+03,5.94E+02,6.18E+00,4.80E+01
1.45E+03,-2.22E+03,5.76E+02,6.06E+00,4.75E+01
1.47E+03,-2.18E+03,5.60E+02,5.95E+00,4.71E+01
1.48E+03,-2.14E+03,5.44E+02,5.84E+00,4.66E+01
1.50E+03,-2.10E+03,5.29E+02,5.73E+00,4.62E+01
1.51E+03,-2.06E+03,5.14E+02,5.62E+00,4.57E+01
1.53E+03,-2.02E+03,5.00E+02,5.52E+00,4.53E+01
1.54E+03,-1.98E+03,4.86E+02,5.41E+00,4.49E+01
1.56E+03,-1.95E+03,4.73E+02,5.32E+00,4.45E+01
1.57E+03,-1.91E+03,4.60E+02,5.22E+00,4.40E+01
1.59E+03,-1.88E+03,4.47E+02,5.13E+00,4.36E+01
1.61E+03,-1.84E+03,4.36E+02,5.04E+00,4.32E+01
1.62E+03,-1.81E+03,4.24E+02,4.95E+00,4.29E+01
1.64E+03,-1.78E+03,4.13E+02,4.86E+00,4.25E+01
1.65E+03,-1.75E+03,4.02E+02,4.78E+00,4.21E+01
1.67E+03,-1.72E+03,3.92E+02,4.70E+00,4.17E+01
1.68E+03,-1.69E+03,3.82E+02,4.62E+00,4.14E+01
1.70E+03,-1.66E+03,3.72E+02,4.54E+00,4.10E+01
1.71E+03,-1.63E+03,3.63E+02,4.46E+00,4.07E+01
1.73E+03,-1.61E+03,3.54E+02,4.39E+00,4.03E+01
1.74E+03,-1.58E+03,3.45E+02,4.32E+00,4.00E+01
1.76E+03,-1.55E+03,3.37E+02,4.25E+00,3.96E+01
1.77E+03,-1.53E+03,3.28E+02,4.18E+00,3.93E+01
1.79E+03,-1.50E+03,3.20E+02,4.11E+00,3.90E+01
1.81E+03,-1.48E+03,3.13E+02,4.04E+00,3.87E+01
1.82E+03,-1.46E+03,3.05E+02,3.98E+00,3.84E+01
1.84E+03,-1.43E+03,2.98E+02,3.92E+00,3.80E+01
1.85E+03,-1.41E+03,2.91E+02,3.86E+00,3.77E+01
1.87E+03,-1.39E+03,2.84E+02,3.80E+00,3.74E+01
1.88E+03,-1.37E+03,2.78E+02,3.74E+00,3.71E+01
1.90E+03,-1.35E+03,2.71E+02,3.68E+00,3.69E+01
1.91E+03,-1.32E+03,2.65E+02,3.63E+00,3.66E+01
1.93E+03,-1.30E+03,2.59E+02,3.57E+00,3.63E+01
1.94E+03,-1.28E+03,2.53E+02,3.52E+00,3.60E+01
1.96E+03,-1.27E+03,2.48E+02,3.47E+00,3.57E+01
1.98E+03,-1.25E+03,2.42E+02,3.41E+00,3.55E+01
1.99E+03,-1.23E+03,2.37E+02,3.36E+00,3.52E+01

2.01E+03,-1.21E+03,2.32E+02,3.32E+00,3.49E+01
2.02E+03,-1.19E+03,2.27E+02,3.27E+00,3.47E+01
2.04E+03,-1.18E+03,2.22E+02,3.22E+00,3.44E+01
2.05E+03,-1.16E+03,2.17E+02,3.17E+00,3.42E+01
2.07E+03,-1.14E+03,2.12E+02,3.13E+00,3.39E+01
2.08E+03,-1.13E+03,2.08E+02,3.09E+00,3.37E+01
2.10E+03,-1.11E+03,2.04E+02,3.04E+00,3.35E+01
2.11E+03,-1.09E+03,1.99E+02,3.00E+00,3.32E+01
2.13E+03,-1.08E+03,1.95E+02,2.96E+00,3.30E+01
2.14E+03,-1.06E+03,1.91E+02,2.92E+00,3.28E+01
2.16E+03,-1.05E+03,1.87E+02,2.88E+00,3.25E+01
2.18E+03,-1.04E+03,1.84E+02,2.84E+00,3.23E+01
2.19E+03,-1.02E+03,1.80E+02,2.80E+00,3.21E+01
2.21E+03,-1.01E+03,1.76E+02,2.77E+00,3.19E+01
2.22E+03,-9.94E+02,1.73E+02,2.73E+00,3.17E+01
2.24E+03,-9.81E+02,1.69E+02,2.69E+00,3.14E+01
2.25E+03,-9.68E+02,1.66E+02,2.66E+00,3.12E+01
2.27E+03,-9.55E+02,1.63E+02,2.62E+00,3.10E+01
2.28E+03,-9.43E+02,1.60E+02,2.59E+00,3.08E+01
2.30E+03,-9.31E+02,1.57E+02,2.56E+00,3.06E+01
2.31E+03,-9.19E+02,1.54E+02,2.52E+00,3.04E+01
2.33E+03,-9.07E+02,1.51E+02,2.49E+00,3.02E+01
2.35E+03,-8.95E+02,1.48E+02,2.46E+00,3.00E+01
2.36E+03,-8.84E+02,1.45E+02,2.43E+00,2.98E+01
2.38E+03,-8.73E+02,1.42E+02,2.40E+00,2.96E+01
2.39E+03,-8.62E+02,1.40E+02,2.37E+00,2.95E+01
2.41E+03,-8.51E+02,1.37E+02,2.34E+00,2.93E+01
2.42E+03,-8.41E+02,1.35E+02,2.31E+00,2.91E+01
2.44E+03,-8.31E+02,1.32E+02,2.28E+00,2.89E+01
2.45E+03,-8.20E+02,1.30E+02,2.26E+00,2.87E+01
2.47E+03,-8.11E+02,1.27E+02,2.23E+00,2.86E+01
2.48E+03,-8.01E+02,1.25E+02,2.20E+00,2.84E+01
2.50E+03,-7.91E+02,1.23E+02,2.18E+00,2.82E+01
2.51E+03,-7.82E+02,1.21E+02,2.15E+00,2.80E+01
2.53E+03,-7.72E+02,1.18E+02,2.13E+00,2.79E+01
2.55E+03,-7.63E+02,1.16E+02,2.10E+00,2.77E+01
2.56E+03,-7.54E+02,1.14E+02,2.08E+00,2.75E+01
2.58E+03,-7.46E+02,1.12E+02,2.05E+00,2.74E+01
2.59E+03,-7.37E+02,1.10E+02,2.03E+00,2.72E+01
2.61E+03,-7.28E+02,1.09E+02,2.01E+00,2.71E+01
2.62E+03,-7.20E+02,1.07E+02,1.98E+00,2.69E+01
2.64E+03,-7.12E+02,1.05E+02,1.96E+00,2.68E+01
2.65E+03,-7.04E+02,1.03E+02,1.94E+00,2.66E+01
2.67E+03,-6.96E+02,1.01E+02,1.92E+00,2.65E+01
2.69E+03,-6.88E+02,9.97E+01,1.90E+00,2.63E+01
2.70E+03,-6.80E+02,9.80E+01,1.87E+00,2.62E+01

2.72E+03,-6.73E+02,9.64E+01,1.85E+00,2.60E+01
2.73E+03,-6.65E+02,9.48E+01,1.83E+00,2.59E+01
2.75E+03,-6.58E+02,9.33E+01,1.81E+00,2.57E+01
2.76E+03,-6.51E+02,9.18E+01,1.79E+00,2.56E+01
2.78E+03,-6.44E+02,9.03E+01,1.78E+00,2.54E+01
2.79E+03,-6.37E+02,8.88E+01,1.76E+00,2.53E+01
2.81E+03,-6.30E+02,8.74E+01,1.74E+00,2.52E+01
2.82E+03,-6.23E+02,8.60E+01,1.72E+00,2.50E+01
2.84E+03,-6.17E+02,8.46E+01,1.70E+00,2.49E+01
2.85E+03,-6.10E+02,8.33E+01,1.68E+00,2.48E+01
2.87E+03,-6.04E+02,8.20E+01,1.67E+00,2.46E+01
2.89E+03,-5.97E+02,8.07E+01,1.65E+00,2.45E+01
2.90E+03,-5.91E+02,7.95E+01,1.63E+00,2.44E+01
2.92E+03,-5.85E+02,7.83E+01,1.61E+00,2.42E+01
2.93E+03,-5.79E+02,7.71E+01,1.60E+00,2.41E+01
2.95E+03,-5.73E+02,7.59E+01,1.58E+00,2.40E+01
2.96E+03,-5.67E+02,7.47E+01,1.57E+00,2.39E+01
2.98E+03,-5.61E+02,7.36E+01,1.55E+00,2.37E+01
2.99E+03,-5.56E+02,7.25E+01,1.53E+00,2.36E+01
3.01E+03,-5.50E+02,7.14E+01,1.52E+00,2.35E+01
3.02E+03,-5.44E+02,7.03E+01,1.50E+00,2.34E+01
3.04E+03,-5.39E+02,6.93E+01,1.49E+00,2.33E+01
3.06E+03,-5.34E+02,6.83E+01,1.48E+00,2.31E+01
3.07E+03,-5.28E+02,6.73E+01,1.46E+00,2.30E+01
3.09E+03,-5.23E+02,6.63E+01,1.45E+00,2.29E+01
3.10E+03,-5.18E+02,6.53E+01,1.43E+00,2.28E+01
3.12E+03,-5.13E+02,6.44E+01,1.42E+00,2.27E+01
3.13E+03,-5.08E+02,6.34E+01,1.41E+00,2.26E+01
3.15E+03,-5.03E+02,6.25E+01,1.39E+00,2.25E+01
3.16E+03,-4.98E+02,6.16E+01,1.38E+00,2.24E+01
3.18E+03,-4.93E+02,6.08E+01,1.37E+00,2.23E+01
3.19E+03,-4.89E+02,5.99E+01,1.35E+00,2.22E+01
3.21E+03,-4.84E+02,5.91E+01,1.34E+00,2.20E+01
3.22E+03,-4.79E+02,5.82E+01,1.33E+00,2.19E+01
3.24E+03,-4.75E+02,5.74E+01,1.32E+00,2.18E+01
3.26E+03,-4.70E+02,5.66E+01,1.30E+00,2.17E+01
3.27E+03,-4.66E+02,5.58E+01,1.29E+00,2.16E+01
3.29E+03,-4.62E+02,5.51E+01,1.28E+00,2.15E+01
3.30E+03,-4.57E+02,5.43E+01,1.27E+00,2.14E+01
3.32E+03,-4.53E+02,5.36E+01,1.26E+00,2.13E+01
3.33E+03,-4.49E+02,5.28E+01,1.25E+00,2.12E+01
3.35E+03,-4.45E+02,5.21E+01,1.23E+00,2.11E+01
3.36E+03,-4.41E+02,5.14E+01,1.22E+00,2.10E+01
3.38E+03,-4.37E+02,5.07E+01,1.21E+00,2.09E+01
3.39E+03,-4.33E+02,5.01E+01,1.20E+00,2.08E+01
3.41E+03,-4.29E+02,4.94E+01,1.19E+00,2.08E+01

3.43E+03,-4.25E+02,4.87E+01,1.18E+00,2.07E+01
3.44E+03,-4.21E+02,4.81E+01,1.17E+00,2.06E+01
3.46E+03,-4.18E+02,4.75E+01,1.16E+00,2.05E+01
3.47E+03,-4.14E+02,4.69E+01,1.15E+00,2.04E+01
3.49E+03,-4.10E+02,4.62E+01,1.14E+00,2.03E+01
3.50E+03,-4.07E+02,4.56E+01,1.13E+00,2.02E+01
3.52E+03,-4.03E+02,4.51E+01,1.12E+00,2.01E+01
3.53E+03,-4.00E+02,4.45E+01,1.11E+00,2.00E+01
3.55E+03,-3.96E+02,4.39E+01,1.10E+00,1.99E+01
3.56E+03,-3.93E+02,4.33E+01,1.09E+00,1.99E+01
3.58E+03,-3.90E+02,4.28E+01,1.08E+00,1.98E+01
3.59E+03,-3.86E+02,4.23E+01,1.07E+00,1.97E+01
3.61E+03,-3.83E+02,4.17E+01,1.07E+00,1.96E+01
3.63E+03,-3.80E+02,4.12E+01,1.06E+00,1.95E+01
3.64E+03,-3.76E+02,4.07E+01,1.05E+00,1.94E+01
3.66E+03,-3.73E+02,4.02E+01,1.04E+00,1.94E+01
3.67E+03,-3.70E+02,3.97E+01,1.03E+00,1.93E+01
3.69E+03,-3.67E+02,3.92E+01,1.02E+00,1.92E+01
3.70E+03,-3.64E+02,3.87E+01,1.01E+00,1.91E+01
3.72E+03,-3.61E+02,3.82E+01,1.01E+00,1.90E+01
3.73E+03,-3.58E+02,3.78E+01,9.97E-01,1.90E+01
3.75E+03,-3.55E+02,3.73E+01,9.89E-01,1.89E+01
3.77E+03,-3.52E+02,3.69E+01,9.81E-01,1.88E+01
3.78E+03,-3.49E+02,3.64E+01,9.73E-01,1.87E+01
3.80E+03,-3.46E+02,3.60E+01,9.66E-01,1.86E+01
3.81E+03,-3.44E+02,3.56E+01,9.58E-01,1.86E+01
3.83E+03,-3.41E+02,3.51E+01,9.50E-01,1.85E+01
3.84E+03,-3.38E+02,3.47E+01,9.43E-01,1.84E+01
3.86E+03,-3.35E+02,3.43E+01,9.36E-01,1.83E+01
3.87E+03,-3.33E+02,3.39E+01,9.28E-01,1.83E+01
3.89E+03,-3.30E+02,3.35E+01,9.21E-01,1.82E+01
3.90E+03,-3.28E+02,3.31E+01,9.14E-01,1.81E+01
3.92E+03,-3.25E+02,3.27E+01,9.07E-01,1.81E+01
3.93E+03,-3.22E+02,3.24E+01,9.00E-01,1.80E+01
3.95E+03,-3.20E+02,3.20E+01,8.93E-01,1.79E+01
3.97E+03,-3.17E+02,3.16E+01,8.86E-01,1.78E+01
3.98E+03,-3.15E+02,3.13E+01,8.80E-01,1.78E+01
4.00E+03,-3.12E+02,3.09E+01,8.73E-01,1.77E+01
4.01E+03,-3.10E+02,3.06E+01,8.66E-01,1.76E+01
4.03E+03,-3.08E+02,3.02E+01,8.60E-01,1.76E+01
4.04E+03,-3.05E+02,2.99E+01,8.54E-01,1.75E+01
4.06E+03,-3.03E+02,2.95E+01,8.47E-01,1.74E+01
4.07E+03,-3.01E+02,2.92E+01,8.41E-01,1.74E+01
4.09E+03,-2.98E+02,2.89E+01,8.35E-01,1.73E+01
4.10E+03,-2.96E+02,2.86E+01,8.29E-01,1.72E+01
4.12E+03,-2.94E+02,2.82E+01,8.23E-01,1.72E+01

4.14E+03,-2.92E+02,2.79E+01,8.17E-01,1.71E+01
4.15E+03,-2.90E+02,2.76E+01,8.11E-01,1.70E+01
4.18E+03,-2.85E+02,2.70E+01,7.99E-01,1.69E+01
4.20E+03,-2.83E+02,2.67E+01,7.93E-01,1.68E+01
4.21E+03,-2.81E+02,2.64E+01,7.88E-01,1.68E+01
4.23E+03,-2.79E+02,2.62E+01,7.82E-01,1.67E+01
4.24E+03,-2.77E+02,2.59E+01,7.76E-01,1.67E+01
4.26E+03,-2.75E+02,2.56E+01,7.71E-01,1.66E+01
4.27E+03,-2.73E+02,2.53E+01,7.65E-01,1.65E+01
4.30E+03,-2.69E+02,2.48E+01,7.55E-01,1.64E+01
4.32E+03,-2.67E+02,2.45E+01,7.49E-01,1.64E+01
4.34E+03,-2.65E+02,2.43E+01,7.44E-01,1.63E+01
4.35E+03,-2.63E+02,2.40E+01,7.39E-01,1.62E+01
4.38E+03,-2.60E+02,2.35E+01,7.29E-01,1.61E+01
4.40E+03,-2.58E+02,2.33E+01,7.24E-01,1.61E+01
4.41E+03,-2.56E+02,2.30E+01,7.19E-01,1.60E+01
4.43E+03,-2.54E+02,2.28E+01,7.14E-01,1.60E+01
4.46E+03,-2.51E+02,2.23E+01,7.04E-01,1.58E+01
4.47E+03,-2.49E+02,2.21E+01,7.00E-01,1.58E+01
4.49E+03,-2.47E+02,2.19E+01,6.95E-01,1.57E+01
4.51E+03,-2.45E+02,2.17E+01,6.90E-01,1.57E+01
4.54E+03,-2.42E+02,2.12E+01,6.81E-01,1.56E+01
4.55E+03,-2.40E+02,2.10E+01,6.77E-01,1.55E+01
4.57E+03,-2.39E+02,2.08E+01,6.72E-01,1.55E+01
4.60E+03,-2.35E+02,2.04E+01,6.63E-01,1.54E+01
4.61E+03,-2.34E+02,2.02E+01,6.59E-01,1.53E+01
4.64E+03,-2.31E+02,1.98E+01,6.51E-01,1.52E+01
4.66E+03,-2.29E+02,1.96E+01,6.46E-01,1.52E+01
4.67E+03,-2.28E+02,1.94E+01,6.42E-01,1.51E+01
4.71E+03,-2.25E+02,1.90E+01,6.34E-01,1.50E+01
4.72E+03,-2.23E+02,1.88E+01,6.30E-01,1.50E+01
4.75E+03,-2.20E+02,1.85E+01,6.22E-01,1.49E+01
4.77E+03,-2.19E+02,1.83E+01,6.18E-01,1.48E+01
4.80E+03,-2.16E+02,1.80E+01,6.10E-01,1.47E+01
4.81E+03,-2.15E+02,1.78E+01,6.06E-01,1.47E+01
4.85E+03,-2.12E+02,1.74E+01,5.99E-01,1.46E+01
4.86E+03,-2.10E+02,1.73E+01,5.95E-01,1.45E+01
4.89E+03,-2.08E+02,1.70E+01,5.88E-01,1.44E+01
4.91E+03,-2.06E+02,1.68E+01,5.84E-01,1.44E+01
4.94E+03,-2.04E+02,1.65E+01,5.77E-01,1.43E+01
4.95E+03,-2.02E+02,1.63E+01,5.74E-01,1.42E+01
4.98E+03,-2.00E+02,1.60E+01,5.67E-01,1.42E+01
5.00E+03,-1.98E+02,1.59E+01,5.62E-01,1.41E+01
5.02E+03,-1.97E+02,1.57E+01,5.58E-01,1.40E+01
5.05E+03,-1.95E+02,1.54E+01,5.53E-01,1.40E+01
5.08E+03,-1.93E+02,1.52E+01,5.47E-01,1.39E+01

5.10E+03,-1.91E+02,1.50E+01,5.42E-01,1.38E+01
5.13E+03,-1.89E+02,1.48E+01,5.37E-01,1.38E+01
5.15E+03,-1.87E+02,1.46E+01,5.32E-01,1.37E+01
5.18E+03,-1.85E+02,1.44E+01,5.27E-01,1.36E+01
5.21E+03,-1.83E+02,1.42E+01,5.22E-01,1.36E+01
5.24E+03,-1.81E+02,1.40E+01,5.18E-01,1.35E+01
5.26E+03,-1.80E+02,1.38E+01,5.13E-01,1.34E+01
5.29E+03,-1.78E+02,1.36E+01,5.08E-01,1.33E+01
5.32E+03,-1.76E+02,1.34E+01,5.03E-01,1.33E+01
5.35E+03,-1.74E+02,1.32E+01,4.98E-01,1.32E+01
5.38E+03,-1.72E+02,1.30E+01,4.94E-01,1.31E+01
5.41E+03,-1.70E+02,1.28E+01,4.89E-01,1.31E+01
5.43E+03,-1.69E+02,1.26E+01,4.84E-01,1.30E+01
5.46E+03,-1.67E+02,1.24E+01,4.80E-01,1.29E+01
5.49E+03,-1.65E+02,1.22E+01,4.75E-01,1.29E+01
5.53E+03,-1.63E+02,1.20E+01,4.71E-01,1.28E+01
5.56E+03,-1.61E+02,1.19E+01,4.66E-01,1.27E+01
5.59E+03,-1.60E+02,1.17E+01,4.62E-01,1.26E+01
5.62E+03,-1.58E+02,1.15E+01,4.57E-01,1.26E+01
5.65E+03,-1.56E+02,1.13E+01,4.53E-01,1.25E+01
5.68E+03,-1.54E+02,1.12E+01,4.49E-01,1.24E+01
5.71E+03,-1.53E+02,1.10E+01,4.44E-01,1.24E+01
5.75E+03,-1.51E+02,1.08E+01,4.40E-01,1.23E+01
5.78E+03,-1.49E+02,1.07E+01,4.36E-01,1.22E+01
5.81E+03,-1.47E+02,1.05E+01,4.32E-01,1.22E+01
5.85E+03,-1.46E+02,1.03E+01,4.28E-01,1.21E+01
5.88E+03,-1.44E+02,1.02E+01,4.23E-01,1.20E+01
5.92E+03,-1.42E+02,1.00E+01,4.19E-01,1.19E+01
5.95E+03,-1.41E+02,9.86E+00,4.15E-01,1.19E+01
5.99E+03,-1.39E+02,9.70E+00,4.11E-01,1.18E+01
6.02E+03,-1.37E+02,9.55E+00,4.07E-01,1.17E+01
6.06E+03,-1.36E+02,9.40E+00,4.03E-01,1.17E+01
6.10E+03,-1.34E+02,9.25E+00,3.99E-01,1.16E+01
6.13E+03,-1.32E+02,9.10E+00,3.95E-01,1.15E+01
6.17E+03,-1.31E+02,8.96E+00,3.91E-01,1.14E+01
6.21E+03,-1.29E+02,8.81E+00,3.87E-01,1.14E+01
6.25E+03,-1.28E+02,8.67E+00,3.84E-01,1.13E+01
6.29E+03,-1.26E+02,8.53E+00,3.80E-01,1.12E+01
6.33E+03,-1.24E+02,8.39E+00,3.76E-01,1.12E+01
6.37E+03,-1.23E+02,8.25E+00,3.72E-01,1.11E+01
6.41E+03,-1.21E+02,8.11E+00,3.68E-01,1.10E+01
6.45E+03,-1.20E+02,7.98E+00,3.65E-01,1.09E+01
6.49E+03,-1.18E+02,7.85E+00,3.61E-01,1.09E+01
6.54E+03,-1.17E+02,7.72E+00,3.57E-01,1.08E+01
6.58E+03,-1.15E+02,7.59E+00,3.54E-01,1.07E+01
6.62E+03,-1.14E+02,7.46E+00,3.50E-01,1.07E+01

6.67E+03,-1.12E+02,7.33E+00,3.46E-01,1.06E+01
6.71E+03,-1.10E+02,7.20E+00,3.43E-01,1.05E+01
6.76E+03,-1.09E+02,7.08E+00,3.39E-01,1.04E+01
6.80E+03,-1.07E+02,6.96E+00,3.36E-01,1.04E+01
6.85E+03,-1.06E+02,6.84E+00,3.32E-01,1.03E+01
6.90E+03,-1.05E+02,6.72E+00,3.28E-01,1.02E+01
6.94E+03,-1.03E+02,6.60E+00,3.25E-01,1.02E+01
6.99E+03,-1.02E+02,6.48E+00,3.21E-01,1.01E+01
7.41E+03,-8.99E+01,5.52E+00,2.91E-01,9.48E+00
7.46E+03,-8.85E+01,5.42E+00,2.88E-01,9.41E+00
7.52E+03,-8.71E+01,5.31E+00,2.85E-01,9.34E+00
7.58E+03,-8.57E+01,5.21E+00,2.81E-01,9.26E+00
7.63E+03,-8.44E+01,5.11E+00,2.78E-01,9.19E+00
7.69E+03,-8.30E+01,5.00E+00,2.74E-01,9.11E+00
7.75E+03,-8.16E+01,4.90E+00,2.71E-01,9.04E+00
7.81E+03,-8.02E+01,4.79E+00,2.67E-01,8.96E+00
7.87E+03,-7.89E+01,4.68E+00,2.64E-01,8.89E+00
7.94E+03,-7.75E+01,4.58E+00,2.60E-01,8.81E+00
8.00E+03,-7.62E+01,4.48E+00,2.57E-01,8.73E+00
8.06E+03,-7.49E+01,4.38E+00,2.53E-01,8.66E+00
8.13E+03,-7.36E+01,4.28E+00,2.50E-01,8.58E+00
8.19E+03,-7.23E+01,4.19E+00,2.46E-01,8.50E+00
8.27E+03,-7.10E+01,4.09E+00,2.43E-01,8.43E+00
8.33E+03,-6.97E+01,4.00E+00,2.39E-01,8.35E+00
8.40E+03,-6.84E+01,3.90E+00,2.36E-01,8.27E+00
8.48E+03,-6.72E+01,3.81E+00,2.33E-01,8.20E+00
8.55E+03,-6.59E+01,3.72E+00,2.29E-01,8.12E+00
8.62E+03,-6.47E+01,3.64E+00,2.26E-01,8.04E+00
8.69E+03,-6.34E+01,3.55E+00,2.23E-01,7.97E+00
8.78E+03,-6.22E+01,3.46E+00,2.20E-01,7.89E+00
8.85E+03,-6.10E+01,3.38E+00,2.16E-01,7.81E+00
8.93E+03,-5.98E+01,3.30E+00,2.13E-01,7.73E+00
9.01E+03,-5.86E+01,3.22E+00,2.10E-01,7.66E+00
9.09E+03,-5.74E+01,3.14E+00,2.07E-01,7.58E+00
9.17E+03,-5.62E+01,3.06E+00,2.04E-01,7.50E+00
9.26E+03,-5.51E+01,2.98E+00,2.01E-01,7.42E+00
9.35E+03,-5.39E+01,2.91E+00,1.98E-01,7.34E+00
9.44E+03,-5.27E+01,2.84E+00,1.95E-01,7.27E+00
9.53E+03,-5.16E+01,2.76E+00,1.92E-01,7.19E+00
9.61E+03,-5.05E+01,2.69E+00,1.89E-01,7.11E+00
9.71E+03,-4.94E+01,2.62E+00,1.87E-01,7.03E+00
9.81E+03,-4.83E+01,2.56E+00,1.84E-01,6.95E+00
9.90E+03,-4.72E+01,2.49E+00,1.81E-01,6.87E+00
1.00E+04,-4.61E+01,2.43E+00,1.79E-01,6.79E+00
1.01E+04,-4.50E+01,2.36E+00,1.76E-01,6.71E+00
1.02E+04,-4.39E+01,2.30E+00,1.73E-01,6.63E+00

1.03E+04,-4.29E+01,2.24E+00,1.71E-01,6.55E+00
1.04E+04,-4.18E+01,2.18E+00,1.69E-01,6.47E+00
1.05E+04,-4.08E+01,2.12E+00,1.66E-01,6.39E+00
1.06E+04,-3.98E+01,2.07E+00,1.64E-01,6.31E+00
1.08E+04,-3.87E+01,2.01E+00,1.62E-01,6.23E+00
1.09E+04,-3.77E+01,1.96E+00,1.60E-01,6.15E+00
1.10E+04,-3.67E+01,1.91E+00,1.58E-01,6.06E+00
1.11E+04,-3.58E+01,1.86E+00,1.56E-01,5.98E+00
1.12E+04,-3.48E+01,1.81E+00,1.54E-01,5.90E+00
1.14E+04,-3.38E+01,1.77E+00,1.52E-01,5.82E+00
1.15E+04,-3.28E+01,1.72E+00,1.50E-01,5.73E+00
1.16E+04,-3.19E+01,1.68E+00,1.49E-01,5.65E+00
1.18E+04,-3.09E+01,1.64E+00,1.47E-01,5.57E+00
1.19E+04,-3.00E+01,1.60E+00,1.46E-01,5.48E+00
1.21E+04,-2.91E+01,1.56E+00,1.45E-01,5.40E+00
1.22E+04,-2.82E+01,1.52E+00,1.44E-01,5.31E+00
1.23E+04,-2.73E+01,1.49E+00,1.43E-01,5.22E+00
1.25E+04,-2.64E+01,1.46E+00,1.42E-01,5.14E+00
1.27E+04,-2.55E+01,1.43E+00,1.41E-01,5.05E+00
1.28E+04,-2.46E+01,1.40E+00,1.41E-01,4.96E+00
1.30E+04,-2.37E+01,1.37E+00,1.41E-01,4.88E+00
1.32E+04,-2.29E+01,1.35E+00,1.41E-01,4.79E+00
1.33E+04,-2.20E+01,1.33E+00,1.42E-01,4.70E+00
1.35E+04,-2.12E+01,1.31E+00,1.42E-01,4.61E+00
1.37E+04,-2.04E+01,1.30E+00,1.44E-01,4.51E+00
1.39E+04,-1.95E+01,1.28E+00,1.45E-01,4.42E+00
1.41E+04,-1.87E+01,1.27E+00,1.47E-01,4.33E+00
1.43E+04,-1.79E+01,1.27E+00,1.49E-01,4.23E+00
1.45E+04,-1.71E+01,1.26E+00,1.52E-01,4.14E+00
1.47E+04,-1.63E+01,1.26E+00,1.56E-01,4.04E+00
1.49E+04,-1.55E+01,1.27E+00,1.60E-01,3.94E+00
1.52E+04,-1.48E+01,1.27E+00,1.66E-01,3.84E+00
1.54E+04,-1.40E+01,1.29E+00,1.72E-01,3.74E+00
1.56E+04,-1.32E+01,1.30E+00,1.79E-01,3.64E+00
1.59E+04,-1.25E+01,1.32E+00,1.87E-01,3.53E+00
1.61E+04,-1.17E+01,1.35E+00,1.97E-01,3.43E+00
1.64E+04,-1.10E+01,1.39E+00,2.09E-01,3.32E+00
1.67E+04,-1.02E+01,1.43E+00,2.23E-01,3.20E+00
1.69E+04,-9.47E+00,1.48E+00,2.39E-01,3.09E+00
1.72E+04,-8.73E+00,1.54E+00,2.59E-01,2.97E+00
1.75E+04,-7.99E+00,1.60E+00,2.82E-01,2.84E+00
1.79E+04,-7.25E+00,1.69E+00,3.11E-01,2.71E+00
1.82E+04,-6.50E+00,1.79E+00,3.48E-01,2.57E+00
1.85E+04,-5.74E+00,1.92E+00,3.95E-01,2.43E+00
1.89E+04,-4.96E+00,2.09E+00,4.60E-01,2.27E+00
1.92E+04,-4.17E+00,2.33E+00,5.51E-01,2.12E+00

1.96E+04,-3.39E+00,2.66E+00,6.78E-01,1.96E+00
2.00E+04,-2.65E+00,3.11E+00,8.46E-01,1.84E+00
2.04E+04,-2.03E+00,3.67E+00,1.04E+00,1.76E+00
2.08E+04,-1.58E+00,4.31E+00,1.23E+00,1.76E+00
2.13E+04,-1.34E+00,4.93E+00,1.37E+00,1.80E+00
2.17E+04,-1.27E+00,5.42E+00,1.47E+00,1.85E+00
2.22E+04,-1.27E+00,5.75E+00,1.52E+00,1.89E+00
2.27E+04,-1.25E+00,5.96E+00,1.56E+00,1.92E+00
2.33E+04,-1.18E+00,6.12E+00,1.59E+00,1.93E+00
2.38E+04,-1.12E+00,6.28E+00,1.62E+00,1.94E+00
2.44E+04,-1.11E+00,6.40E+00,1.64E+00,1.95E+00
2.50E+04,-1.12E+00,6.44E+00,1.65E+00,1.96E+00
2.56E+04,-1.09E+00,6.39E+00,1.64E+00,1.95E+00
2.63E+04,-9.71E-01,6.31E+00,1.65E+00,1.92E+00
2.70E+04,-7.88E-01,6.27E+00,1.66E+00,1.89E+00
2.78E+04,-5.92E-01,6.32E+00,1.70E+00,1.86E+00
2.86E+04,-4.50E-01,6.44E+00,1.73E+00,1.86E+00
2.94E+04,-4.07E-01,6.58E+00,1.76E+00,1.87E+00
3.03E+04,-4.69E-01,6.70E+00,1.77E+00,1.90E+00
3.12E+04,-6.13E-01,6.74E+00,1.75E+00,1.92E+00
3.23E+04,-7.98E-01,6.66E+00,1.72E+00,1.94E+00
3.33E+04,-9.63E-01,6.45E+00,1.67E+00,1.93E+00

A11.2.5. Dielectric function for MgO in MgO.csv

wavn,e
250.728,16.1583761
254.585,16.474475
258.442,16.8113171
262.3,17.1709821
266.157,17.5555352
270.014,17.9676297
273.872,18.4103087
277.729,18.8867033
281.586,19.4008029
285.444,19.9572531
289.301,20.561012
293.159,21.2185574
297.016,21.9368227
300.873,22.7246278
304.731,23.5926085
308.588,24.5528922
312.445,25.6210428
316.303,26.816384
320.16,28.1620158
324.017,29.6882291
327.875,31.4341149

331.732,33.4492079
335.589,35.8011466
339.447,38.5822587
343.304,41.9193035
347.161,45.9978257
351.019,51.0962448
354.876,57.6468139
358.733,66.3737823
362.591,78.5792941
366.448,96.8459813
370.305,127.183525
374.163,187.47232
378.02,365.070528
381.878,13489.1238
385.735,-375.646335
389.592,-182.72369
393.45,-119.598592
397.307,-88.2679463
401.164,-69.5411414
405.022,-57.08479
408.879,-48.2059041
412.736,-41.5560577
416.594,-36.3887257
420.451,-32.2602198
424.308,-28.8854102
428.166,-26.0747799
432.023,-23.6991283
435.88,-21.6644573
439.738,-19.9020255
443.595,-18.3615192
447.452,-17.0033112
451.31,-15.7966977
455.167,-14.7182788
459.025,-13.7483013
462.882,-12.8717166
466.739,-12.0755623
470.597,-11.3491749
474.454,-10.6841804
478.311,-10.0730485
482.169,-9.50942945
486.026,-8.9883398
489.883,-8.50509031
493.741,-8.05567237
497.598,-7.63693286
501.455,-7.24581335
505.313,-6.8796457

509.17,-6.53636089
513.027,-6.21386164
516.885,-5.91030627
520.742,-5.62428532
524.599,-5.3543165
528.457,-5.09907806
532.314,-4.85758188
536.171,-4.62874491
540.029,-4.41160062
543.886,-4.20543355
547.744,-4.00938024
551.601,-3.82286468
555.458,-3.64520303
559.316,-3.47578769
563.173,-3.31417755
567.03,-3.15985034
570.888,-3.01232177
574.745,-2.87126185
578.602,-2.73625166
582.46,-2.6069071
586.317,-2.48297002
590.174,-2.36410129
594.032,-2.24999187
597.889,-2.14043595
601.746,-2.03515628
605.604,-1.93389517
609.461,-1.83648894
613.318,-1.74270694
617.176,-1.65233542
621.033,-1.56524157
624.891,-1.48120666
628.748,-1.40011743
632.605,-1.32179883
636.463,-1.24608826
640.32,-1.17288957
644.177,-1.10205772
648.035,-1.03345099
651.892,-0.966991758
655.749,-0.902554651
659.607,-0.840019999
663.464,-0.779324725
667.321,-0.7203602
671.179,-0.66302472
675.036,-0.607267759
678.893,-0.552995192
682.751,-0.500122973

686.608,-0.448608551
690.465,-0.398373378
694.323,-0.349344213
698.18,-0.301490177
702.037,-0.254743642
705.895,-0.209042627
709.752,-0.164364738
713.609,-0.120653676
717.467,-0.077856389
721.324,-0.035956971
725.182,0.005101336
729.039,0.045331866
732.896,0.084776246
736.754,0.12347197
740.611,0.161426734
744.468,0.198676053
748.326,0.235251748
752.183,0.271155244
756.04,0.306417058
759.898,0.341064418
763.755,0.375095533
767.612,0.408535326
771.47,0.44140662
775.327,0.473706487
779.184,0.505455232
783.042,0.536672943
786.899,0.567354363
790.756,0.597517582
794.614,0.627179936
798.471,0.65633493
802.329,0.685006884
806.186,0.713188423
810.043,0.740894984
813.901,0.768141189
817.758,0.794920039
821.615,0.82124552
825.473,0.847131654
829.33,0.872571082
833.187,0.897577749
837.045,0.922164311
840.902,0.946324354
844.759,0.970070605
848.617,0.993415954
852.474,1.01635403
856.331,1.03889786
860.189,1.06105896

864.046,1.08283277
867.903,1.10423097
871.761,1.12526578
875.618,1.1459321
879.476,1.16624765
883.333,1.18620791
887.19,1.2058249
891.048,1.22510988
894.905,1.24405902
898.762,1.26268364
902.62,1.28099524
906.477,1.29899027
910.334,1.31667992
914.192,1.33407464
918.049,1.35117168
921.906,1.36798176
925.764,1.38451511
929.621,1.40076908
933.478,1.41675386
937.336,1.43247915
941.193,1.44794262
945.05,1.46315387
948.908,1.47812231
952.765,1.4928456
956.622,1.50733299
960.48,1.5215933
964.337,1.5356241
968.195,1.5494377
972.052,1.56303163
975.909,1.57641456
979.767,1.5895942
983.624,1.60256847
987.481,1.61534519
991.339,1.62793195
995.196,1.64032607
999.053,1.65253524
1002.911,1.66456649
1006.768,1.67641725
1010.625,1.68809464
1014.483,1.69960535
1018.34,1.71094669
1022.197,1.72212546
1026.055,1.73314758
1029.912,1.74401095
1033.769,1.75472137
1037.627,1.76528472

1041.484,1.77569855
1045.342,1.78597133
1049.199,1.79610032
1053.056,1.80609135
1056.914,1.81594941
1060.771,1.82567213
1064.628,1.83526466
1068.486,1.84473198
1072.343,1.85407145
1076.2,1.86328797
1080.058,1.87238635
1083.915,1.88136386
1087.772,1.89022523
1091.63,1.89897487
1095.487,1.9076104
1099.344,1.91613597
1103.202,1.9245556
1107.059,1.9328673
1110.916,1.94107483
1114.774,1.94918207
1118.631,1.95718679
1122.489,1.96509482
1126.346,1.97290388
1130.203,1.98061751
1134.061,1.98823938
1137.918,1.99576718
1141.775,2.00320454
1145.633,2.01055459
1149.49,2.01781541
1153.347,2.02499011
1157.205,2.03208193
1161.062,2.03908852
1164.919,2.04601347
1168.777,2.05285935
1172.634,2.05962436
1176.491,2.06631143
1180.349,2.07292342
1184.206,2.07945814
1188.063,2.08591861
1191.921,2.09230742
1195.778,2.09862276
1199.635,2.10486718
1203.493,2.11104338
1207.35,2.11714935
1211.208,2.12318919
1215.065,2.12916089

1218.922,2.13506705
1222.78,2.1409101
1226.637,2.146688
1230.494,2.15240331
1234.352,2.15805836
1238.209,2.16365097
1242.066,2.16918379
1245.924,2.17465909
1249.781,2.18007487
1253.638,2.1854332
1257.496,2.19073648
1261.353,2.19598285
1265.21,2.20117418
1269.068,2.20631298
1272.925,2.21139705
1276.782,2.21642872
1280.64,2.22140994
1284.497,2.22633869
1288.354,2.23121708
1292.212,2.23604733
1296.069,2.24082728
1299.927,2.24556012
1303.784,2.25024431
1307.641,2.25488156
1311.499,2.25947371
1315.356,2.26401892
1319.213,2.26851918
1323.071,2.27297627
1326.928,2.27738837
1330.785,2.28175726
1334.643,2.28608455
1338.5,2.29036871
1342.357,2.2946115
1346.215,2.29881432
1350.072,2.30297552
1353.929,2.30709697
1357.787,2.31118003
1361.644,2.31522337
1365.501,2.31922819
1369.359,2.32319632
1373.216,2.32712594
1377.073,2.33101886
1380.931,2.33487624
1384.788,2.33869675
1388.646,2.34248273
1392.503,2.34623269

1396.36,2.34994807
1400.218,2.35363032
1404.075,2.35727793
1407.932,2.36089219
1411.79,2.3644745
1415.647,2.36802338
1419.504,2.37154023
1423.362,2.37502628
1427.219,2.3784802
1431.076,2.38190308
1434.934,2.38529641
1438.791,2.38865873
1442.648,2.39199125
1446.506,2.39529515
1450.363,2.39856912
1454.22,2.40181448
1458.078,2.40503213
1461.935,2.40822103
1465.792,2.4113822
1469.65,2.41451667
1473.507,2.41762339
1477.365,2.42070419
1481.222,2.42375763
1485.079,2.42678512
1488.937,2.4297875
1492.794,2.43276361
1496.651,2.43571444
1500.509,2.43864109
1504.366,2.44154239
1508.223,2.44441932
1512.081,2.44727296
1515.938,2.45010203
1519.795,2.45290747
1523.653,2.4556905
1527.51,2.45844975
1531.367,2.46118625
1535.225,2.46390096
1539.082,2.4665927
1542.939,2.4692625
1546.797,2.47191121
1550.654,2.47453771
1554.511,2.47714295
1558.369,2.47972778
1562.226,2.48229118
1566.084,2.48483469
1569.941,2.48735717

1573.798,2.48985951
1577.656,2.49234252
1581.513,2.49480527
1585.37,2.49724851
1589.228,2.49967311
1593.085,2.502078
1596.942,2.50446399
1600.8,2.50683199
1604.657,2.5091809
1608.514,2.51151149
1612.372,2.51382468
1616.229,2.5161193
1620.086,2.5183963
1623.944,2.52065634
1627.801,2.52289843
1631.658,2.52512341
1635.516,2.52733198
1639.373,2.52952316
1643.231,2.53169831
1647.088,2.53385639
1650.945,2.53599821
1654.803,2.53812453
1658.66,2.54023425
1662.517,2.54232823
1666.375,2.54440716
1670.232,2.54647001
1674.089,2.54851757
1677.947,2.55055051
1681.804,2.55256788
1685.661,2.55457041
1689.519,2.55655874
1693.376,2.55853204
1697.233,2.56049086
1701.091,2.56243591
1704.948,2.56436635
1708.805,2.56628279
1712.663,2.5681859
1716.52,2.57007472
1720.378,2.57195048
1724.235,2.57381232
1728.092,2.57566081
1731.95,2.57749659
1735.807,2.57931883
1739.664,2.58112811
1743.522,2.58292506
1747.379,2.5847088

1751.236,2.58648001
1755.094,2.58823925
1758.951,2.58998566
1762.808,2.59171985
1766.666,2.59344238
1770.523,2.59515256
1774.38,2.59685076
1778.238,2.59853771
1782.095,2.60021255
1785.952,2.60187582
1789.81,2.60352813
1793.667,2.60516867
1797.525,2.60679836
1801.382,2.60841657
1805.239,2.61002373
1809.097,2.61162042
1812.954,2.61320586
1816.811,2.61478058
1820.669,2.6163451
1824.526,2.61789874
1828.383,2.61944188
1832.241,2.62097514
1836.098,2.62249773
1839.955,2.62401019
1843.813,2.62551303
1847.67,2.62700546
1851.527,2.62848807
1855.385,2.62996125
1859.242,2.63142434
1863.099,2.63287784
1866.957,2.63432217
1870.814,2.63575671
1874.672,2.63718226
1878.529,2.63859816
1882.386,2.64000487
1886.244,2.64140283
1890.101,2.64279138
1893.958,2.64417102
1897.816,2.64554209
1901.673,2.64690404
1905.53,2.64825726
1909.388,2.64960223
1913.245,2.65093821
1917.102,2.65226573
1920.96,2.65358518
1924.817,2.65489591

1928.674,2.6561984
1932.532,2.65749298
1936.389,2.65877911
1940.246,2.66005716
1944.104,2.66132752
1947.961,2.66258964
1951.818,2.6638439
1955.676,2.66509067
1959.533,2.6663294
1963.391,2.66756077
1967.248,2.66878418
1971.105,2.6700001
1974.963,2.67120886
1978.82,2.67240985
1982.677,2.67360351
1986.535,2.67479019
1990.392,2.67596932
1994.249,2.67714125
1998.107,2.6783064
2001.964,2.67946419
2005.821,2.68061498
2009.679,2.68175912
2013.536,2.6828961
2017.393,2.68402621
2021.251,2.68514987
2025.108,2.68626654
2028.965,2.68737653
2032.823,2.68848016
2036.68,2.68957698
2040.537,2.69066731
2044.395,2.69175144
2048.252,2.69282891
2052.11,2.69390028
2055.967,2.6949651
2059.824,2.69602369
2063.682,2.69707632
2067.539,2.69812255
2071.396,2.69916265
2075.254,2.700197
2079.111,2.70122504
2082.968,2.70224716
2086.826,2.7032636
2090.683,2.70427394
2094.54,2.70527844
2098.398,2.70627743
2102.255,2.70727044

2106.112,2.70825776
2109.97,2.70923969
2113.827,2.71021576
2117.684,2.71118631
2121.542,2.71215158
2125.399,2.71311114
2129.257,2.71406552
2133.114,2.71501424
2136.971,2.71595764
2140.829,2.71689596
2144.686,2.71782882
2148.543,2.71875643
2152.401,2.71967906
2156.258,2.72059635
2160.115,2.72150853
2163.973,2.72241588
2167.83,2.72331796
2171.687,2.72421503
2175.545,2.72510743
2179.402,2.72599465
2183.259,2.72687697
2187.117,2.72775467
2190.974,2.72862738
2194.831,2.7294953
2198.689,2.73035869
2202.546,2.73121716
2206.404,2.73207118
2210.261,2.73292035
2214.118,2.73376495
2217.976,2.73460516
2221.833,2.73544066
2225.69,2.73627165
2229.548,2.73709837
2233.405,2.73792045
2237.262,2.73873813
2241.12,2.73955166
2244.977,2.74036063
2248.834,2.74116531
2252.692,2.74196591
2256.549,2.74276205
2260.406,2.74355399
2264.264,2.74434195
2268.121,2.74512553
2271.978,2.745905
2275.836,2.74668058
2279.693,2.74745191

2283.551,2.74821938
2287.408,2.74898264
2291.265,2.74974195
2295.123,2.75049747
2298.98,2.75124887
2302.837,2.75199637
2306.695,2.7527402
2310.552,2.75348004
2314.409,2.75421602
2318.267,2.75494842
2322.124,2.75567683
2325.981,2.75640153
2329.839,2.7571227
2333.696,2.75784001
2337.553,2.75855368
2341.411,2.75926387
2345.268,2.75997027
2349.125,2.76067309
2352.983,2.76137253
2356.84,2.76206826
2360.698,2.76276068
2364.555,2.76344942
2368.412,2.76413468
2372.27,2.76481667
2376.127,2.76549509
2379.984,2.76617011
2383.842,2.76684194
2387.699,2.76751027
2391.556,2.76817524
2395.414,2.76883709
2399.271,2.76949548
2403.128,2.77015062
2406.986,2.77080271
2410.843,2.77145142
2414.7,2.77209691
2418.558,2.77273939
2422.415,2.7733786
2426.272,2.77401462
2430.13,2.77464774
2433.987,2.77527759
2437.844,2.7759044
2441.702,2.77652829
2445.559,2.77714902
2449.417,2.77776686
2453.274,2.7783816
2457.131,2.77899335

2460.989,2.77960231
2464.846,2.7802082
2468.703,2.78081114
2472.561,2.78141139
2476.418,2.78200857
2480.275,2.78260293
2484.133,2.78319461
2487.99,2.7837833
2491.847,2.78436918
2495.705,2.78495244
2499.562,2.78553282
2503.419,2.78611041
2507.277,2.78668545
2511.134,2.78725763
2514.991,2.7878271
2518.849,2.78839406
2522.706,2.78895821
2526.563,2.7895197
2530.421,2.79007872
2534.278,2.79063502
2538.135,2.79118868
2541.993,2.79173994
2545.85,2.79228847
2549.708,2.79283464
2553.565,2.79337811
2557.422,2.79391909
2561.28,2.79445771
2565.137,2.79499367
2568.994,2.79552722
2572.852,2.79605842
2576.709,2.79658707
2580.566,2.79711332
2584.424,2.79763728
2588.281,2.79815872
2592.138,2.79867779
2595.996,2.79919463
2599.853,2.79970896
2603.71,2.80022102
2607.568,2.80073086
2611.425,2.80123827
2615.282,2.80174342
2619.14,2.80224638
2622.997,2.80274699
2626.854,2.80324534
2630.712,2.80374158
2634.569,2.80423551

2638.427,2.80472731
2642.284,2.80521681
2646.141,2.80570414
2649.999,2.80618944
2653.856,2.80667245
2657.713,2.80715332
2661.571,2.80763218
2665.428,2.80810884
2669.285,2.80858337
2673.143,2.80905592
2677,2.80952629
2680.857,2.80999462
2684.715,2.81046098
2688.572,2.81092522
2692.429,2.8113874
2696.287,2.81184771
2700.144,2.81230587
2704.001,2.81276207
2707.859,2.8132164
2711.716,2.81366861
2715.573,2.81411891
2719.431,2.81456737
2723.288,2.81501379
2727.146,2.81545837
2731.003,2.81590097
2734.86,2.81634165
2738.718,2.81678055
2742.575,2.81721744
2746.432,2.81765249
2750.29,2.81808582
2754.147,2.81851716
2758.004,2.81894668
2761.862,2.81937448
2765.719,2.81980035
2769.576,2.82022445
2773.434,2.82064685
2777.291,2.82106736
2781.148,2.82148608
2785.006,2.82190316
2788.863,2.8223184
2792.72,2.82273186
2796.578,2.82314373
2800.435,2.82355377
2804.292,2.82396209
2808.15,2.82436883
2812.007,2.82477375

2815.865,2.8251771
2819.722,2.82557869
2823.579,2.82597861
2827.437,2.82637697
2831.294,2.82677358
2835.151,2.82716857
2839.009,2.82756201
2842.866,2.82795375
2846.723,2.82834389
2850.581,2.82873252
2854.438,2.82911947
2858.295,2.82950482
2862.153,2.82988869
2866.01,2.83027092
2869.867,2.8306516
2873.725,2.83103084
2881.439,2.83178447
2885.297,2.83215911
2889.154,2.83253215
2893.011,2.83290366
2896.869,2.8332738
2900.726,2.83364232
2904.583,2.83400938
2908.441,2.83437509
2912.298,2.83473922
2916.156,2.83510197
2920.013,2.83546321
2927.728,2.83618144
2931.585,2.83653839
2935.442,2.83689388
2939.3,2.83724809
2943.157,2.83760081
2947.014,2.83795213
2950.872,2.83830215
2954.729,2.83865072
2958.586,2.8389979
2966.301,2.83968828
2970.158,2.8400314
2974.016,2.84037327
2977.873,2.84071371
2981.73,2.84105282
2985.588,2.84139072
2993.302,2.84206237
2997.16,2.84239635
3001.017,2.84272891
3004.875,2.84306032

3008.732,2.84339033
3012.589,2.84371911
3020.304,2.8443729
3024.161,2.84469788
3028.019,2.84502171
3031.876,2.8453442
3035.733,2.84566547
3039.591,2.84598558
3047.305,2.84662201
3051.163,2.84693851
3055.02,2.84725371
3058.877,2.84756771
3066.592,2.84819225
3070.449,2.84850271
3074.307,2.84881209
3078.164,2.84912023
3082.021,2.8494272
3089.736,2.85003779
3093.594,2.85034141
3097.451,2.85064381
3101.308,2.85094509
3109.023,2.85154437
3112.88,2.8518423
3116.738,2.85213919
3120.595,2.85243493
3128.31,2.85302319
3132.167,2.85331565
3136.024,2.85360703
3139.882,2.85389743
3147.596,2.85447486
3151.454,2.85476207
3155.311,2.85504815
3163.026,2.85561726
3166.883,2.85590022
3170.741,2.85618223
3178.455,2.85674304
3182.313,2.85702198
3186.17,2.85729986
3190.027,2.85757673
3197.742,2.85812754
3201.599,2.85840143
3205.457,2.85867441
3213.171,2.85921728
3217.029,2.85948732
3220.886,2.85975635
3228.601,2.86029157

3232.458,2.86055772
3236.315,2.86082294
3244.03,2.86135059
3247.888,2.86161306
3255.602,2.86213507
3259.46,2.86239477
3263.317,2.86265347
3271.032,2.86316826
3274.889,2.86342425
3278.746,2.86367936
3286.461,2.86418696
3290.318,2.8644394
3298.033,2.86494172
3301.89,2.86519153
3309.605,2.86568864
3313.462,2.86593588
3317.32,2.86618231
3325.035,2.86667259
3328.892,2.86691643
3336.607,2.86740166
3340.464,2.867643
3348.179,2.86812327
3352.036,2.86836214
3355.893,2.8686002
3363.608,2.86907395
3367.465,2.8693096
3375.18,2.86977854
3379.037,2.87001179
3386.752,2.87047601
3390.609,2.87070691
3398.324,2.87116645
3402.182,2.87139508
3409.896,2.87184996
3413.754,2.87207631
3421.468,2.87252665
3425.326,2.87275076
3433.04,2.8731966
3436.898,2.87341849
3444.612,2.87385992
3448.47,2.8740796
3456.184,2.87451668
3463.899,2.87495096
3467.756,2.87516699
3475.471,2.875597
3479.329,2.87581098
3487.043,2.87623672

3490.901,2.87644862
3498.615,2.87687024
3506.33,2.87728918
3510.187,2.8774976
3517.902,2.87791249
3521.759,2.87811889
3529.474,2.87852979
3537.189,2.87893805
3541.046,2.87914118
3548.761,2.87954552
3552.618,2.87974671
3560.333,2.88014721
3568.048,2.88054517
3571.905,2.88074318
3579.62,2.88113737
3587.334,2.88152903
3591.192,2.88172397
3598.906,2.88211194
3606.621,2.88249754
3610.478,2.8826894
3618.193,2.88307138
3625.908,2.88345099
3629.765,2.88363989
3637.48,2.88401596
3645.195,2.88438971
3652.909,2.88476111
3656.767,2.884946
3664.481,2.88531398
3672.196,2.88567975
3679.911,2.88604328
3683.768,2.8862242
3691.483,2.8865844
3699.197,2.88694238
3706.912,2.88729825
3710.77,2.88747539
3718.484,2.88782797
3726.199,2.88817848
3733.914,2.88852689
3741.628,2.88887316
3745.486,2.88904556
3753.2,2.88938874
3760.915,2.88972991
3768.63,2.89006905
3776.344,2.89040614
3784.059,2.89074129
3787.917,2.89090813

3795.631,2.89124028
3803.346,2.8915705
3811.061,2.8918988
3818.775,2.89222513
3826.49,2.8925496
3834.205,2.89287219
3841.919,2.89319287
3849.634,2.89351171
3857.349,2.89382873
3861.206,2.89398653
3868.921,2.89430081
3876.635,2.89461324
3884.35,2.89492393
3892.065,2.89523285
3899.78,2.89554
3907.494,2.89584537
3915.209,2.89614905
3922.924,2.896451
3930.638,2.89675122
3938.353,2.89704978
3946.068,2.89734667
3953.782,2.89764186
3961.497,2.89793543
3969.212,2.89822736
3976.927,2.89851768
3984.641,2.89880635
3992.356,2.89909345
4000.071,2.89937898
4011.643,2.89980429
4019.357,2.90008588
4027.072,2.90036595
4034.787,2.9006445
4042.501,2.90092148
4050.216,2.90119701
4057.931,2.90147104
4065.646,2.90174358
4073.36,2.90201463
4084.932,2.9024185
4092.647,2.90268595
4100.362,2.90295197
4108.076,2.90321654
4115.791,2.90347973
4127.363,2.90387188
4135.078,2.90413161
4142.792,2.90438991
4150.507,2.90464691

4158.222,2.90490254
4169.794,2.90528347
4177.509,2.90553577
4185.223,2.90578674
4192.938,2.90603643
4204.51,2.90640852
4212.225,2.90665499
4219.939,2.90690016
4231.512,2.90726562
4239.226,2.90750766
4246.941,2.90774849
4258.513,2.90810742
4266.228,2.90834519
4273.942,2.90858174
4285.514,2.90893434
4293.229,2.90916794
4304.801,2.90951613
4312.516,2.90974681
4320.23,2.90997631
4331.803,2.91031848
4339.517,2.91054514
4351.089,2.91088305
4358.804,2.91110695
4370.376,2.91144071
4378.091,2.91166186
4389.663,2.91199154
4397.377,2.91220998
4408.95,2.9125357
4416.664,2.91275148
4428.236,2.91307325
4435.951,2.91328647
4447.523,2.91360437
4455.238,2.91381504
4466.81,2.91412915
4474.524,2.9143373
4486.097,2.91464772
4497.668,2.91495588
4505.383,2.91516013
4516.955,2.9154647
4528.527,2.91576713
4536.242,2.91596759
4547.814,2.91626651
4559.386,2.91656335
4567.101,2.91676009
4578.673,2.91705352
4590.245,2.91734491

4597.959,2.91753804
4609.532,2.91782614
4621.104,2.91811225
4632.676,2.9183964
4640.391,2.91858478
4651.962,2.91886572
4663.535,2.91914481
4675.106,2.91942198
4686.679,2.91969734
4698.25,2.91997082
4705.965,2.92015215
4717.538,2.92042266
4729.109,2.92069134
4740.682,2.9209583
4752.253,2.92122346
4763.826,2.92148693
4775.397,2.92174864
4786.97,2.92200871
4798.542,2.92226706
4810.114,2.92252377
4821.686,2.92277882
4833.258,2.92303223
4844.83,2.92328404
4856.402,2.92353424
4867.974,2.92378287
4879.546,2.92402993
4891.118,2.92427544
4902.69,2.92451941
4914.262,2.92476186
4929.691,2.92508278
4941.264,2.92532177
4952.836,2.92555925
4964.408,2.92579529
4975.98,2.92602988
4987.552,2.92626304
5002.981,2.92657171
5014.553,2.9268016
5026.125,2.9270301
5041.555,2.92733264
5053.127,2.92755797
5064.699,2.92778195
5076.271,2.92800461
5091.7,2.92829943
5103.272,2.92851904
5118.702,2.92880987
5130.274,2.9290265

5141.846,2.92924188
5157.275,2.92952711
5168.847,2.92973959
5184.277,2.93002103
5195.849,2.93023069
5211.278,2.93050839
5222.85,2.93071529
5238.279,2.93098934
5249.852,2.93119356
5265.281,2.93146406
5280.71,2.93173254
5292.282,2.93193261
5307.712,2.93219767
5319.284,2.93239518
5334.713,2.93265686
5350.143,2.93291665
5365.572,2.93317457
5377.144,2.93336679
5392.573,2.93362148
5408.003,2.93387438
5423.432,2.93412546
5435.004,2.93431263
5450.434,2.93456067
5465.863,2.93480695
5481.292,2.93505154
5496.722,2.93529445
5512.151,2.93553567
5527.581,2.93577527
5543.01,2.93601321
5558.439,2.93624956
5573.869,2.93648433
5589.298,2.93671751
5604.728,2.93694916
5620.157,2.93717925
5635.586,2.93740783
5651.016,2.93763492
5666.445,2.93786052
5681.875,2.93808467
5701.161,2.93836281
5716.591,2.93858373
5732.02,2.93880322
5747.45,2.93902135
5766.736,2.93929203
5782.166,2.93950708
5797.595,2.93972076
5816.882,2.93998602

5832.311,2.94019674
5851.598,2.94045834
5867.027,2.94066617
5882.457,2.94087277
5901.744,2.94112925
5917.173,2.94133304
5936.459,2.94158609
5955.747,2.94183727
5971.176,2.94203689
5990.462,2.94228476
6009.749,2.94253084
6025.179,2.94272643
6044.465,2.94296934
6063.752,2.94321052
6079.182,2.94340224
6098.468,2.94364037
6117.755,2.94387684
6137.042,2.94411167
6156.329,2.94434489
6175.615,2.9445765
6194.902,2.94480655
6214.189,2.94503506
6233.476,2.94526203
6252.762,2.94548748
6272.049,2.94571146
6291.336,2.94593396
6310.623,2.94615503
6329.909,2.94637464
6353.053,2.94663634
6372.34,2.9468529
6391.627,2.94706809
6410.914,2.94728194
6434.058,2.94753678
6453.344,2.94774771
6472.631,2.94795736
6495.775,2.94820725
6515.062,2.94841411
6538.206,2.94866071
6557.493,2.94886488
6580.637,2.94910828
6603.781,2.94934999
6623.068,2.94955013
6646.212,2.94978878
6669.356,2.95002581
6692.5,2.95026123
6711.787,2.95045621

6734.931,2.95068877
6758.075,2.95091979
6781.219,2.9511493
6804.363,2.95137733
6827.507,2.9516039
6850.651,2.95182903
6873.795,2.95205274
6896.939,2.95227507
6923.941,2.95253272
6947.085,2.9527521
6970.229,2.95297015
6993.373,2.9531869
7020.375,2.95343816
7043.519,2.95365214
7070.52,2.95390023
7093.664,2.95411155
7120.666,2.95435659
7143.81,2.95456533
7170.811,2.9548074
7197.813,2.95504792
7220.957,2.95525287
7247.958,2.95549057
7274.959,2.95572681
7301.961,2.9559616
7328.962,2.95619497
7355.964,2.95642695
7382.965,2.95665754
7409.967,2.9568868
7436.968,2.95711473
7463.97,2.95734137
7490.971,2.95756673
7521.83,2.95782275
7548.832,2.95804546
7575.833,2.95826696
7606.691,2.95851864
7633.693,2.95873763
7664.552,2.95898651
7695.411,2.95923394
7722.412,2.95944926
7753.271,2.95969403
7784.129,2.95993742
7814.988,2.96017948
7845.847,2.96042021
7876.706,2.96065966

A11.2.6. Dielectric function for CaF_2 in CaF2.csv

wavn,e
100.291,7.35083803
104.148,7.42358917
108.006,7.50120254
111.863,7.58394957
115.72,7.67219044
119.578,7.76632438
123.435,7.86671352
127.293,7.97386311
131.15,8.08821818
135.007,8.21036194
138.865,8.3409491
142.722,8.48060774
146.579,8.63015325
150.437,8.79051631
154.294,8.96262704
158.151,9.14768785
162.009,9.34709898
165.866,9.56232461
169.723,9.79525376
173.581,10.04813
177.438,10.3234211
181.295,10.6243087
185.153,10.9546694
189.01,11.3189679
192.867,11.7230182
196.725,12.1741041
200.582,12.6810497
204.439,13.255564
208.297,13.9129151
212.154,14.6727064
216.012,15.5622446
219.869,16.6181833
223.726,17.8933464
227.584,19.465253
231.441,21.450613
235.298,24.0381408
239.156,27.5507855
243.013,32.5859347
246.87,40.4007101
250.728,54.1550739
254.585,84.6657482
258.442,209.722608
262.3,-372.754756
266.157,-94.7604834

270.014,-53.0317086
273.872,-36.2248609
277.729,-27.1737186
281.586,-21.5304458
285.444,-17.6854726
289.301,-14.9067044
293.159,-12.8097526
297.016,-11.1764187
300.873,-9.87136511
304.731,-8.80691402
308.588,-7.92437305
312.445,-7.18185383
316.303,-6.54910265
320.16,-6.00413581
324.017,-5.52989196
327.875,-5.11323794
331.732,-4.74419626
335.589,-4.41457092
339.447,-4.11781968
343.304,-3.8488564
347.161,-3.6033424
351.019,-3.37773795
354.876,-3.16928734
358.733,-2.97556867
362.591,-2.79458289
366.448,-2.62480251
370.305,-2.46484417
374.163,-2.31355826
378.02,-2.17010648
381.878,-2.03364963
385.735,-1.90363106
389.592,-1.77948916
393.45,-1.66075991
397.307,-1.54713971
401.164,-1.43829201
405.022,-1.3339303
408.879,-1.23388441
412.736,-1.13793328
416.594,-1.04587936
420.451,-0.957614499
424.308,-0.872969561
428.166,-0.791788398
432.023,-0.713983197
435.88,-0.639407773
439.738,-0.567921687
443.595,-0.499441028

447.452,-0.433827541
451.31,-0.370947973
455.167,-0.310717285
459.025,-0.252989259
462.882,-0.19767871
466.739,-0.144658293
470.597,-0.093805351
474.454,-0.045037786
478.311,0.00176241
482.169,0.046708528
486.026,0.089874562
489.883,0.131367514
493.741,0.171287464
497.598,0.209700526
501.455,0.246698938
505.313,0.282369932
509.17,0.316768496
513.027,0.349974115
516.885,0.382060422
520.742,0.413072037
524.599,0.443075312
528.457,0.472132299
532.314,0.500278078
536.171,0.527567897
540.029,0.554052366
543.886,0.579758945
547.744,0.604739967
551.601,0.629017436
555.458,0.652632255
559.316,0.67562055
563.173,0.698000094
567.03,0.719803407
570.888,0.741061649
574.745,0.761786929
578.602,0.782006983
582.46,0.801747466
586.317,0.821017242
590.174,0.839839728
594.032,0.858236069
597.889,0.876212671
601.746,0.893789213
605.604,0.910984149
609.461,0.927801529
613.318,0.944258213
617.176,0.960369794
621.033,0.976138734

624.891,0.991584191
628.748,1.00670729
632.605,1.02152162
636.463,1.03603973
640.32,1.05026248
644.177,1.06420107
648.035,1.07786719
651.892,1.09126072
655.749,1.10439192
659.607,1.11727092
663.464,1.12989706
667.321,1.14227987
671.179,1.15442835
675.036,1.16634144
678.893,1.1780281
682.751,1.18949591
686.608,1.20074421
690.465,1.21178082
694.323,1.22261315
698.18,1.23323991
702.037,1.24366854
705.895,1.25390591
709.752,1.26395062
713.609,1.2738094
717.467,1.28348884
721.324,1.29298766
725.182,1.30231433
729.039,1.31146791
732.896,1.32045436
736.754,1.32927913
740.611,1.33794126
744.468,1.34644652
748.326,1.35480019
752.183,1.3630009
756.04,1.37105425
759.898,1.37896536
763.755,1.38673297
767.612,1.39436214
771.47,1.40185766
775.327,1.40921863
779.184,1.4164496
783.042,1.42355524
786.899,1.43053453
790.756,1.4373919
794.614,1.4441317
798.471,1.45075291

802.329,1.45726159
806.186,1.46365665
810.043,1.4699422
813.901,1.4761222
817.758,1.48219569
821.615,1.48816651
825.473,1.49403846
829.33,1.49981052
833.187,1.50548644
837.045,1.5110697
840.902,1.51655937
844.759,1.52195887
848.617,1.52727162
852.474,1.53249659
856.331,1.53763716
860.189,1.54269631
864.046,1.5476733
867.903,1.55257108
871.761,1.55739267
875.618,1.56213708
879.476,1.56680852
883.333,1.57140604
887.19,1.57593248
891.048,1.58039046
894.905,1.58477908
898.762,1.58910092
902.62,1.59335857
906.477,1.59755109
910.334,1.60168097
914.192,1.60575049
918.049,1.60975883
921.906,1.6137083
925.764,1.6176011
929.621,1.62143636
933.478,1.62521626
937.336,1.62894283
941.193,1.63261525
945.05,1.63623554
948.908,1.63980566
952.765,1.64332476
956.622,1.64679478
960.48,1.65021754
964.337,1.65359218
968.195,1.65692137
972.052,1.66020422
975.909,1.66344256

979.767,1.66663797
983.624,1.66978968
987.481,1.67289931
991.339,1.67596845
995.196,1.67899619
999.053,1.68198415
1002.911,1.68493382
1006.768,1.68784432
1010.625,1.69071716
1014.483,1.69355377
1018.34,1.69635327
1022.197,1.69911711
1026.055,1.70184658
1029.912,1.70454093
1033.769,1.70720142
1037.627,1.70982933
1041.484,1.71242386
1045.342,1.71498695
1049.199,1.71751777
1053.056,1.72001758
1056.914,1.7224875
1060.771,1.72492679
1064.628,1.72733657
1068.486,1.72971798
1072.343,1.73207021
1076.2,1.73439437
1080.058,1.73669155
1083.915,1.73896094
1087.772,1.74120361
1091.63,1.74342058
1095.487,1.74561113
1099.344,1.74777621
1103.202,1.74991675
1107.059,1.75203214
1110.916,1.75412325
1114.774,1.75619097
1118.631,1.75823466
1122.489,1.7602557
1126.346,1.76225345
1130.203,1.76422874
1134.061,1.76618241
1137.918,1.76811382
1141.775,1.77002381
1145.633,1.77191313
1149.49,1.77378122
1153.347,1.77562881

1157.205,1.77745667
1161.062,1.77926415
1164.919,1.7810521
1168.777,1.78282114
1172.634,1.78457074
1176.491,1.78630162
1180.349,1.78801445
1184.206,1.78970863
1188.063,1.79138489
1191.921,1.79304385
1195.778,1.79468499
1199.635,1.79630895
1203.493,1.79791637
1207.35,1.79950669
1211.208,1.80108094
1215.065,1.80263856
1218.922,1.80418018
1222.78,1.80570641
1226.637,1.80721667
1230.494,1.8087116
1234.352,1.81019178
1238.209,1.8116566
1242.066,1.81310672
1245.924,1.81454271
1249.781,1.81596401
1253.638,1.81737113
1257.496,1.81876468
1261.353,1.82014414
1265.21,1.82150998
1269.068,1.82286283
1272.925,1.82420208
1276.782,1.82552832
1280.64,1.82684204
1284.497,1.82814268
1288.354,1.82943079
1292.212,1.83070691
1296.069,1.83197047
1299.927,1.83322227
1303.784,1.8344619
1307.641,1.83568978
1311.499,1.83690638
1315.356,1.83811119
1319.213,1.83930473
1323.071,1.84048744
1326.928,1.84165883
1330.785,1.84281934

1334.643,1.8439694
1338.5,1.84510857
1342.357,1.8462373
1346.215,1.84735597
1350.072,1.8484641
1353.929,1.84956217
1357.787,1.85065055
1361.644,1.85172886
1365.501,1.8527974
1369.359,1.85385665
1373.216,1.85490611
1377.073,1.85594624
1380.931,1.85697736
1384.788,1.85799908
1388.646,1.85901202
1392.503,1.86001576
1396.36,1.8610107
1400.218,1.86199718
1404.075,1.86297482
1407.932,1.86394393
1411.79,1.86490488
1415.647,1.86585726
1419.504,1.86680144
1423.362,1.86773774
1427.219,1.86866579
1431.076,1.86958588
1434.934,1.87049839
1438.791,1.87140292
1442.648,1.87229979
1446.506,1.8731893
1450.363,1.8740711
1454.22,1.87494554
1458.078,1.87581283
1461.935,1.8766727
1465.792,1.87752542
1469.65,1.87837125
1473.507,1.8792099
1477.365,1.88004186
1481.222,1.88086673
1485.079,1.88168488
1488.937,1.88249654
1492.794,1.88330138
1496.651,1.88409966
1500.509,1.88489168
1504.366,1.88567711
1508.223,1.8864562

1512.081,1.88722926
1515.938,1.88799591
1519.795,1.88875642
1523.653,1.88951109
1527.51,1.89025957
1531.367,1.89100212
1535.225,1.89173899
1539.082,1.89246986
1542.939,1.893195
1546.797,1.89391464
1550.654,1.89462847
1554.511,1.89533674
1558.369,1.89603968
1562.226,1.89673701
1566.084,1.89742913
1569.941,1.89811573
1573.798,1.89879706
1577.656,1.89947332
1581.513,1.90014426
1585.37,1.90081008
1589.228,1.901471
1593.085,1.90212674
1596.942,1.90277752
1600.8,1.90342356
1604.657,1.90406458
1608.514,1.90470077
1612.372,1.90533239
1616.229,1.90595911
1620.086,1.90658118
1623.944,1.90719878
1627.801,1.90781164
1631.658,1.90841999
1635.516,1.909024
1639.373,1.90962342
1643.231,1.9102186
1647.088,1.91080926
1650.945,1.91139562
1654.803,1.91197788
1658.66,1.91255574
1662.517,1.91312943
1666.375,1.91369914
1670.232,1.91426458
1674.089,1.91482596
1677.947,1.91538347
1681.804,1.91593684
1685.661,1.91648626

1689.519,1.91703192
1693.376,1.91757358
1697.233,1.91811139
1701.091,1.91864554
1704.948,1.9191758
1708.805,1.91970232
1712.663,1.92022531
1716.52,1.92074448
1720.378,1.92126018
1724.235,1.92177216
1728.092,1.92228057
1731.95,1.9227856
1735.807,1.92328702
1739.664,1.92378497
1743.522,1.92427963
1747.379,1.92477075
1751.236,1.92525853
1755.094,1.92574311
1758.951,1.92622426
1762.808,1.92670213
1766.666,1.92717688
1770.523,1.92764833
1774.38,1.92811656
1778.238,1.92858178
1782.095,1.92904375
1785.952,1.92950262
1789.81,1.92995855
1793.667,1.93041132
1797.525,1.93086118
1801.382,1.93130796
1805.239,1.93175176
1809.097,1.93219276
1812.954,1.93263072
1816.811,1.93306581
1820.669,1.93349815
1824.526,1.93392756
1828.383,1.93435415
1832.241,1.93477808
1836.098,1.93519913
1839.955,1.93561745
1843.813,1.93603319
1847.67,1.93644611
1851.527,1.93685639
1855.385,1.93726412
1859.242,1.93766913
1863.099,1.93807155

1866.957,1.93847149
1870.814,1.93886879
1874.672,1.93926366
1878.529,1.93965593
1882.386,1.94004571
1886.244,1.94043312
1890.101,1.94081799
1893.958,1.94120044
1897.816,1.94158058
1901.673,1.94195825
1905.53,1.94233355
1909.388,1.94270662
1913.245,1.94307725
1917.102,1.94344559
1920.96,1.94381175
1924.817,1.94417553
1928.674,1.94453708
1932.532,1.94489649
1936.389,1.9452536
1940.246,1.94560852
1944.104,1.94596135
1947.961,1.94631195
1951.818,1.9466604
1955.676,1.94700682
1959.533,1.94735106
1963.391,1.9476933
1967.248,1.94803336
1971.105,1.9483714
1974.963,1.94870748
1978.82,1.94904145
1982.677,1.94937342
1986.535,1.94970349
1990.392,1.95003151
1994.249,1.95035756
1998.107,1.95068177
2001.964,1.95100397
2005.821,1.95132426
2009.679,1.95164273
2013.536,1.95195926
2017.393,1.95227391
2021.251,1.95258679
2025.108,1.95289778
2028.965,1.95320693
2032.823,1.95351435
2036.68,1.95381991
2040.537,1.9541237

2044.395,1.95442579
2048.252,1.95472606
2052.11,1.95502466
2055.967,1.95532147
2059.824,1.95561658
2063.682,1.95591005
2067.539,1.95620178
2071.396,1.95649182
2075.254,1.9567803
2079.111,1.95706704
2082.968,1.95735216
2086.826,1.95763573
2090.683,1.95791762
2094.54,1.95819791
2098.398,1.9584767
2102.255,1.95875384
2106.112,1.95902942
2109.97,1.95930352
2113.827,1.95957602
2117.684,1.959847
2121.542,1.96011653
2125.399,1.96038449
2129.257,1.96065103
2133.114,1.96091602
2136.971,1.96117954
2140.829,1.96144167
2144.686,1.9617023
2148.543,1.96196148
2152.401,1.96221929
2156.258,1.96247564
2160.115,1.96273058
2163.973,1.96298419
2167.83,1.96323635
2171.687,1.96348713
2175.545,1.96373663
2179.402,1.9639847
2183.259,1.96423142
2187.117,1.96447687
2190.974,1.96472094
2194.831,1.9649637
2198.689,1.9652052
2202.546,1.96544535
2206.404,1.96568427
2210.261,1.96592186
2214.118,1.96615818
2217.976,1.9663933

2221.833,1.96662711
2225.69,1.96685967
2229.548,1.96709107
2233.405,1.96732117
2237.262,1.96755007
2241.12,1.96777782
2244.977,1.96800431
2248.834,1.96822961
2252.692,1.96845379
2256.549,1.96867673
2260.406,1.96889851
2264.264,1.9691192
2268.121,1.96933867
2271.978,1.969557
2275.836,1.96977426
2279.693,1.96999034
2283.551,1.97020536
2287.408,1.97041921
2291.265,1.97063196
2295.123,1.97084367
2298.98,1.97105424
2302.837,1.97126372
2306.695,1.9714722
2310.552,1.97167956
2314.409,1.97188586
2318.267,1.97209116
2322.124,1.97229536
2325.981,1.97249853
2329.839,1.97270072
2333.696,1.97290184
2337.553,1.97310195
2341.411,1.97330109
2345.268,1.97349919
2349.125,1.97369629
2352.983,1.97389245
2356.84,1.97408758
2360.698,1.9742818
2364.555,1.97447499
2368.412,1.97466722
2372.27,1.97485853
2376.127,1.97504886
2379.984,1.97523824
2383.842,1.97542674
2387.699,1.97561426
2391.556,1.97580085
2395.414,1.97598657

2399.271,1.97617133
2403.128,1.97635518
2406.986,1.97653819
2410.843,1.97672026
2414.7,1.97690143
2418.558,1.97708177
2422.415,1.97726119
2426.272,1.97743973
2430.13,1.97761746
2433.987,1.97779428
2437.844,1.97797025
2441.702,1.97814541
2445.559,1.97831969
2449.417,1.97849316
2453.274,1.97866577
2457.131,1.97883755
2460.989,1.97900855
2464.846,1.9791787
2468.703,1.97934802
2472.561,1.97951659
2476.418,1.97968431
2480.275,1.97985124
2484.133,1.98001742
2487.99,1.98018277
2491.847,1.98034734
2495.705,1.98051117
2499.562,1.9806742
2503.419,1.98083645
2507.277,1.98099799
2511.134,1.98115873
2514.991,1.98131872
2518.849,1.981478
2522.706,1.9816365
2526.563,1.98179426
2530.421,1.98195132
2534.278,1.98210763
2538.135,1.9822632
2541.993,1.9824181
2545.85,1.98257223
2549.708,1.98272571
2553.565,1.98287843
2557.422,1.98303045
2561.28,1.98318181
2565.137,1.98333244
2568.994,1.98348238
2572.852,1.98363167

2576.709,1.98378025
2580.566,1.98392815
2584.424,1.98407542
2588.281,1.98422197
2592.138,1.98436787
2595.996,1.98451314
2599.853,1.98465771
2603.71,1.98480164
2607.568,1.98494495
2611.425,1.98508758
2615.282,1.98522957
2619.14,1.98537096
2622.997,1.98551168
2626.854,1.98565177
2630.712,1.98579127
2634.569,1.98593012
2638.427,1.98606838
2642.284,1.98620599
2646.141,1.98634299
2649.999,1.98647943
2653.856,1.98661522
2657.713,1.98675041
2661.571,1.98688503
2665.428,1.98701904
2669.285,1.98715245
2673.143,1.98728531
2677,1.98741755
2680.857,1.98754923
2684.715,1.98768035
2688.572,1.98781087
2692.429,1.98794081
2696.287,1.98807023
2700.144,1.98819905
2704.001,1.98832731
2707.859,1.98845506
2711.716,1.9885822
2715.573,1.98870881
2719.431,1.9888349
2723.288,1.98896042
2727.146,1.98908542
2731.003,1.98920986
2734.86,1.98933377
2738.718,1.98945717
2742.575,1.98958001
2746.432,1.98970233
2750.29,1.98982417

2754.147,1.98994545
2758.004,1.99006621
2761.862,1.99018649
2765.719,1.99030623
2769.576,1.99042547
2773.434,1.99054424
2777.291,1.99066247
2781.148,1.99078019
2785.006,1.99089746
2788.863,1.9910142
2792.72,1.99113045
2796.578,1.99124625
2800.435,1.99136153
2804.292,1.99147633
2808.15,1.99159068
2812.007,1.99170452
2815.865,1.99181792
2819.722,1.99193082
2823.579,1.99204325
2827.437,1.99215524
2831.294,1.99226674
2835.151,1.99237778
2839.009,1.99248839
2842.866,1.99259851
2846.723,1.99270819
2850.581,1.99281744
2854.438,1.99292621
2858.295,1.99303454
2862.153,1.99314244
2866.01,1.99324988
2869.867,1.99335689
2873.725,1.99346349
2881.439,1.99367532
2885.297,1.99378062
2889.154,1.99388547
2893.011,1.99398989
2896.869,1.99409391
2900.726,1.99419749
2904.583,1.99430065
2908.441,1.99440343
2912.298,1.99450576
2916.156,1.99460771
2920.013,1.99470922
2927.728,1.99491105
2931.585,1.99501136
2935.442,1.99511125

2939.3,1.99521078
2943.157,1.99530989
2947.014,1.9954086
2950.872,1.99550694
2954.729,1.99560488
2958.586,1.99570242
2966.301,1.99589638
2970.158,1.99599277
2974.016,1.99608881
2977.873,1.99618445
2981.73,1.99627971
2985.588,1.99637463
2993.302,1.99656329
2997.16,1.99665709
3001.017,1.9967505
3004.875,1.99684358
3008.732,1.99693626
3012.589,1.99702859
3020.304,1.9972122
3024.161,1.99730346
3028.019,1.99739439
3031.876,1.99748494
3035.733,1.99757515
3039.591,1.99766503
3047.305,1.99784371
3051.163,1.99793257
3055.02,1.99802106
3058.877,1.9981092
3066.592,1.99828452
3070.449,1.99837166
3074.307,1.9984585
3078.164,1.99854498
3082.021,1.99863114
3089.736,1.99880249
3093.594,1.9988877
3097.451,1.99897255
3101.308,1.99905709
3109.023,1.99922524
3112.88,1.99930883
3116.738,1.99939212
3120.595,1.99947509
3128.31,1.99964011
3132.167,1.99972214
3136.024,1.99980387
3139.882,1.99988532
3147.596,2.00004727

3151.454,2.00012781
3155.311,2.00020803
3163.026,2.00036761
3166.883,2.00044695
3170.741,2.00052602
3178.455,2.00068324
3182.313,2.00076143
3186.17,2.00083932
3190.027,2.00091693
3197.742,2.00107131
3201.599,2.00114806
3205.457,2.00122456
3213.171,2.00137668
3217.029,2.00145234
3220.886,2.00152772
3228.601,2.00167766
3232.458,2.00175221
3236.315,2.0018265
3244.03,2.00197429
3247.888,2.0020478
3255.602,2.00219398
3259.46,2.0022667
3263.317,2.00233914
3271.032,2.00248326
3274.889,2.00255492
3278.746,2.00262633
3286.461,2.00276841
3290.318,2.00283906
3298.033,2.00297963
3301.89,2.00304953
3309.605,2.00318862
3313.462,2.00325779
3317.32,2.00332672
3325.035,2.00346386
3328.892,2.00353206
3336.607,2.00366776
3340.464,2.00373525
3348.179,2.00386953
3352.036,2.00393631
3355.893,2.00400286
3363.608,2.00413528
3367.465,2.00420114
3375.18,2.00433219
3379.037,2.00439737
3386.752,2.00452707
3390.609,2.00459158

3398.324,2.00471994
3402.182,2.0047838
3409.896,2.00491083
3413.754,2.00497404
3421.468,2.00509977
3425.326,2.00516234
3433.04,2.00528679
3436.898,2.00534872
3444.612,2.00547191
3448.47,2.00553321
3456.184,2.00565515
3463.899,2.00577629
3467.756,2.00583655
3475.471,2.00595647
3479.329,2.00601614
3487.043,2.00613484
3490.901,2.00619391
3498.615,2.00631143
3506.33,2.00642819
3510.187,2.00648627
3517.902,2.00660186
3521.759,2.00665936
3529.474,2.00677381
3537.189,2.0068875
3541.046,2.00694406
3548.761,2.00705664
3552.618,2.00711264
3560.333,2.00722411
3568.048,2.00733485
3571.905,2.00738995
3579.62,2.00749961
3587.334,2.00760855
3591.192,2.00766276
3598.906,2.00777064
3606.621,2.00787783
3610.478,2.00793116
3618.193,2.00803732
3625.908,2.0081428
3629.765,2.00819528
3637.48,2.00829974
3645.195,2.00840354
3652.909,2.00850666
3656.767,2.00855799
3664.481,2.00866013
3672.196,2.00876163
3679.911,2.00886249

3683.768,2.00891268
3691.483,2.00901258
3699.197,2.00911185
3706.912,2.00921051
3710.77,2.00925961
3718.484,2.00935732
3726.199,2.00945443
3733.914,2.00955095
3741.628,2.00964684
3745.486,2.00969458
3753.2,2.00978959
3760.915,2.00988402
3768.63,2.00997786
3776.344,2.01007111
3784.059,2.01016381
3787.917,2.01020994
3795.631,2.01030177
3803.346,2.01039305
3811.061,2.01048377
3818.775,2.01057393
3826.49,2.01066354
3834.205,2.01075262
3841.919,2.01084114
3849.634,2.01092914
3857.349,2.0110166
3861.206,2.01106013
3868.921,2.01114681
3876.635,2.01123296
3884.35,2.0113186
3892.065,2.01140373
3899.78,2.01148834
3907.494,2.01157245
3915.209,2.01165607
3922.924,2.01173919
3930.638,2.0118218
3938.353,2.01190394
3946.068,2.0119856
3953.782,2.01206676
3961.497,2.01214745
3969.212,2.01222768
3976.927,2.01230743
3984.641,2.01238671
3992.356,2.01246553
4000.071,2.0125439
4011.643,2.01266059
4019.357,2.01273782

4027.072,2.01281461
4034.787,2.01289095
4042.501,2.01296685
4050.216,2.01304232
4057.931,2.01311736
4065.646,2.01319196
4073.36,2.01326614
4084.932,2.01337662
4092.647,2.01344974
4100.362,2.01352246
4108.076,2.01359476
4115.791,2.01366665
4127.363,2.01377373
4135.078,2.01384461
4142.792,2.01391509
4150.507,2.01398519
4158.222,2.01405489
4169.794,2.0141587
4177.509,2.01422744
4185.223,2.01429578
4192.938,2.01436375
4204.51,2.014465
4212.225,2.01453204
4219.939,2.01459869
4231.512,2.01469801
4239.226,2.01476376
4246.941,2.01482915
4258.513,2.01492657
4266.228,2.01499108
4273.942,2.01505522
4285.514,2.0151508
4293.229,2.01521409
4304.801,2.01530838
4312.516,2.01537081
4320.23,2.0154329
4331.803,2.01552543
4339.517,2.0155867
4351.089,2.01567799
4358.804,2.01573845
4370.376,2.01582852
4378.091,2.01588818
4389.663,2.01597706
4397.377,2.01603593
4408.95,2.01612365
4416.664,2.01618174
4428.236,2.01626831

4435.951,2.01632565
4447.523,2.01641109
4455.238,2.01646768
4466.81,2.01655201
4474.524,2.01660786
4486.097,2.01669111
4497.668,2.0167737
4505.383,2.01682841
4516.955,2.01690995
4528.527,2.01699086
4536.242,2.01704445
4547.814,2.01712433
4559.386,2.0172036
4567.101,2.0172561
4578.673,2.01733437
4590.245,2.01741203
4597.959,2.01746348
4609.532,2.01754018
4621.104,2.0176163
4632.676,2.01769183
4640.391,2.01774188
4651.962,2.01781647
4663.535,2.01789052
4675.106,2.01796401
4686.679,2.01803696
4698.25,2.01810935
4705.965,2.01815732
4717.538,2.01822884
4729.109,2.01829982
4740.682,2.01837029
4752.253,2.01844024
4763.826,2.01850968
4775.397,2.0185786
4786.97,2.01864704
4798.542,2.01871497
4810.114,2.01878241
4821.686,2.01884936
4833.258,2.01891583
4844.83,2.01898182
4856.402,2.01904734
4867.974,2.01911239
4879.546,2.01917698
4891.118,2.0192411
4902.69,2.01930477
4914.262,2.01936799
4929.691,2.01945159

4941.264,2.01951377
4952.836,2.01957552
4964.408,2.01963683
4975.98,2.01969772
4987.552,2.01975817
5002.981,2.01983813
5014.553,2.01989761
5026.125,2.01995668
5041.555,2.0200348
5053.127,2.02009293
5064.699,2.02015065
5076.271,2.02020798
5091.7,2.0202838
5103.272,2.02034022
5118.702,2.02041485
5130.274,2.02047037
5141.846,2.02052552
5157.275,2.02059848
5168.847,2.02065276
5184.277,2.02072458
5195.849,2.02077802
5211.278,2.02084872
5222.85,2.02090133
5238.279,2.02097093
5249.852,2.02102274
5265.281,2.02109127
5280.71,2.0211592
5292.282,2.02120975
5307.712,2.02127665
5319.284,2.02132644
5334.713,2.02139232
5350.143,2.02145763
5365.572,2.02152237
5377.144,2.02157056
5392.573,2.02163433
5408.003,2.02169756
5423.432,2.02176024
5435.004,2.0218069
5450.434,2.02186865
5465.863,2.02192988
5481.292,2.02199058
5496.722,2.02205078
5512.151,2.02211047
5527.581,2.02216966
5543.01,2.02222835
5558.439,2.02228656

5573.869,2.02234428
5589.298,2.02240152
5604.728,2.02245829
5620.157,2.02251458
5635.586,2.02257042
5651.016,2.0226258
5666.445,2.02268072
5681.875,2.0227352
5701.161,2.02280267
5716.591,2.02285615
5732.02,2.0229092
5747.45,2.02296183
5766.736,2.02302701
5782.166,2.02307869
5797.595,2.02312995
5816.882,2.02319346
5832.311,2.02324381
5851.598,2.02330618
5867.027,2.02335564
5882.457,2.02340471
5901.744,2.0234655
5917.173,2.02351371
5936.459,2.02357343
5955.747,2.02363258
5971.176,2.02367949
5990.462,2.0237376
6009.749,2.02379516
6025.179,2.02384081
6044.465,2.02389738
6063.752,2.02395341
6079.182,2.02399785
6098.468,2.02405292
6117.755,2.02410747
6137.042,2.02416151
6156.329,2.02421503
6175.615,2.02426806
6194.902,2.02432059
6214.189,2.02437263
6233.476,2.02442418
6252.762,2.02447526
6272.049,2.02452587
6291.336,2.02457601
6310.623,2.02462569
6329.909,2.02467492
6353.053,2.02473339
6372.34,2.02478164

6391.627,2.02482945
6410.914,2.02487683
6434.058,2.02493311
6453.344,2.02497956
6472.631,2.02502558
6495.775,2.02508028
6515.062,2.02512541
6538.206,2.02517904
6557.493,2.0252233
6580.637,2.02527589
6603.781,2.02532793
6623.068,2.02537088
6646.212,2.02542193
6669.356,2.02547244
6692.5,2.02552243
6711.787,2.0255637
6734.931,2.02561275
6758.075,2.02566129
6781.219,2.02570934
6804.363,2.02575689
6827.507,2.02580396
6850.651,2.02585056
6873.795,2.02589668
6896.939,2.02594234
6923.941,2.02599503
6947.085,2.02603971
6970.229,2.02608394
6993.373,2.02612772
7020.375,2.02617827
7043.519,2.02622112
7070.52,2.02627059
7093.664,2.02631254
7120.666,2.02636097
7143.81,2.02640204
7170.811,2.02644945
7197.813,2.02649633
7220.957,2.0265361
7247.958,2.026582
7274.959,2.0266274
7301.961,2.0266723
7328.962,2.02671669
7355.964,2.0267606
7382.965,2.02680403
7409.967,2.02684699
7436.968,2.02688947
7463.97,2.02693149

7490.971,2.02697306
7521.83,2.02702002
7548.832,2.02706064
7575.833,2.02710082
7606.691,2.02714622
7633.693,2.02718549
7664.552,2.02722987
7695.411,2.02727371
7722.412,2.02731164
7753.271,2.0273545
7784.129,2.02739686
7814.988,2.02743871
7845.847,2.02748007
7876.706,2.02752094

A11.3. Python codes for Chapter 4
The structure of the directory is given by:

```
Root/
    run.py
    bin/
        __init__.py
        config.py
        constants.py
        convert.py
        dataprocessors.py
        experiments.py
        global_variables.py
        math.py
        optics.py
        physics.py
        plot.py
```

The following pages will display the contents for each file. __init__.py is empty.

A11.3.1. run.py

```
import bin.global_variables as glv
import bin.config
import bin.experiments as expt
import bin.dataprocessors as dp
import bin.plot as plot

#start experiments
experiment = expt.MultiWavExpt(Nanoparticle = glv.Gold2, Molecule = glv.Molecule,
Molecule_cmpr = glv.Molecule_cmpr)
#experiment2 = expt.MultiWavelengthExpt(Laser=glv.Laser, Nanoparticle = glv.Gold2, \
#    Molecule = glv.Molecule, Detector=glv.Detector)

#experiment.plot_multi_ang()
experiment.plot_sg_ang()
#experiment2 = expt.EFMultiRadiiExpt(Laser=glv.Laser, Nanoparticle = glv.Gold_radii, \
#    Molecule = glv.Molecule_radii, Detector=glv.Detector_radii)
#experiment2.plot()
max = dp.find_max(glv.wavl_nm,experiment.signals)
```

A11.3.2. config.py

```
import numpy as np
import bin.constants as const
import bin.convert as cv
import bin.dataprocessors as dp
import bin.global_variables as glv
```

```
import bin.optics as op
from pandas import read_csv

glv.freq = dp.sampline(cv.wavlength_nm2freq_rad(632.9), cv.wavlength_nm2freq_rad(633.1), 100) ## equal sampling the points in frequency regime: start, end, points.
glv.angle_deg = np.arange(0,1,1)

#the radius needs to initiallize first
glv.metal_radius = 15e-9 #in meters
glv.metal_dens = 1.4e17 #particle per meter cubed
glv.Molecule_par_dict = {
"dens" : cv.conc2dens(10e-6), #This does not contribute to the molecular dielectric function
"surface_concentration_factor" : 180000, #This means how could the surface concentrate the molecules
"res_freq" : cv.wavlength_nm2freq_rad(592),
"damp_freq_abs" : cv.wavn2rad(1000),
"damp_freq_Raman" : cv.wavn2rad(1000),
"Raman_shift" : cv.wavn2rad(1605),
"radius": 1.2e-9,
"distance":2e-10, #in meters
"parallel_rate":0, #0 to 1, this is relative to the scattering plane. Actually means molecules are perpendicular to the surface
"metal_dens":glv.metal_dens,
}
glv.Molecule_per_dict = {
"dens" : cv.conc2dens(1e-6), #This does not contribute to the molecular dielectric function
"surface_concentration_factor" : 360000, #This means how could the surface concentrate the molecules
"res_freq" : cv.wavlength_nm2freq_rad(592),
"damp_freq_abs" : cv.wavn2rad(1000),
"damp_freq_Raman" : cv.wavn2rad(1000),
"Raman_shift" : cv.wavn2rad(1605),
"radius": 0.848528e-9, #assume 1 parallel molecule is replaced by 3 perpendicular molecules
"distance":2e-10, #in meters
"parallel_rate":1, #0 to 1, this is relative to the scattering plane. Actually means molecules are perpendicular to the surface
"metal_dens":glv.metal_dens,
}
glv.Molecule_dict = glv.Molecule_par_dict
glv.Molecule_cmpr_dict = {
"dens" : cv.conc2dens(5e-4), # *0.5 means the estimation of sum dipoles on x axis, because the dipoles are randomly polarized
"surface_concentration_factor" : 1,
"res_freq" : cv.wavlength_nm2freq_rad(592),
"damp_freq_abs" : cv.wavn2rad(1000),
"damp_freq_Raman" : cv.wavn2rad(1000),
```

```
"Raman_shift" : cv.wavn2rad(1605),
"radius": 1.2e-9,
"distance":2e-10, #in meters. This is used to calculate the volume of interest.
}

glv.detector_distance = 1 #1m

#glv.freq = mt.sampline(cv.wavlength_nm2freq_rad(589), cv.wavlength_nm2freq_rad(591),
100, cv.wavlength_nm2freq_rad(590), cv.wavlength_nm2freq_rad(590)+cv.wavn2rad(1605),
cv.wavlength_nm2freq_rad(538.7755102040817))



#### Do not change the contents below ::::::::::::::::::::::::::::
#converting units
glv.wavl_nm = cv.freq_rad2wavlength_nm(glv.freq)
glv.wavl_m = glv.wavl_nm * 1e-9
glv.k = 2*np.pi/glv.wavl_m
glv.angle = cv.deg2rad(glv.angle_deg)

#describe the theta angle, for integrate
glv.cos_theta = np.linspace(-1,1,180)

#set up laser parameters

glv.laser_dict = {
   "power_W" : 0.02,
   "crossec_m2" : 0.000004,
   "wavelength_m":glv.wavl_nm/1e9,
   #"wavelength_m1":cv.wavnumbers2wavlength_nm(glv.freq_cm)/1e9,
}

#set up optics
glv.Laser = op.Laser(freq=glv.freq,**glv.laser_dict)
glv.Detector = op.Detector(angle=glv.angle,distance = glv.detector_distance)

#molecules
glv.Molecule = op.Molecule(freq=glv.freq, metal_radius=glv.metal_radius,
**glv.Molecule_dict)
glv.Molecule_cmpr = op.Molecule_cmpr(freq=glv.freq, metal_radius=glv.metal_radius,
**glv.Molecule_cmpr_dict)

#conductors
#prepare conductor parameters
glv.csv_folder="dielectric_functions/" #this is relative to the location of run.py, which is the root
directory of this program
```

```
glv.gold_dict = {
"radius_m" : np.asarray([glv.metal_radius]),
"file" : read_csv(glv.csv_folder+"Gold.csv"),
}
glv.silver_dict = {
"radius_m" : np.asarray([glv.metal_radius]),
"file" : read_csv(glv.csv_folder+"Yang_PhysRevB_15_Ag_C_corrected.csv"),
}
glv.Gold = op.Nanoparticle(freq=glv.freq,k=glv.k,**glv.gold_dict)
glv.Silver = op.Nanoparticle(freq=glv.freq,k=glv.k,**glv.silver_dict)
glv.Gold2 = op.NanoparticleModel(freq=glv.freq,k=glv.k,**glv.gold_dict)

#for multiple radius
glv.gold_radii_dict = {
"radius_m" : 1e-9*np.arange(5,21,1),
"file" : read_csv(glv.csv_folder+"Gold.csv"),
}
radii_freq = np.asarray([glv.Molecule_dict['res_freq']])
radii_k = np.asarray([cv.freq_rad2k(glv.Molecule_dict['res_freq'])])

glv.Detector_radii = op.Detector(angle=0,distance = glv.detector_distance)
glv.Gold_radii = op.NanoparticleModel(freq=radii_freq,k=radii_k,**glv.gold_radii_dict)
glv.Molecule_radii = op.Molecule(freq=radii_freq, metal_radius=glv.metal_radius,
**glv.Molecule_dict)
```

A11.3.3. constants.py

```
import numpy as np
import pandas as pd
#fundamental constants
import numpy as np

CONST_DICT={
'C': 2.998e8,
'E': 1.602e-19,
'NA': 6.022e23,
'EP0': 8.854e-12,
'ME': 9.109e-31,
'H': 6.626e-34,
'H_BAR': 1.054571817e-34,
'DEBYE': 3.33564e-30,
'MU0': 4 *np.pi * 1e-7,
'COULOMB_CONST': 1/4/np.pi/8.854e-12,
'Z0':376.730313668,
'R0Rm':0.02,
}
```

```
class _const:
    class ConstError(TypeError): pass
    class ConstCaseError(ConstError): pass
    def __init__(self):
        self.__dict__.update(CONST_DICT)
    def __setattr__(self, name, value):
        if name in self.__dict__:
            raise self.ConstError("Can't change const.%s" % name)
        if not name.isupper():
            raise self.ConstCaseError("const name %s is not all uppercase'" % name)
        self.__dict__[name] = value

import sys
sys.modules[__name__]=_const() #so that you may call the module directly to access the _const.
#i.const.E. the moledule is _const itself
```

A11.3.4. convert.py

```
import numpy as np
import bin.constants as const

#math conversions
cmplx_conjugate = lambda cmplx : cmplx.real - 1j*cmplx.imag
sin2cos = lambda x: np.sqrt(1-x**2+0j)
cos2sin = sin2cos

deg2rad = lambda angle: np.pi*angle/180
rad2deg = lambda angle: angle*180/np.pi


#frequency, wavelength, wavenumbers
wavn2rad = lambda wavn: wavn * const.C * 100 * 2 * np.pi #wavn: wavenumber in cm-1
rad2wavn = lambda omega: omega/const.C/100/2/np.pi

wavlength_nm2freq_rad = lambda wavl_nm: const.C/wavl_nm * 1e9 * 2 * np.pi
freq_rad2wavlength_nm = wavlength_nm2freq_rad

wavnumbers2wavlength_nm = lambda wavn: 1/ wavn / 100 * 1e9
wavlength_nm2wavnumbers = wavnumbers2wavlength_nm

eV2freq_rad = lambda eV: eV*const.E/const.H_BAR
freq_rad2k = lambda omega: omega/const.C

#convert scattering efficiency per steradian to scattering efficiency
sr2intensity = lambda intensity_per_sr,radius: intensity_per_sr/radius**2
```

```
#concentration and number density
conc2dens = lambda concentration: concentration*const.NA*1000 #concentration in mol/L, dens
in number/m^3
```

A11.3.5. dataprocessors.py

```
import numpy as np
import scipy.interpolate as inp
import bin.math as mt
import bin.global_variables as glv

def sampline(start, end, num_points, *args):
    points = np.linspace(start,end,num_points)
    step = (end - start)/(num_points - 1)
    if args:
        for new_point in args:
            idx = int((new_point - start)//step+1)
            points = np.insert(points, idx, new_point)
    return points

class VecDetector():
    def __init__(self,signal):
    #position,incident_E,freq,angle
        self.Signal = signal

def dataProcessor(signal,conductor,molecule):
    z = (signal - conductor)/molecule
    z = np.maximum(z,0)
    return z

def find_max(wavl,signal):
    ratio = signal[3]
    max_ef = 0
    max_idx = 0
    for i in range(len(ratio)):
        if ratio[i][0] > max_ef:
            max_idx = i
            max_ef = ratio[i][0]
    return (wavl[max_idx],signal[3][max_idx][0])

def interpolate(raw_x,raw_y,target_x):
    smoothed_y = inp.splrep(raw_x,raw_y)
    return inp.splev(target_x,smoothed_y)
```

A11.3.6. experiments.py

```
import numpy as np
```

```
import bin.global_variables as glv
import bin.physics as phys
import bin.optics as op
import bin.plot as plot
import bin.dataprocessors as dp

#spherical experiments
class SimpleSphExperiment():
    def __init__(self,**kwargs): #Laser, Nanoparticle, Molecule, Distance, Detector
        self.Laser = glv.Laser
        self.Detector = glv.Detector
        self.__dict__.update(kwargs)
        self.static()
        #self.mie()
        self.mol_dipole()
        self.img_dipole()
        self.total_dipole()
        self.surface_scatter()
        self.sol_scatter()
    def mie(self):
        #return relative intensity
        self.int_E = \
            phys.mie(self.Nanoparticle.n[self.freq_ct], self.Laser.E_xi, glv.cos_theta,
self.Nanoparticle.k[self.freq_ct], self.Nanoparticle.radius_m, self.Molecule.parallel_rate)
        #we assume the incident E is on -theta direction. then the parallel means the
        #scattered E is at theta&r direction, the perpendicular means the scattered light is at phi
direction
        #the sum of the E field is on x direction
    def static(self):
        #incident E:
        self.inc_E = self.Laser.E_xi
        #total intigrated E
        self.int_E = phys.static_sca(self.Nanoparticle.epsilon[self.freq_ct],\
            self.Molecule.epsilon[self.freq_ct], self.inc_E, \
            self.Nanoparticle.radius_m, self.Molecule.distance, self.Molecule.parallel_rate)
    def mol_dipole(self):
        self.dipole_x = phys.total_dipole(self.int_E, self.Molecule.a_Raman[self.freq_ct],
self.Molecule.surface_number)
    def img_dipole(self):
        self.img_p_x = phys.img_dipole(self.Molecule.epsilon[self.freq_ct], self.Molecule.distance,
\
            self.dipole_x, self.Nanoparticle.epsilon[self.freq_ct], self.Nanoparticle.radius_m)
    def total_dipole(self):
        self.total_p_x = self.dipole_x + self.img_p_x
    def surface_scatter(self):
        self.sca_E = phys.dipole_scatter_E(self.Detector.distance, self.total_p_x,\
```

```
            self.Detector.angle, self.Laser.freq[self.freq_ct], self.Molecule.Raman_shift)
        self.sca_S = phys.E2S(self.sca_E)* self.Molecule.metal_dens
    def sol_scatter(self):
        self.single_p = phys.total_dipole(self.inc_E, self.Molecule.a_Raman[self.freq_ct], 1) *0.5
#*0.5: random direction
        self.sca_E_sol = phys.dipole_scatter_E(self.Detector.distance, self.single_p,\
            self.Detector.angle, self.Laser.freq[self.freq_ct], self.Molecule.Raman_shift)
        self.sca_S_sol = self.Molecule.sol_number * phys.E2S(self.sca_E_sol)

class MoleculeOnly(SimpleSphExperiment):
    def __init__(self,**kwargs):
        self.Laser = glv.Laser
        self.Detector = glv.Detector
        self.__dict__.update(kwargs)
        self.static()
        #self.mie()
        self.sol_scatter()
    def mie(self):
        #self.int_E = phys.empty_mol_E(self.Laser.E_xi, self.Nanoparticle.k[self.freq_ct],
self.Nanoparticle.radius_m) #has phase change, with a hollow particle
        self.int_E = self.Laser.E_xi #no phase difference, compared to no nanoparticle. *0.5 means
the dipoles are randomized. The estimation on x axis is a half
    def static(self):
        self.int_E = self.Laser.E_xi #*0.5 means the dipoles are randomized. The estimation on x
axis is a half
        self.inc_E = self.int_E

class ConductorSignal(SimpleSphExperiment):
    def total_dipole(self):
        self.total_p_x = self.img_p_x

class NoImg(SimpleSphExperiment):
    def img_dipole(self):
        self.img_p_x = 0

class MultiWavExpt():
    def __init__(self,**kwargs):#Laser, Nanoparticle, Molecule, Detector
        self.__dict__.update(kwargs)

        #initiallizing data series
        self.metal_mol = []
        self.metal = []
        self.empty_mol = []
        self.signals = self.expt(**kwargs)

    def expt(self,**kwargs):
```

```
        #because mie program won't work with ndarrays, has to break down the ndarrays for each
single frequency at a time
        for freq_ct in range(len(glv.freq)):
            self.exp_metal_mol = SimpleSphExperiment(freq_ct=freq_ct, Nanoparticle =
self.Nanoparticle, Molecule = self.Molecule)
            self.exp_metal = ConductorSignal(freq_ct=freq_ct, Nanoparticle = self.Nanoparticle,
Molecule = self.Molecule)
            self.exp_empty_mol = MoleculeOnly(freq_ct=freq_ct, Nanoparticle = self.Nanoparticle,
Molecule = self.Molecule_cmpr)

            #generating data series

self.metal_mol.append((self.exp_metal_mol.sca_S+self.exp_metal_mol.sca_S_sol)/self.exp_met
al_mol.Molecule.dens)
            self.metal.append(self.exp_metal.sca_S)

self.empty_mol.append(self.exp_empty_mol.sca_S_sol/self.exp_empty_mol.Molecule.dens)

        #finallize data series
        self.metal_mol = np.asarray(self.metal_mol)
        self.metal = np.asarray(self.metal)
        self.empty_mol = np.asarray(self.empty_mol)
        return self.metal_mol, self.metal, self.empty_mol, self.metal_mol/self.empty_mol

    def plot_multi_ang(self):
        self.titles = ["signal","Img","Molecule","ratio"]
        plot.multi_plots(plot_type=plot.polar_contour,
signals=self.signals,row=2,column=2,titles=self.titles)

    def plot_sg_ang(self):
        self.title = "REP w/ and w/o nanoparticle"
        signal = self.signals[0].T[0]
        molecule = self.signals[2].T[0]
        plot.double_linear_plot(x=glv.wavl_nm,y1=signal,y2=molecule,
y3=signal/molecule,x_label = "wavelength nm", y_label = "signal W/$\mathregular{m^{2}}$",\
            y2_label="EF on same wavelength",y1_legend = "w/ Au", y2_legend = "w/o
Au",y3_legend = "EF", title=self.title)
```

A11.3.7. gloval_variables.py

```
# -*- coding: UTF-8 -*-
''' Set a class to store global variables. '''

class GlobalVariables:
    def __init__(self,**kwargs):
        self.__dict__.update(kwargs)
    #def __setattr__(self, name, value):
```

```
    #    self.__dict__[name] = value
import sys
sys.modules[__name__]=GlobalVariables() #so that you may call the module directly to access the _const.
#i.e. the moledule is _const itself
```

A11.3.8. maths.py

```
import numpy as np
import bin.convert as cv
'''
vector defined in structure
'''

def cross_rxxxr(v1_x,v2_r,v2_theta):
    #first obtain v1_z cross v2_r. The direction is on y axis.
    v_xxr = v1_x * v2_r * np.cos(v2_theta) #np.sin(np.pi/2-v2_theta), assume the detector is on xz plane
    #then evaluate the triple cross product
    #rxxxr:= r cross x cross r
    v_rxxxr = v2_r * v_xxr #*np.sin(np.pi/2)
    #since we do not care about the direction, just return the abs values
    return v_rxxxr


#spherical surface integral for vectors on theta direction.
#The input is symmetric about z direction, and is not a function of phi
#Hence the result is a vector on z direction
def int_E_over_steradian(E_xi, cos_theta, kR, S1, S2, parallel_rate):
    #for each vector on theta direction, the z component is -1 * sin(theta), which is the "y"-axis of np.trapz.
    #The "x"-axis for np.trapz is actually sin(theta)d(theta), which is d(cos(theta)), which is coordinate z.
    perpendicular_rate = 1 - parallel_rate
    ikR = 1j*kR
    pref = np.pi*E_xi/ikR
    eikR = np.exp(ikR)
    e_ikR = np.exp(-1*ikR) #_ as negative
    integrant = np.exp(-1*ikR*cos_theta)*(S2*cos_theta*parallel_rate + S1*perpendicular_rate)
    int_over_stardian = np.trapz(integrant, cos_theta) #np.trapz: integrate(y,x)
    int_E = pref*(2*(eikR - e_ikR) - eikR*int_over_stardian)
    return int_E

def int_Ei_over_steradian(E_xi, kR):
    ikR = 1j*kR
    pref = np.pi*E_xi/ikR
    eikR = np.exp(ikR)
```

```
    e_ikR = np.exp(-1*ikR) #_ as negative
    int_Ei = pref*2*(eikR - e_ikR)
    return int_Ei

sphere_volume = lambda radius: 4/3*np.pi*radius**3
sphere_surface_area = lambda radius: 4*np.pi*radius**2
area = lambda radius:np.pi*radius**2
```

A11.3.9. optics.py

```
import numpy as np
import bin.constants as const
import bin.physics as phys
import bin.math as mt
import bin.convert as cv
import bin.dataprocessors as dp
from bin.config import *
#A laser generates the light source within the coords
class Laser: #power_W, crossec_m2
    def __init__(self, **kwargs):
        self.__dict__.update(kwargs)
        #self.E = phys.pow_cross2Em(self.power_W,self.crossec_m2) # this is the magnitude, set
on z direction
        self.E_xi = phys.I2E(1) # this is the magnitude, set on z direction


class Detector: #angle, distance
    def __init__(self, **kwargs):
        self.__dict__.update(kwargs)

class Material:
    def __init__(self,**kwargs): #dielectric function and refractive index
        self.__dict__.update(kwargs)
        self.epsilon = self.get_epsilon() #dielectric function
        self.n = self.get_refractive_index() #refractive index
        #self.x = 4*np.pi*self.radius_m/glv.wavl_m
    def get_epsilon(self):
        return 1
    def get_refractive_index(self):
        n = np.sqrt(self.epsilon)
        return n

class Molecule(Material): #distance, dens, damp_freq, res_freq, Raman_shift
    def __init__(self,**kwargs):
        Material.__init__(self,**kwargs)
        self.surface_number = self.get_surface_number()
        self.sol_number = self.get_sol_number()
```

```
    def ccm_epsilon(self):
        epsilon_raw = phys.ccm_epsilon\

(self.dens,self.surface_concentration_factor,self.freq,self.damp_freq_abs,res_freq=self.res_freq)
        self.get_Raman_polarizability()
        #print("epsilon raw mol\n",epsilon_raw)
        epsilon = phys.ccm_epsilon_Raman(epsilon_raw, self.dens,
self.surface_concentration_factor, self.a_Raman)
        return epsilon
    def get_Raman_polarizability(self):
        self.a_Raman =
phys.ccm_Raman_polarizability(self.freq,self.res_freq,self.damp_freq_Raman,self.Raman_shift,
const.R0Rm)
    def get_epsilon(self):
    #light,resfreq_cm,dampfreq_cm,depth_nm
        epsilon = self.ccm_epsilon()
        return epsilon
    def get_surface_number(self):
        #volume_of_interest = mt.sphere_volume(self.metal_radius + self.distance) -
mt.sphere_volume(self.metal_radius)
        #number = self.dens * volume_of_interest * self.surface_concentration_factor
        number = mt.sphere_surface_area(self.metal_radius) / mt.area(self.radius)
        return number
    def get_sol_number(self):
        number = self.dens - self.surface_number*self.metal_dens
        return number

class Molecule_cmpr(Molecule):
    def get_surface_number(self):
        return 0
    def get_sol_number(self):
        return self.dens

class Nanoparticle(Material): #radius_m radius in meter
    #self.file is pd.Dataframe, obtained from pd.read_csv()
    def get_epsilon(self):
        self.epsilon_real_raw = dp.interpolate(self.file['freq'],self.file['ep1'],self.freq)
        self.epsilon_real = self.epsilon_real_raw
        if 'ep2' in self.file: # imaginary parts
            self.epsilon_imag_raw = dp.interpolate(self.file['freq'],self.file['ep2'],self.freq)
        else:
            self.epsilon_imag_raw = 0
        self.epsilon_imag = self.epsilon_imag_raw
        epsilon_raw = self.epsilon_real_raw + 1j*self.epsilon_imag_raw
        self.epsilon = epsilon_raw
        return self.epsilon
```

```
    def get_refractive_index(self):
        self.n_real_raw = dp.interpolate(self.file['freq'],self.file['n'],self.freq)
        self.n_imag_raw = dp.interpolate(self.file['freq'],self.file['k'],self.freq)
        n_raw = self.n_real_raw + 1j*self.n_imag_raw
        self.n = n_raw
        return self.n

class NanoparticleModel(Material):
    def get_epsilon(self):
        epsilon_Di = 9.84 - cv.eV2freq_rad(9.010)**2/(self.freq**2 + 1j *(cv.eV2freq_rad(0.072)
+ 0.33*1.4e6/self.radius_m)*self.freq)
        #radius is the first dimension, freq is the second one
        delta_epsilon = 5.6/(1 + np.exp((cv.eV2freq_rad(2.4) - self.freq)/cv.eV2freq_rad(0.17)))
        self.epsilon = epsilon_Di + 1j*delta_epsilon
        return self.epsilon
```

A11.3.10. physics.py

```
import numpy as np
#import PyMieScatt as ps
import bin.constants as const
import bin.global_variables as glv
import bin.convert as cv
import bin.math as mt

### MIE SCATTERING ###
#miescattering when environment has a epsilon == 1
#returns the relative intensity parallel and perpendicular
def mie(mCore, E_xi, cos_theta, k, R, parallel_rate):
    xCore = k*R
    S1, S2 = [],[]
    for i in range(len(cos_theta)):
        S1_i, S2_i = ps.MieS1S2(mCore, xCore, cos_theta[i]) #cos_theta can only be a single value
        S1.append(S1_i)
        S2.append(S2_i)
    S1, S2 = np.asarray(S1), np.asarray(S2)
    int_E = mt.int_E_over_steradian(E_xi, cos_theta, xCore, S1, S2, parallel_rate)
    int_E = int_E / (4*np.pi) #
    return int_E
    #Note that the scattered light should on r direction.
    #If assume the incident E is on theta
    #The rel_E field is given by:

def static_sca(epsilon_nano, epsilon_mol, E_xi, R, d, parallel_rate): #d: distance between
molecule and the particle
    perpendicular_rate = 1 - parallel_rate
    geometric = (epsilon_nano - epsilon_mol)/(epsilon_nano + 2*epsilon_mol)
```

```
    #geometric = (epsilon_nano - 1)/(epsilon_nano + 2)
    int_E = E_xi * ((1/3*(parallel_rate + perpendicular_rate)) + geometric*(R/(R + d))**3 *
(2/3*(parallel_rate - perpendicular_rate)))
    return int_E

def empty_mol_E(E_xi, k, R):
    xCore = k*R
    int_E = mt.int_Ei_over_steradian(E_xi, xCore)
    int_E = int_E / (4*np.pi)
    return int_E
###Dipole and Raman dipole related

#figure out the total dipole on x direction
def total_dipole(E, polarizability, numbers):
    total_dipole = numbers*E*polarizability
    return total_dipole

#parallel image dipole
def img_dipole(mol_epsilon, distance, dipole, nano_epsilon, nano_radius_m):
    radius_ratio = nano_radius_m/(nano_radius_m + distance)
    #this is the correction of imagecharge with dielectrics, the origin of the plasmon
    #gamma = (nano_epsilon - 1)/(nano_epsilon + 1)
    gamma = (nano_epsilon - mol_epsilon)/(nano_epsilon + mol_epsilon)
    #Dipole is a Vector, with r theta phi projection data for each position (described by r theta phi
coordinate)
    img_dipole = -1 * dipole * gamma * radius_ratio**3
    return img_dipole

#dipole scattering
def dipole_scatter_E(r,p,angle,freq,freq_Raman_shift): #freq: laser freq
    vecrpr = mt.cross_rxxxr(p,r,angle)
    #prepare for the prefectors incase of recalculating in a loop
    #freq_angle = np.stack((self.freq,)*angs, axis = 1) # reshaping freq
    #freq_Raman = self.freq-self.Raman_shift # reshaping freq
    #space_phase = np.exp(1j*rm*freq_Raman/const.C) #this will be cancelled after complex
conjugate
    pref_rad = 1/const.C**2/r**3*(freq-freq_Raman_shift)**2
    sca_E = const.COULOMB_CONST*pref_rad*vecrpr
    #ignore the elecstatic field since the detector is far away.
    #pref_stat = 1/rm**5 - 1j*freq_angle/const.C/rm**4
    #self.sca_E = SI_pref*(pref_rad*vecrpr + pref_stat*(3*r*dotrp-self.p*rm**2))
    return sca_E

###Plane waves

E2S =lambda E: (E.real**2 + E.imag**2) / const.Z0 * 0.5
```

```
E2I = E2S

def pow_cross2Em(power,crosssection):#laser S to magnitude
    S_avg = power / crosssection
    return np.sqrt(2 * S_avg * const.Z0)

#convert light intensity on r direction to E on theta or phi direction
I2E = lambda I_sph: np.sqrt(2 * I_sph * const.Z0)
S2E = I2E
## CCM
def damping_frequency(mu, rel_eff_mass):
    return const.E/mu/rel_eff_mass/const.ME/2

def
ccm_epsilon(dens,surface_concentration_factor,freq,damp_freq,res_freq=0,ep_inf=1,rel_eff_ma
ss=1):
    plsm_freq_square =
dens*surface_concentration_factor*const.E**2/const.ME/rel_eff_mass/const.EP0
    epsilon = ep_inf + plsm_freq_square / \
            (res_freq**2 - freq**2 - 2j * freq * damp_freq)
    return epsilon

def ccm_Raman_polarizability(freq,res_freq,damp_freq,Raman_shift,r0rm):
        #delta_k = 4 * const.ME * freq * r0rm * damp_freq
        delta_k = 0.005
        ####### delta_k = 1.63739e-4
        prefactor = const.E**2/const.ME**2*delta_k
        a_raman = prefactor / (freq - res_freq - Raman_shift + damp_freq * 1j) \
            / (freq - res_freq + damp_freq * 1j) / 4 / res_freq**2
        return a_raman

def ccm_epsilon_Raman(epsilon_raw,dens,surface_concentration_factor,a_Raman):
    return epsilon_raw + a_Raman*dens*surface_concentration_factor/const.EP0
#these last three functions can be further simplified
```

A11.3.11. plot.py

```
import numpy as np
import matplotlib.pyplot as plt
from mpl_toolkits import mplot3d
import bin.global_variables as glv
import bin.convert as cv

###single plots
def easy_plot(yscale="linear",**kwargs):
    fig,ax = plt.subplots()
    ax.plot(kwargs['x'],kwargs['y'])
```

```
    ax.set_xlabel(kwargs['x_label'])
    ax.set_ylabel(kwargs['y_label'])
    ax.set_yscale(kwargs['yscale'])
    ax.set_title(kwargs['title'])
    plt.show()

def double_linear_plot(**kwargs):
    fig,ax = plt.subplots()
    lns1 = ax.plot(kwargs['x'],kwargs['y1'],label = kwargs['y1_legend'])
    lns2 = ax.plot(kwargs['x'],kwargs['y2'],label = kwargs['y2_legend'])
    ax.set_xlabel(kwargs['x_label'])
    ax.set_ylabel(kwargs['y_label'])
    ax.set_title(kwargs['title'])
    plt.legend()
    ax2 = ax.twinx()
    lns3 = ax2.plot(kwargs['x'],kwargs['y3'],label = kwargs['y3_legend'],color="red")
    ax2.set_ylabel(kwargs['y2_label'])
    ax2.tick_params(axis='y', colors='red')
    lns = lns1+lns2+lns3
    labs = [l.get_label() for l in lns]
    ax.legend(lns, labs, loc=0)
    plt.show()

def polar_plot(wavelength_nm,theta_deg,r,fig,counter,**kwargs):
    ax = fig.add_subplot(*counter.get_count(), projection='polar')
    for i in range(len(wavelength_nm)):
        polar = ax.plot(cv.deg2rad(theta_deg), r[i], label="%d nm"%wavelength_nm[i])
    #ax.set_rmax(2)
    #ax.set_rticks([0.5, 1, 1.5, 2])  # Less radial ticks
    ax.set_rlabel_position(-22.5)  # Move radial labels away from plotted line
    ax.grid(True)
    ax.set_title(kwargs['title'], va='bottom')
    counter.next()
    return polar

def threeDcontour(x,y,z,fig,counter,**kwargs): # requires ax = fig.add_subplot(a, b, c,
projection='3d')
    ax = fig.add_subplot(*counter.get_count(), projection='3d')
    Y,X = np.meshgrid(y,x)
    ax.set_xlabel('wavenumbers [$\vectorregular{cm^{-1}}$]')
    ax.set_ylabel('angle [${^{\circ}}$]')
    ax.set_zlabel('Signal')
    ax.set_title(kwargs['title'])
    counter.next()
    return ax.contour3D(X, Y, z, 50,**kwargs)
```

```
def contour(x,y,z,fig,counter,**kwargs):
    ax = fig.add_subplot(*counter.get_count())
    #fig, ax = plt.subplots(figsize=(12,10),dpi=600)
    #ax.set(xlim = [15000,25000], ylim = [45,70])
    ax.set_xlabel('wavenumbers [$\mathregular{cm^{-1}}$]')
    Y,X = np.meshgrid(y,x)
    #xmajorLocator = MultipleLocator(500)
    #ymajorLocator = MultipleLocator(1)
    ax.set_ylabel('angle [${^{\circ}}$]')
    ax.tick_params(axis='x')
    ax.tick_params(axis='y')
    ax.set_title(kwargs['title'])
    #levels = np.linspace(0,2,30)
    contour = ax.contourf(X, Y, z, 50, cmap='inferno')
    #contour = ax.contourf(X, Y, z, levels=levels, cmap='inferno')
    #ax.contour(X, Y, z, cmap='inferno', linewidths=0, linestyles='None')
    cbar = fig.colorbar(contour)
    #cbar = fig.colorbar(contour, ticks=levels)
    #show figure on canvas
    counter.next()
    return contour

def polar_contour(wavelength_nm,theta_deg,z,fig,counter,**kwargs):
    ax = fig.add_subplot(*counter.get_count(), projection='polar')
    T,W = np.meshgrid(theta_deg,wavelength_nm)
    ax.set_title(kwargs['title'])
    #levels = np.linspace(0,2,30)
    contour = ax.contourf(T, W, z, 50, cmap='inferno')
    cbar = fig.colorbar(contour)
    #cbar = fig.colorbar(contour, ticks=levels)
    #show figure on canvas
    counter.next()
    return contour
### multi plots

class Counter(): #automatically rearrange the subplots pattern
    def __init__(self,row,column,count=1):
        self.row = row
        self.column = column
        self.count = count
    def next(self):
        self.count += 1
    def set_zero(self):
        self.count = 0
    def get_count(self):
        return (self.row, self.column, self.count)
```

```
def multi_plots(plot_type,signals,titles,row=3,column=1):
    fig = plt.figure() #figsize=[5,10]
    counter = Counter(row=row,column=column)
    for signal,title in zip(signals,titles):
        plot_type(glv.Laser.wavelength_m*1e9, glv.angle_deg, signal, fig, counter, title=title)
    fig.tight_layout(pad=0.05,h_pad=0.05, w_pad=0.05)
    plt.legend()
    plt.show()
```

Appendix References

(1) Jackson, J. D. Classical Electrodynamics. American Association of Physics Teachers 1999.

(2) Maier, S. A. Plasmonics: Fundamentals and Applications; 2007.

(3) Zou, W.; Tao, Y.; Freindorf, M.; Cremer, D.; Kraka, E. Local Vibrational Force Constants– From the Assessment of Empirical Force Constants to the Description of Bonding in Large Systems. Chem. Phys. Lett. 2020, 748, 137337.